Catalytic Combustion of Ventilation Air Methane Released from Coal Mines

A Thesis Submitted for the Degree of

Doctor of Philosophy

By

Adi Setiawan
BEng, MEng

School of Engineering
Faculty of Engineering and Built Environment
The University of Newcastle

2015

(Submitted January, 28th 2015)

Statement of Originality

*The thesis contains no material which has been accepted for the award of any other degree or diploma in any university or other tertiary institution and, to the best of my knowledge and belief, contains no material previously published or written by another person, except where due reference has been made in the text. I give consent to the final version of my thesis being made available worldwide when deposit in the University's Digital Repository**, subject to the provisions of the Copyright Act 1968.*

**Unless an Embargo has been approved for a determined period.

Signature:  Date: 28-01-2015

Statement of Authorship

I hereby certify that the work embodied in this thesis contains published papers of which I am a joint author. I have included as part of the thesis a written statement endorsed by my supervisor, attesting to my significant contribution to the joint publications.

Signature:  Date: 28-01-2015

Statement of Contribution of Others

We, the undersigned, attest that Research Higher Degree candidate, Adi Setiawan, has carried out the experiments, result analysis and writing in all papers included in this thesis.

Associate Professor Michael Stockenhuber Date: 27/01/2015

Professor Eric Kennedy Date: 27/01/15

Professor Bogdan Dlugogorski Date:

Acknowledgments

I would like to express my gratitude to my principal supervisor Associate Professor Michael Stockenhuber for all professional guidance and knowledge that have been given. I am also thankful to my co-supervisors Professor Eric Kennedy and Professor Bogdan Dlugogorski for their advice and guidance towards the right direction. I would also like to thank Professor Adesoji Adesina, Dr. Olga Tkachenko and Dr. Glenn Bryant for their contributions in the journal publications.

My pray and gratitude are always for my mother and my father. I would also like to thank my dearest wife, Mina Andhina and my lovely son, Muhammad A. Shamil for their love, patient, and sacrifices and pray. I would not be able to reach this point without their unconditional love and supports. Thank you also to my brothers, sisters and my mother in law for their help and supports.

I would like to thank the Aceh Province Government, Indonesia for providing me the scholarship which covers the living allowance and health insurance. I would like to acknowledge The University of Newcastle for awarding me the International Postgraduate Research Scholarship (UNIPRS) which covers tuition fees and completion scholarship. I would also acknowledge the financial support for our VAM research project from Australian Coal Association Research Program (ACARP).

My special thank is due to Jarrod Friggieri for his cooperative work and contributions in our VAM project. I really appreciate the help from Matthew Drewery in proofreading the chapters. I would acknowledge Jane Hamson for her assistance with ICP-OES analysis and TGA-MS. I am grateful to the Electron Microscope and X-Ray Unit of the University of Newcastle Australia and their staff (Dave Phelan, Jennifer Zobec, Dylan Cuskelly and Michael Griffiths) for their help with the SEM and XRD analyses. Thanks are also due to Dr. Viswanathan Arcotumapathy for his help with chemisorption analysis at UNSW, Sydney.

Last but not least, I would also like to thank my colleagues (Dr. Jerry Li, Naseer, Gizelle, Luke, Hadi *etc*) and technical staff at Priority Research Centre for Energy (PRCfE) and Chemical Engineering Department at the University of Newcastle (Scott Molloy, James Wilson, Con Safouris, and David Dlugogorski) for their help and support given during my research in PRCfE.

Abstract

This thesis presents a series of investigation on catalytic combustion of lean methane mixtures emitted from coal mine ventilation air. The study involves catalyst preparation, catalytic activity and stability evaluation under simulated ventilation air methane (VAM) gas, and understanding the catalyst deactivation phenomena. The investigation on the chemical and physical properties of catalysts employed a number of techniques including nitrogen physisorption, hydrogen chemisorption, temperature-programmed desorption (TPD), powder X-ray diffraction (XRD), scanning electron microscopy (SEM), transmission electronic microscopy and X-ray photoelectron spectroscopy (XPS) analyses.

Investigation on the influence of pre-treatment conditions on Pd/Al_2O_3 catalysts discloses significant differences in the light off temperatures and the extent of coke deposition, depending on whether the catalysts were pre-treated under oxidising or reducing conditions. The oxidised palladium catalysts were reduced by methane under reaction conditions and exhibited similar activity compared to catalysts which were activated under hydrogen. The long-term stability tests suggest that the primary factor responsible for low temperature catalyst deactivation is the water vapour present in the feed stream. Although no palladium hydroxide phase was observed during short-term experiment, extended exposure to wet feed results in the formation of palladium hydroxide, which appears to match the progressive deactivation of the Pd/Al_2O_3 catalyst. Introducing VAM dust causes a variation in catalytic activity originating from

coal-dust ignition and the effect of chloride on the surface of the catalyst. Nevertheless, in the presence of inhibiting agents, an average methane conversion of higher than 75 % over 1,100 h was achieved at reaction temperatures below 600 ºC.

Although supported Pd catalysts are higher in activity, nano-sized Co_3O_4 catalysts exhibit excellent stability. No changes in oxidation/chemical states were observed from the Co_3O_4 catalyst after time on stream experiments. In contrast, the presence of strongly bonded hydroxyl species on the surface of Fe_2O_3 catalysts highlights the role of water vapour in catalyst deactivation. Oxygen TPD shows that higher oxygen surface coverage of Co_3O_4 is suggested to be responsible for a higher activity in comparison with Fe_2O_3 catalysts. Co-precipitating gold particles with cobalt oxide or iron oxide does not enhance the activity of the catalyst, which is most likely due to blocking the active site of support by the gold particles.

Enhanced hydrothermal stability was observed over a novel Pd/TS-1 catalyst during 1,900 h time-on-stream experiments, where a 90 % methane conversion level was successfully maintained at temperature < 500 °C. Surface oxygen mobility and coverage plays a major role for the activity and stability of this catalyst in the presence of a large excess of water. It was identified that water adsorption and in turn hydrophobicity of the catalyst support was a major factor influencing the long term stability of combustion catalysts. The hydrophobicity and competitive adsorption of water with oxygen is suggested to influence oxygen surface coverage and in turn apparent activation energy over the catalysts.

Catalyst characterization of Pd/Al_2O_3 confirms that the deactivation is due to palladium migration and particle growth and is the most prominent in the presence of water in the feed. The formation of α-Al_2O_3 during long-term stability tests explains the changes in pore structures which is responsible for the re-dispersion of palladium particles. Four accelerated ageing procedures were performed with a target of mimicking the properties of long-term used catalysts. Interestingly, no formation of α-Al_2O_3 phase was found from the aged catalysts suggesting that, the transformation of alumina phase occurs at a very slow rate. Among the four procedures, ageing under wet-oxygen in helium provides the most similarity to the properties of long-term used catalysts. Increasing the aging temperature up to 830 °C leads to depletion of surface palladium, which permanently reduces the performance of the catalyst.

List of Publications

Journal Articles

Setiawan, A., Kennedy, E.M., Dlugogorski B.Z., Adesina A.A., Stockenhuber, M., *The stability of Co_3O_4, Fe_2O_3, Au/Co_3O_4 and Au/Fe_2O_3 catalysts in the catalytic combustion of lean methane mixtures in the presence of water*, Catalysis Today, 2014, http://dx.doi.org/10.1016/j.cattod.2014.11.031.

Setiawan, A., Friggieri, J., Kennedy E.M., Dlugogorski, B.Z., Stockenhuber, M., *Catalytic combustion of ventilation air methane (VAM) – long term catalyst stability in the presence of water vapour and mine dust,* Catalysis Science & Technology, 4(6):1793-1802, 2014.

Setiawan, A., Kennedy, E.M., Dlugogorski, B.Z., Adesina A.A, Tkachenko, O., Stockenhuber, M., *Evidence of the formation of surface palladium carbide during the catalytic combustion of lean methane/air mixtures*, Energy Technology, 2(3):243-249, Mar 2014.

Conference Papers

Setiawan, A., Kennedy, E.M., Dlugogorski, B.Z, Stockenhuber, M., *Hydrothermal stability evaluation of cobalt and iron oxides catalysts during total oxidation of lean*

methane mixtures, 8th International Conference on Environmental Catalysis, Asheville, NC, USA, 24-27 August 2014.

Setiawan, A., Stockenhuber, M., Kennedy, E.M., Dlugogorski, B.Z., *Low temperature methane combustion over palladium supported on a mixture of TiO_2 and ZSM-5 catalyst in the presence of water*, 8th World Congress on Oxidation Catalysis, St. Louis, USA, 9-12 June 2013.

Setiawan, A., Dlugogorski, B.Z., Kennedy, E.M., Stockenhuber, M., *Catalytic combustion of methane - mechanistic insights into the effect of contaminants present in ventilation air methane*, 10th Natural Gas Conversion Symposium (NGCS10), Doha, 2-7 March 2013.

Stockenhuber, M., Setiawan, A., Kennedy, E.M., Dlugogorski, B.Z., *Study on the inhibitory effect of water on palladium and gold catalysts during catalytic combustion of ventilation air methane*, 15th International Congress on Catalysis, Munich, Germany, 1-6 July 2012.

Table of Contents

Appendices

List of Figures

List of Tables

List of Abbreviations

A	The rate pre-exponential factor
BE	Binding Energy
BE	Backscattered Electron
CBM	Coal-Bed Methane
CFBC	Coal Fluidized Bed Combustion
CFRR	Catalytic Flow Reverse Reactor
CMR	Catalytic-Monolith Reactor
DP	Deposition-Precipitation
E	Activation energy
E_{ads}	Activation energy for adsorption
EDS	Energy-Dispersive X-ray Spectroscopy
E_{dsb}	Activation energy for desorption
E_{gas}	Activation energy for gas phase reaction
E_{sur}	Activation energy for surface reaction
FTIR	Fourier Transform Infrared Spectroscopy
FWHM	Full Width at Half Maximum (The line broadening at half the maximum intensity)
GC	Gas Chromatography
GHG	Green-House Gas
GHSV	Gas Hourly Space Velocity
GWP	Global-warming potential
HDP	Homogenous Deposition Precipitation
ICP-OES	Inductively Coupled Plasma-Optical Emission Spectrometer
IUPAC	International Union of Pure and Applied Chemistry
k_A	The specific reaction rate
MS	Mass Spectrometer
NIST	National Institute of Standards and Technology

P_0	Saturation pressure
PT	Pressure Transmitter
R	The gas constant
RH	relative humidity
RMR	Relative Molar Response
SE	Secondary Electron
SEM	Scanning Electron Microscopy
STEM	Scanning Transmission Electron Microscope
T	Temperature
TCD	Thermal Conductivity Detector
TEM	Transmission Electron Microscopy
TFRR	Thermal Flow Reverse Reactor
TGA	Thermogravimetric Analysis
TGA	Thermogravimetric Analysis
TOC	Total Organic Carbon
TOF	Turn-Over Frequency
TOS	Time On Stream
TPD	Temperature Programmed Desorption
TS-1	Titanium silicalite
UHV	Ultra-High Vacuum
VAM	Ventilation Air Methane
VOC	Volatile Organic Compounds
X	Conversion
XPS	X-ray Photoelectron Spectroscopy
XRD	X-Ray Diffraction

CHAPTER 1

INTRODUCTION

1.1. Research Background

Methane (CH_4) is the main constituent of natural gas and is an important energy source. As a greenhouse gas, methane can exist in the atmosphere for periods of up to15 years and it is 21 times more effective in trapping heat in the atmosphere over a 100-year period compared to carbon dioxide [1]. A number of natural (such as wetlands) and anthropogenic sources such as coal mining, landfills, natural gas and petroleum systems, agricultural activities, and waste water treatment contribute to methane emissions [2].

One of the primary sources of methane is associated coal mining activities. Methane emitted from coal mines around the world represents approximately 8 % of the world's anthropogenic methane emissions, which themselves constitute a 17 % contribution to total anthropogenic greenhouse gas emissions [3]. Coal and methane gas are formed during the coalification process, in which biomass is converted by biological and geological processes into coal [4]. Methane is deposited in coal seams and adjacent rock strata, called coal-bed methane (CBM). The process of coal extraction releases CBM into the mine working areas. CBM drained in advance of mining is extracted at high concentrations and often meets the specification of natural gas pipeline quality [3]. Mixing with air, this coal mine methane presents a substantial danger of fire and explosion when the methane concentration is in the range of 5 – 15 %. To ensure mine safety and maintain continuous production, the mine operators employ large-scale ventilation systems to dilute, as well as remove coal mine methane from mining areas. This diluted methane is discharged to the atmosphere and is referred as ventilation air methane (VAM).

There are three sources of methane gas released from coal mines: (1) mine ventilation air (0.1-1 % CH_4), (2) gas drained from mine working area e.g. goafs (30-95 % CH_4), and (3) gas drained from the coal seam prior to mining (60-95 % CH_4). Prior to mining, the concentration of methane in the gas is high, but it rapidly decreases as mining activities commence. Although ventilation air methane has a much lower methane concentration compared to the other sources, it is considered to be the most significant net contributor to gases released into the atmosphere, accounting for 60-70 % of all coal mining related methane emitted [3, 5, 6]. These reasons lead to the conclusion that methane capture, mitigation and utilization in VAM is an important and urgent issue because (1) it represents the majority of methane emissions from coal mines; and (2) it is most difficult to capture and use as the air volume is large and the methane resource is dilute and variable in concentration and flow rate [5].

Currently, a number of technologies for VAM mitigation and utilization are under development. In general, these technologies are classified into two categories, ancillary uses and principal uses [5, 7]. For ancillary uses, the VAM gas is utilized as combustion air for boilers, turbines and internal combustion engines while for principal uses the VAM is oxidized in a reactor to reduce methane emissions and in part, recover the waste energy. One potential technological solution for treatment of VAM is catalytic combustion, where methane is oxidized to carbon dioxide on a catalytically active solid surface. This flameless combustion is ideal for highly diluted air-methane streams, such as VAM, as the concentration of methane is outside the typical flammability range. Production of NO_x is essentially absent and the reaction temperature is relatively low (generally below 500 ºC).

The catalytic oxidation of methane at low temperature has been extensively investigated, especially over Pd and Pt based catalysts. A comprehensive review of methane oxidation over noble metal based catalysts where it appears most researchers agree that supported Pd catalysts are the most active materials [8]. However, palladium catalysts can be susceptible to poisoning by water vapour and other contaminants, which may result in severe deactivation when used in the catalytic combustion of VAM. These challenges and considerations motivate us to embark on the present study to understand the activity and deactivation phenomena of catalysts in catalytic combustion of VAM.

1.2. Objective of Current Study

This research aims to further the understanding of catalytic combustion of VAM emitted from coal-mine ventilation systems where the methane concentration is below 1 %, and other components most notably $H_2O_{(v)}$. The specific objectives are: (i) to prepare catalytic materials applicable for combustion of VAM; (ii) to improve the stability of the catalysts against contaminants and (iii) to investigate the deactivation behaviour of the catalysts. The investigation considers the extremely humid conditions of ventilation streams and the presence of particulates (coal dust, calcium oxides, iron oxides, clay, quartz etc) at maximum particle size of 0.5 μm and a dust loading of 4.5 mg m^{-3}.

Achieving this objective requires a number of steps as follows:

a. Designing and installing experimental facilities for methane oxidation reactors for short and long term experiments;
b. Preparing catalytic materials (based on current progress on catalyst development) and examining the activity and durability of catalysts in total oxidation of methane in the presence of water;
c. Performing long-term stability tests over the most active catalysts under simulated ventilation air methane (VAM) stream.
d. Investigating the characteristics of the catalysts prepared for this research by using H_2-chemisorption, temperature programmed desorption (TPD), powder x-ray diffraction (XRD), scanning electron microscopy (SEM), transmission electron microscopy (TEM), and x-ray photoelectron spectroscopy (XPS).
e. Designing a new catalyst and evaluating the performance and durability of the catalyst for an extended period of time (up to 2,000 h) under a simulated VAM stream.
f. Investigating the physical and chemical properties of the new catalyst and comparing it with the properties of a commercially available catalyst to gain new insight into catalyst stability and deactivation phenomena.
g. Designing and evaluating the procedures for aging treatment of the catalysts to mimic the properties of long-term used catalysts as well as understanding the deactivation phenomena.

1.3. Structure of the Thesis

The work is presented in the following order:

Chapter 2 provides a literature review of the previous studies on catalytic combustion of lean methane mixtures. This chapter also assembles and reviews existing research progress on the characteristics of ventilation air methane streams, the technological options for methane mitigation and utilization, and the current progress on catalyst development for methane combustion.

Chapter 3 describes the catalyst synthesis procedures, the experimental set-up for catalytic activity and stability tests including the analytical methodology. The catalyst characterization techniques employed in this research including N_2-physisorption, H_2-chemisorption, TPD, XRD, SEM, TEM, XPS and elemental analyses are described in detail.

Chapter 4 examines the effect of pre-treatment conditions on the activity of palladium supported on aluminium catalyst for combustion of air mixtures containing low concentrations of methane (0.2-0.8%). The experiments performed for this chapter disclose the formation of carbonaceous deposits and are able to correlate coke deposition with catalyst activation procedures. The time-on-stream behaviours of methane combustion and the activity of Pd/Al_2O_3 catalyst at different gas hourly space velocities are also reported in this chapter.

Chapter 5 reports the effect of water and coal mine dust present on supported palladium catalysts during the catalytic combustion of a surrogate VAM gas. This chapter evaluates the stability of the Pd/Al_2O_3 catalysts in long term experiments (up to 1,100 hours time-on-stream) with simulated ventilation air methane in order to understand the deactivation phenomena of the catalyst. The effect of coal

mine dust is assessed by adding it to the catalyst and noting any effect it has on catalyst activity and stability. The combustion tests are operated under conditions where the level of methane conversion is maintained at or above 90 % by increasing the catalyst bed temperature.

Chapter 6 presents the investigation results on the effect of water vapour present in catalytic combustion of lean methane mixtures over pure metal oxide (Co_3O_4 and Fe_2O_3) and supported gold (Au/Fe_2O_3, Au/Co_3O_4) catalysts. An understanding of the inhibitory effect of water vapour is explored by performing temperature-programmed desorption of water from fresh and used samples supported by other characterization techniques such as N_2 adsorption desorption, XRD, TEM, SEM and XPS analyses.

Chapter 7 reports a new palladium catalyst supported on titanium silicalite (TS-1) zeolite. A notable increase in hydrothermal stability observed over 1,900 hours time-on-stream experiments are discussed in this chapter. This chapter presents the physical and chemical properties of Pd/TS-1 catalyst in comparison with conventional palladium on alumina catalysts to understand the advantages of this catalyst and the deactivation mechanism.

Chapter 8 examines the properties of Pd/Al_2O_3 catalyst after long-term stability tests in the presence of water and coal mine dust in lean-methane combustion. Using four accelerated ageing procedures, catalyst deactivation phenomena are explored. In this chapter, the properties of the aged catalysts are compared with the properties of used catalysts tested in long-term stability experiments to explore effective strategies for

accelerating the ageing process in order to reduce the time that is typically required for catalyst stability tests.

Chapter 9 summarises the major findings obtained during this research and provides suggestion for future investigation.

References

1. Solomon, S., D. Qin, M. Manning, R.B. Alley, T. Berntsen, N.L. Bindoff, Z. Chen, A. Chidthaisong, J.M. Gregory, G.C. Hegerl, M. Heimann, B. Hewitson, B.J. Hoskins, F. Joos, J. Jouzel, V. Kattsov, U. Lohmann, T. Matsuno, M. Molina, N. Nicholls, J. Overpeck, G. Raga, V. Ramaswamy, J. Ren, M. Rusticucci, R. Somerville, T.F. Stocker, P. Whetton, R.A. Wood, and D. Wratt, *Technical summary*, in c*limate change 2007: the physical science basis. Contribution of working group I to the fourth assessment report of the intergovernmental panel on climate change*, S. Solomon, et al., Editors. 2007: Cambridge, United Kingdom and New York, NY, USA p. 996.
2. Bousquet, P., B. Ringeval, I. Pison, E.J. Dlugokencky, E.G. Brunke, C. Carouge, F. Chevallier, A. Fortems-Cheiney, C. Frankenberg, D.A. Hauglustaine, P.B. Krummel, R.L. Langenfelds, M. Ramonet, M. Schmidt, L.P. Steele, S. Szopa, C. Yver, N. Viovy, and P. Ciais, *Source attribution of the changes in atmospheric methane for 2006–2008.* Atmospheric Chemistry Physics, 2011. 11: p. 3689–3700.
3. Schultz, H.L., P. Carothers, R. Watts, and R. McGuckin, *Assessment of the worldwide market potential for oxidising coal mine ventilation air methane*. 2003, United States Environmental Protection Agency, Air and Radiation (US-EPA)
4. Warmuzinski, K., *Harnessing methane emissions from coal mining.* The Institution of Chemical Engineers (IChemE), 2008. 86: p. 315 - 320.

5. Karakurt, I., G. Aydin, and K. Aydiner, *Mine ventilation air methane as a sustainable energy source.* Renewable and Sustainable Energy Reviews, 2011. 15(2): p. 1042-1049.

6. Carothers, P. and M. Deo, *Technical and economic assessment: mitigation of methane emissions from coal mine ventilation air*, in *Coalbed Methane Outreach Program*. 2000, Climate Protection Division, U.S. Environmental Protection Agency.

7. Su, S., A. Beath, H. Guo, and C. Mallett, *An assessment of mine methane mitigation and utilisation technologies.* Progress in Energy and Combustion Science, 2005. 31(2): p. 123-170.

8. Gelin, P. and M. Primet, *Complete oxidation of methane at low temperature over noble metal based catalysts: a review.* Applied Catalysis B: Environmental, 2002. 39: p. 1-37.

CHAPTER 2

LITERATURE REVIEW

2.1. Introduction

Coal mining is a significant contributor to the emission of methane, which has a greenhouse gas potency that is 23 times greater than that of CO_2 [1]. The total oxidation of methane to carbon dioxide is seen as a technological option to curb net greenhouse gas emissions. In excess of 60 % of the total coal mining-related methane emissions originate from the ventilation air system. The successful development of a technology for methane mitigation and utilization would greatly reduce greenhouse gas emissions associated with coal mining [2].

This chapter summarises previous studies dealing with the characterization and treatment of ventilation air methane streams. The technological developments for methane mitigation and utilization are described, including their benefits and drawbacks. The review commences with the discussion on catalytic combustion in general, followed by a specific discussion on the process of methane total oxidation. Subsequently, current progresses in catalyst investigation for methane combustion are discussed, *i.e.* supported palladium catalysts, gold-based catalysts and single metal oxide catalysts. Finally, this review identifies the knowledge gaps and proposes further research priorities needed to enhance the understanding of the activity and behaviour of catalysts in combustion process of ventilation air methane.

2.2. Characteristic of ventilation air methane (VAM)

Developing an efficient technology for ventilation air methane (VAM) utilization and mitigation requires detail information on the characteristics of coal mining emissions. In

general, coal-mine ventilation air consists of nitrogen, oxygen, methane, carbon dioxide and water vapour where the methane concentration is below 1 % [2-4]. Traces of CO, C_2H_2 and higher hydrocarbons, He, H_2, HCN, NH_3, NO_x, H_2S, SO_2 or organic sulphur compounds may be present in the VAM [4].

The characteristics of ventilation air methane was investigated in detail by Shi Su et al. at four mines located in eastern Australia [3]. It was found that in addition to air, the mine-ventilation streams contained CH_4, H_2O, and traces of CO, H_2S and SO_2. Methane concentration varied considerably but was below 1 % while H_2S and SO_2 concentrations were less than 1 ppm. CO spikes were detected at a maximum of 28 ppm during shift changes which was most-likely due to diesel equipment being started. Humidity measurements suggested that the ventilation air of all mines tested varied between 70 % and 100 % relative saturation. It was reported also that the effect of mining activities on the concentration of methane in the ventilation air was significant. During mine production, many coal and other particles such as calcium oxides, iron oxides, clay, quartz *etc.* were detected. The dust loading was 4.47 mg m^{-3} with the maximum particles size of 0.5 μm. A low concentration of particles was observed in the VAM stream when the mine was not producing. In general, the flow rate of "gassy" mines ventilation air stream is in the range of 150-300 $m^3.s^{-1}$ however methane concentration, temperature and flow rate is not constant, especially when mine operations are changing.

Based on the above-mentioned characteristics of VAM of the gassy mines, catalytic combustion technology would be a prospective way to mitigate the methane emission. This is due to its capability to oxidise lean methane in air mixtures with fluctuating

methane concentration. A relatively low reaction temperature characteristic of this flameless combustion brings a great benefit in designing a self-sustainable system for capturing the energy and oxidising methane. Moreover, NO_x emissions can be minimized if the combustion occurs at low temperatures. For these reasons, a catalytic combustion facility for methane was prepared and used to evaluate this technology by improving the activity of the catalyst as well as increasing its stability against poisons.

2.3. Technology options for utilization and mitigation of VAM

The very low concentration of methane in mine ventilation air and the presence of water vapour and solid particulates generate major challenges with respect to utilisation and mitigation. The typically high volumetric flow rates of VAM leads to significant contribution to the world's anthropogenic methane emission (*ca.* 8 %). This requires either treatment in its dilute state, or concentration of the feed stream to levels that can be used in conventional methane-fuelled engines [3].

In general, mitigation and utilization technologies of VAM are classified into two categories, ancillary uses and principal uses [5-7]. For the ancillary uses, the VAM gas is used as supplemental fuel, added to input air of various combustion systems. Only a fraction of VAM gas can be used with this technique while the remainder of the methane gas is released to the atmosphere. As principal use, VAM gas is utilized as the primary fuel and oxidized in a reactor mainly for reducing greenhouse gas (GHG) emissions as well as producing heat or electricity. Selection of one of these options for providing the best solution for a mine depends on several factors such as: (a) highest investment return, (b) governmental policy, such as carbon credit only for ventilation air

methane or for all the mine methane, (c) mine-site specifications, and (d) mine safety [5].

Fig. 2.1 illustrates the current technological options available for VAM mitigation and utilization. The first group of options makes use of ventilation air as a combustion air for above ground installations such as boilers, engines and turbines to provide heat or power at the mine site. Using this option, the energy recovery of the process is quantifiable, but only contributes a small percentage of the total fuel used for conventional gas turbines and gas engines [8]. The safety aspects of the connection between the unit and mine shaft becomes a major issue. The presence of coal-dust in VAM stream leads to a higher cost of filtering of the dust. The impact of coal-dust can be reduced if the VAM stream is utilized in pulverized coal-fired boiler, nevertheless lack of pulverised fuel power station are established near to the coal mines. Fluctuations in the flow rate and methane concentration of VAM gas may negatively influence the performance of the power plant equipment, *i.e.* damage boiler furnace, slagging and residuals due to methane concentration increases [5].

The use of coal mine ventilation air in hybrid waste/coal/tailings/methane combustion systems can be considered as an alternative option for methane mitigation. This technology can mitigate mine methane and utilise waste coal as well as recover waste energy for power generation. Either oxidizing methane in a rotary kiln or fluidized bed has similar benefits to the use of ventilation air methane in pulverized coal boilers. However, additional system/regulations are needed to control the combustion process and provide a sustainable operation [6].

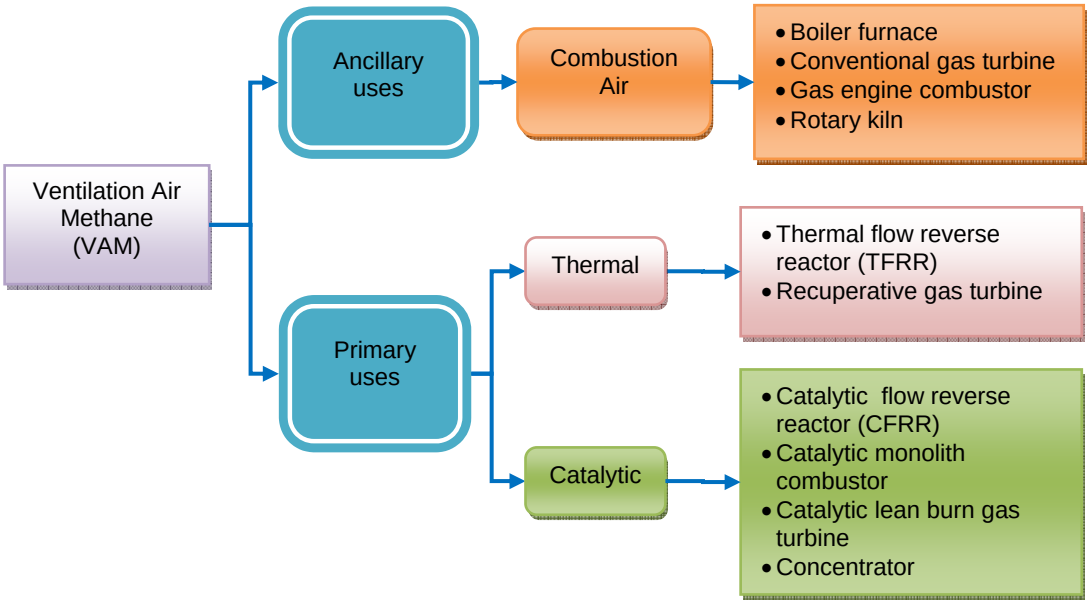

Fig. 2.1. Technologies for ventilation air methane [6, 7, 9]

To hybridize waste/coal, several companies have developed rotating (rotary) kilns, however maintaining the stability of the combustion process requires input gas or fuel of high and relatively constant concentration. Somewhat disappointing process performance was reported when the rotary kiln was fed with low grade solid fuels, such as anthracite culm and difficulties in relation to maintaining sustained combustion, even when large quantities of supplemental fuels were used [10].

Fluidized bed technology can also be used to combust waste coal through mixing with ventilation air methane. During the combustion process in fluidized beds, solid fuels are suspended by upward-blowing jets of air, resulting in the turbulent mixing of gas and solids. The bubbling fluid provides a media for high chemical reaction rates and rates of heat transfer. The mixing action of the fluidised bed can facilitate flue gases contacting with a sulphur-absorbing chemicals, such as limestone or dolomite that has been added to the bed [5]. This insight was reported during studies in Pennsylvania, where there are

14 circulating fluidised bed combustion (CFBC) power plants burning waste coals including anthracite Culm. These power plants successfully operate using advanced CFBC technology and can directly fire unprocessed waste coal with ash content ranging from 50 to 70% by weight, corresponding to a heating value of 7 MJ/kg (the minimum requirement for stable boiler operation) [11]. Nevertheless, for hybrid waste coal/methane fluidized bed combustion, more experimental studies are needed to establish that the methane can be fully combusted.

Internal combustion engines are also considered as possible option for VAM mitigation and utilization. In this technology, "medium" quality gas is used as the primary fuel to generate electric and the mine ventilation air is introduced to the engine as combustion air. The capital cost required is relatively low if the engines can be located near the coal mine, and results in no or little additional cost involved for supplying VAM stream to the engines. However, since the combustion process takes place at high temperatures, the formation of NO_x is notable [8] and can become a major emission concern. Although the capital cost is relatively low, only a small fraction of methane in ventilation air can be utilized in internal combustion engines. Likewise, a small percentage of methane in ventilation air can contribute to the total fuel consumed in a conventional gas turbine. Coal mine ventilation air can be used for diluting the combustion process and cooling the turbines, however it is likely that methane passes through the turbine without combustion. To deal with this problem, more complex turbine systems are required including a compressed ventilation air system [5].

The second group of technologies available for VAM mitigation and utilization is to thermally or catalytically oxidize the lean methane mixtures in reactors. Using these

options, VAM can potentially be utilized as primary fuel in combustion processes. However, the principal uses of VAM gas can be effective if the combustion system can operate at methane concentrations below its lower flammability limit. In this group of technologies, VAM gas is used as the primary feed for thermal flow reverse reactors (TFRR), catalytic flow reversal reactor (CFRR), catalytic monolith reactors, lean burn gas turbines and concentrators/membrane reactors.

Thermal flow reversal reactors (TFRR) employ the flow-reversal principal to transfer the heat of combustion initially to a solid medium then back to incoming air to increase its temperature until it reaches the auto-ignition temperature of methane [9]. A TFRR system consists of a ceramic or silica gravel bed located in the centre of the reactor and electric heating elements as the bed pre-heater. Fig. 2.2 illustrates the flow-reversal process of this system. Initially, ventilation air is fed from one end to the reactor by opening valve A and heated until the oxidation takes places around the centre of the bed. When the temperature at the other side of reactor reaches the oxidation temperature (> 1000 °C), the direction of airflow is automatically reversed, allowing the incoming VAM gas flow through valve B to encounter auto-oxidation temperatures near the centre of the bed and then oxidizes. The hot gases again transfer heat to the near (cold) side of the bed and exit the reactor. Then, the process again reverses [2]. This flow-reversal process is managed by a programmable logic controller to maintain the hot area of the bed in the middle of the oxidizer. This controller supports the oxidation of a constant stream of VAM over time. Laboratory and field studies suggested that TFRR can sustain operation with ventilation air containing methane concentrations as low as 0.1 percent [8]. Unfortunately, the upper limit of bed temperature increases the likelihood of NO_x gases formation. The operational and maintenance costs of this unit is

relatively high since the heater consumes energy and the presence of particulates in the VAM stream [3] may create major problems, including corrosion of the reactor.

Methane emissions from VAM can be treated also in a recuperative gas turbine, where the heat from the combustion process is used to preheat the air containing methane reaching the auto-ignition temperature (in the range 700–1000 °C), with the combusted gas is being used to drive a turbine. It was reported that this gas turbine can operate continuously when the methane concentration in air is higher than 1.6 %, which leads to the air being preheated to 700 °C before combustion. Therefore, additional substantial quantities of methane to the ventilation air is required to reach adequate methane concentrations [5]. This adds significant cost to the VAM processing.

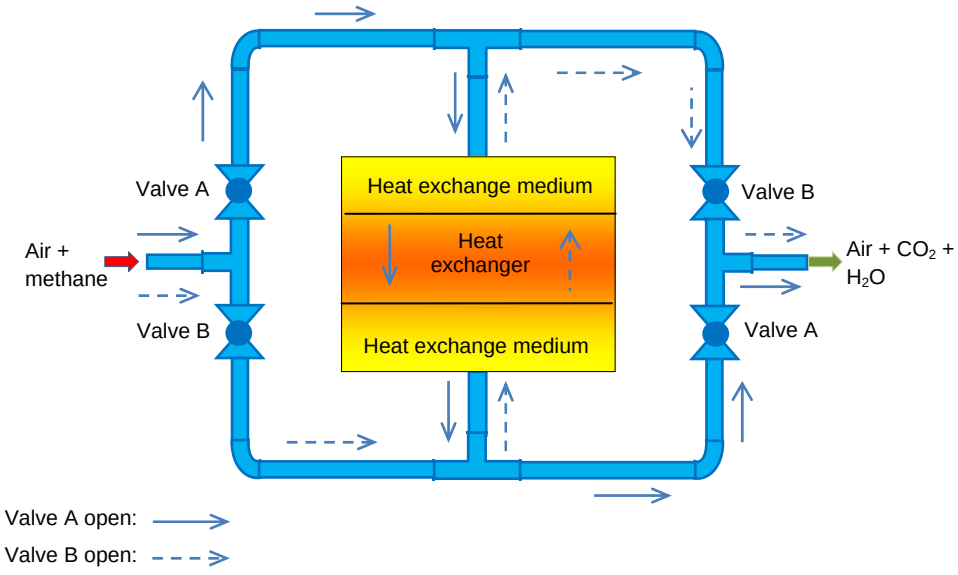

Fig. 2.2. Schematic of thermal flow-reversal process

Catalytic flow reversal reactors (CFRR) offers benefits with regard to auto-ignition temperature of methane and the absence of NO_x formation. CFRR adapts the thermal flow-reversal technology described above by using a catalyst to reduce the auto-oxidation temperature of methane to a temperature as low as 350 °C [2]. It was reported that in order to sustain process operation, a pilot scale CFRR required the minimum methane concentration in the ventilation air to be 0.19 % [12], however there was no information on how long the CFRR unit can be operated at this low methane concentration. The overall performance of this system depends on methane concentration, cycle time and velocity. The catalyst selection plays important role in fixing the main operation variables in order to obtain a stable and auto-thermal operation [13]. A recent lab-scale study of VAM combustion in a vertical CFFR suggested that this reactor was successfully operated under a wide range of operating conditions with self-sustaining operation even at methane concentration as low as 0.13 vol. % [14].

The uses of monolithic reactors for lean methane combustion were demonstrated as a potential solution for destruction of coal mine methane emission, as well as extracting the heat from the combustion reaction [15, 16]. Catalytic-monolith reactors (CMR) employ a honeycomb type-monolith-reactor to oxidize the methane with very low pressure drop even though the flow rate is very high. Monoliths used consists of a structure of a parallel channels with walls coated by a porous support containing catalytically active particles [6]. Compared to the other reactor technologies, CMR units are reduced in size due to the high surface activity. However, an additional heating system is required, i.e. heat exchanger to pre-heat the ventilation air. To reach auto-ignition temperature, a monolith reactor should be operated above 500 °C, which is

higher compared to CFRR. An experimental study suggested that the methane concentration required for sustainable CMR operation is ≥ 0.4 % [5].

Development of a lean-burn gas turbine is still in progress and mostly focuses on reducing required limit of methane concentration in air. The combination of a lean-burn gas turbine and catalytic combustor is an effective strategy for increasing the efficiency of the system. Currently, Energy Development Limited (EDL)'s recuperative gas turbine, CSIRO lean-burn catalytic turbine and Ingersoll-Rand (IR)'s micro-turbine are being developed with a catalytic combustor [5]. It was reported that the CSIRO catalytic turbine and the IR catalytic micro-turbine can operate at a methane concentration of 1 %, while EDL recuperative turbine required at least 1.6 % of methane in air. Therefore, additional quantities of methane will need to be added to the VAM stream. Using lean burn gas turbine, not only low methane concentration can be utilized, methane captured from pre and post mining may also be added as fuel.

Concentrators can also be an alternative solution to enrich the methane concentration in ventilation air to meet the gas turbine requirement since the air volume is large and methane concentration is not constant. Usually, concentrators are used to capture volatile organic compounds (VOC). Potentially processing via a concentrator, ventilation air containing 0.1 – 0.9 % of methane can be enriched up to 20 %, which can be used to generate the electric power. Vortex tubes could be a potential method for VAM utilization and mitigation as gas separation devices leading to produce a higher concentration of methane [17]. However, effective technology to enrich methane concentration is still under development. Overall, the assessment on the technology

available for VAM mitigation and utilization suggested that the lean-burn turbine is capable of using most of the ventilation air methane [5].

A fluid bed concentrator is considered as an alternative way to increase the methane concentration. This concentrator consists of an adsorber, a vessel containing adsorbent fluid with adsorbed methane, methane desorption system and a feeding system for the adsorbent medium. The adsorber is a combination of fluidized and moving bed systems which consists of a series of adsorbent fluid beds. The inlet of ventilation air is at the bottom of adsorber passing upward through the fluidized beds. The methane adsorption process leads to an increase in the adsorbent density, causing the saturated adsorbent to drop to the bottom of the adsorber. The saturated adsorbent is then discharged to the storage vessel and subsequently transferred into the desorber. Activated carbon or zeolite is suitable adsorbent medium. These materials can be re-generated by increasing the temperature results in the release of concentrated methane into a lower volume stream. After methane desorption process (adsorbent regeneration), the adsorbent medium can be stored back to the adsorber for reuse. Unfortunately, recent experiments on this technology were unsuccessful [5]. To be considered as a viable technology for application in VAM, further development is required based on cost-effective processing of the waste methane in a variety of site/plant conditions.

In conclusion, mitigation and utilization of ventilation air methane faces significant challenges due to its low and variable concentration of methane, as well as its high volumetric flow. Utilization of VAM gas mainly can be categorized as ancillary and principal uses. Ancillary uses of ventilation air methane benefit mainly in reducing the greenhouse effect of methane. In principal uses, both harnessing energy and methane

emission reduction may be achieved. To enrich methane concentration in ventilation air, concentrators are considered to be useful devices when methane concentration in ventilation air does not meet the requirement. Mine site specific conditions are the main factors to be evaluated in assessing the applicability of technology for mitigation and utilization of coal mine ventilation air at any site. It is very important to investigate any possible safety issue when any type of technologies is connected to the mine site. Globally, the greenhouse gas effect from underground coal mines ventilation air could be reduced about 95 % by using oxidation methods. On the other hand emissions from coal mining could be reduced to 67 % [6].

Due to its low methane concentration, ventilation air methane does not support the combustion, so flaring is not feasible. Adding higher concentration of methane to the ventilation air and burning it would offer some remedy, but overall it would add to the total emission of greenhouse gases. Enrichment of methane using membrane separation or pressure swing adsorption is also potentially feasible for methane mitigation and utilization. The enriched methane gas can be fed directly to gas turbines or reciprocating engines to produce power. Another way of using VAM is to oxidise the methane to carbon dioxide in thermal flow-reversal reactors. Flameless combustion is more practical but the low caloric value of lean methane mixture makes self-sustaining operation difficult. Finally, recent technological developments in the catalytic oxidation of methane may be a prospective way to ease the methane emission, despite problems with catalyst deactivation during operation.

2.4. Catalytic combustion

2.4.1. General

Catalysis is defined as a process whereby a reaction occurs at an enhanced rate compared to the rate of reaction in absence of catalyst. A catalyst is a substance that enhances a reaction rate by promoting alternative reaction pathway(s) [18, 19]. There are two broad types of catalysis, homogeneous and heterogeneous. However, in this section the discussion is focussed on heterogeneous catalysis as it is more relevant to the current study. Catalysis is termed heterogeneous when the catalyst and reactant are in different phases. A simple example is CO oxidation on a metal surface (such a occurring in automotive exhaust catalysts) where the reactants are in gas phase and the catalyst is solid phase. In this and most catalytic processes, the catalytic cycle involves gas phase diffusion, molecular adsorption, dissociative adsorption, surface diffusion, surface reaction, adsorbed product and product desorption.

In heterogeneous catalysis, the nature of the top atomic layer of a solid catalyst determines the rate of a catalytic reaction. The availability of bonding sites on the surface of the catalyst provides a lower energy pathway for molecules to react. Fig. 2.3 illustrates a simplified energy profile for a heterogeneous catalytic process [18]. In the absence of catalyst (gas phase reaction) the activation energy (ΔE_{gas}) is high since a barrier has to overcome to enable breaking of bonds before the product is formed. In a heterogeneous catalytic reaction, the gas phase molecules are adsorbed on the surface during the process, stabilising the transition state of the reaction. As a result, the energy barriers are lower than un-catalysed process and the reaction is kinetically accelerated.

This means a catalyst enhances reaction rates by lowering activation barriers, accelerates the approach to equilibrium, however the equilibrium concentration is not affected.

Heterogeneous catalysis is widely used in many industrial processes. One of the most widespread applications is in catalytic converters where hydrocarbons emissions are oxidised on catalytically active materials. Moreover, catalytic oxidation is more popular today as an alternative way of producing energy. Instead of working within fuel flammability limits, a suitable catalyst is able to oxidise hydrocarbon over a broad range of concentrations. A lower reaction temperature utilised by catalytic combustion offers a number of important benefits, minimising the production of unwanted nitrogen oxides and avoiding sintering of catalyst caused by a higher reaction temperature, reducing heat losses and potentially improving mine safety.

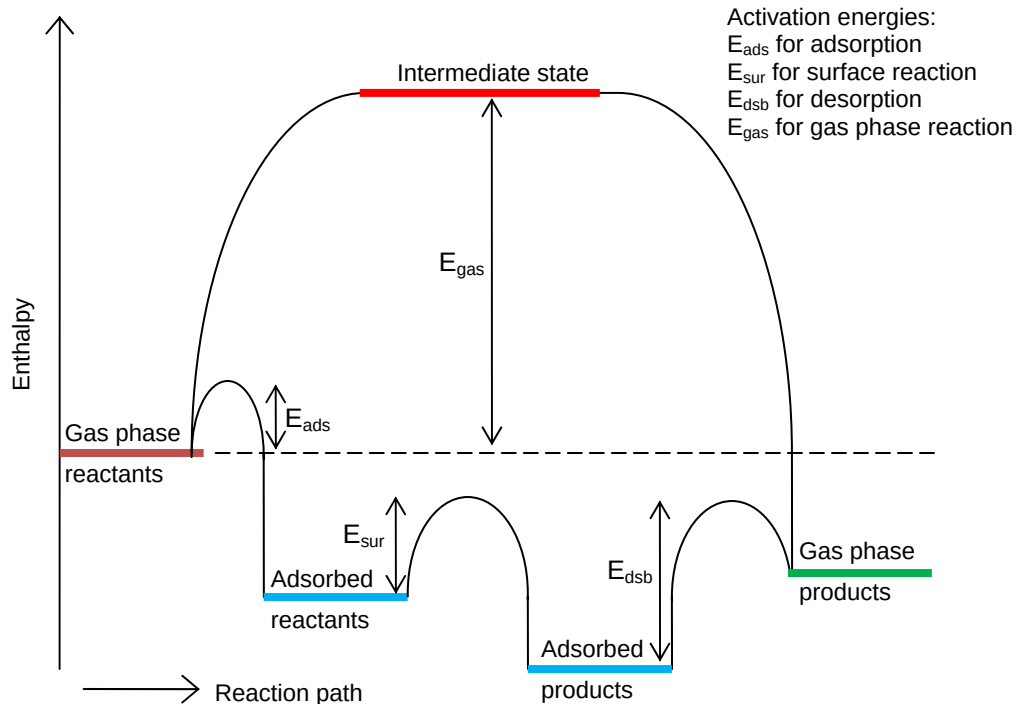

Fig. 2.3. Simplified energy profile of a heterogeneous catalytic reaction [18]

In general the catalytic oxidation of hydrocarbons follows the pattern depicted in Fig. 2.4. The oxidation is starting in region A where the initial reaction temperature depends on the properties of catalyst and hydrocarbon. A further increase in temperature (region B) results in an exponential increase in reaction rate to the point where heat generated by combustion is much greater that heat supplied. The reaction becomes mass transfer controlled (region C) after which further increases are limited by reactant availability (region D) [20]

A common parameter in catalytic oxidation is the light-off temperature. It refers to the temperature at which mass transfer control becomes rate limiting and conversion makes little difference such as in regions A-B and D. At the light-off temperatures, the heat generated by combustion is much greater than heat supplied. Usually the light-off temperature occurs as conversion reaches 10 %, 20 % or 90 %. Once light-off occurs, mass and heat transfer become important parameters.

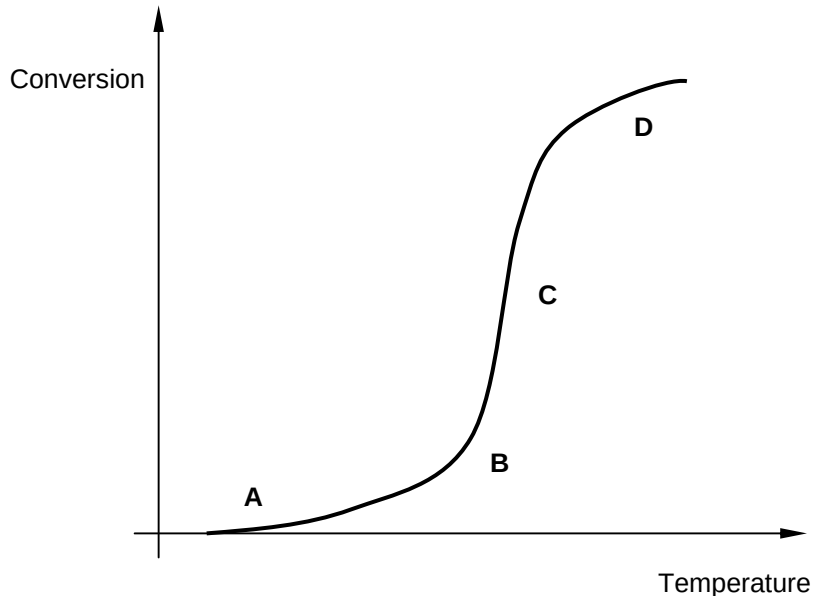

Fig. 2.4. Conversion versus temperature in catalytic combustion [20]

The geometry of the catalytic combustor and porosity of the catalyst/support have much more influence in this region. At region D, the reaction nearly reaches full-conversion where the heat generated from the combustion is raised significantly as well as increasing catalyst temperature. Therefore, the stability of the catalyst at higher reaction temperature is considered as important benchmarks for catalyst performance and durability investigations.

In calculating conversion, one of the reactants should be selected as the basis for calculation and then related with other species involved in the reaction. For instance, a general reaction is written as:

$$aA + bB \rightarrow cC + dD \quad (2.1.)$$

Then, the conversion of A (X_A) is defined as the number of moles of A that have reacted per mole of A fed to the system.

$$X_A = \frac{Moles\ of\ A\ reacted}{Moles\ of\ A\ fed} \quad (2.2)$$

In a continuous flow system, the conversion increases with increasing reactor volume. The additional time allows the reactants to flow completely through the reactor and thus, the more time for reaction to proceed. However, for catalytic plug flow reactor systems, the conversion increases with the increasing of the catalyst bed temperature and pressure (see Fig. 2.4).

The dependence of the reaction rate on the concentrations of the species present in reactant mixture is usually determined by experimental measurements. In general, the

form of this dependence is the power rate law model. Refer to a general reaction in equation (2.1), the rate law can be written as:

$$-r_A = k_A C_A^{\alpha} C_B^{\beta} \tag{2.3}$$

The exponents of the concentrations is referred as the order of reaction where α is order with respect to reactant A, and β order with respect to reactant B. The overall order of reaction is the sum of these two order of reaction (α + β). The units of $-r_A$ are expressed in term of concentration per unit time while the unit of k_A (specific reaction rate) is depending on the order of reaction.

For heterogeneous reactions over a solid catalyst, the rate can be defined as the rate of disappearance of reactant (in our case is methane) per mass of catalyst ($-r_A'$). The rate of reaction per unit weight of catalyst is related to the bulk density of the catalyst particles (ρ) and the rate of reaction per unit volume $(-r_A)$ which can be written as:

$$-r_A = \rho \times (-r_A') = \frac{moles}{time \cdot volume} = \left(\frac{mass}{volume}\right)\left(\frac{moles}{time \cdot mass}\right) \tag{2.4}$$

The specific rate of reaction is an important parameter to understand the process of catalytic combustion. Arrhenius suggested that the temperature dependence of the specific reaction rate (k_A) can be correlated as in the following equation:

$$k_A(T) = Ae^{-E/RT} \tag{2.5.}$$

Where, A is the pre-exponential factor (frequency factor); E is activation energy (J mol^{-1}), R is the gas constant (8.314 J mol^{-1} K^{-1}) and T is the absolute temperature (K). Postulation of this equation is the greatest achievement in chemical kinetics and remains useful until today. The activation energy (E) is determined experimentally by

performing the reaction at several different temperatures. After taking the natural logarithm of equation (2.5), the equation can be written as:

$$\ln k_A = \ln A - \frac{E}{R}\left(\frac{1}{T}\right) \tag{2.6}$$

By plotting ln k_A as a function of reaction temperature of (1/T) in a semi-log plot, the activation energy can be determined from the slope of the plot $\left(-\frac{E}{R}\right)$.

The main parameters for evaluation of a catalyst are the catalytic activity and selectivity. The activity of a catalyst is referred to the rate of reactant consumption, although the activity to a particular product can also be specified, whereas selectivity is the fraction of the total products which a particular substance represents [18]. To quantify the activity of a catalyst, we can use the turnover frequency (TOF) number. TOF is the number of molecules reacting per active site per unit of time. When using a supported catalyst (such as Pd or Pt deposited on Al_2O_3 catalysts), the noble metal atoms are considered as the active sites. This can be estimated based on the dispersion (D) measured from chemisorption analysis. Dispersion is the fraction of the active metal atoms deposited on the support material and available to catalyse a surface reaction.

2.4.2. Catalytic Combustion of Methane

The catalytic process of methane oxidation is well known and has been used since the end of the 20th century as a method of energy production from natural gas without emitting nitrogen oxides. In general the reaction process can be described by the equation:

$$CH_4 + 2O_2 \Rightarrow CO_2 + 2H_2O, \quad \Delta H_{289} = -802.7 \text{ kJ/mol [21]} \tag{2.7}$$

This combustion process can produce CO_2 and CO depending on the air fuel ratio. Oxygen enriched reaction results in the formation of CO_2 as the only carbonaceous product while partial oxidation will produce carbon monoxide. The reactions can be described as follows:

$$CH_4 + 2O_2 \Rightarrow CO_2 + 2\,H_2O \quad (2.8)$$

$$CH_4 + \tfrac{3}{2}\,O_2 \Rightarrow CO + 2\,H_2O \quad (2.9)$$

Catalysts are able to replace flame combustion and oxidize lean methane mixtures, even when the concentration of methane is less than 5 %. Catalytic combustion enables the utilization of pure methane and low-concentration gases, which can be used as an environmentally friendly source of energy that contributes to a complete management of methane in mines [4]. Although methane oxidation will produce carbon dioxide which is another greenhouse gas, this gas (i) has a reduced GHG potential and (ii) may be absorbed whereas the alkanes cannot.

A possible mechanistic pathway of methane oxidation over noble metals has been outlined by Oh and co-workers [22] as shown in Fig. 2.5. Since the O_2 adsorption occurs at a faster rate than methane adsorption, the surface of the catalyst is initially fully occupied by oxygen and then chemisorption of CH_4 on the surface of catalyst takes place. The chemisorption of methane onto noble metals then cleaves the hydrogen atoms from CH_4 and produces methyl or methylene radicals. The adsorbed atoms subsequently react with adsorbed oxygen to produce carbon dioxide and H_2O in direct oxidation or chemisorbed formaldehyde. This chemisorbed formaldehyde is either desorbed as HCHO or decomposed as adsorbed CO and adsorbed H atoms. Subsequently, adsorbed CO and H atoms are either desorbed as CO and H_2 or reacted

with adsorbed O_2 to produce CO_2 and H_2O, depending on the composition of the reactant mixture.

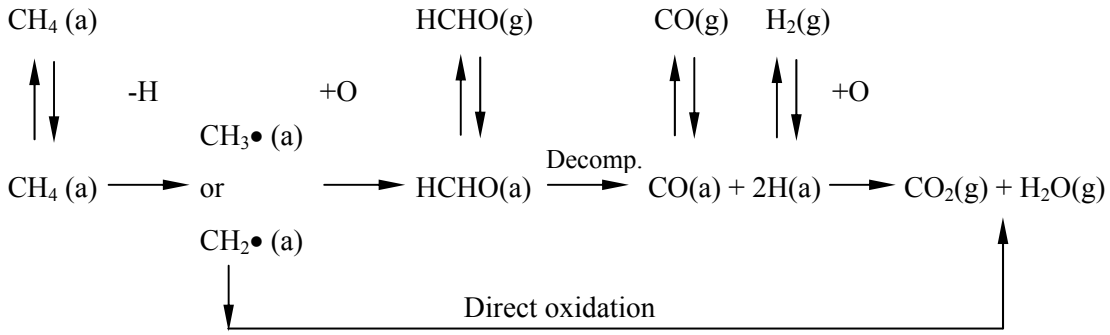

Fig. 2.5. A possible mechanism for catalytic oxidation of methane, (a) adsorbed, (g) gas phase [22]

2.5. Progress in catalyst development for methane combustion

Methane is included in the group of hydrocarbons which are very challenging to oxidize using catalysts. Developments in catalytic oxidation were initiated with an overarching aim of reducing hydrocarbons emissions from internal combustion engines. It was reported that reasonable activity can be achieved at temperatures below 400 °C [23-25]. Catalytic oxidation techniques were established as a potential strategy for producing energy in gas turbine combustors, as well as reducing emissions. For these applications, noble metal catalysts such as Pt or Pd on an Al_2O_3 support were reported to be the most attractive catalysts [26]. A number of investigations were devoted to designing a catalytic material which is operable at high temperatures for long periods of time, and in humid and oxygen-rich conditions. Low reaction temperatures would be a distinct advantage in VAM application because: (1) the production of NOx gases can be minimised (essentially zero), (2) a self-sustaining system of methane mitigation and

utilization can be designed based on the catalyst activity. It is expected that a self-sustaining system is feasible at reaction temperatures of 200 °C because thermodynamically, the adiabatic temperature rise of complete-methane oxidation is (very approximately) 23 K per 0.1 % of methane in air (see our COSILAB calculation result in Appendix A). Therefore, most of the recent studies are focussed on developing a low temperature methane oxidation catalyst.

Recent developments in catalytic materials for methane oxidation enable operation at approximately 100 % conversion of CH_4 to CO_2 at reaction temperatures of 320-400 °C depending on the system and catalyst characteristics. Currently, palladium supported on alumina catalyst is identified as the most active catalyst for total methane oxidation [20, 27]. Supported gold catalysts have also been shown as active materials where significant conversions were observed at the temperature as low as 350 °C in catalytic oxidation of lean methane mixtures [28-30]. Single metal oxide catalysts (such as Co_3O_4, Mn_2O_3 etc.) are also reported, mainly because of low cost and higher resistance to deactivation [31].

2.5.1. Palladium-based catalysts

Supported palladium catalysts are widely used in many catalytic combustion and converter systems. The mechanism of methane oxidation over Pd-based catalyst is complex. A number of papers have focussed on understanding the oxidation behaviour and catalytic properties of supported Pd catalysts, examining aspects as diverse as role of feed ratio, particle size and dispersion, pre-treatment effects, poisoning effect of water, chlorine and sulphur poisoning and deactivation. [20, 32-40]. Progress on

development and investigation of palladium catalysts will be reviewed in this section. The specific issues related to VAM application such as water inhibition and catalyst deactivation are explored and discussed in detail.

Earlier works on palladium-based catalysts were focussed on establishing the influence of O_2/CH_4 ratio during catalytic combustion of air-methane-mixtures, in order to understand the mechanism of methane oxidation. When methane is oxidised under oxygen-rich conditions over Pd-based catalyst, carbon dioxide is the only carbonaceous compound found in the outlet gas mixture [41, 42]. On the other hand, under oxygen-deficient oxidation, the formation of carbon monoxide was detected where the selectivity of CO has strong correlation with the reaction temperature. Under these conditions, the production of CO_2 and H_2O increases with increasing temperature until the oxygen is totally consumed, where the formation of carbon monoxide is observed thereafter [42]. At higher temperature the selectivity to CO is enhanced and lower feed ratio ($[O_2]/[CH_4]$) CO dominant to CO_2 at the outlet. Moreover, the characteristics of methane oxidation were investigated in the presence or absence of CO in the feed [22]. It was reported that under both O_2-rich and O_2-deficient conditions, the characteristics of methane conversion with CO-free feed were similar to those observed with the feed containing CO, suggesting the presence of carbon monoxide in the feed does not affect the characteristics of methane oxidation. Similarly, adding carbon dioxide into the feed stream have been shown no significant effect on the activity [43], which is important for the VAM application.

The influence of H_2, He and O_2 used for catalyst activation procedure were investigated for palladium supported on metal oxides catalysts [24, 44]. It is generally agreed that

catalyst pre-treatment plays an important role in controlling the activity and durability of catalysts. Earlier studies reported that pre-treatment under hydrogen increased the activity of catalysts whereas O_2 pre-treatment decreased the activity [24, 45]. Subsequent investigations also found that reduced Pd was an important active site for the catalytic combustion reaction [44, 46, 47]. However, others reported that reactant mixtures were also used as pre-treatment gases [26, 42, 48, 49] where catalyst activation under reactant mixtures (O_2-CH_4-carrier gas) leads to catalysts being more active than those pre-treat with hydrogen [50, 51]. It was suggested that the mechanism of catalyst activation on initial exposure to reaction condition can possibly be: (a) poisoning the active site by the substances left in catalyst from its precursor (primarily chlorine) [24, 46, 50]; (b) transformation from an initially amorphous PdO state to a crystalline state [26, 52, 53] and (c) interactions with the support phase, especially at low Pd coverage [33].

Under oxygen-rich conditions, for palladium catalysts, it is suggested that PdO is formed and this phase represents the active phase for methane oxidation [27]. Prior investigations have clearly shown the importance of PdO for methane combustion [54-57]. It was suggested that the transformation of PdO ↔ Pd is reversible in presence of oxygen [58, 59] and metallic Pd is less active than PdO. The reactivity of oxygen chemisorbed on Pd metal and oxide ions for Pd/Al_2O_3 catalysts was compared by Burch and Urbano [55]. The catalyst was prepared by impregnating alumina with palladium nitrate and submitted to oxidation and reduction treatments at 500 °C before measuring the catalytic activities. Catalytic steady-state and pulse experiments suggested that metallic Pd is not active while the pre-oxidized sample is active. However, the time on stream experiment at 300 °C over the pre-reduced sample revealed that the oxidation

begin with a very fast formation of a monolayer of oxygen followed by a slower oxidation step leading to almost complete oxidation of palladium. It was found also that fully oxidised bulk PdO is the optimum state of the active site for methane oxidation and the intermediate state corresponding to a layer of PdO on a Pd metal core has no greater activity compared to the bulk PdO [57, 60].

The presence of both PdO and Pd metal on the catalysts under reaction conditions was reported in the literature [53, 61]. Lyubovsky and Pfefferle initially found that Pd metallic surface is formed after pre-treatment at temperatures > 800 °C followed by transformation into a highly dispersed PdO clusters during cooling cycle leading to increase in conversion with decreasing temperature [61]. On the other hand, an investigation by Datye and co-workers proposed that the PdO → Pd transformation is initiated at the surface upon heating and causes small domains of Pd metal to form on the surface of PdO [53]. Upon cooling step, these small domains are re-oxidised easily which is not the case when complete transformation into Pd metal (at T > 925 °C) is achieved. It was suggested that complete oxidation of the Pd metal can possibly results in the formation of polycrystalline PdO with a roughening of the particle surfaces. Re-activation of the Pd metal catalysts upon cooling could be associated to two possible mechanisms: (i) PdO re-formation (increase in the fraction of Pd metal particles fully re-oxidised into bulk PdO) or (ii) a reaction mechanism which involves metallic Pd.

Palladium supported on ceria-zirconium oxide catalysts have been prepared by Ciuparu and Pfefferle in order to investigate the influence of the oxygen content in supported Pd/PdO particles on the activity in methane oxidation [62]. The amount of metallic Pd was varied by controlled chemical reduction with methane. It was observed that catalyst

activity initially increases with the degree of reduction, reaching a maximum and then decreasing continuously as the oxygen is depleted. This indicates that slight reduction results in more improvement in the catalytic activity compared to either fully oxidised or fully reduced metallic particles. Moreover, the partially reduced sample was found to be easier to re-oxidise than the completely reduced one.

More recent investigation suggested that the surface structure of the Pd-based catalysts changes with time-on-stream under fuel-rich conditions [63]. For this investigation, 5 wt% Pd/Al_2O_3 were used and tested under oxidation–reduction cycles (pulse reactor studies). The results showed that the initial methane combustion activity of the oxidized catalyst (PdO/Al_2O_3) is much higher than that of the reduced form (Pd^0/Al_2O_3). The methane combustion activity of the partially reduced and oxidized catalysts is strongly influenced by the degree of PdO reduction and Pd oxidation, respectively; it decreases with increasing Pd^0 content but increases with increasing PdO content. It was suggested that along with the relative concentration of PdO, the PdO formation pathway is also critical in deciding the methane combustion activity of the catalyst. Overall, there are still uncertainties regarding the relationship between pre-treatment history and the activity of catalyst. The clear question that arises from these investigations is how to optimise the catalytic activity and what kinds of gases are suitable for a particular catalyst and its support. It is of great importance that this matter is addressed further in order to improve the behaviour in the reactor and understand the process.

Several kinetic studies of methane combustion over supported Pd catalysts were reported in the literature [24, 51, 64-67]. Under oxidising or stoichiometric conditions, the order of reaction over Pd/Al_2O_3 catalysts is first order with respect to methane and

almost zero with respect to oxygen concentration. While CO_2 was suggested to have no effect on reaction rate, a strong inhibition was observed upon adding H_2O into the feed where the order with respect to H_2O was reported in the range of -0.6 to -1.0 [66-68]. Under dry feed conditions, apparent activation energies were ranging between 70 and 90 kJ mol^{-1}[51, 66, 67]. The activation energy increased to 151 ± 15 kJ mol^{-1} when adding 2 vol% H_2O to the feed [66]. It seems that kinetic data under humid conditions is still insufficient to understand the inhibition effect of water. It can be suspected that varying the concentration of water in the feed and modification of support material will have some influences on the nature of active site.

Possible effects of fouling by carbon (or coke) on the activity of supported metal catalysts are increasing since the temperature reaction of VAM combustion is targeting low temperature processes. Deactivation of supported metal catalysts by coke may occur chemically due to chemisorption or carbide formation. It may also occur physically due to blocking of surface sites, metal crystallite encapsulation, plugging of pores and destruction of catalyst pellets by carbon whiskers [69]. While coking of transition metal catalysts was reported during the combustion of methane at higher concentrations [70, 71] and reaction temperatures [71], carbon deposition on palladium catalyst under lean methane conditions at low temperatures has not been addressed yet. Furthermore, recent investigation showed that methane can be activated over Pd catalysts at temperatures as low as 180 °C [63]. The presence of coke on Pd catalysts at this temperature could have important consequences on catalytic activity and this requires more detail investigation.

Although it is well recognized that water strongly inhibits the activity of catalysts, the mechanism of catalyst deactivation is still uncertain [72]. Some earlier studies reported that the water produced by reaction significantly inhibits the activity of Pd/Al_2O_3 at lower temperatures due to competition with methane for active sites [43, 67, 73]. Furthermore, an irreversible deactivation can possibly be induced by the presence of water where the active site (PdO) transforms into a less active site (palladium hydroxide) [43, 67, 73, 74]. The rate of Pd/Al_2O_3 catalyst deactivation in the presence of water, either present in the feed (such as the case in VAM) or produced in the reaction, is heavily dependent on reaction temperature [43, 74]. The inhibiting effect of water is more significant at lower temperatures and becomes less apparent at temperatures higher than 450 °C [43]. Ciuparu et al suggested that the hydroxyl groups produced by reaction are bound strongly on the surface and when the external water is introduced the surface becomes saturated and the rate of desorption of water from the surface of the catalyst is inhibited due to the high concentration of water vapour in the feed and product stream [68]. Recent work by Schwartz et al. proposes an alternative explanation regarding deactivation of palladium supported on various metal oxides [72, 75]. Hydroxyl groups formed during the reaction accumulate on the catalyst support and inhibit the rate of exchange of oxygen between the support and PdO, [75] which is necessary for surface reaction. This accumulation of hydroxyl groups prevents the migration of oxygen from the support to the Pd active site, as well as reducing the availability of oxygen involved in the oxidation of methane [72]. Clearly the primary mechanisms leading to deactivation is still contentious as the hydroxyls form on both the Pd site and the support in high concentrations [72] and deactivation can potentially originate from surface on either the support or palladium.

Recently, Di Carlo and co-workers reported an improved tolerance against water poisoning in catalytic combustion of methane over palladium catalysts by using a support which inhibited or delayed the reaction between Pd and H_2O [76], however no long-term stability test results were reported. The application of a catalytic process for VAM abatement requires long-term evaluation of the catalyst stability and durability under humid feed condition. An extended period of time of hydrocarbon oxidation activity was reported by Yamamoto and Uchida reported over Pt and Pd supported on alumina for lean-burn natural gas engine exhausts [77] where the total hydrocarbon conversion dropped from 80 % to 50 % within 2,500 h at 385 °C. More recent investigation by Liu et al. [78] reported that during 3,200 h methane combustion experiment at 600 °C, Pd supported on Ni-modified alumina catalyst demonstrated a stability improvement. It was suggested that the stability of Pd/NiO-Al_2O_3 catalyst was improved by optimizing the Ni/Al ratio. Nevertheless, the catalyst stability tests at reaction temperatures less than 600 °C or the effect of CO_2 in the feed for long term catalyst stability tests have not been reported yet. In addition, to our knowledge there is no literature reporting on the effect of coal mine dust on the catalytic combustion of ventilation air methane.

The effect of Pd particle size on catalytic activity is still unclear, while most of the research groups have reported that methane combustion is a structure sensitive reaction, there have been some contradictory suggestions [79]. The effect of palladium particle size on catalytic activity were investigated to confirm the structure sensitivity of Pd during CH_4 oxidation [50]. A more detailed study was carried-out by Baldwin and Burch where palladium was dispersed on Al_2O_3 support within average diameter of 2-74 nm. Pd dispersion was obtained by varying the calcination temperature and tested

under continuous-flow conditions of 1 vol. % CH_4 in air [26]. Unfortunately, the relationship between palladium particle size and reaction rate of methane oxidation was not clearly explained. Meanwhile, Burch and Loader reported that there was no evidence of a particle size affecting the catalytic behaviour of Pd and Pt catalysts [80]. This idea was supported by Ribeiro *et al.* who prepared Pd catalysts supported on Al_2O_3, ZrO_2 and Si-Al_2O_3 and calculated the turnover rate on the basis of Pd dispersion measured after reaction. It was concluded that the reaction was not structure-sensitive, however, some variation of the activity with the particle size was considered. A recent work on Pd load and dispersion on catalytic activity in methane combustion and on redox behaviour of palladium supported on alumina catalysts suggested that the catalyst with lower Pd load and higher metal dispersion exhibits a lower specific catalytic activity [38]. Therefore, more detailed investigation is needed to clearly address the relationship between the catalytic activity and the particle size, especially for the catalysts which have been operated under extremely humid conditions.

Despite considerable effort, the mechanism of catalyst deactivation is not fully understood [72]. Deactivation can occur through chemical, mechanical and thermal processes [69]. Thermal deactivation processes include the loss of active-site surface area as a result of particle aggregation and collapse of the support pore structure through re-crystallization. Chemical transformation can also result in the loss of active metal sites [69]. Pd/Al_2O_3 catalyst activity can be affected by both thermal and chemical transformations [81].

These deactivation processes can be accelerated under high-temperature hydrothermal ageing. A study of hydrothermal ageing on methane combustion over Ce-promoted

PdO/ZrO_2 catalysts highlighted the impact that ageing temperature plays on catalyst deactivation [82]. Hydro-thermal treatments for two weeks on various supported Pd catalysts at 900 °C under simulated domestic boiler exhaust gas were performed to understand the ageing mechanism in natural gas combustion [83]. Deactivation studies were reported recently for natural-gas vehicle catalysts [84] and diesel oxidation catalysts [85] where significant changes in morphology and chemical poisoning were observed. A very recent article reported that support phase transformation and particle sintering were found after thermal (at 900 °C in air) and stoichiometric (at 900°C, air-fuel equivalent ratio = 1) ageing over $Pd/YFeO_3$ three-way-catalyst [86]. However, the effects caused by thermal ageing and chemical poisoning are still inconclusive, and, in particular, the ageing process under simulated VAM gas has not been considered.

2.5.2. Supported gold catalysts

Investigations focussed on low temperature catalytic oxidation over gold catalysts were pioneered by Haruta et al.[87]. They used gold supported on transition metal oxides to oxidise carbon monoxide. It was reported that this type of catalyst has been used successfully for CO oxidation at temperatures as low as -70 °C. Gold catalysts were reported to be more active in carbon monoxide oxidation compared to traditional platinum or palladium supported catalysts. The earlier studies also found that the catalysts for CO oxidation can be used to promote methane oxidation by using transition metal oxides as supports.

An earlier investigation by Waters and co-workers [88] studied the methane combustion over transition metal oxide supported gold catalysts prepared by co-precipitation. A

micro-reactor was used to observe the trend in activities of Au/Co_3O_4, Au/NiO, Au/MnO_x, Au/Fe_2O_3, and Au/CeO. They have found that the best catalytic performance was obtained with Co_3O_4 as the support which is active in the range of 200-250 °C.

Gold catalysts on metal oxide supports were prepared by Solsona et al. [29] and tested for the total oxidation of methane, ethane and propane. The catalyst was made by several methods including co-precipitation, deposition-precipitation and impregnation. The catalysts were tested at atmospheric pressure in a fixed-bed stainless steel tubular flow reactor and analysed by online gas chromatography. They found that Au/CoOx prepared by co-precipitation method was the most active catalyst which can complete oxidation of methane at 350°C. Based on their activity, the order of catalysts was: $Au/CoO_x > Au/MnO_x > Au/CuO > Au/Fe_2O_3 > Au/CeO_2 > Au/TiO_2$. This order has the same reactivity as observed for the supports. The behavioural observations on Au-free and Au-containing catalysts indicated that Au gave a positive influence on catalyst performance, except for TiO_2. However, there is no clear explanation has been proposed on the role of gold in activating methane combustion process and correlation between the redox properties of the catalysts and catalytic activity.

Gold catalysts supported on iron oxide were prepared recently by Choudhary et al. for methane oxidation experiment using different preparation methods: deposition-precipitation (DP) and homogenous deposition precipitation (HDP). Gold with different loadings was deposited on various supports such as Fe_2O_3, MnO_2, CoO_x, CeO_2, Ga_2O_3, Al_2O_3 and TiO_2. Prior to the activity measurement, each sample was heated in nitrogen at 600 °C for 1 h and then 1 vol. % CH_4 in air was continuously passed through the catalyst at the flow rate of 100 ml min^{-1} [30]. It was reported that the Au/Fe_2O_3 prepared

by HDP showed higher activity compared to those prepared by DP. The transmission electron microscopy images show that an HPD method leads to catalysts with much higher Au loading and smaller Au particle size. Under different space velocities, the performance of Au/Fe_2O_3 (HDP) was also evaluated. An increase of the gas hourly space velocity from 10,000 to 100,000 h^{-1} increased the ignition temperature (for 10 % CH_4 conversion) from ca. 200 °C to 350 °C. At 500 °C (100 % conversion) the time-on-stream activity of Au/Fe_2O_3 (HDP) catalyst was observed during 50 hours. The catalytic activity was slightly decreased to 80 % conversion but then remained constant until 50 h oxidation. Unfortunately, there is no explanation why this catalyst is stable once the conversion reaches 80 %. In addition, during experiments there were three gold species detected: Au^0, Au^{1+} and Au^{3+}, but none of these are claimed as an active phase of gold.

The effect of support on the catalytic performance of Au/Co_3O_4-CeO_2 catalysts for methane oxidation was reported by Liotta and co-workers [89]. They prepared gold-based catalysts supported on Co_3O_4, CeO_2, and mixed Co_3O_4-CeO_2 using co-precipitation method. Prior to catalytic activity measurement, the catalysts was treated with a mixture of 5 vol. % of O_2 balanced with helium at 350°C for 30 minutes and purged with helium during cooling down to room temperature. The methane oxidation experiment results show that Au/Co_3O_4 is the most active catalyst, followed by Au/Co_3O_4-CeO_2 and then by Au/CeO_2 catalyst [89]. It was suggested that the better performance of cobalt containing support is due the presence of Co^{2+} and Co^{3+} ions, being active sites for oxygen and methane activation, respectively. On the basis of the increased reducibility of the oxides, gold is acting as the promoter for the oxygen mobility.

Nano-size AuOx/$Ce_{0.6}Zr_{0.3}Y_{0.1}O_2$ (AuOx/CZY) catalysts were successfully produced by adopting the cetyltrimethyl ammonium bromide (CTAB)-assisted hydrothermal treatment method [90]. The Au weight percentage (y) was varied by using a novel in-situ reduction method. The characterization result confirmed that the CZY and gold were nano-sized particles where the diameter is in the range of 5-50 nm and 2-20 nm, respectively. Among the catalysts investigated in this work, the 0.2 % AuOx/CZY catalyst appeared most active for methane oxidation where 100 % conversion was achieved at ca. 640 °C. It was concluded that the catalytic performance of the CZY-supported gold catalyst is dependent to the AuOx dispersion, Au^{3+}/Au^0 molar ratio, Au and CZY particle sizes and catalyst reducibility. On the other hand, the activity of catalyst is far too low compared to what has been reported by previous authors.

Bimetallic Au-Pt and Au-Pd supported on cobalt oxide catalysts were investigated by Miao and Deng under reactant mixture of 1 vol% CH_4 and 5 vol% O_2 in N_2 [28]. The Au-Pt/Co_3O_4 and Au-Pd/Co_3O_4 catalysts at different Au, Pt and Pd loading were prepared by co-precipitation method in order to find a better Au-containing catalyst for low oxidation temperature of methane. All samples were calcined in air at 500 °C for 5 h and then reduced in hydrogen at 400 °C for 3 h. The result showed that Au-Pt/Co_3O_4 was the highest Au-containing catalyst activity where 100 % conversion was achieved at 360°C. Unfortunately, the detailed mechanism on the interaction between Au, Pt and support was not described in this report. The role of gold in promoting the methane oxidation reaction has not been addressed. It seems that the development of supported gold catalysts is still in the early stage. To improve the activity and stability of this type of catalyst, a number of investigations are required to address some issues such as the

active site of gold, the role of gold and its interactions with support material and the effect of water.

2.5.3. Single metal oxide catalysts

Transition metal oxides have been considered as catalysts for total oxidation of methane due to their higher stability and lower cost when compared to noble metals [79]. Earlier work reported the use of single-metal oxides (such as Cr_2O_3, NiO, Mn_2O_3, Co_3O_4, and CuO) and these studies evaluated the activities and deactivation phenomena during lean methane combustion [31]. Among those tested, Co_3O_4 was the most active catalyst but was less stable compared to Mn_2O_3. Preparing different morphologies of cobalt oxide was demonstrated recently as a strategy for improving the catalytic activity [91]. Enhanced activity and stability was reported for Co_3O_4 nanotube prepared using a morphology-directed technique [92]. The higher activity observed from these nanotubes catalysts was reported to be due to the prominence and exposure of the (112) crystal plane and high reactivity of the surface oxygen. However, the issue of catalyst stability in the presence of water vapour in the feed has not been addressed yet.

The performances of Co_3O_4 and Co_3O_4-MOx binary oxides have recently been evaluated and correlated with the synthesis methods, morphological and structural properties [93]. The advances in the synthesis strategies and the characteristics of cobalt oxide catalysts enlighten potential application for this type of catalyst in various catalytic processes. It is highlighted that the information about relationship between reactive planes/redox properties and catalytic activity of Co_3O_4 in methane oxidation are still limited. Current investigations suggest that the activity of Co_3O_4 is related to either

the reactive {112}/{110} planes or the surface oxygen species, bulk oxygen mobility, re-oxidation of cobalt species, and active oxygen vacancies of nano-sized Co_3O_4 with controlled size. A better understanding of this issue need more investigations to be performed under different reaction conditions. Particularly for lean methane oxidation under extremely humid condition, the rate limiting step and catalyst deactivation are not fully addressed.

2.6. Summary

Supported palladium catalysts are the most active materials and widely used for catalytic combustion of lean methane mixtures. It is commonly agreed that PdO is the active phase. However, its sensitivity to water vapour presents in the VAM is a major disadvantage to its use as efficient catalyst for methane emissions abatement from coal mine ventilation systems. A number of fundamental studies have been reported and have contributed to improving the understanding the reaction pathways and catalyst deactivation phenomena. However, there are remaining significant uncertainties and obstacles to explain the influence of parameters such as the pre-treatment history, palladium particle size and the presence of contaminants on the catalytic behaviour of Pd catalysts. Particularly for VAM application, there are many important practical aspects in which further detail investigation such as catalyst deactivation phenomena, the stability of catalyst under extremely humid conditions, the effect of coal dust on catalytic activity and stability.

Attempts to improve the catalytic activity of Pd catalysts in methane combustion have not yet been achieved. The intrinsic activity of PdO for the reaction could potentially be

increased by increasing the degree of dispersion of PdO. However, improving the catalytic activity of Pd catalysts is not necessarily the key issue with respect to the use of these catalysts, compared to the effect of water vapour. It is highly desirable for the current study to develop strategies for improving the catalysts resistance to water vapour rather than only improving catalytic activity. The literature suggests that the mechanism of water vapour inhibition of Pd-based catalysts remains uncertain.

Although supported gold catalysts are not as active as palladium-based catalysts, an understanding on the nature of nano-sized gold can further the understanding of the deactivation process and in turn how to enhance the catalyst activity and stability. Limited data regarding the characteristics and catalytic activity of supported gold catalyst specifically for combustion of lean methane-air mixtures is available. The role of gold and the interaction between methane and gold are still uncertain. Methane combustion in the presence of water over gold-based catalysts has not yet been investigated in detail.

Another route for preparing efficient catalysts for VAM combustion could be improving the catalytic activity of transition metal oxide catalysts. Nano-sized cobalt oxide catalysts have drawn much attention due to its lower cost and higher stability compared to noble metal catalysts. Enhanced activity and stability reported in the literature over nano-sized cobalt oxide catalysts offers a good prospect for VAM combustion. In order to meet the requirements of the VAM application, it appears essential that more studies should focus on the influence of water and coal dust particles on the catalytic activity in order to evaluate the limitations of the catalyst.

References

1. Solomon, S., D. Qin, M. Manning, R.B. Alley, T. Berntsen, N.L. Bindoff, Z. Chen, A. Chidthaisong, J.M. Gregory, G.C. Hegerl, M. Heimann, B. Hewitson, B.J. Hoskins, F. Joos, J. Jouzel, V. Kattsov, U. Lohmann, T. Matsuno, M. Molina, N. Nicholls, J. Overpeck, G. Raga, V. Ramaswamy, J. Ren, M. Rusticucci, R. Somerville, T.F. Stocker, P. Whetton, R.A. Wood, and D. Wratt, *Technical summary*, in *Climate change 2007: the physical science basis. contribution of working group I to the fourth assessment report of the intergovernmental panel on climate change*, S. Solomon, et al., Editors. 2007: Cambridge, United Kingdom and New York, NY, USA p. 996.
2. Schultz, H.L., P. Carothers, R. Watts, and R. McGuckin, *Assessment of the worldwide market potential for oxidising coal mine ventilation air methane*. 2003, United States Environmental Protection Agency, Air and Radiation (US-EPA)
3. Su, S., H. Chen, P. Teakle, and S. Xue, *Characteristics of coal mine ventilation air flows.* Journal of Environmental Management, 2008. 86: p. 44 - 62.
4. Stasinska, B. and A. Machocki, *Catalysts for the utilization of methane from the coal mine ventilation air.* Polish Journal of Chemical Technology, 2007. 9(3): p. 29 - 32.
5. Su, S., A. Beath, H. Guo, and C. Mallett, *An assessment of mine methane mitigation and utilisation technologies.* Progress in Energy and Combustion Science, 2005. 31(2): p. 123-170.
6. Karakurt, I., G. Aydin, and K. Aydiner, *Mine ventilation air methane as a sustainable energy source.* Renewable and Sustainable Energy Reviews, 2011. 15(2): p. 1042-1049.
7. Baris, K., *Assessing ventilation air methane (VAM) mitigation and utilization opportunities: A case study at Kozlu Mine, Turkey.* Energy for Sustainable Development, 2013. 17(1): p. 13-23.
8. Carothers, P. and M. Deo, *Technical and economic assessment: mitigation of methane emissions from coal mine ventilation air*, in *Coalbed Methane*

Outreach Program. 2000, Climate Protection Division, U.S. Environmental Protection Agency.

9. Su, S. and J. Agnew, *Catalytic combustion of coal mine ventilation air methane.* FUEL, 2006. 85: p. 1201-1210.

10. Cobb, J.T., *Coal desulfurization in a rotary kiln combustor*. 1992, Pittsburgh, Pa. BCR National Laboratory, Pennsylvania Energy Development Authority.

11. Mallett, C.W. and S. Su, *Investigation into waste coal handling facilities*, in *Exploration and Mining Report*. 2003, CSIRO Brisbane.

12. Salomons, S., R.E. Hayes, M. Poirier, and H. Sapoundjiev, *Flow reversal reactor for the catalytic combustion of lean methane mixtures.* Catalysis Today, 2003. 83: p. 59-69.

13. Hevia, M.A.G., S. Ordonez, and F.V. Diez, *Effect of the catalyst properties on the performance of a reverse flow reactor for methane combustion in lean mixtures.* Chemical Engineering Journal, 2007. 129: p. 1-10.

14. Wang, Y., C. Man, and D. Che, *Catalytic combustion of ventilation air methane in a reverse-flow reactor.* Energy & Fuels, 2010. 24(9): p. 4841-4848.

15. Kushwaha, A., M. Poirier, R.E. Hayes, and H. Sapoundjiev, *Heat extraction from a flow reversal reactor in lean methane combustion.* Institution of Chemical Engineers, Chemical Engineering Research and Design, 2005. 83(A2): p. 205-213.

16. Gosiewski, K., Y.S. Matros, K. Warmuzinski, and M. Jaschik, *Homogeneous vs. catalytic combustion of lean methane-air mixtures in reverse-flow reactors.* Chemical Engineering Science, 2008. 63: p. 5010 - 5019.

17. Kulkarni, M.R. and C.R. Sardesai, *Enrichment of methane concentration via separation of gases using vortex tubes.* Journal of Energy Engineering, 2002. 128(1): p. 1-12.

18. Bowker, M., *The basis and application of heterogeneous catalysis*. Oxford Chemistry Primers, ed. R.G. Compton. 1998, New York: Oxford University Press.

19. Fogler, H.S., *Elements of chemical reaction engineering*. 4th ed. 2008, Massachusettes: Pearson Education.

20. Lee, J.H. and D.L. Trimm, *Catalytic combustion of methane.* Fuel Processing Technology, 1995. 42: p. 339-359.

21. Semenov, N.N., *Some problems of chemical kinetics and reactivity*. Vol. 1. 1958, London: Pergamon Press.

22. Oh, S.H., P.J. Mitchell, and R.M. Siewert, *Methane oxidation over noble metal catalysts as related to controlling natural gas vehicle exhaust emissions.* ACS Symposium Series, 1992. 495: p. 12-25.

23. Mezaki, R., and C.C. Watson, *Catalytic oxidation of methane.* Industrial & Engineering Chemistry Process Design and Development, 1966. 5.

24. Cullis, C.F. and B.M. Willatt, *Oxidation of methane over supported precious metal catalysts.* Journal of Catalysis, 1983. 83: p. 267-285.

25. Trimm, D.L., *Catalytic combustion (review).* Applied Catalysis, 1983. 7(3): p. 249-282.

26. Baldwin, T.R. and R. Burch, *Catalytic combustion of methane over supported palladium catalysts. II. Support and possible morphological effects.* Applied Catalysis, 1990. 66: p. 359-381.

27. Gelin, P. and M. Primet, *Complete oxidation of methane at low temperature over noble metal based catalysts: a review.* Applied Catalysis B: Environmental, 2002. 39: p. 1-37.

28. Miao, S. and Y. Deng, *Au-Pt/Co_3O_4 catalyst for methane combustion.* Applied Catalysis B: Environmental, 2011. 31: p. L1-L2.

29. Solsona, B.E., T. Garcia, C. Jones, S.H. Taylor, A.F. Carley, and G.J. Hutchings, *Supported gold catalysts for the total oxidation of alkanes and carbon monoxide.* Applied Catalysis A: General, 2006. 312: p. 67-76.

30. Choudhary, V.R., V.P. Patil, P. Jana, and B.S. Uphade, *Nano-gold supported on Fe_2O_3: A highly active catalyst for low temperature oxidative destruction of methane green house gas from exhaust/waste gases.* Applied Catalysis A: General, 2008. 350: p. 186-190.

31. Paredes, J.R., E. Diaz, F.V. Diez, and S. Ordonez, *Combustion of methane in lean mixtures over bulk transition-metal oxides: evaluation of the activity and self-deactivation.* Energy & Fuels, 2009. 23(1): p. 86-93.

32. Lampert, J.K., M.S. Kazi, and R.J. Farrauto, *Palladium catalyst performance for methane emissions abatement from lean burn natural gas vehicles.* Applied Catalysis B: Environmental, 1997. 14(3-4): p. 211-223.

33. Ciuparu, D., M.R. Lyubovsky, E. Altman, L.D. Pfefferle, and A. Datye, *Catalytic combustion of methane over palladium-based catalysts.* Catalysis Reviews, 2002. 44(4): p. 593-649.

34. Janbey, A., W. Clark, E. Noordally, S. Grimes, and S. Tahir, *Noble metal catalysts for methane removal.* Chemosphere, 2003. 52: p. 1041-1046.

35. Roth, D., P. Gelin, A. Kaddouri, E. Garbowski, M. Primet, and E. Tena, *Oxidation behaviour and catalytic properties of Pd/Al_2O_3 catalysts in the total oxidation of methane.* Catalysis Today, 2006. 112: p. 134-138.

36. Lapisardi, G., L. Urfels, P. Gelin, M. Primet, A. Kaddouri, E. Garbowski, S. Toppi, and E. Tena, *Superior catalytic behaviour of Pt-doped Pd catalysts in the complete oxidation of methane at low temperature.* Catalysis Today, 2006. 117: p. 564-568.

37. Escandón, L.S., S. Ordóñez, A. Vega, and F.V. Díez, *Sulphur poisoning of palladium catalysts used for methane combustion: effect of the support.* Journal of Hazardous Materials, 2008. 153(1-2): p. 742-750.

38. Castellazzi, P., G. Groppi, P. Forzatti, A. Baylet, P. Marecot, and D. Duprez, *Role of Pd loading and dispersion on redox behaviour and CH_4 combustion activity of Al_2O_3 supported catalysts.* Catalysis Today, 2010. 155: p. 18-26.

39. Colussi, S., A. Trovarelli, E. Vesselli, A. Baraldi, G. Comelli, G. Groppi, and J. Llorca, *Structure and morphology of Pd/Al_2O_3 and $Pd/CeO_2/Al_2O_3$ combustion catalysts in Pd-PdO transformation hysteresis.* Applied Catalysis A: General, 2010. 390: p. 1-10.

40. Colussi, S., F. Arosio, T. Montanari, G. Busca, G. Groppi, and A. Trovarelli, *Study of sulphur poisoning on Pd/Al_2O_3 and $Pd/CeO_2/Al_2O_3$ methane combustion catalysts.* Catalysis Today, 2010. 155: p. 59-65.

41. Trimm, D.L. and C.-W. Lam, *The combustion of methane on platinum-alumina fibre catalysts-I.* Chemical Engineering Science, 1980. 35: p. 1405-1413.

42. Mouaddib, N., C. Feumi-Jantou, E. Garbowski, and M. Primet, *Catalytic oxidation of methane over palladium supported on alumina: influence of the oxygen-to-methane ratio.* Applied Catalysis A, 1992. 87: p. 129-144.

43. Burch, R., F.J. Urbano, and P.K. Loader, *Methane combustion over palladium catalysts: the effect of carbon dioxide and water on activity.* Applied Catalysis A: General, 1995. 123(1): p. 173-184.

44. Oh, S.H., P.J. Mitchell, and R.M. Siewert, *Methane oxidation over alumina-supported noble metal catalysts with and without cerium additives.* Journal of Catalysis, 1991. 132(2): p. 287-301.

45. Otto, K., *Methane oxidation over Pt on γ-alumina: kinetics and structure sensitivity.* Langmuir, 1989. 5: p. 1364-9.

46. Hicks, R.F., H. Qi, M.L. Young, and R.G. Lee, *Structure sensitivity of methane oxidation over platinum and palladium.* Journal of Catalysis, 1990. 122(2): p. 280-294.

47. Lyubovsky, M. and L. Pfefferle, *Complete methane oxidation over Pd catalyst supported on alpha-alumina. Influence of temperature and oxygen pressure on the catalyst activity.* Catalysis Today, 1999. 47(1-4): p. 29-44.

48. Briot, P., A. Auroux, D. Jones, and M. Primet, *Effect of particle size on the reactivity of oxygen-adsorbed platinum supported on alumina.* Applied Catalysis, 1990. 59: p. 141-152.

49. Hoyos, L.J., H. Praliaud, and M. Primet, *Catalytic combustion of methane over palladium supported on alumina and silica in presence of hydrogen sulfide.* Applied Catalysis A, 1993. 98(125-138).

50. Hicks, R.F., H. Qi, M.L. Young, and R.G. Lee, *Effect of catalyst structure on methane oxidation over palladium on alumina.* Journal of Catalysis, 1990. 122(2): p. 295-306.

51. Baldwin, T.R. and R. Burch, *Catalytic combustion of methane over supported palladium catalysts. I. Alumina supported catalysts.* Applied Catalysis, 1990. 66(1): p. 337-358.

52. Carstens, J.N., S.C. Su, and A.T. Bell, *Factors affecting the catalytic activity of Pd/ZrO_2 for the combustion of methane.* Journal of Catalysis, 1998. 176(1): p. 136-142.

53. Datye, A.K., J. Bravo, T.R. Nelson, P. Atanasova, M. Lyubovsky, and L. Pfefferle, *Catalyst microstructure and methane oxidation reactivity during the Pd↔PdO transformation on alumina supports.* Applied Catalysis A: General, 2000. 198(1–2): p. 179-196.

54. Farrauto, R.J., J.K. Lampert, M.C. Hobson, and E.M. Waterman, *Thermal decomposition and reformation of PdO catalysts: support effects.* Applied Catalysis B: Environmental, 1995. 6(3): p. 263-270.

55. Burch, R. and F.J. Urbano, *Investigation of the active state of supported palladium catalysts in the combustion of methane.* Applied Catalysis A: General, 1995. 124(1): p. 121-138.

56. Su, S.C., J.N. Carstens, and A.T. Bell, *A study of the dynamics of Pd oxidation and PdO reduction by H_2 and CH_4.* Journal of Catalysis, 1998. 176(1): p. 125-135.

57. Burch, R., *Low NOx options in catalytic combustion and emission control.* Catalysis Today, 1997. 35(1–2): p. 27-36.

58. Farrauto, R.J., M.C. Hobson, T. Kennelly, and E.M. Waterman, *Catalytic chemistry of supported palladium for combustion of methane.* Applied Catalysis A: General, 1992. 81(2): p. 227-237.

59. Groppi, G., C. Cristiani, L. Lietti, and P. Forzatti, *Study of PdO/Pd transformation over alumina supported catalysts for natural gas combustion*, in *Studies in Surface Science and Catalysis*, F.V.M.S.M. Avelino Corma and G.F. José Luis, Editors. 2000, Elsevier. p. 3801-3806.

60. Burch, R., *Low NOx options in catalytic combustion and emission control.* Pure and Applied Chemistry, 1996. 68(2): p. 377-385.

61. Lyubovsky, M. and L. Pfefferle, *Methane combustion over the α-alumina supported Pd catalyst: Activity of the mixed Pd/PdO state.* Applied Catalysis A: General, 1998. 173(1): p. 107-119.

62. Ciuparu, D. and L. Pfefferle, *Methane combustion activity of supported palladium catalysts after partial reduction.* Applied Catalysis A: General, 2001. 218(1–2): p. 197-209.

63. Choudhary, T.V., S. Banerjee, and V.R. Choudhary, *Influence of PdO content and pathway of its formation on methane combustion activity.* Catalysis Communications, 2005. 6(2): p. 97-100.

64. Muto, K.-i., N. Katada, and M. Niwa, *Complete oxidation of methane on supported palladium catalyst: support effect.* Applied Catalysis A: General, 1996. 134(2): p. 203-215.

65. Ahlström-Silversand, A.F. and C.U.I. Odenbrand, *Combustion of methane over a catalyst, catalyst activity and stability.* Applied Catalysis A: General, 1997. 153(1-2): p. 157-175.

66. van Giezen, J.C., F.R. van den Berg, J.L. Kleinen, A.J. van Dillen, and J.W. Geus, *The effect of water on the activity of supported palladium catalysts in the catalytic combustion of methane.* Catalysis Today, 1999. 47(1-4): p. 287-293.

67. Ribeiro, F.H., M. Chow, and R.A. Dallabetta, *Kinetics of the complete oxidation of methane over supported palladium catalysts.* Journal of Catalysis, 1994. 146(2): p. 537-544.

68. Ciuparu, D., N. Katsikis, and L. Pfefferle, *Temperature and time dependence of the water inhibition effect on supported palladium catalyst for methane combustion.* Applied Catalysis A: General, 2001. 216(1-2): p. 209-215.

69. Bartholomew, C.H., *Mechanisms of catalyst deactivation.* Applied Catalysis A: General, 2001. 212(1–2): p. 17-60.

70. Euzen, P., J.H. Le Gal, B. Rebours, and G. Martin, *Deactivation of palladium catalyst in catalytic combustion of methane.* Catalysis Today, 1999. 47(1-4): p. 19-27.

71. O'Shea, V.A.D., M.C. Alvarez-Galvan, J. Requies, V.L. Barrio, P.L. Arias, J.F. Cambra, M.B. Guemez, and J.L.G. Fierro, *Synergistic effect of Pd in methane combustion $PdMnO_x/Al_2O_3$ catalysts.* Catalysis Communications, 2007. 8(8): p. 1287-1292.

72. Schwartz, W.R., D. Ciuparu, and L.D. Pfefferle, *Combustion of methane over palladium-based catalysts: catalytic deactivation and role of the support.* The Journal of Physical Chemistry C, 2012. 116(15): p. 8587-8593.

73. Roth, D., P. Gélin, M. Primet, and E. Tena, *Catalytic behaviour of Cl-free and Cl-containing Pd/Al_2O_3 catalysts in the total oxidation of methane at low temperature.* Applied Catalysis A: General, 2000. 203(1): p. 37-45.

74. Mowery, D.L., M.S. Graboski, T.R. Ohno, and R.L. McCormick, *Deactivation of $PdO-Al_2O_3$ oxidation catalyst in lean-burn natural gas engine exhaust: aged catalyst characterization and studies of poisoning by H_2O and SO_2.* Applied Catalysis B: Environmental, 1999. 21(3): p. 157-169.

75. Schwartz, W.R. and L.D. Pfefferle, *Combustion of methane over palladium-based catalysts: support interactions.* The Journal of Physical Chemistry C, 2012. 116(15): p. 8571-8578.

76. Carlo, G.D., G. Melaet, N. Kruse, and L.F. Liotta, *Combined sulfating and non-sulfating support to prevent water and sulfur poisoning of Pd catalysts for methane combustion.* Chemical Communication, 2010. 46: p. 6317-6319.

77. Yamamoto, H. and H. Uchida, *Oxidation of methane over Pt and Pd supported on alumina in lean-burn natural-gas engine exhaust.* Catalysis Today, 1998. 45(1–4): p. 147-151.

78. Liu, Y., S. Wang, T. Sun, D. Gao, C. Zhang, and S. Wang, *Enhanced hydrothermal stability of high performance lean fuel combustion alumina-supported palladium catalyst modified by nickel.* Applied Catalysis B: Environmental, 2012. 119–120(0): p. 321-328.

79. Choudhary, T.V., S. Banerjee, and V.R. Choudhary, *Catalysts for combustion of methane and lower alkanes.* Applied Catalysis A: General, 2002. 234(1-2): p. 1-23.

80. Burch, R. and P.K. Loader, *Investigation of Pt/Al_2O_3 and Pd/Al_2O_3 catalysts for the combustion of methane at low concentrations.* Applied Catalysis B: Environmental, 1994. 5(1-2): p. 149-164.

81. Peterson, E.J., A.T. DeLaRiva, S. Lin, R.S. Johnson, H. Guo, J.T. Miller, J. Hun Kwak, C.H.F. Peden, B. Kiefer, L.F. Allard, F.H. Ribeiro, and A.K. Datye, *Low-temperature carbon monoxide oxidation catalysed by regenerable atomically dispersed palladium on alumina.* Nature Communications, 2014. 5.

82. Escandon, L.S., D. Nino, E. Diaz, S. Ordonez, and F.V. Diez, *Effect of hydrothermal ageing on the performance of Ce-promoted PdO/ZrO_2 for methane combustion.* Catalysis Communications, 2008. 9(13): p. 2291-2296.

83. Specchia, S., P. Palmisano, E. Finocchio, and G. Busca, *Ageing mechanisms on PdOx-based catalysts for natural gas combustion in premixed burners.* Chemical Engineering Science, 2009. 65(1): p. 186-192.

84. Honkanen, M., M. Kärkkäinen, V. Viitanen, H. Jiang, K. Kallinen, M. Huuhtanen, M. Vippola, J. Lahtinen, R. Keiski, and T. Lepistö, *Structural characteristics of natural-gas-vehicle-aged oxidation catalyst.* Topics in Catalysis, 2013. 56(9-10): p. 576-585.

85. Winkler, A., D. Ferri, and M. Aguirre, *The influence of chemical and thermal aging on the catalytic activity of a monolithic diesel oxidation catalyst.* Applied Catalysis B: Environmental, 2009. 93(1–2): p. 177-184.

86. Lu, Y., S. Keav, V. Marchionni, G.L. Chiarello, A. Pappacena, M. Di Michiel, M.A. Newton, A. Weidenkaff, and D. Ferri, *Ageing induced improvement of methane oxidation activity of $Pd/YFeO_3$.* Catalysis Science & Technology, 2014. 4(9): p. 2919-2931.

87. Haruta, M., T. Kobayashi, H. Sano, and N. Yamada, *Novel gold catalysts for the oxidation of carbon monoxide at a temperature far below 0 ^oC.* Chemistry Letters, 1987: p. 405-408.

88. Waters, R.D., J.J. Weimer, and J.E. Smith, *An investigation of the activity of coprecipitated gold catalysts for methane oxidation.* Catalysis Letters, 1995. 30: p. 181-188.

89. Liotta, L.F., G. DiCarlo, A. Longo, G. Pantaleo, and A.M. Venezia, *Support effect on the catalytic performance of Au/Co_3O_4-CeO_2 catalysts for CO and CH_4 oxidation.* Catalysis Today, 2008. 139: p. 174-179.

90. Zhang, Y., J. Deng, L. Zhang, W. Qiu, H. Dai, and H. He, *$AuO_x/Ce_{0.6}Zr_{0.3}Y_{0.1}O_2$ nano-sized catalysts active for the oxidation of methane.* Catalysis Today, 2008. 139: p. 29-36.

91. Hu, L., Q. Peng, and Y. Li, *Selective synthesis of Co_3O_4 nanocrystal with different shape and crystal plane effect on catalytic property for methane combustion.* Journal of the American Chemical Society, 2008. 130(48): p. 16136-16137.

92. Fei, Z., S. He, L. Li, W. Ji, and C.-T. Au, *Morphology-directed synthesis of Co_3O_4 nanotubes based on modified Kirkendall effect and its application in CH_4 combustion.* Chemical Communications, 2012. 48(6): p. 853-855.

93. Liotta, L.F., H. Wu, G. Pantaleo, and A.M. Venezia, *Co_3O_4 nanocrystals and Co_3O_4-MOx binary oxides for CO, CH_4 and VOC oxidation at low temperatures: a review.* Catalysis Science & Technology, 2013. 3(12): p. 3085-3102.

CHAPTER 3

EXPERIMENTAL METHODS

3.1. Catalyst preparation

Catalysts containing 0.1-1.2 wt% Pd were prepared by the wet impregnation technique where a Pd (II) nitrate solution (10 wt% in 10 wt% nitric acid, Sigma-Aldrich) was mixed with gamma-delta-alumina (γ-δ-Al_2O_3, Chem-Supply) using a mortar and pestle. Water was added drop-wise while mixing until a paste was formed. The resulting paste was dried in an oven at 110 °C for approximately 20 hours. The dried catalyst was then pressed to a pellet with a maximum force of 5 tonnes. The maximum force was limited at 5 tonnes to prevent damage to the lattice structure of sample. After pelletizing, the catalysts were crushed into small pieces and sieved to 250-425µm.

After sizing the catalyst, activation procedures were performed in-situ in air (40 ml min^{-1}) at 500 ºC for 1 hour with a ramp of 10 ºC min^{-1}. The activation of the catalyst was then continued by purging in-situ with helium for 30 minutes then reduced in 99.99 % H_2 (20 ml min^{-1}) at 300 ºC for 2 h. The activation process was completed by purging with helium while adjusting the temperature to the desired reaction temperature (referred to calcined-reduced sample). A portion of the Pd/Al_2O_3 catalysts was activated in air only at 500 ºC for 1-2 h in order to investigate the effect of pre-treatment conditions on the catalyst activity (referred to calcined sample). For hydrothermal stability investigations of Pd/Al_2O_3 catalyst, a commercially available 1.0 wt% Pd/Al_2O_3 (Sigma-Aldrich) was used and activated under similar conditions as mentioned above.

Gold supported on iron oxide catalyst was prepared by a co-precipitation method [1]. A solution of 35.08 grams of $Fe(NO_3)_3 \cdot 9H_2O$ (Sigma-Aldrich) dissolved in 868.4 ml of

water (0.1 M) was prepared. This solution was then mixed with 0.299 grams of $HAuCl_4 \cdot 9H_2O$ (Acros-Organic) dissolved in 1.313 ml of HCl (0.58 M). The solution was then adjusted to a pH of 9 while being stirred at 80°C using Na_2CO_3 (0.1 M). The resulting solution was filtered under vacuum and washed with hot and cold water. The precipitate was then collected and dried in an oven at 110 °C for approximately 20 hours and then treated using the above procedures to pelletize and sieve catalysts. For catalyst activation, the sample was pre-treated ex-situ in air at 400 °C for 4 h ensuring the removal of any residual precursors. A similar method was used for preparing a 2.2 wt. % Au/Co_3O_4 catalyst where 23.97 g of $Co(NO_3)_2.6H_2O$ (Sigma-Aldrich) dissolved in water (0.1 M) was mixed with 307.2 mg of $HAuCl_4.9H_2O$ (Acros-Organic) dissolved in HCl at 0.58 $mol.L^{-1}$. The solutions were stirred at 80 ºC and Na_2CO_3 solution (0.25 M) was added drop wise until a pH of 8.2 was reached [1]. The resulting paste was then filtered, washed, dried and calcined under the same procedure as described above.

Nano-sized cobalt oxide catalyst was prepared using the so-called precipitation method. $Co(NO_3)_2.6H_2O$ (Sigma-Aldrich) was dissolved in water (0.1 M), the solution was stirred at 80 ºC and cobalt species precipitated by adjusting to a pH of 9 using Na_2CO_3 solution (0.25 M). The resulting precipitate was filtered, washed with hot and cold water and dried in an oven at 110 °C for 20 h [1]. Prior to catalyst activity measurements, the sample was pre-treated ex-situ in air at 400 °C for 4 h.

In order to investigate the effect of surface area on the catalytic activity and stability of iron oxide, a high surface area Fe_2O_3 catalyst was prepared by adding 0.33 mL of an aqueous solution of 0.36 M $Al(H_2PO_4)_3$ (Alfa Aesar) into 15.1 mL of 2.33 M $Fe(NO_3)_3$ (Sigma-Aldrich) in a flask [2]. The mixture was then placed in a rotary evaporator at 60

ºC for 2 h. The resulting paste was transferred in to an alumina boat and heated in a furnace to 380 ºC with a temperature ramp of 4 ºC min^{-1} for 1 h. The resulting paste was then dried in an oven at 110 °C for approximately 20 h and calcined in static air at 400 °C for 4 h to activate the catalyst as well as remove any residual phosphorus and nitrate originating from sample precursors. Finally the sample was purged with helium for 30 min prior to reaction.

Catalyst containing 1.4 wt% Pd/TS-1 was prepared by wet impregnation of a commercial titanium silicalite (TS-1) support (ENI-Polimeri Europa SpA) with an aliquot of Pd (II) nitrate solution (10 wt% in 10 wt% nitric acid, Sigma-Aldrich) mixed using a mortar and pestle. Water was added drop-wise while mixing, until a paste was formed. The resulting paste was dried in an oven at 110 °C for approximately 20 h. The dried catalyst was then ground, pressed and sieved to 250 μm - 425 μm. A tubular fixed-bed reactor was employed for the calcination of the dried solid catalyst in air at 500 ºC for 2 h followed by purging in helium while slowly cooling the catalyst to the desired reaction temperature.

3.2. Catalytic activity and stability measurements

The catalyst activity measurements were performed in a tubular stainless steel micro reactor operating in a steady-state plug flow mode. The reactant mixtures were then varied in the range of 0.2-0.8 % CH_4 balanced with air at various space velocities refer to the methane composition reported for ventilation air methane streams [3-6]. The inlet and outlet mixtures were analyzed using a dedicated ATI Unicam 610 gas chromatograph equipped with a thermal conductivity detector (TCD) and concentric

packed column (Alltech CTR-I). For the experimental data reported in Chapter 8, a new GC Shimadzu GC-2014, was installed and used for analysis. This Shimadzu GC was equipped with SRI 8610C column. For both gas chromatographs, Valco 6-port injection valves served for injecting the reactor feed and effluent streams to the columns. The GC's were calibrated by injecting standard calibration gases consist of (i) 1 % of each CO, CO_2, CH_4, H_2, O_2, N_2 in helium (Matheson MicroMAT^{TM}-14) and (ii) 0.2 % of each CH_4, CO_2, CO, n-butane, iso-butene, propane, propene, ethane, ethene in helium (Coregas) to the Unicam and Shimadzu gas chromatographs, respectively.

As shown in Fig. 3.1, the apparatus employed in the catalytic activity measurements was constructed with safety devices such as a flame arrester and relief valve. Methane and compressed-air flows were controlled using mass flow controllers (Brooks and Aalborg). In all experiments, helium was used as the GC carrier gas. Injections were repeated three times and the standard deviation of the conversion was ± 3 %. No methane conversion was detected when the feed was heated up to 650 ºC in the absence of catalyst. For humid feed experiments, the reactant mixture was passed through a saturator and a humidity probe was installed at the gas outlet. The bed temperature was determined by placing a thermocouple at the exit edge of the catalyst bed. The catalyst bed was loaded into the reactor by weighing a predetermined amount of pre-sized catalyst, depending upon the required gas hourly space velocity. Quartz wool was packed into the centre of reactor tube and the catalyst was then poured into the tube. A second piece of quartz wool was placed into the reactor so the catalyst formed a plug secured in place on each side by the quartz wool. This system is known as a packed bed micro-reactor. Fig. 3.2 illustrates the detail of packed catalyst bed used in the current research project.

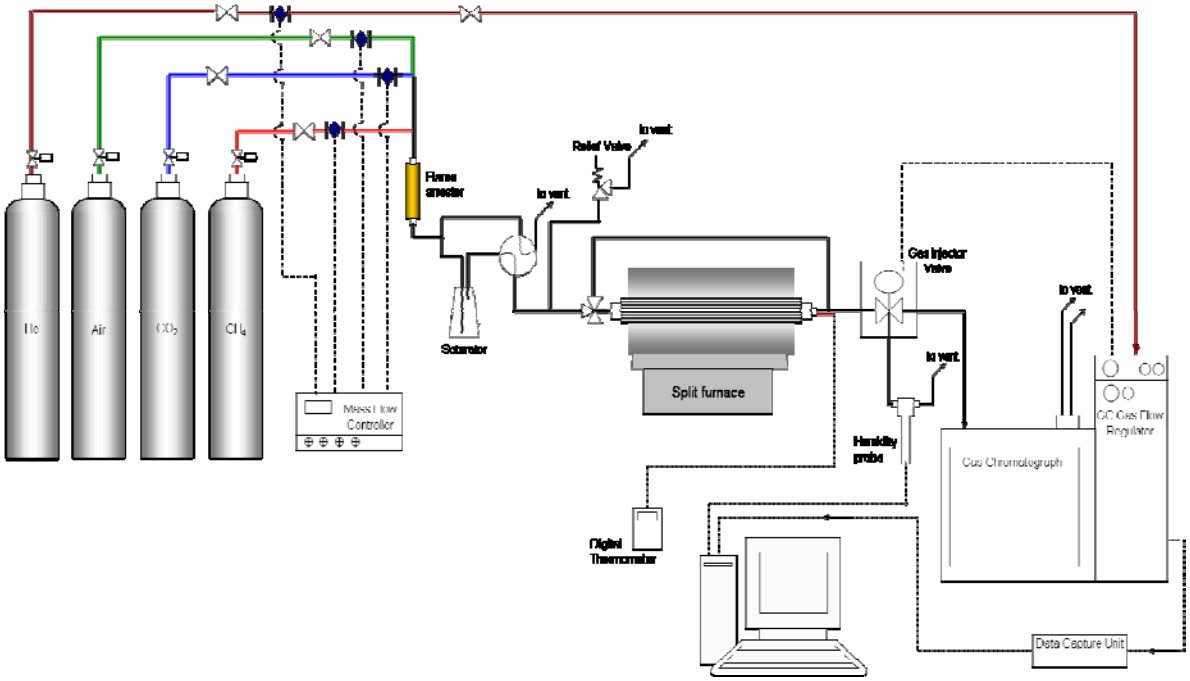

Fig. 3.1. Experimental set-up for catalyst activity measurement.

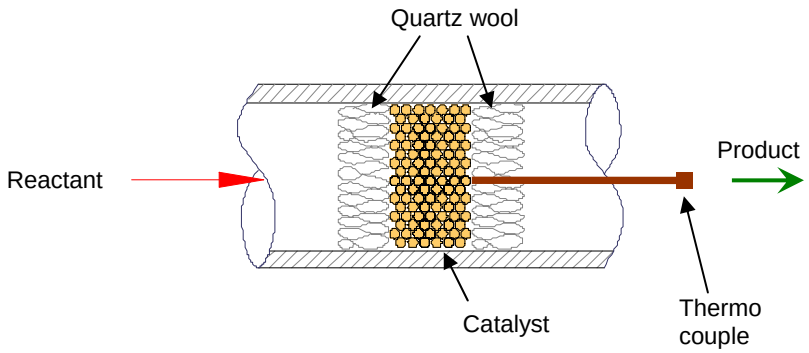

Fig. 3.2. Detail section of catalyst bed.

For catalytic stability studies, a separate set-up was used and operated continuously with varying conditions. Throughout the study, the composition of methane and carbon dioxide were set at 7,000 ppm and 10,000 ppm, respectively. The water content was measured within the range of 75 % to 85 % relative humidity (RH) for the saturator system used (T = 25 °C ± 3°C, ambient), corresponding to a $H_2O_{(v)}$ pressure of approximately 30,000 – 40,000 ppm. This level was based on information in the open literature [4] where the relative humidity of VAM stream ranges from 70 % to 100 %

RH. Thus, our saturator system was aimed producing humidity within this range. The feed gas hourly space velocity (GHSV) was maintained at 100,000 h^{-1} for the majority of the tests. The GHSV was varied to a limited extent between 75,000 h^{-1} and 110,000 h^{-1} in order to examine its effect on the total methane conversion. The targeted 90 % methane conversion was maintained by increasing the catalyst bed temperature as the catalyst deactivated during time on stream.

Fig. 3.3a shows a typical chromatogram (detector signal, in mV, versus retention time, in min) of feed composition with peak 6 (methane) corresponding to 7000 ppm of methane in air. A typical product trace at the conversion of methane is 90 % are shown in Fig. 3.3b. Peak no. 3 corresponds to CO_2 detected in the outlet stream of the reactor. The concentration of methane and carbon dioxide present in the feed and product were analysed based on response factors obtained from GC calibrations as mentioned above. Methane conversion and carbon balance were calculated using equation (3.1) and (3.2).

$$\text{Methane conversion (\%)} = \frac{\left(CH_{4,\,feed} - CH_{4,\,product}\right)}{CH_{4,\,feed}} \times 100 \tag{3.1}$$

$$\text{Carbon balance (\%)} = \left[1 - \left(\frac{Carbon_{total,\,feed} - Carbon_{total,\,product}}{Carbon_{total,\,feed}}\right)\right] \times 100 \tag{3.2}$$

3.3. Catalysts characterization

In order to understand the chemical and physical properties of the catalysts studied in this research, a number of techniques were employed including nitrogen physisorption, hydrogen chemisorption, temperature-programmed desorption (TPD), powder X-ray diffraction (XRD), scanning electron microscopy (SEM), transmission electron

microscopy and X-ray photoelectron spectroscopy XPS. The elemental composition of all catalysts was analysed using an inductively coupled plasma optical emission spectrometer (ICP-OES). The understanding of catalyst deactivation phenomena was explored by testing the post-run samples (used) under similar characterization procedures. To minimize the possibility of sample contamination, special procedures were taken such as purging in helium and transferring the used samples into sealed containers. In the following sub-sections, the individual procedure of each characterization technique is explained in detail.

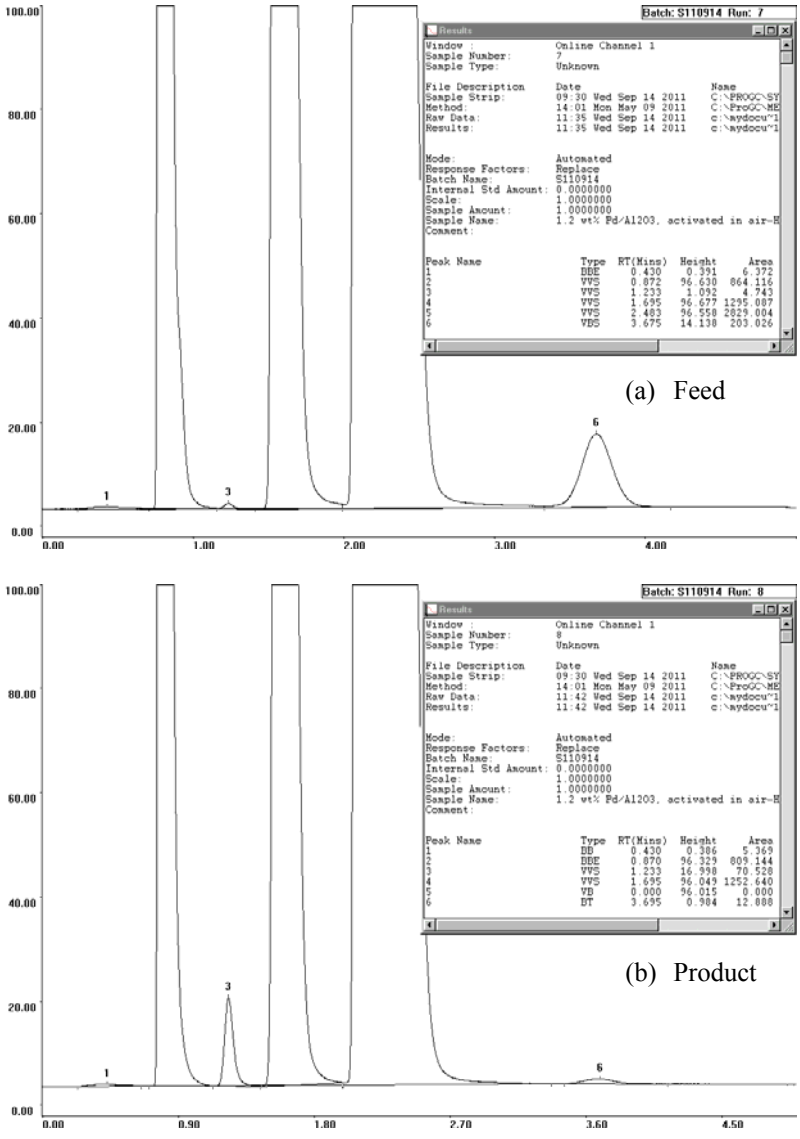

Fig. 3.3. Typical gas chromatographic trace of (a) feed gas (approximately 7,000 ppm of methane in air, (b) product gas composition, at a methane conversion level of 90 %.

3.3.1. Elemental Analysis

In order to determine the chemical compositions of the samples, analyses using an inductively coupled plasma optical emission spectrometer (ICP-OES) was performed for each catalyst prepared for this research. Prior to analysis, each sample was dissolved in a solution of 4.5 ml HNO_3 (65 %); 4.5 ml HCl (37 %) and 3 ml HBF_4 (50 %). All samples were then digested by means of Milestone Start D Microwave Unit. In plasma emission spectroscopy (OES), a sample solution is introduced into the core of inductively coupled argon plasma (ICP), which generates temperature of approximately 8,000 °C. At this temperature all elements become thermally excited and emit photons at their characteristic wavelengths. This light is collected by the spectrometer and passes through a diffraction grating that serves to resolve the light into a spectrum of its constituent wavelengths. Within the spectrometer, this diffracted light is then collected by wavelength and amplified to yield an intensity measurement that can be converted to an elemental concentration by comparison with calibration standards.

3.3.2. Nitrogen physisorption analysis

Physical adsorption (physisorption) of N_2 gas is a widely used technique to determine the surface area and pore-size distribution of solid materials. At low temperature, nitrogen molecules form a monolayer over the surface of any porous material. The N_2 molecules pack together as close as they can, independent of the substrate atomic structure. In general, physisorption measurements are performed at constant temperature and thus involve the determination of an adsorption isotherm,

$$n^a = f\left(p / p_0\right)_{T,gas,solid} \tag{3.3}$$

Where n^a is the amount of gas adsorbed which is plotted as a function of the equilibrium relative pressure, p/p_0. The shape of isotherm plot suggests the nature of the gas-solid interactions, the surface area and pore parameters of the solid [7].

The equation derived by Brunauer, Emmett and Teller (the BET equation) is commonly used for determination of the surface area of porous materials. It is recognized in this method that multilayer of adsorbed gas can form as the monolayer is being filled. Equation 3.4. presents the BET equation in linear form.

$$\frac{p}{n^a \cdot (p_0 - p)} = \frac{1}{n_m^a \cdot C} + \frac{(C-1)}{n_m^a \cdot C} \cdot \frac{p}{p_0} \tag{3.4}$$

Where, p is the equilibrium pressure for a particular surface coverage, n^a is the amount of adsorbed gas at the relative pressure p/p_0, n_m^a is the monolayer capacity and C is a constant related exponentially to the heat of adsorption in the first adsorbed layer. The BET equation invokes a linear relation between $\frac{p}{n_a(p_0 - p)}$ and $\frac{p}{p_0}$ (i.e. the BET plot) where the range of linearity is usually within the p/p0 range of 0.05-0.30. The surface area is then calculated using the following equations:

$$SA = n_m^a \cdot L \cdot a_m \tag{3.5}$$

$$SSA = \frac{SA}{W} \tag{3.6}$$

Where SA and SSA are respectively the total and specific surface areas of the adsorbent, W is the weight of sample used in this measurement, a_m is molecular cross-sectional area occupied by the adsorbate molecules in the complete monolayer and L is the Avogadro constant.

At the beginning of this research, nitrogen adsorption-desorption was carried-out using a Micromeritics Gemini 11 2370 at a temperature of 77 K (data reported in Chapters 4-5). Due to an up-grade of the physisorption instrument, later analyses were performed using a Micromeritics TriStar 3000, operating under similar conditions. Both instruments were calibrated using a surface area reference material, carbon black (Micromeritics).

In preparation for analysis, 150-200 mg of sample was charged in a quartz tube and weighted using a digital scale. The sample was degassed under vacuum for 6-12 h at 80 °C. This was undertaken to remove any the pre-adsorbed compounds. Following degassing, the mass of the sample was re-measured and then placed in the instrument for analysis. The saturation pressure (P_0) was automatically measured before the beginning of each analysis. During analyses, pressure changes and the volume of N_2 adsorbed were logged to the computer and analysed by the TriStar 3000 analysis software (version 6.08).

3.3.3. Chemisorption analysis

In order to correlate catalyst properties with its catalytic performance, quantitative information on the active metal phase such as metal surface area, metal dispersion and metal crystallite size are required. Chemical gas adsorption (chemisorption) is usually used to obtain this information. Chemisorption is a strong adsorption which involves bond breaking or weakening in the reactant and formation of bonds of the adsorbant with the surface. The availability of the adsorption site is an important aspect when evaluating the performance of a catalyst. In some cases, the particles of active metal are

at the surface, but there are also active metal particle located below the surface which is inaccessible for the reactant to adsorb. Therefore, an important design criterion is to maximize the number of active site per unit of metal. The activity of a catalyst is also strongly related to the rate that chemisorption occurs and the strength (energy) of the chemisorption bond. If the bond is too weak, the molecule may desorb prior to reacting; if too strong, the release of the product and regeneration of the site may be inhibited. Isothermal chemisorption methods as well as temperature-programmed chemisorption methods can be used to study surface energy distribution.

There are two techniques that can be used to obtained isothermal chemisorption analyses: (a) static volumetric chemisorption, and b) dynamic (flowing gas) chemisorption. The volumetric technique is suitable for obtaining high-accuracy measurements of the chemisorption isotherm from very low to atmospheric pressure at any temperatures which requires precise dosing steps to achieve equilibrium. The flowing gas (dynamic) technique operates at ambient pressure. After removing the physisorbed species from the surface of the adsorbent, small injections (doses) of accurately known aliquots of adsorptive gas are introduced to the sample in pulses until the sample is saturated. This technique is also called 'pulse chemisorption'. A calibrated thermal conductivity detector (TCD) monitors the quantity of adsorptive that is not taken up by active metals [8]. The first few injections may be completely adsorbed by the sample, resulting in little or no change in signal of the adsorbate on the detector. As the sample approaches saturation, peaks disclosing the concentration of un-adsorbed gas appear. Once reaction is complete, each of the discretely injected gases emerge from the sample tube are characterised by having a constant in peak area. The quantity of molecules chemisorbed is quantified from the difference between the total amount of

reactant gas injected and the sum amount that did not react with the active sites of the sample as measured by the detector. Number of moles of chemisorbed adsorbate is then calculated by using the ideal gas law:

$$P \cdot V = N_m \cdot R \cdot T \tag{3.7}$$

Quantification of surface atoms involved in chemisorption should consider the stoichiometry factor of the surface reaction. For instance, a hydrogen molecule may dissociate into two hydrogen atoms and react with two active surface atoms. Therefore, the number of hydrogen molecules taken up by the active surface (N_m) must be multiplied by a stoichiometry factor (Fs) of 2. Thus, the number of surface atoms (N_s) mathematically given by:

$$N_s = F_s \times N_m \tag{3.8}$$

where N_s and N_m are calculated per gram of sample.

In catalysis, metal dispersion is defined as the number of active metal atoms available for reaction compared to the total number of metal atoms in the catalyst material. The total amount of active metal deposited on support material per unit mass of catalyst (N_T) is determined after catalyst preparation using elemental analysis. Chemisorption analysis as described above is used to determine the quantity of active metal per gram that is available for reaction. The percent dispersion is the ratio of the available quantity to total quantity of active molecules times 100 %, or

$$D(\%) = \left(\frac{N_s}{N_T} \right) \times 100\% \tag{3.9}$$

Dispersion is expressed as the ratio of available metal to total metal atoms. Another fraction that is determined from the synthesis procedure is the ratio of the weight of

metal to the mass of the bulk catalyst material, expressed as a decimal fraction or as a percentage.

For catalysts reported in Chapters 4 and 5, the assessment of the active particle size and metal dispersion employed a Micromeritics 2910 AutoChem analysis unit (Micromeritics Instruments Corp., USA) by performing a number of H_2 pulse-chemisorption experiments. A 150-200 mg of sample was loaded to the sample tube and plugged with quartz wool. The sample was pre-treated *in-situ* by calcining in air at 500 °C for 1 h and reducing in H_2 at 300 °C for 1 h. As adsorbate, 10 % H_2 in N_2 was injected through a sample loop at a temperature of 109 °C. A thermal conductivity detector (TCD) detected the un-reacted adsorbate at the outlet. The injections were repeated several times and stopped automatically as the sample reached saturation. The Micromeritics WIN 2910 V5.01 software was used to calculate the total amount of reactant gas injected and the total amount that did not react with the active sites of the sample as measured by the TCD.

For catalysts reported in Chapter 7, a volumetric glass apparatus was used to determine the active particle size and metal dispersion by performing hydrogen chemisorption at 35 ºC, where the pressure range was 30-90 mbar (vacuum measurement by Pfeiffer CMR 362-TPG 261, data logging by LabVIEW version 7.1.1). Fig. 3.4 is a schematic of the set-up of the volumetric chemisorption analysis system, which consists of glass flasks (bulbs), a glass-manifold, a u-shape quartz tube, cock valves, a furnace, a Eurotherm 815P (Worthing, England) temperature controller complete with a k-type thermocouple, vacuum gauges, rough (rotary) vacuum pump and turbo pumps. The volume of the flasks and manifold were measured carefully before the analysis. For

calibration, a standard reference material 0.5% Pt on γ-Al_2O_3 (Catal International Ltd.) was tested with the results showing good agreement to the certificate of analysis provided with the reference material.

A sample of 400-500 mg of catalyst was charged into the u-shape quartz tube and activated using procedure as described above. To remove pre-adsorbed compounds, the system was evacuated (10^{-3} to 10^{-2} mbar) at 400 °C for 30 min followed by cooling to 35 °C. Approximately 90 mbar of hydrogen (99.99 %) was stored in bulb V_1. Chemisorption was commenced by releasing the adsorbate stored in V_1 to the manifold and sample tube. Based on changes in pressure and accurately knowing the volume of the system, the amount of adsorbed gas can be calculated (assuming ideal gas conditions). A ratio of H/Pd = 1/1 stoichiometry was assumed for H_2 chemisorption on metallic palladium [9], thus the amount of adsorbed hydrogen is equal to the number of accessible Pd sites.

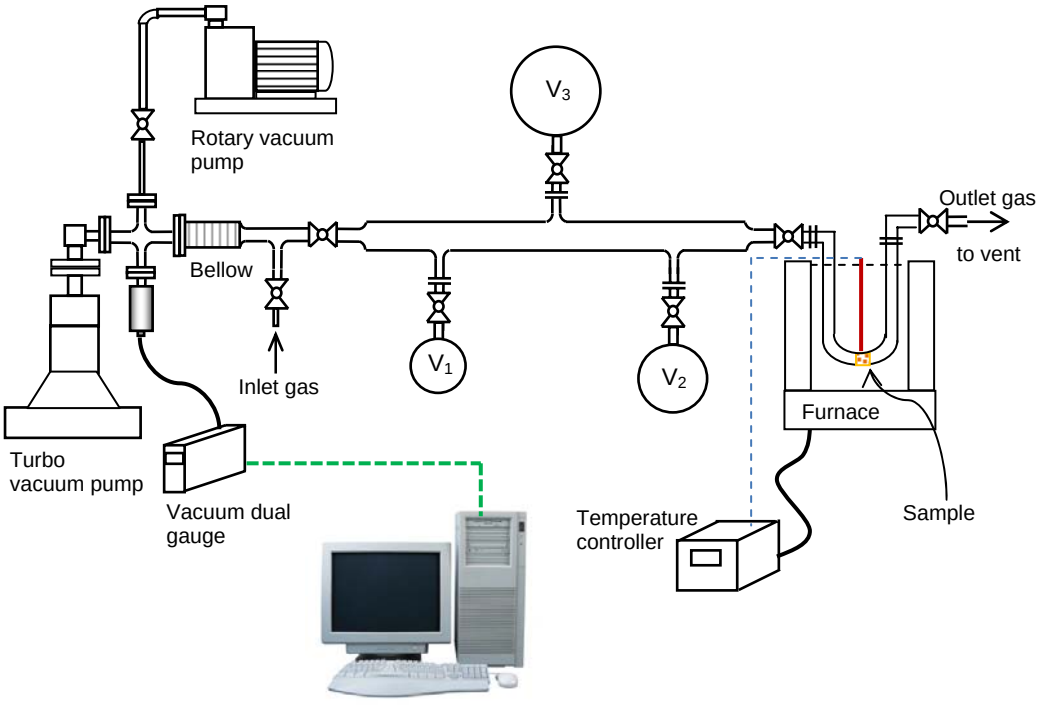

Fig. 3.4. Volumetric chemisorption experimental set-up.

The dispersion is defined as the number of moles of accessible metal divided by total amount of metal. Mean particle diameter was estimated based on dispersion values using equation 3.10.

$$dp = \frac{6 \times Ca \times M \times 10^9}{\rho \times D \times Na} \tag{3.10}$$

Where, Ca is concentration of surface metal atom (equal to 1.27×10^{19} atoms m^{-2}), M is Pd atomic mass, ρ is Pd volumetric mass (equal to 12.02×10^6 g m^{-3}) [10], D is metal dispersion and Na is Avogadro number.

3.3.4. Temperature-programmed desorption (TPD) analysis

Determination of kinetic and thermodynamic parameters of desorption process or decomposition reactions over the surface of catalysts employed temperature programmed desorption (TPD) analysis. In this technique, a sample is heated at a constant temperature ramp and the desorbed molecules are analyzed and quantified by mass spectrometry. For TPD experiments, it is desirable to undertake analysis under ultra-high vacuum (UHV) conditions, whereby the vacuum regime is lower than 10^{-8} mbar. At this low pressure, the gas molecules will collide and react with the sample substrate in the UHV chamber many times over before colliding with each other, ensuring that all interactions take place on the substrate surface.

Throughout this research, a purpose built apparatus with a Pfeiffer Prisma quadrupole mass spectrometer served for TPD experiments. Fig. 3.5 illustrates TPD apparatus set-up. The system consists of two turbo pumps and one rotary (rough) vacuum pump installed in the system to achieve UHV conditions (<10^{-8} mbar). The pressure at three

different locations in the vacuum manifold are monitored *via* pressure transmitters (PT) connected to a Pfeiffer single gauge (TPG 261) and a Pfeiffer dual gauge (TPG 252A). The furnace temperature was programmed and recorded *via* a Eurotherm RS232 temperature controller.

Analysis is started by charging 50-100 mg of sample into the sample tube and covered with quartz wool. To remove any pre-adsorbed species, the sample was heated under vacuum to a temperature equal to activation or reaction temperatures of catalysts for 1 h. The furnace temperature was then set to the adsorption temperature. The adsorption was carried out at room temperature or at elevated temperatures depends on the specific target of investigation and the nature of the catalyst and adsorbate. The actual adsorption temperature is mentioned in each plot of TPD spectra.

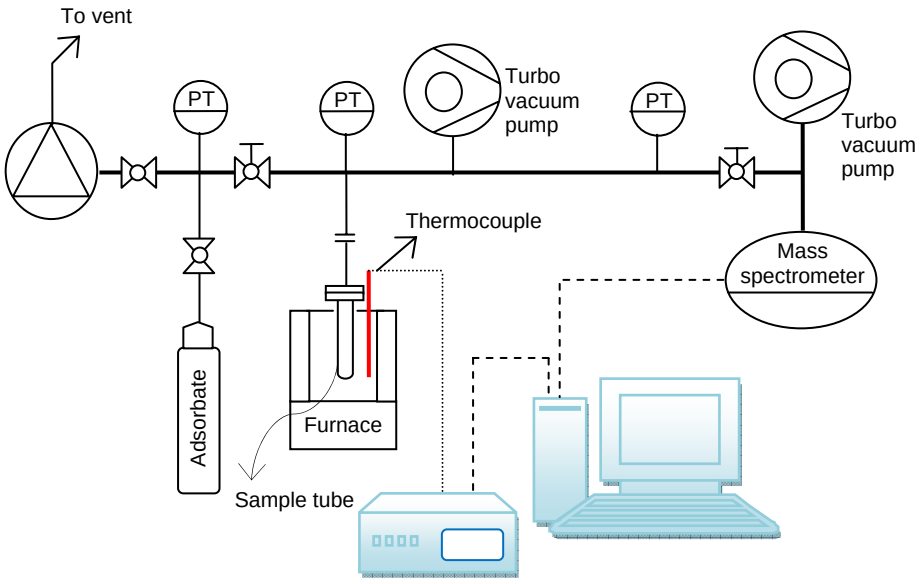

Fig. 3.5. Schematic of temperature programmed desorption (TPD) apparatus

By opening the adsorbate gas cylinder slowly, the pressure of the system is increased from $<10^{-4}$ mbar to 1 mbar and the valve is then closed. A decrease in pressure was observed signalling the adsorption was in process with the pressure stabilizing once the sample has reached saturation. Any excess adsorbate was then evacuated from the system by opening the turbo pump valve.

Temperature programmed desorption was performed from room temperature to a selected temperature depending on the objective of analysis and specific properties of the catalyst. For all TPD experiments, the heating ramp was set at 5 °C min^{-1}. At the outlet, the mass spectrometer (MS) Pfeiffer Prisma quadrupole QMA 200 detected the desorbed species and the data logged to the computer. The spectrum calibration was performed by introducing the MS with various known gases such as water vapour, 99.995 % CH_4, 99.95 % CO_2, 99.95 % O_2 *etc*. For quantification of water and CO_2, sodium bicarbonate ($NaHCO_3$) was decomposed in the TPD apparatus using various amounts of sample.

Fig. 3.6 illustrates the basic components of the quadrupole mass spectrometer used in the study. The quadrupole MS consists of (a) the ion source with electron impact ionizer and ion extraction optics, (b) four cylindrical rod quadrupole analyser, and (c) an ion detector (electron multiplier). The rods are arranged symmetrically and have a fixed direct current (DC) and alternating radio frequency (RF) potentials applied to them. The ions are generated by electron impact ionisation. The emitted electrons are accelerated by a potential difference (typically 70 V) between the filament and the grid. Ionisation takes place in the area between grid and aperture, which are at approximately equal potentials. The ions are then focussed and passed through the middle of quadrupole. The

ion motion depends on the electric fields and only ions of a certain mass to charge ratio (*m/z)* will have a stable trajectory passing through to the detector. The RF is varied in order to bring different *m/z* in to focus on the detector, thus building up a mass spectrum. Ions that possess unstable trajectories will hit the quadrupole and will not be detected. The mass range and resolution of the device is determined by the length and diameter of the rods.

The data obtained from MS consists of the intensity variation of each recorded mass fragment as a function of temperature or time. Fig. 3.7 shows typical spectra obtained from a TPD experiment following the adsorption of oxygen onto Pd/Al_2O_3 catalyst at 110 °C. The following points are noteworthy information that we can obtain from a TPD plot.

- The area under the peak represents the amount of adsorbed species, i.e. proportional to the surface coverage.

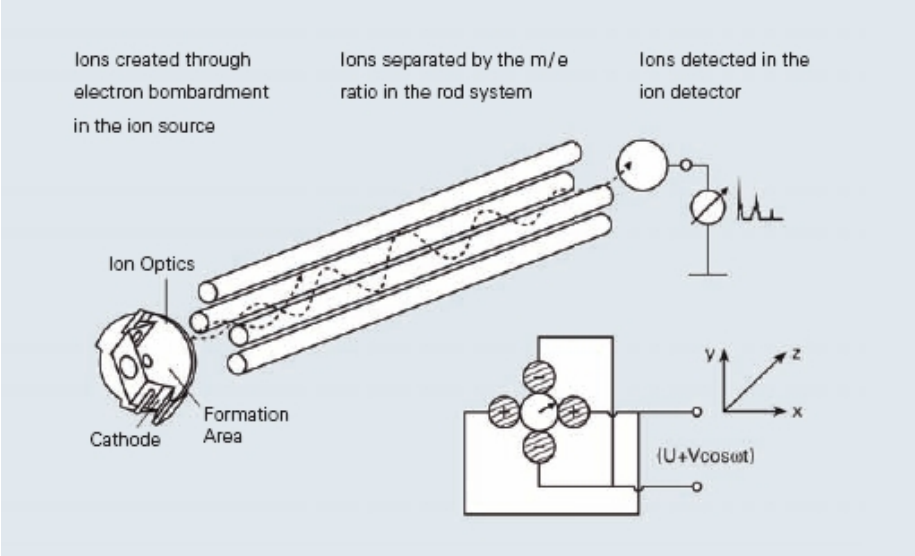

Fig. 3.6. Schematic of a quadrupole mass spectrometer (QMS) by Pfeiffer Vacuum.

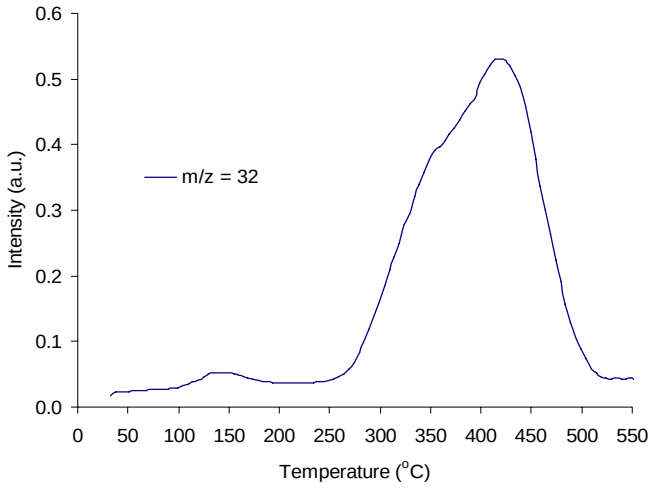

Fig. 3.7. Typically O_2-TPD spectra desorbed from Pd/Al_2O_3 catalyst.

- The kinetics of desorption obtained from the peak profile and the coverage dependence of the desorption characteristics enabling the study of the state of aggregation of the adsorbed species.
- The position of the peak (the temperature at maximum peak intensity) is related to the enthalpy of adsorption, i.e. to the strength of binding to the surface. The presence of multiple peaks in the TPD spectrum suggests that there is more than one binding state for the species desorbed from the surface and give different adsorption enthalpies.

3.3.5. Powder X-Ray Diffraction (XRD) analysis

Identification of crystalline phases of the fresh and used catalyst was performed using x-ray diffraction (XRD) analysis. XRD is the classical technique for determination of the bulk structure of crystalline solids. The analysis is based on constructive interference of monochromatic X-rays and a crystalline sample. The X-rays beam are generated by a cathode ray tube to produce monochromatic radiation, collimated to concentrate, and directed toward the sample. The interaction of the incident rays with the sample

produces constructive interference and a diffracted X-ray when conditions satisfy Bragg's Law ($n\lambda=2d \sin \theta$). This law relates the wavelength of electromagnetic radiation to the diffraction angle and the lattice spacing in a crystalline sample.

For fresh catalyst, 200-300 mg of catalyst was ground and charged in a sample holder. As the mass of used catalyst is less than 100 mg, a low background (smaller size) sample holder was used. X-Ray diffraction patterns of catalysts were examined using Cu Kα radiation with a Philips X'Pert diffractometer. Diffractrograms were collected in the 2θ angle range from 2° to 90° with 0.008° 2θ step resolutions. Software (HighScore from PANalytical) assisted in diffraction pattern analysis, profile fitting and phase identification. The line broadening at half the maximum intensity (FWHM) of the most intense reflection of each phases allowed the estimation of particle size by X'Pert Data Viewer (PANalytical) software calculated from the Scherrer formula in the following equation:

$$\tau = \frac{K \times \lambda}{\beta \times \cos\phi} \tag{3.11}$$

Where, K is shape factor, λ is x-ray wavelength (nm), β is the line broadening at half the maximum intensity (º2θ) and ϕ is the Bragg angle (º2θ). For this calculation, we assume there is no significant difference in the disorder of the metal due to the heat treatment. The shape factor used in this calculation was 0.9 as recommended by Klug and Alexander [11]. This calculation procedure was used to estimate the particle size of the catalysts reported in Chapter 6 due their higher crystallinity. For palladium supported catalysts, minute reflections attributed to Pd or PdO phases overlapping with support peaks restricted the accurately of the analysis using this procedure.

3.3.6. Scanning Electron Microscopy (SEM) analysis

The external morphology (texture), surface topography and crystalline structure of the catalyst prepared were determined using scanning electron microscopy (SEM). This technique allows for the exploration of the possibility of a morphological transformation after methane oxidation reactions. SEM consists of an electron gun which produces the electron beam, electromagnetic optics guide the beam and focus it. The electrons, either direct scattered or emitted from the sample, are collected by a detector and the energy of the detected electrons, together with their intensity and location of emission, is used to produce the image [12]. Often an energy dispersive photon detector is used for SEM to provide analysis of x-rays that are emitted from the specimen due to the interactions of incident electrons with the atoms of the sample.

Briefly, the components and the function of SEM are, in many ways, analogous to the light microscope (LM). A comparison of these microscopes is illustrated in Fig. 3.8 which is frequently used in textbooks when starting a discussion about SEM. The following points outline some of the advantages provided by SEM in comparison with the light microscope (LM):

(i) Resolution at high magnification, the best resolution can possibly be gained in a LM is about 200 nm whereas SEM can provide a resolution higher than 10 nm.

(ii) The height of a specimen (depth of field) that appears in focus in an SEM image is equal to 300 times depth of field in a LM. This means under SEM a great topographical detail can be captured. SEM allows the three dimensional (3D) appearance of the specimen image and provide much more information.

(iii) SEM allows the analysis of sample composition including information about crystallography, chemical composition, magnetic and electrical characteristics.

In SEM analysis, a beam of high energy electrons is generated by an electron gun and processed by magnetic lenses. The beam is focused at the specimen surface and systematically scanned across the surface of a specimen. Different to a light microscope, the image observed under SEM actually is not a real image of the sample. The SEM image is in the form of a serial data stream i.e. it is an electronic image. It is a result of the beam probe illuminating the sample one point at a time in a rectangular scanning pattern, with the strength of the signal generated from each point being a reflection of differences (e.g. topographical or compositional) in the sample.

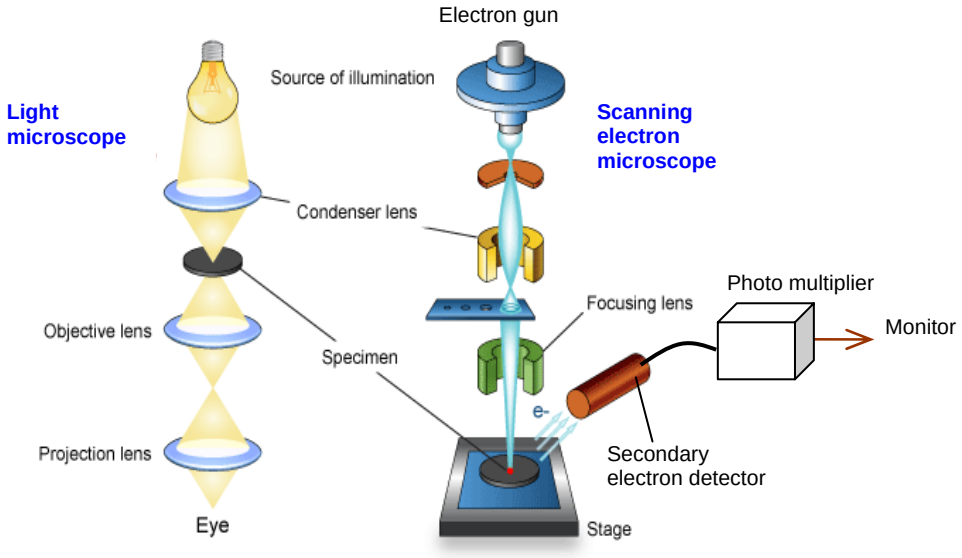

Fig. 3.8. The basic function of light microscope compared with scanning electron microscope.

The type of image to be generated using SEM analysis is based on the detector used during analysis. There are two types of detectors, first is a secondary electron detector (SED). As the primary beam hits the surface of specimen, it interacts with the atoms in the sample and scatters electrons from a range of different depth [13]. The low energy secondary electrons (2-50 eV) are ejected from near surface layer and collected to produce secondary electron images (micrographs). The low energy of these electrons enables them to be collected easily and makes secondary electron detector ideal for capturing topographical information. To attract these low-energy electrons, the collector cage applies a small bias voltage at the front end of the detector to attract the negative electrons towards the detector. A higher kV (e.g. 7 to 12kV) is applied inside the cage to accelerate the electrons into the screen.

The second detector is backscattered electron detector (BSD). By using backscattered electron, the information in relation to topographical, physical and chemical characteristics of the sample can be obtained. The BSD is mounted below the objective lens centred-line with the optic axis. As the electron beam scans the surface of the sample, back scattered electrons (BE) are generated and bounced back out of the sample. The electrons exiting the sample are collected to produce the backscattered image. Compositional or topographical backscattered electron images (BEI) is recorded depending on the window of electron energies selected for image formation.

Prior to analysis, the sample holder was coated by a thin layer of carbon liquid tape. A few mg of sample was poured over the coated area and dried in the oven for 15 minutes at 60-80 °C. The sample was then transferred into the chamber for analysis. Zeiss Sigma VP FESEM served to capture the SEM images of the fresh and used sample using a

secondary electron detector and backscattered electron detector. Bruker light element SSD Energy-dispersive X-ray spectroscopy (EDS) detector allowed for the elemental analysis while capturing the SEM images.

3.3.7. Transmission Electron Microscopy (TEM) analysis

The study on particle size, size distribution and morphology of the fresh and used catalysts requires submicron imaging. Transmission electronic microscopy (TEM) is a rigorous tool for directly imaging the nano-materials. A modern high resolution TEM (HRTEM) can magnify an image ca 800,000 times to 1,500,000 times at maximum [14]. This technique enables the investigation of crystal structures, orientations and chemical compositions of phases, and contaminants through diffraction patterns, characteristic X-ray, and electron energy loss analysis.

In terms of its optical configuration, TEM has similarity with a light microscope. However, instead of a light source generating a beam of photons that passes through a series of glass lenses, the electron microscope is equipped with an electron gun under vacuum conditions that generates an electron beam and electromagnetic lenses. The image is produced by illuminating the sample with the electron beam. The electrons pass through (unscattered), are subsequently scattered, or absorbed by the sample, generating a projection on a fluorescent screen, a photographic film, or a charge-coupled device (CCD) chip, which represents a 2D electron density map of the sample [15]. When electrons interact with a specimen, information can be collected with respect to the interaction events for further analysis. Fig. 3.9 illustrates the electrons interaction with a sample and how they are used in different types of analysis.

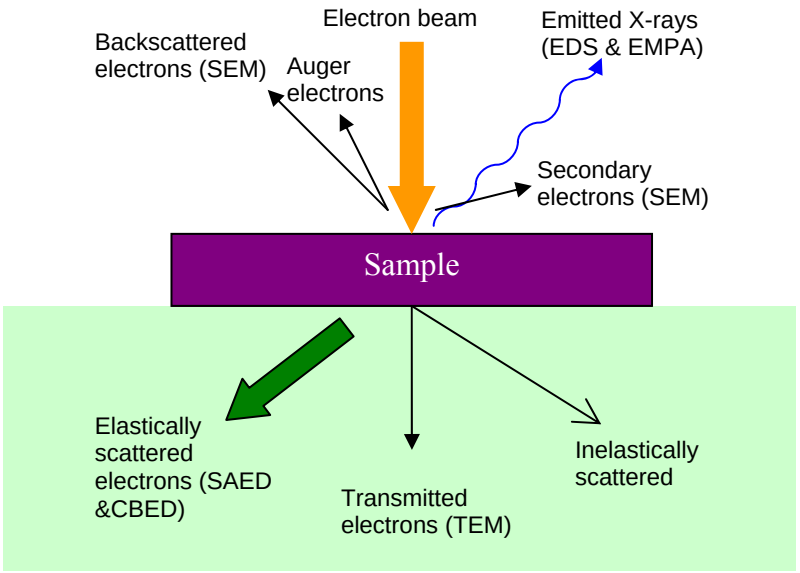

Fig. 3.9. Representation of information produced by the interaction between specimen and the electron beam.

Fig. 3.10 shows a simplified set up of a TEM, which consists of four main components, *i.e* electron source, electromagnetic lens system, sample holder, and imaging system. The electron source comprises a cathode and an anode. As a cathode, a tungsten filament emits electrons while being heated. A negative cap confines the electrons into a loosely focused beam. The beam is then accelerated towards the specimen by the positive anode. Electrons at the rim of the beam will fall onto the anode while the others at the centre will pass through the small hole of the anode. The electron source works like a cathode ray tube. After leaving the electron source, the electron beam is tightly focused using electromagnetic lens and metal apertures. The system only allows electrons within a small energy range to pass through, and as a consequence the electrons in the electron beam will have a well-defined energy. As the sample mount, a mechanical arm is used for holding the specimen and controlling its position. Acquiring the images employs a second electromagnetic lens system and a screen. The electromagnetic lens system consists of two lens systems, one for refocusing the electrons after they emitted from the specimen, and the other for enlarging the image

and projecting it onto the screen. The screen has a phosphorescent plate which illuminates when impacted by electrons.

Sample preparation for TEM analysis involves dispersing the sample in ethyl alcohol and loading it on the sample grid. Initially, about 5 mg of sample was mixed with 5 ml of ethyl alcohol in a vial and placed in a sonic bath for 5-10 minutes. Using a pipette the solution was dropped on a TEM sample grid (strong carbon film on 200 mesh Cu, GSCu200C-50, ProSciTech). The sample grid was dried in an oven at 80 °C for 5 minutes and then transferred into the TEM chamber. TEM images of the catalysts reported in Chapters 4-6 were taken with a JEOL 2100 TEM. For the catalysts reported in Chapters 7-8, A JEOL 2200 FS TEM featured with EDS and scanning transmission electron microscope (STEM) system was used for imaging nano-sized Pd particles and support as well as measuring the particle size distribution. Particle size measurement was carried out by using Gatan DigitalMicrograph software.

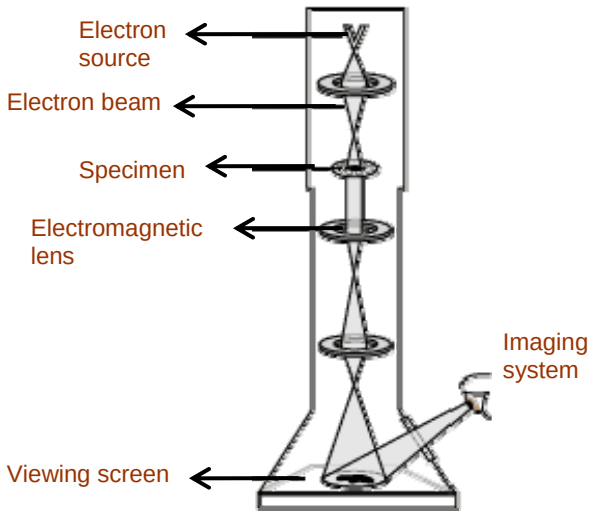

Fig. 3.10. The schematic outline of a TEM.

3.3.8. X-Ray Photoelectron Spectroscopy (XPS) analysis

Understanding intrinsic the activity and deactivation phenomena of the catalysts prepared in this research requires surface elemental analysis and an understanding of the chemical/oxidation state of the elements that exist on the surface of the catalyst. X-ray photoelectron spectroscopy (XPS) is a suitable technique for surface analysis. XPS analysis involves irradiating the solid sample under vacuum with mono-energetic soft x-rays and analysing the emitted electrons at each energy interval. The obtained spectrum is plotted as the number of detected electrons per energy interval versus their kinetic energy [16].

X-ray Photoelectron Spectroscopy (XPS) is also known as Electron Spectroscopy for Chemical Analysis (ESCA). A basic description of the XPS analysis technique is illustrated in Fig. 3.11, where a low energy X-ray beam irradiates the surface of sample and excites the electrons in the sample atoms. Due to its lower binding energy compared to the X-ray energy, electrons are ejected from the parent atom as photoelectrons. Most of these electrons are reabsorbed by the sample, and only electrons emitted from atoms near the sample surface (the outmost photoelectrons) are able to escape from the sample surface. The ejected electrons are energy filtered via a hemispherical analyzer (HSA) by placing a negative charge on the outside plate to repel the electrons and a positive charge on the inner plate to attract the electrons (see Fig. 3.11). The potential difference between these two plates will only allow photoelectrons of a certain voltage to make it through the hemisphere. A photoelectron spectrum is recorded by counting ejected electrons over a range of electron kinetic energies. Peaks appear in the spectrum as a result of atoms emitting electrons of a particular characteristic energy. The energies and

intensities of the photoelectron peaks enable identification and quantification of all surface elements (except hydrogen).

To generate mono-energetic soft X-rays, XPS instrument employs Mg Kα x-rays (1253.6 eV) or Al Kα x-rays (1486.6 eV). These photons have limited penetrating power in a solid, of the order of 1-10 micrometers. The photons interact with atoms at the surface of the sample by photoelectric effect, causing the electrons to be ejected. This can occur if the energy of the impinging photon (hv) is greater than the energy required to remove the electron from the system. This latter is expressed as a sum of two parameters: firstly, the binding energy (BE) describing the energy required to remove an electron from a certain orbital, and secondly the work function of spectrometer (ϕ_s), which is the energy for taking an electron from inside the sample to the vacuum level [17]. Therefore, the binding energy of an electron can simply be determined by measuring the energy-dependent photocurrent using the equation 3.12.

$$BE = h\nu - KE - \phi_s \tag{3.12}$$

Where *KE* is the measured kinetic energy of the emitted electron [16, 17].

The different in chemical environments, can give a different in the binding energy of a particular core level in the same atom. The energy difference observed in binding energies is called the chemical shift. The occurrence of chemical shift is related to different screening of the Coulomb interaction between the nucleus and the probe orbital via valence electrons. Hence, the binding energies are correlated with the partial charge on an atom, *i.e.* increasing positive charge on an atom of a molecule increases the binding energy and *vice versa*.

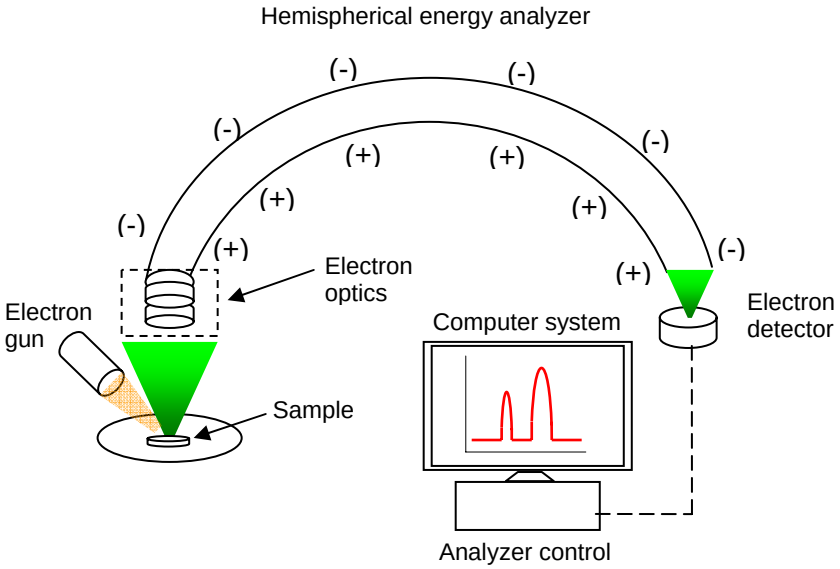

Fig. 3.11. The schematic outline of XPS analysis

Binding energy is characteristic of the analysed elements and the orbit from which the electrons are emitted. The BE can be calculated using the equation 3.12 by measuring the kinetic energy with known ϕ_s. The spectrum of XPS is typically presented as a plot of the number of photoelectrons ejected as a function of binding energies of detected electrons [18]. Identification of the elements detected from the surface of sample is based on the XPS peaks rising at their characteristics binding energies. The peak area represents the quanta of each element in which the atomic ratio of the surface elements can be determined following normalization. The popularity of XPS is due to its ability to (i) identify and quantify the elemental composition of the outer 10 nm or less of any solid surface with any element from Li to U, (ii) reveal the chemical environment where the respective element exists in, (iii) obtained the above information with a minimum sample preparation work [19].

For surface analysis on catalysts reported in Chapter 4, XPS analysis was undertaken using Al Kα radiation. The emitted photoelectrons were analysed using a PHOIBOS 100 hemispherical analyser manufactured by SPECS GmbH. Used samples were collected immediately after terminating the reaction by cooling in helium and the catalyst was then stored in a sealed container. The sample was mounted on an XPS sample holder using indium tape. The exposure time of samples in air was minimised in order to reduce the likelihood of water adsorption or oxidation of any carbon that may have been deposited on the catalyst. The energy scale was shifted relative to the adventitious carbon peak at 284.6 eV. The shift was cross checked with the position of O1s from Al_2O_3, which is found at 531 eV.

XPS analyses of catalysts reported in Chapters 5-8 were performed using monochromated Al K alpha (energy 1486.68 eV) radiation and the emitted photoelectrons were analyzed using an ESCALAB250Xi manufactured by Thermo Scientific, UK. Background vacuum was lower than 2×10^{-9} mbar. To minimize the possibility of sample contamination, spent samples were immediately transferred into sealed containers after stopping the reaction by cooling in helium. The samples were mounted on the stub using indium tape. The energy scale in the XPS spectra was referenced to the adventitious carbon adsorption at 284.6 eV. The spectrometer was calibrated against binding energies of Au $4f_{7/2}$ = 83.96 eV, Ag $3d_{5/2}$ = 368.21 eV and Cu $2p_{3/2}$ = 932.62 eV.

References

1. Solsona, B.E., T. Garcia, C. Jones, S.H. Taylor, A.F. Carley, and G.J. Hutchings, *Supported gold catalysts for the total oxidation of alkanes and carbon monoxide.* Applied Catalysis A: General, 2006. 312: p. 67-76.

2. Liu, Y., H. Tuysuz, C.-J. Jia, M. Schwickardi, R. Rinaldi, A.-H. Lu, W. Schmidt, and F. Schuth, *From glycerol to allyl alcohol: iron oxide catalyzed dehydration and consecutive hydrogen transfer.* Chemical Communications, 2010. 46(8): p. 1238-1240.

3. Schultz, H.L., P. Carothers, R. Watts, and R. McGuckin, *Assessment of the worldwide market potential for oxidising coal mine ventilation air methane*. 2003, United States Environmental Protection Agency, Air and Radiation (US-EPA)

4. Su, S., H. Chen, P. Teakle, and S. Xue, *Characteristics of coal mine ventilation air flows.* Journal of Environmental Management, 2008. 86: p. 44 - 62.

5. Su, S. and J. Agnew, *Catalytic combustion of coal mine ventilation air methane.* FUEL, 2006. 85: p. 1201-1210.

6. Stasinska, B. and A. Machocki, *Catalysts for the utilization of methane from the coal mine ventilation air.* Polish Journal of Chemical Technology, 2007. 9(3): p. 29 - 32.

7. Sing, K.W., *Physisorption of nitrogen by porous materials.* Journal of Porous Materials, 1995. 2(1): p. 5-8.

8. Webb, P.A., *Introduction to chemical adsorption analytical techniques and their applications to catalysis.* MIC Technical Publications, 2003.

9. Castellazzi, P., G. Groppi, and P. Forzatti, *Effect of Pt/Pd ratio on catalytic activity and redox behavior of bimetallic Pt-Pd/Al_2O_3 catalysts for CH_4 combustion.* Applied Catalysis B: Environmental, 2010. 95: p. 303-311.

10. Anderson, J.R. and K.C. Pratt, *Introduction to characterisation and testing of catalysts*. 1985: Academic Press.

11. Klug, H.P. and L.E. Alexander, *X-ray diffraction procedures: for polycrystalline and amorphous materials*. 2nd ed. 1974, New York: John Wiley & Sons, Inc.

12. Mehta, R., *Interactions, imaging and spectra in SEM*, in *Scanning Electron Microscopy*, V. Kazmiruk, Editor. 2012, InTech.

13. Khursheed, A., *Scanning electron microscope optics and spectrometers*. 2010, River Edge, NJ, USA: World Scientific Publishing Co.

14. Zhou, W., *Transmission electron microscopy*. Metal oxide catalysis, ed. S.D. Jackson and J.S.J. Hargreaves. Vol. 1. 2009, WILEY-VCH Verlag GmbH & Co. KGaA: Weinheim

15. Beniash, E., A. Dey, and N.A.J.M. Sommerdijk, *Transmission electron microscopy in biomineralization research: Advances and challenges*. 2014, Taylor & Francis Group, LLC.

16. Moulder, J.F., W.F. Stickle, P.E. Sobol, and K.D. Bomben, *Handbook of x-ray photoelectron spectroscopy*. A reference book of standard spectra for identification and interpretation of XPS data. 1992, Minnesota, USA: Perkin-Elmer Corporation.

17. Teschner, D., E.M. Vass, and R. Schlogl, *Photoelectron spectroscopy of catalytic oxide materials*. Metal oxide catalysis, ed. S.D. Jackson and J.S.J. Hargreaves. Vol. 1. 2009, WILEY-VCH Verlag GmbH & Co. KGaA: Weinheim.

18. Lu, K., *Nanoparticulate materials : synthesis, sharacterization, and processing*. 2012: Wiley.

19. van der Heide, P., *X-ray photoelectron spectroscopy: an introduction to principles and practices*. 2011: Wiley.

CHAPTER 4

Evidence of the Formation of Surface Palladium Carbide during the Catalytic Combustion of Lean Methane/Air Mixtures

---

Published in:

Energy Technology (Wiley-VCH Verlag GmbH&Co. KGaA, Weinheim) 2014, 2, 243 – 249, (DOI: 10.1002/ente.201300119)

Appendix B supplied the supporting information of this chapter.

4.1. Introduction

Methane is a gas with a GHG potential which is 23 times greater than that of CO_2 [1] and under certain circumstances the oxidation of methane to CO_2 is considered a viable option to reduce net greenhouse gas emissions, especially where the concentration of methane is well below its lower explosion limit of 5 %. Catalytic oxidation of methane is one of the most promising technologies to mitigate methane emissions as it can operate under a wide range of methane concentrations and at low reaction temperatures. The relatively low temperature of catalytic combustion for lean methane streams is an important advantage over other combustion technologies because of its potential to achieve a significant reduction in energy usage due to minimal heat losses from the process, significantly reduced requirements for the addition of fuel to the process as well as limited reaction of most contaminants with the solid catalyst. High conversion at high space velocities can be achieved, which in turn reduces the reactor size compared to high temperature combustion technology.

Palladium catalysts are well known to be highly active catalytic materials for the total combustion of methane. These catalysts exhibit high activity for oxidation of alkanes at low temperatures, especially when supported on high surface area oxides such as γ-alumina. The high specific surface area of the support enables high metal dispersion which in turn results in high catalytic activity [2]. A wide range of research has been performed in recent years to investigate the oxidation behaviour and catalytic properties of metal oxides [3] and noble metal based catalysts, with a number of comprehensive reviews published in this area [2, 4]. Recently, supported palladium catalysts were investigated experimentally in a laboratory-scale monolithic reactor study and by

simulation [5, 6] with the aim of developing more cost effective and efficient catalytic combustion technologies [6].

It is generally agreed that catalyst pre-treatment plays an important role in controlling the activity and durability of catalysts. Under oxygen-rich conditions, for palladium catalysts, it is suggested that PdO is formed and this phase represents the active phase for methane oxidation [2]. Other investigators claim that reduced Pd was an important active site for the catalytic combustion reaction [7-9], while others have suggested that the surface structure of the Pd-based catalysts changes with time-on-stream under fuel-rich conditions [10].

Although the coking of transition metal catalysts was reported during the combustion of methane at higher concentrations [11, 12] and reaction temperatures [12], we have observed the formation of significant quantities of carbonaceous material under highly oxygen-rich conditions which, to our knowledge, has not been previously reported. Furthermore, we have observed that methane can be activated at temperatures as low as 180 ºC, which could have important consequences for development of technologies for the low temperature catalytic combustion of methane.

The dependency of light off curves and overall catalytic activity depends on the pre-treatment history of catalysts and the deactivation behaviour needs further investigation in order to improve the performance of the catalytic system. Moreover, the chemical nature of carbon deposits, identified as Pd carbide [13] formed under reaction conditions is under debate [14].

In this study, we examined the effect of pre-treatment conditions on the activity of palladium supported on aluminium catalyst for combustion of air mixtures containing low concentrations of methane (0.2-0.8%). We observed the formation of carbonaceous deposits and are able to correlate coke deposition with catalyst activation procedures. We also examined catalyst deactivation during time-on-stream methane combustion experiments undertaken in conditions where the level of methane conversion was over 90%.

4.2. Experimental

4.2.1. Catalyst Preparation

Catalysts containing 0.1-1.2 wt% Pd were prepared by wet impregnation of an alumina (gamma and delta Al_2O_3, Chem-Supply) support with a Pd (II) nitrate solution (10 wt% in 10 wt% nitric acid, Sigma-Aldrich). The dried catalyst (110 °C) was ground, pressed and sieved to 250-400 μm. The solid was then calcined in air at 500 ºC (40 ml min^{-1}) for 1 h in a tubular fixed-bed reactor and purged with helium (40 ml min^{-1}) for 30 min. The sample was then reduced in 99.99% H_2 at 300 ºC (20 ml min^{-1}) for approximately 2 h and the activation was completed by purging with helium while bringing the temperature to the desired reaction value (calcined-reduced sample). Some Pd/Al_2O_3 catalyst samples were activated at 500 ºC for 1 h in air in order to investigate the effect of pre-treatment conditions on the catalyst activity (calcined sample).

4.2.2. Catalytic activity measurements

The catalytic measurements were performed using a tubular stainless steel micro reactor. The composition of the reaction mixtures was varied in the range of 0.2-0.8% of CH_4, balanced with air at various flow rates. The inlet and outlet mixture compositions were analysed using a gas chromatograph equipped with a thermal conductivity detector (TCD) and concentric packed column (Alltech CTR-1). Methane (99.95%) and compressed air flows were adjusted by means of mass flow controllers. Reactor feed and effluent streams were injected on the GC column through a Valco 6-port injection valve. In all experiments, helium was used as a GC carrier gas. Injections were repeated three times and the standard deviation of the conversion was ± 3%. No methane conversion was detected when the feed was heated up to 650 ºC in the absence of catalyst. Details of the experimental setup are shown in Supporting Information (SI) Figure A.1.

4.2.3. Characterization of catalysts

The surface area of fresh and used catalysts were determined by nitrogen adsorption at 77 K using a Gemini 11 2370 surface area analyser using the Brunauer-Emmet-Teller (BET) method. Powder X-Ray diffraction patterns of fresh and used catalysts were examined using Cu Kα radiation with a Philips X'Pert diffractometer. Diffractrograms were collected in the 2θ angle range from 2° to 90° with 0.008° 2θ step resolution. For surface analysis, ex-situ X-ray photoelectron spectroscopy (XPS) was carried out using Al Kα radiation. The emitted photoelectrons were analysed using a PHOIBOS 100 hemispherical analyser manufactured by SPECS GmbH. Used samples were collected immediately after terminating the reaction by cooling in helium and the catalyst was then stored in a sealed container. The sample was mounted on an XPS sample holder

using indium tape. The exposure time of samples in air was minimised in order to reduce the likelihood of water adsorption or oxidation of the carbon deposited on the catalyst. The energy scale was shifted relative to the adventitious carbon peak at 284.6 eV. The shift was cross checked with the position of O 1s from Al_2O_3, which is found at 531 eV. For measuring the metal dispersion of the catalysts, pulse chemisorption experiments utilising a mixture of 10% H_2 in N_2 were performed at 109.1 ºC using Micromeritics 2910 AutoChem (Micromeritics Instruments Corp., USA). Transmission Electronic Microscopy (TEM) images of the sample were taken with a JEOL 2100 TEM.

The elemental composition of the catalyst was determined by inductively coupled plasma optical emission spectrometry (ICP-OES) using a Varian 715 ES spectrometer. Prior to analysis, the sample was dissolved in a solution of 4.5 ml HNO_3 (65 %); 4.5 ml HCl (37 %); 3 ml HBF_4 (50 %) and 600 µl Tm internal standard (1,000 ppmv) as added as an internal standard. All samples were then digested using a Milestone Start D Microwave Unit for a minimum time of 2 h. No sample contamination of nitrate was observed (detection limit of 30 ppm, based on the solid).

4.3. Results and Discussion

4.3.1. Catalytic activity

Pre-treatment procedures were varied for the 1.2 wt% Pd/Al_2O_3 catalysts in order to examine the effect of oxygen and hydrogen pretreatment on the catalytic activity. The methane conversion curves obtained from these samples are plotted in Fig. 4.1. At lower temperatures (below 280 ºC), the catalyst activated in air shows a higher

conversion level compared to the sample reduced in hydrogen. At temperatures higher than T_{50} (temperature at 50% conversion) the activity of both samples was essentially the same. In addition, the calcined-reduced sample demonstrates the same activity during heating and cooling cycles, i.e., showing no hysteresis (see Fig. A.2 of SI).

The surface area of a 1.2 wt% Pd/Al_2O_3 catalyst decreased after reaction, suggesting pore blocking of the support (see Table 4.1). Consistent with our carbon balance analysis, we suggest that methane is reducing the Pd species under our reaction conditions and forming carbonaceous deposits. The existence of these deposits has been substantiated using XPS analysis (see below). At higher temperatures (once the Pd is reduced) these deposits are removed as indicated by the observation of a carbon balance in excess of 100 % at elevated temperatures.

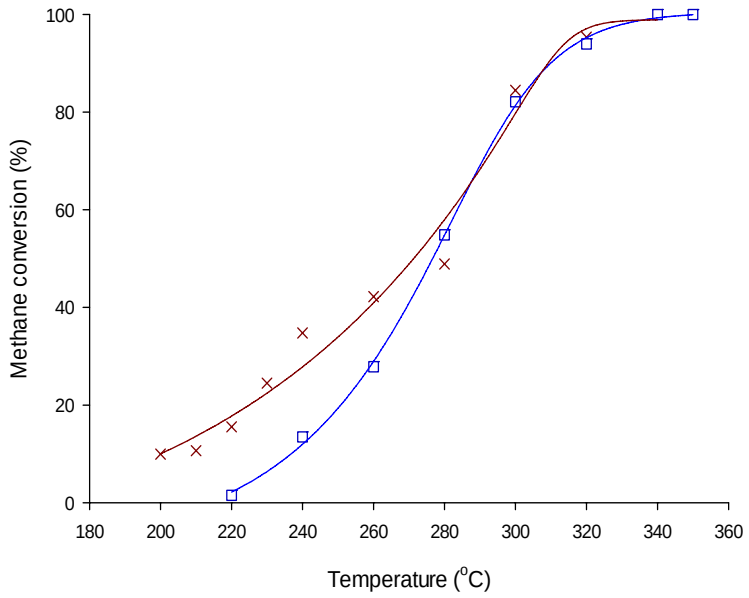

Fig. 4.1. Methane conversion over 1.2 wt% Pd/Al_2O_3 catalysts activated in air-He-H_2 (calcined-reduced) and activated in air (calcined). Inlet mixture: 6,000 ppm CH_4 in air, 250 mg catalyst, GHSV = 33,000 h^{-1}. × = calcined sample, □ = calcined-reduced sample.

Table 4.1. BET Surface area.

No	Sample	Surface Area (m^2 g^{-1})
1.	Alumina, 99%	63.7
2.	0.1 wt. % Pd/Al_2O_3, fresh	61.1
3.	1.2 wt. % Pd/Al_2O_3, fresh	58.6
4.	1.2 wt. % Pd/Al_2O_3, used	47.5

It is suggested that a low oxidation state palladium species is formed at higher temperatures, which is the active phase for complete oxidation. The oxidised Pd can activate methane as indicated by the high conversion at temperatures below 350 °C. The presence of PdO at lower temperatures has been reported in the published literature where it was suggested, that the oxidized PdO phase is more active compared to its reduced form [10]. Without a separate reduction step, PdO starts reacting with methane at T_{10} = 180 ºC while over a hydrogen reduced Pd/Al_2O_3 catalyst a similar conversion is achievable only at temperatures ≥ 220 ºC [10].

Figure 4.2 shows the methane conversion and carbon balance changes of methane oxidation experiments over Pd/Al_2O_3 catalyst at a reaction temperature of 180 °C where the feed is 5,000 ppm CH_4 in air. To illustrate the differences in carbon balance at low and high temperatures the analysed concentrations are compared in Fig. A3 of the supplementary section. These data support the argument that CH_4 is adsorbed and reacts on the catalyst to form carbonaceous species at lower temperatures consistent with the observed deficit in the mass balance. Along with a decrease in methane conversion, the carbon balance increases with time on stream, and approaches 100 % at 180 °C. This

indicates that after 40 min on stream, maximum coverage with coke is observed. The formation of coke is quite surprising, because only 0.5 % methane was present in the air and it is evident that methane is being activated at a very low temperature. The amount of coke deposited at 180 °C corresponds to approximately 1×10^{-5} mol C g^{-1} of catalyst, compared with a loading of surface Pd species (based on Pd $3d_{5/2}$ photoelectrons) of 4×10^{-5} mol Pd g^{-1} of catalyst. Thus only a fraction of accessible Pd is covered by coke and consequently only a fraction was involved in methane activation at low temperatures. To determine the fate of the carbon species deposited, spent catalyst was heated in zero-air from 400 ºC to 800 ºC, where CO_2 was detected in the outlet of the reactor and which suggests the existence of coke on the catalyst. The CO_2 was quantified and the balance with the deposited carbon closed within 0.4 % (relative), suggesting that all the carbon could be removed by heating in air at 400 ºC. The existence of carbon deposits was further substantiated by TGA and TOC analyses. Carbon deposition on Pd catalysts with methane has been reported before at low temperatures by Dropsch and Baerns, but only under higher methane concentrations (20 % CH_4 balanced He) [15].

It is interesting to note that at higher temperatures (350 °C), we observed only minor catalyst deactivation of palladium supported on alumina catalyst in the time on stream experiment. There was only a 5 % drop in methane conversion from 100 % conversion observed over a period of 35 h for the catalyst calcined in air (Fig. 4.3, inlet methane = 6,000 ppm). It should be noted that the catalyst was operating at close to 100 % conversion. However, a significant level of deactivation was observed at lower space velocities and temperatures during time-on-stream experiments using the Pd catalyst (see Figure A.4 of SI). It was explained that the deactivation with time on stream is due

to transformation of active sites (PdO) into less active sites, $Pd(OH)_2$ [16, 17], which can be a result of poisoning of the active sites by H_2O produced by the reaction. By purging the deactivated catalyst in a dry carrier gas stream above 500 °C, the initial catalytic activity was at least partially restored.

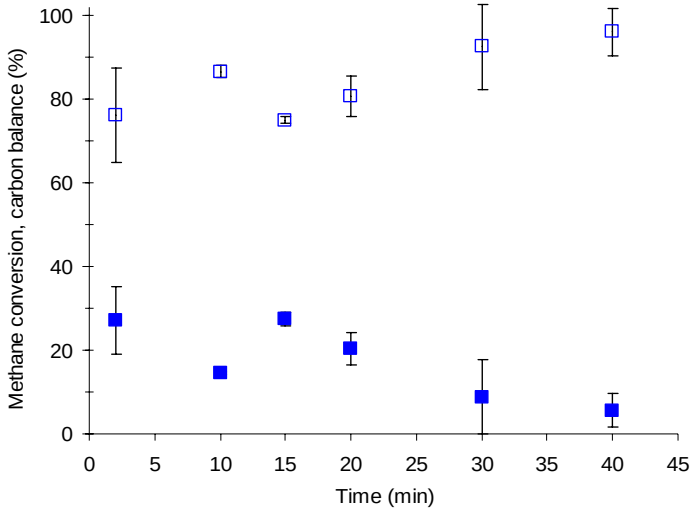

Fig. 4.2. Carbon balance and methane conversion as a function of time during methane oxidation over 1.2 wt% Pd/Al_2O_3 catalysts at 180 °C. The sample was pre-treated in air at 500 ºC for 1 h. Inlet mixture: 5,000 ppm CH_4 in air, 250 mg catalyst, GHSV = 33,000 h^{-1}. ■ = methane conversion; □ = carbon balance.

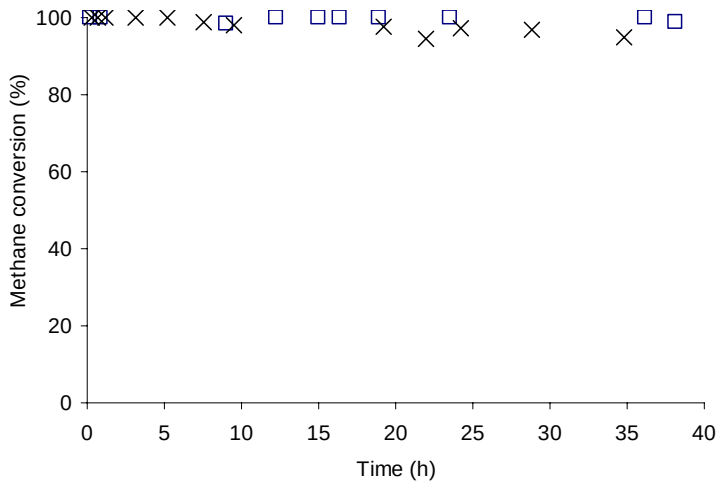

Fig. 4.3. Evaluation of time-on-stream behaviour. □ = at 350 °C over 1.2 wt. % Pd/Al_2O_3 catalysts activated in air and subsequently reduced in hydrogen (300 °C), feed = 6,000 ppm CH_4 in air at space velocity of 33,000 h^{-1}; × = calcined in air.

We also observed hydrogen in the product stream of this reactivation process which is confirming the reverse decomposition of $Pd(OH)_2$ into a PdO phase. This is in agreement to what has been reported by Roth et al. and Castellazzi *et al*.[18, 19].

Methane conversion as a function of reaction temperature at different GHSV's as shown in Fig. 4.4 indicates that the Pd-based catalysts remain active, even at very high space velocities. The light-off temperature (T_{10}, the temperature in which noticeable oxidation occurs) at a gas velocity of 50,000 h^{-1} was 240 ºC, while at the same temperature there is no significant methane conversion at higher space velocities. At 50,000 h^{-1} maximum conversion was achieved at the reaction temperature of 330 ºC, while the air-methane mixture at a GHSV of 80,000 h^{-1} requires temperatures of up to 350 ºC for complete combustion. In addition, when the space velocity was increased up to 200,000 h^{-1}, the level of highest conversion of methane was achieved at 370 ºC. In the temperature range between 280 °C and 320 °C, an almost linear dependency of the conversion with space velocity was observed, similar to what others have reported in methane oxidation over magnesium and manganese supported catalysts in plug flow reactors [20, 21]. The methane combustion outside this temperature range is likely to become mass or heat transfer controlled [4].

The effect of palladium loading on the catalytic combustion was investigated using 0.1 wt% and 1.2 wt% Pd supported on gamma alumina catalysts (see Fig. A.5 of SI). In this experiment the inlet methane concentration was set at 6,000 ppm where the flow rate and GHSV were maintained at 33,000 h^{-1}. It was found by Cullis and Willatt that the loading of precious metal on the support contributes significantly to catalyst activity at much higher CH_4 concentration [22]. The light off temperature of a feedstock

containing 0.6 % methane in air is much lower over 1.2 wt% Pd compared to the 0.1 wt% Pd/Al_2O_3 catalyst (see SI). Low conversion of methane over 0.1 % loading was observed at 300 ºC while using 1.2 wt% Pd/Al_2O_3 catalyst at this temperature 80 % methane was converted to CO_2. Estimation of the turnover number suggested a significant difference in activity between the catalysts (4×10^{-2} s^{-1} at 250 ºC for 1.2 wt% Pd, (GHSV = 200,000 h^{-1}) and 9.5×10^{-3} s^{-1} for 0.1 wt% Pd (GHSV = 10,000 h^{-1} conversion over both catalysts was below 5 %), which is consistent with previous studies [19, 23]. This change suggests a variation of the chemical properties of the active sites which is influenced by the loading and particle size. Even at the low methane concentrations used in this study, a clear trend of increased activity with catalyst loading is observed. Interestingly, the lower palladium loaded sample also shows rapid deactivation at temperatures higher than 450 ºC. Over this catalyst, 100 % oxidation could not be achieved at temperatures as high as 650 ºC.

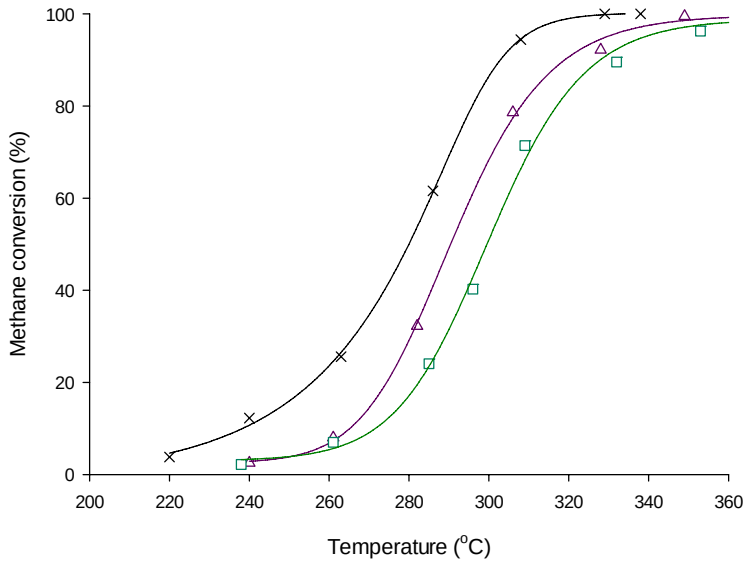

Fig. 4.4. Methane conversion over Pd/Al_2O_3 catalysts as a function of temperature at various space velocities. Feed: 8,000 ppm CH_4 in air. Activated in air at 500 ºC for 1 h, purged with He for 30 min at 300 ºC and reduced in H_2 at 300 ºC for 2 h. × = 50,000 h^{-1}; Δ = 80,000 h^{-1}; □ = 200,000 h^{-1}.

4.3.2. The nature of the sites active in methane combustion

In general, the specific surface areas of all samples were in the range of 50-60 $m^2 g^{-1}$ as listed in Table 4.1. An increase in the palladium loading decreased the surface area of the catalyst slightly. The used 1.2 wt% Pd/Al_2O_3 catalyst has a BET surface area of 47.5 $m^2 g^{-1}$ while the fresh sample exhibits 58.6 $m^2 g^{-1}$ disclosing a 19 % loss of surface area of the Pd/Al_2O_3 catalyst during methane oxidation.

XRD patterns of palladium-based catalysts, in comparison with γ-δ alumina, reveal minute Pd or PdO reflections (identified by slightly increased intensities and widths of reflections from the support) consistent with the low metal loading and the highly dispersed nature of the palladium particles on the support. H_2-chemisorption analysis suggested a dispersion level of 68 % for the palladium calcined in air (see Supporting Information in Appendix B). Based on this measurement, it is estimated that the average size of active palladium particles is 1.6 nm. This is consistent with the XRD result. For Pd/Al_2O_3 reduced in H_2, the dispersion decreases to 9 % and the average particle diameter to 12.2 nm. This lower dispersion level is likely due to sintering of Pd in the hydrogen atmosphere, which is substantiated by TEM measurements as reported in the Supporting Information. The images of the palladium samples suggest that the palladium particle size of the reduced sample is larger than the calcined Pd/Al_2O_3 (see Fig. A.6 and A.7 of Supporting Information).

Fig. 4.5a displays Pd 3d spectra of Pd/Al_2O_3 catalyst calcined in air and subsequently reduced in hydrogen. Based on the peak shape of the Pd 3d peak, the presence of two Pd

species in the reduced (H_2 treated) catalyst can be suggested. Fitting the Pd $3d_{5/2}$ peak to a Gaussian Lorentzian curve results in two different photoelectron binding energies (BE) at 335.0 eV (Pd $3d_{5/2}$ core level) and 336.3 eV (Pd $3d_{5/2}$ core level). In Table 4.2, the species, atom percentage and Pd/Al ratio are summarized. The chemical species exhibiting the peak at 336.3 eV is identified as Pd^{2+}[24]. The BE peak position at 335.0 eV of the second peak of the reduced sample suggests formation of Pd^0 (metallic palladium clusters) similar to the XPS results reported by Tompos and co-workers [25]. As illustrated in Fig. 4.5b, for calcined Pd/Al_2O_3, the peaks are more intense and slightly broader (Pd $3d_{5/2}$) and fitting an additional peak did not result in significant decrease of Chi^2 of the overall fit. Thus, only a single peak was fitted for Pd $3d_{3/2}$ and Pd $3d_{5/2}$, at BEs of 341.9eV and 336.6 eV, respectively. It is inferred that subsequent to activation in air, only one Pd species exists on the surface.

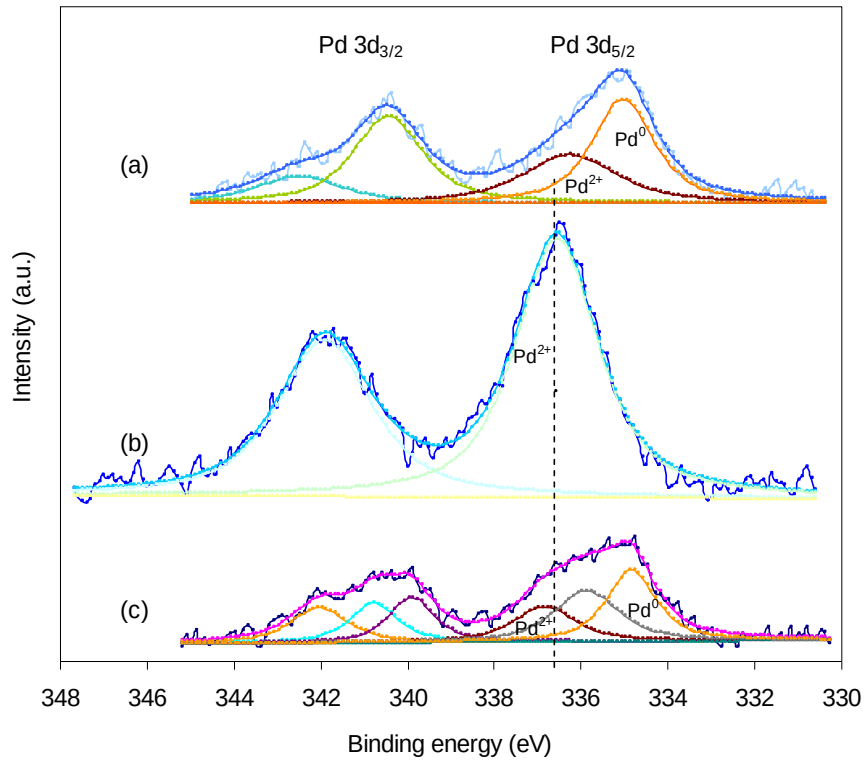

Fig. 4.5. XPS spectra of Pd 3d core level region of Pd/Al_2O_3 catalysts, (a) calcined-reduced sample, (b) calcined sample, (c) coked sample.

Table 4.2. XPS peak position and surface composition of Pd/Al_2O_3 catalysts

	Sample	Peak position Pd $3d_{5/2}$ (eV)	Species and atom percentage	Atomic surface ratio Pd/Al
a.	Calcined-reduced Pd/Al_2O_3	335.0 336.3	(Pd^0) 59% (Pd^{2+}) 41%	0.0046
b.	Calcined Pd/Al_2O_3	336.6	(Pd^{2+}) 100%	0.0055
c.	Coked Pd/Al_2O_3	334.9 335.9 336.9	(Pd^0) 40% (Pd^{2+}) 36% (Pd^{2+}) 24%	0.0047

In Fig. 4.5c, the X-ray photoelectron spectrum of a coked sample reveals three different species at 334.9 eV, 335.9 eV and 336.9 eV (Pd $3d_{5/2}$ core level), suggesting reaction of Pd^{2+} upon low temperature treatment of the oxidised Pd sample with methane and resulting in the formation of an additional Pd^{2+} species and a Pd^0 species. This coked sample was activated in air only. It may be noted that the binding energy of the Pd $3d_{5/2}$ peak identified as Pd^{2+} changed from 336.6 eV to 336.9 eV compared to the precursor sample, i.e., the sample calcined in air. This BE change can be related to the formation of carbonaceous compound in the vicinity of the Pd^{2+} species or changes in the particle size. The Pd $3d_{5/2}$ peak at 335.9 eV can be attributed to PdC_x, which has been reported previously [26]. The BE in the present study are observed to be at a slightly higher energies than corresponding literature values. BE changes in small noble metal particles are not only a result of the oxidation state but also the surrounding atoms (due to changes in the Madelung potential and relaxation) [27, 28]. Meanwhile, the peak at BE of 334.9 eV is consistent with Pd^0 peak position reported in the literature [25, 26]. This is a very low temperature for reduction of Pd^{2+} to Pd^0 with methane [29, 30]. We suggest the discrepancy with the literature may be a result of the decomposition of highly active carbide species that have formed at low temperatures (180 °C).

The particle diameter of 1.2 nm and 1.8 nm that were determined in the present study are within the range of significant differences of nanoparticles compared to bulk species [31]. The difference in BE of the carbide peak compared to the literature [26] is more likely the result of the smaller particle size or the stoichiometry of PdC_x formed on nanoparticles compared to the single crystal studies. The stoichiometry of the carbide species is also expected to have an influence on the photoelectron lines, which might explain the small differences between the present findings and the literature. Evidence of a carbide species was also found in the C 1s spectra (see Fig. 4.6).

The spectra of the carbon 1s core level region of used Pd/Al_2O_3 catalysts are shown in Fig. 4.6. The peak shape and width of the C 1s peak suggests that carbon is present in the form of multiple species (coked sample). For clean samples (without coking), a single peak at 284.6 eV can be observed, which is identified as adventitious carbon. For the coked sample, significant peak broadening and a shoulder peak at 281.5 eV was observed. Thus, two peaks were fitted using the same peak shape as above (30:70 Gaussian:Lorentzian) one peak corresponding to adventitious carbon at a BE of 284.6 eV and a peak at BE = 281.5 eV. The peak at 281.5 eV most likely originates from the formation of carbide-like species. We cannot exclude the possibility of aluminium carbide formation, but suggest aluminium carbide formation to be unlikely due to a constant FWHM of the Al 2p line for the coked and un-coked sample which suggests absence of any aluminium phases other than oxide. In contrast, a Pd $3d_{5/2}$ peak at 335.9eV was observed in the coked samples, providing further evidence for the formation of a PdC_x phases (see above). The peak position at 281.5 eV is, however, found at slightly lower binding energies than Pd carbide and Al-carbides [32].

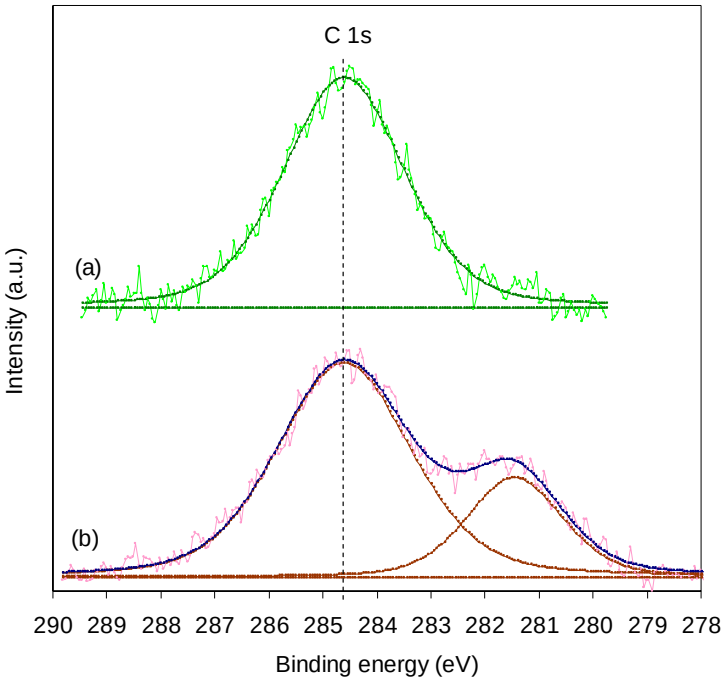

Fig. 4.6. XPS spectra of C 1s core level region of used Pd/Al_2O_3 catalysts: (a) Without coking, (b) coked sample.

The C 1s peak formed from CF_2Cl_2 on Pd catalysts was reported [33] (suggested to be carbide) to be at 282.9 eV, while carbon monoxide decomposition over Pd/alumina led to a carbide C 1s peak at 282 eV [34].

The above illustrates that significant changes in the BE of carbide species have been reported in the literature and may reflect changes in particle size and also stoichiometry of the carbide phase when compared to data reported in the literature. Pd carbide formation from methane was also inferred from XRD measurements of Pd alumina catalysts [35], supporting our assertion of the formation of a carbide species in the present study. Furthermore, we observed an additional peak with a shift of approximate -1.0 eV of the Pd $3d_{5/2}$ BE (Pd^{2+}), which is consistent with an increase of the electron density surrounding Pd^{2+} resulting from the formation of carbide. The C1s peak at 281.5 eV could also originate from graphitic species on alumina but the Pd $3d_{5/2}$ peak at 335.9

eV is evidence for the formation of an additional species formed on the surface. The low binding energy of the C1s species suggests that the carbon is negatively charged or bound to an electropositive species such as Pd. More importantly, the presence of an additional C1s peak strongly supports the findings from the reactor studies, where carbon deposition was inferred as the carbon balance and the conversion data presented in Fig. 4.1 and 4.2. Note that increasing the temperature of the coked sample to 320 °C results in a decrease of the intensity of the C1s peak at 281.7 eV (not shown), suggesting decomposition of the carbide species which is consistent with the formation of CO_2 upon heating to 400 °C.

4.4. Conclusion

Palladium on alumina catalysts were prepared and activated under controlled conditions. Pd/Al_2O_3 catalysts calcined in air and then reduced in hydrogen exhibit a lower catalytic activity at low temperatures compared to those activated in air only. Interestingly, even under very lean conditions, methane is converted at 180 °C and carbon is formed on palladium catalysts. Upon increasing the reaction temperature, the catalysts are reduced by methane and exhibit similar activity to catalysts reduced with hydrogen. Based on XPS analysis it is concluded that the carbon formed at 180 °C is most likely present in the form of a Pd-carbide species. Heating the coked sample to 320 °C in air converts the carbide species to CO_2.

References

1. Solomon, S., D. Qin, M. Manning, Z. Chen, M. Marquis, K.B. Averyt, M. Tignor, and H.L. Miller, *Climate change 2007: the physical science basis*, in *Contribution of working group I to the fourth assessment report of the*

intergovernmental panel on climate change. 2007, Cambridge University Press: Cambridge, United Kingdom and New York, NY, USA

2. Gelin, P. and M. Primet, *Complete oxidation of methane at low temperature over noble metal based catalysts: a review.* Applied Catalysis B: Environmental, 2002. 39: p. 1-37.

3. Li, J., H. Fu, L. Fu, and J. Hao, *Complete combustion of methane over indium tin oxides catalysts.* Environmental Science & Technology, 2006. 40(20): p. 6455-6459.

4. Lee, J.H. and D.L. Trimm, *Catalytic combustion of methane.* Fuel Processing Technology, 1995. 42: p. 339-359.

5. Gosiewski, K., Y.S. Matros, K. Warmuzinski, and M. Jaschik, *Homogeneous vs. catalytic combustion of lean methane - air mixtures in reverse-flow reactors.* Chemical Engineering Science, 2008. 63: p. 5010 - 5019.

6. Su, S. and J. Agnew, *Catalytic combustion of coal mine ventilation air methane.* FUEL, 2006. 85: p. 1201-1210.

7. Oh, S.H., P.J. Mitchell, and R.M. Siewert, *Methane oxidation over alumina-supported noble metal catalysts with and without cerium additives.* Journal of Catalysis, 1991. 132(2): p. 287-301.

8. Hicks, R.F., H. Qi, M.L. Young, and R.G. Lee, *Structure sensitivity of methane oxidation over platinum and palladium.* Journal of Catalysis, 1990. 122(2): p. 280-294.

9. Lyubovsky, M. and L. Pfefferle, *Complete methane oxidation over Pd catalyst supported on α-alumina. Influence of temperature and oxygen pressure on the catalyst activity.* Catalysis Today, 1999. 47(1-4): p. 29-44.

10. Choudhary, T.V., S. Banerjee, and V.R. Choudhary, *Influence of PdO content and pathway of its formation on methane combustion activity.* Catalysis Communication, 2005. 6(2): p. 97-100.

11. Euzen, P., J.H. Le Gal, B. Rebours, and G. Martin, *Deactivation of palladium catalyst in catalytic combustion of methane.* Catalysis Today, 1999. 47(1-4): p. 19-27.

12. O'Shea, V.A.D., M.C. Alvarez-Galvan, J. Requies, V.L. Barrio, P.L. Arias, J.F. Cambra, M.B. Guemez, and J.L.G. Fierro, *Synergistic effect of Pd in methane combustion $PdMnO_x/Al_2O_3$ catalysts.* Catalysis Communications, 2007. 8(8): p. 1287-1292.

13. Seriani, N., F. Mittendorfer, and G. Kresse, *Carbon in palladium catalysts: a metastable carbide.* Journal of Chemical Physics, 2010. 132(2): p. 024711-8.

14. Tew, M.W., M. Nachtegaal, M. Janousch, T. Huthwelker, and J.A. van Bokhoven, *The irreversible formation of palladium carbide during hydrogenation of 1-pentyne over silica-supported palladium nanoparticles: in situ Pd K and L3 edge XAS.* Physical Chemistry Chemical Physics, 2012. 14(16): p. 5761-5768.

15. Dropsch, H. and M. Baerns, *Interaction of methane with supported Pd catalysts studied by adsorption microcalorimetry and TPD/TPSR techniques.* Applied Catalysis A: General, 1997. 165(1–2): p. 159-169.

16. Cullis, C.F., T.G. Nevell, and D.L. Trimm, Journal of the Chemical Society, 1972. 68(1): p. 1406.

17. Burch, R., F.J. Urbano, and P.K. Loader, *Methane combustion over palladium catalysts: the effect of carbon dioxide and water on activity.* Applied Catalysis A: General, 1995. 123(1): p. 173-184.

18. Roth, D., P. Gélin, M. Primet, and E. Tena, *Catalytic behaviour of Cl-free and Cl-containing Pd/Al_2O_3 catalysts in the total oxidation of methane at low temperature.* Applied Catalysis A: General, 2000. 203(1): p. 37-45.

19. Castellazzi, P., G. Groppi, P. Forzatti, and A. Baylet, *Role of Pd loading and dispersion on redox behaviour and CH_4 combustion activity of Al_2O_3 supported catalysts.* Catalysis Today, 2010. 155: p. 18-26.

20. Berg, M. and S. Järås, *Catalytic combustion of methane over magnesium oxide.* Applied Catalysis A: General, 1994. 114(2): p. 227-241.

21. Choudhary, V.R., B.S. Uphade, and S.G. Pataskar, *Low temperature complete combustion of dilute methane over Mn-doped ZrO_2 catalysts: factors influencing the reactivity of lattice oxygen and methane combustion activity of the catalyst.* Applied Catalysis A: General, 2002. 227(1–2): p. 29-41.

22. Cullis, C.F. and B.M. Willatt, *Oxidation of methane over supported precious metal catalysts.* Journal of Catalysis, 1983. 83: p. 267-285.

23. Roth, D., P. Gelin, A. Kaddouri, E. Garbowski, M. Primet, and E. Tena, *Oxidation behaviour and catalytic properties of Pd/Al_2O_3 catalysts in the total oxidation of methane.* Catalysis Today, 2006. 112: p. 134-138.

24. Naumkin, A.V., A. Kraut-Vass, S.W. Gaarenstroom, and C.J. Powell, *NIST standard reference database 20, version 4.1*. 2012.

25. Tompos, A., J.L. Margitfalvi, M. Hegedus, A. Szegedi, J.L.G. Fierro, and S. Rojas, *Characterization of trimetallic Pt-Pd-Au/CeO_2 catalysts combinatorial designed for methane total oxidation.* Combinatorial Chemistry & High Throughput Screening, 2007. 10: p. 71-82.

26. Balmes, O., A. Resta, D. Wermeille, R. Felici, M.E. Messing, K. Deppert, Z. Liu, M.E. Grass, H. Bluhm, R. van Rijn, J.W.M. Frenken, R. Westerstrom, S. Blomberg, J. Gustafson, J.N. Andersen, and E. Lundgren, *Reversible formation of a PdC_x phase in Pd nanoparticles upon CO and O-2 exposure.* Physical Chemistry Chemical Physics, 2012. 14(14): p. 4796-4801.

27. Bouwman, R. and P. Biloen, *Valence state and interaction of platinum and germanium on γ-Al_2O_3 investigated by x-ray photoelectron spectroscopy.* Journal of Catalysis, 1977. 48(1–3): p. 209-216.

28. Karhu, H., A. Kalantar, I.J. Väyrynen, T. Salmi, and D.Y. Murzin, *XPS analysis of chlorine residues in supported Pt and Pd catalysts with low metal loading.* Applied Catalysis A: General, 2003. 247(2): p. 283-294.

29. Ciuparu, D., N. Katsikis, and L. Pfefferle, *Temperature and time dependence of the water inhibition effect on supported palladium catalyst for methane combustion.* Applied Catalysis A: General, 2001. 216(1-2): p. 209-215.

30. Ciuparu, D., M.R. Lyubovsky, E. Altman, L.D. Pfefferle, and A. Datye, *Catalytic Combustion of methane over palladium-based catalysts.* Catalysis Reviews: Science and Engineering, 2002. 44(4): p. 593-649.

31. Marks, F.A., I. Lindau, and R. Browning, *Characterization of the Pd/α-Al_2O_3 supported cluster system.* Journal of Vacuum Science & Technology A, 1990. 8(4): p. 3437-3442.

32. Hinnen, C., D. Imbert, J.M. Siffre, and P. Marcus, *An in situ XPS study of sputter-deposited aluminium thin films on graphite.* Applied Surface Science, 1994. 78(3): p. 219-231.

33. Ahn, B.S., S.G. Jeon, H. Lee, K.Y. Park, and Y.G. Shul, *Hydrogenolysis of CFC-12 (CF_2Cl_2) over Pd/γ-Al_2O_3 pretreated with HCFC-22 (CHF_2Cl).* Applied Catalysis A: General, 2000. 193(1–2): p. 87-93.

34. Johánek, V., I. Stará, N. Tsud, K. Veltruská, and V. Matolín, *CO adsorption on Al_2O_3-supported Pd clusters: XPS study.* Applied Surface Science, 2000. 162–163(0): p. 679-684.

35. Sarkany, A., *Hydrocarbonaceous deposit assisted n-butane formation in hydrogenation of 1,3-butadiene over Pd catalysts.* Applied Catalysis A: General, 1998. 175(1-2): p. 245-253.

CHAPTER 5

Catalytic combustion of ventilation air methane (VAM) – long term catalyst stability in the presence of water vapour and mine dust

---

Published in:

Catalysis Science & Technology, 4(6):1793-1802 2014.

Appendix C supplied the supporting information of this chapter.

5.1. Introduction

Concerns over the rising concentration of greenhouse gases in the atmosphere have generally focused on carbon dioxide, although there is a growing emphasis on lowering methane emissions. Methane has been assigned a CO_2 greenhouse gas warming potential (GWP) of 25 over a 100 year time horizon [1], and the conversion of CH_4 to CO_2 is considered as a potentially viable approach to reduce net emissions of greenhouse gases. Underground ventilation air systems in "gassy" coal mines contribute significantly to net methane emissions, although the concentration of methane in the ventilation air stream is typically below 1 %. The high volumetric flow rates (typically 300 m^3 s^{-1}) and the subsequent net discharge of significant quantities of methane have generated interest in developing technologies to reduce VAM emissions [2]. As reported in the literatures [3, 4], besides air and methane, the VAM stream usually contains water (relative humidity = 70-100 %), CO_2 (<2.5 %), coal dust and others particles (such as calcium oxides, iron oxides, clay and quartz at dust loading range of 0.1-4.5 mg m^{-3}). It may also contains traces of CO, C_2H_6 (higher hydrocarbons), He, H_2, HCN, NH_3, NO_x, H_2S, and SO_2 (organic sulphur compounds).

Basically, mitigation and utilization technologies of VAM are classified into two categories, ancillary uses and principal uses [5, 6]. For the ancillary uses, the VAM gas is used as combustion air for boilers, turbines and internal combustion

engines while for principal uses the VAM is oxidized in a reactor to burn methane emission as well as produce the energy. One potential technological solution for treatment of ventilation air methane (VAM) is catalytic combustion, where methane is oxidized to carbon dioxide on a catalytically active solid surface. This flameless combustion is ideal for highly diluted air-methane streams, such as VAM, as the concentration of methane is outside the typical flammability range for methane in air. Production of NO_x is essentially absent and the reaction temperature is relatively low (generally below 500 ºC).

The catalytic oxidation of methane at low temperature has been extensively investigated, especially over Pd and Pt based catalysts. A comprehensive review of methane oxidation over noble metal based catalysts agrees that, the supported Pd catalysts are the most active materials [7]. However, palladium catalysts can be susceptible to poisoning by water vapour and other contaminants, which may result in severe deactivation when used in the catalytic combustion of VAM. Many recent investigations are focused on catalyst modifications which aim to enhance the durability of catalysts, especially developing resistance against water, sulfur compounds and particulates, as well as enhancing the absolute activity of the catalyst [7].

Although it is well recognised that water vapour strongly inhibits the activity of catalysts, the mechanism of catalyst deactivation is uncertain [8]. Some earlier studies reported that, the water produced by reaction significantly inhibits the

activity of Pd/Al_2O_3 at lower temperatures due to competition with methane for active sites [9-11]. Furthermore, irreversible deactivation can be induced by the presence of water vapour where the active site (PdO) transforms into a less active site (palladium hydroxide) [9-12]. The rate of Pd/Al_2O_3 catalyst deactivation in the presence of water, either present in the feed (such as the case in VAM) or produced in the catalytic combustion reaction, is heavily dependent on reaction temperature [10, 12]. The inhibiting effect of water is more significant at lower temperatures, becoming less apparent at temperatures higher than 450 °C [10]. Ciuparu *et al.* suggested that, the hydroxyl groups produced by the reaction are bound strongly on the surface and when additional external water is introduced, the surface becomes saturated and the rate of desorption of water from the surface of the catalyst is slowed due to the high concentration of water vapour in the feed and product streams [13]. Recent work by Schwartz *et al.* proposes an alternative explanation regarding deactivation of palladium supported on various metal oxides [8, 14]. They suggest that hydroxyl groups formed during the reaction accumulate on the catalyst support and inhibit the rate of exchange of oxygen between the support and PdO [14], a process which is necessary for surface reaction. This accumulation of hydroxyl groups prevents the migration of oxygen from the support to the Pd active site, as well as reducing the availability of oxygen involved in the oxidation of methane [8]. Clearly the primary mechanisms leading to deactivation is contentious, as it is possible that hydroxyls form on both the Pd site and the support in high concentration [8] and deactivation can potentially originate from surface on either the support or

palladium. Recently Di Carlo and co-workers reported improved tolerance against water poisoning in catalytic combustion of methane over palladium catalysts by using a support which inhibited or delayed the reaction between Pd and H_2O [15], however no long time stability test results were reported.

The application of a catalytic process for VAM abatement requires long-term evaluation of the catalyst stability and durability under humid feed condition. There are a limited number of reports on the hydrothermal stability tests of supported palladium catalysts. Yamamoto and Uchida reported longer-lasting hydrocarbon oxidation activity over Pt and Pd supported on alumina for lean-burn natural gas engine exhausts [16] where the total hydrocarbon conversion dropped from 80 % to 50 % within 2,500 h at 385 °C. Enhanced hydrothermal stability data during 3,200 h methane oxidation at 600 °C was published recently by Liu and co-workers [17]. Hydrothermal stability of the catalyst was improved by optimizing the Ni/Al ratio for Ni supported alumina catalysts. Notwithstanding, stability data was not reported at reaction temperatures less than 600 °C or the effect of CO_2 in the feed for long term catalyst stability tests. In addition, to our knowledge, there is no literature reporting on the effect of coal mine dust on the catalytic combustion of ventilation air methane.

In this paper, we report the effect of water and coal mine dust present on supported palladium catalysts during the catalytic combustion of a surrogate VAM gas. Attempts to improve the resistance of catalysts are explored by

determining differences in the physical and chemical characteristics of this catalyst (fresh and following long term activity testing). The stability of the Pd catalysts are evaluated for a long term activity under simulated ventilation air methane (where the feed contains components such as CH_4, CO_2, H_2O and air) in order to understand the deactivation phenomena of Pd/Al_2O_3 catalyst over a long period of time. The effect of coal mine dust is assessed by adding it to the catalyst and noting any effect it has on catalyst activity and stability. The combustion tests are operated under conditions where the level of methane conversion is maintained at or above 90 % by increasing the catalyst bed temperature.

5.2. Experimental

5.2.1. Catalyst preparation

Catalyst containing 1.2 wt% Pd/Al_2O_3 was prepared by wet impregnation of alumina (gamma and delta Al_2O_3, Chem-Supply) support with an aliquot of Pd (II) nitrate solution (10 wt% in 10 wt% nitric acid, Sigma-Aldrich) mixed using a mortar and pestle. Water was added drop-wise while mixing, until a paste was formed. The resulting paste was dried in the oven at 110 °C for approximately 20 h. The dried catalyst was then ground, pressed and sieved to 250-400 μm. A tubular fixed-bed reactor employed for calcination of dried solid catalyst in air at 500 ºC for 1 h followed by purging in helium for 30 min. For activation, the sample was reduced in H_2 at 300 ºC for approximately 2 h and subsequently purged with helium while slowly heating the catalyst to desired reaction

temperature. For long-term stability experiments, we use a commercially available 1.0 wt% Pd/Al_2O_3 (Sigma-Aldrich) and activated it in air at 500 ºC for 4 h followed by purging in H_2 for 2 h.

5.2.2. Catalyst characterization

The surface area of catalysts was measured by nitrogen adsorption at 77 K using Gemini 11 2370 surface area analyzer. Micromeritics 2910 AutoChem (Micromeritics Instruments Corp., USA) assessed the active particle size and metal dispersion by performing a number of H_2 pulse-chemisorption. Temperature-programmed desorption (TPD) analysis was carried out using a purpose built TPD apparatus with a Pfeiffer Prisma quadrupole mass analyser for detection. Transmission Electronic Microscopy (TEM) images of the sample served to capture by JEOL 2100. Palladium loading was quantified using Varian 715-ES inductively coupled plasma optical emission spectrometer (ICP-OES). Powder X-Ray diffraction patterns of catalysts and ventilation air dust were examined using Cu Kα radiation with a Philips X'Pert diffractometer. Diffractrograms were collected in the 2θ angle range from 2° to 90° with 0.008° 2θ step resolution.

For surface analysis, ex-situ X-ray photoelectron spectroscopy (XPS) was carried out using monochromated Al K alpha (energy 1486.68 eV) radiation and the emitted photoelectrons were analyzed using an ESCALAB250Xi manufactured

by Thermo Scientific, UK. To minimize the possibility of sample contamination, spent samples were immediately transferred into sealed containers after stopping the reaction by cooling in helium. The sample was mounted on the stub using indium tape. The energy in the XPS spectra was referenced to the adventitious carbon adsorption at 284.6 eV. The shift was cross checked with the position of O 1s from Al_2O_3 which is found at 531eV.

5.2.3. Catalytic activity measurement

The activity of the catalyst was measured in a tubular stainless steel micro reactor. The reactant mixture composition was varied in the range of 0.6-0.8 % of CH_4 balanced with air at various flow rates. The inlet and outlet mixtures were analyzed using a gas chromatograph equipped with a thermal conductivity detector (TCD) and concentric-packed single column (Alltech CTR-I). For humid feed experiments, the reactant mixture was passed through a saturator and a humidity probe (HumidiProbe, Pico Technology Ltd.) was installed at the outlet. The reaction temperature was measured with a thermocouple placed into the catalyst bed. At constant water vapour pressure, the repeatability of the data is 3.8 %.

For catalytic stability studies, a second, separate reactor set-up was used and operated continuously with varying conditions (temperature was increased in order to maintain a 90 % level of conversion for methane). Throughout the study, the feed concentration of methane and carbon dioxide were kept constant at 7,000

ppm and 10,000 ppm, respectively. During this experiment, our calculation on the total carbon at the inlet and outlet reactor results in average carbon balance of 96 %. The average water content was measured at approximately 85 % relative humidity (RH) for the saturator system used (T = 28 °C ± 3 °C, ambient), corresponding to a $H_2O_{(v)}$ pressure of approximately 32,000 ppm. As reported in the literature [4], the relative humidity of VAM stream is fluctuated, ranging from 70 % to 100 % RH. Thus, our saturator system was aimed producing humidity within this range. The feed gas hourly space velocity (GHSV) was maintained at 100,000 h^{-1} for the majority of the tests, although in a limited number of tests the GHSV was varied between 75,000 h^{-1} and 110,000 h^{-1} by manipulating the feed flow-rate. The targeted 90 % methane conversion was maintained by increasing the catalyst bed temperature as the catalyst deactivated during time on stream.

In order to investigate the effect of the presence of mine dust on the conversion of methane, a 1.0 wt% Pd/Al_2O_3 catalyst was mixed with mine dust and using the surrogate VAM feed described above, and the reaction carried out for more than 1,200 h of continuous operation. The amount of mine dust mixed into the catalyst is estimated as the quantity of dust deposited for one year of operation (dust loading assumption of 2 $mg \cdot m^{-3}$).

5.3. Results and discussion

5.3.1. The activity of catalyst under dry and wet feed

The activity of 1.2 wt% Pd/Al_2O_3 catalyst was measured in alternating dry and wet conditions at a space velocity of 200,000 h^{-1} as shown in Fig. 5.1. A shift in the T_{90} temperatures (which is a measure of activity) to higher values is observed with a humid compared to a dry feed VAM gas. Four alternating cycles of reactions were performed over the same catalyst, highlighting the deactivation phenomena. For the first cycle under a dry feed, complete combustion of methane was obtained at 380 ºC. The addition of approximately 3.2 vol% water vapour into the VAM feed slightly reduces the activity of the catalyst within the second cycle experiment. When feed was switched back to dry (cycle-3), the conversion curve overlaps with the 2nd cycle, highlighting the loss of activity under wet feed conditions. Significant deactivation is revealed in the next wet cycle condition (cycle-4) where complete methane combustion was achieved at temperatures in excess of 470 ºC.

Fig. 5.2 shows the time on stream behaviour of 1.2 wt% Pd/Al_2O_3 at 320 ºC under dry and wet conditions for 12 h. Combustion of 8,000 ppm of methane in dry air was changed to a wet feed (8,000 ppm CH_4, 40,000 ppm H_2O balance air) after 2 h reaction. Once the wet feed was introduced, a sharp decrease in conversion is observed (from ca. 90 % to 40 % conversion). The activity quickly returns to the initial value when the water vapour in the feed is turned off, suggestive of reversible deactivation phenomena occurring, at least within 2 h oxidation under wet feed condition.

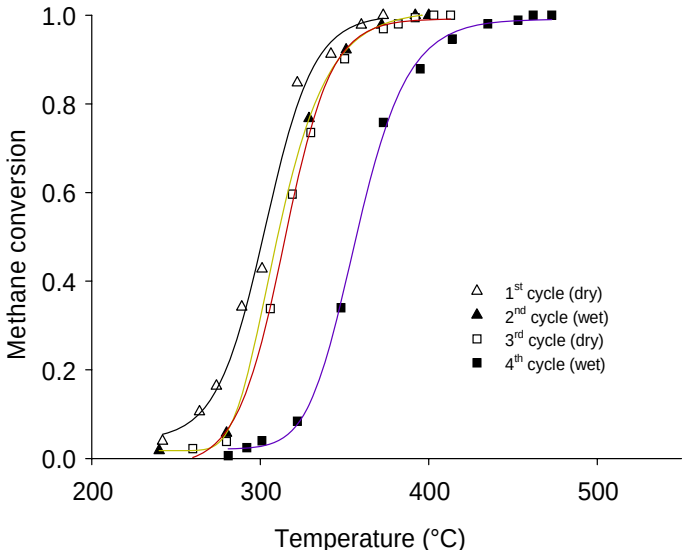

Fig. 5.1. Methane conversion as a function of reaction temperature of methane oxidation over 1.2 wt% Pd/Al_2O_3 catalyst using dry and wet feed. GHSV = 200,000 h^{-1}, CH_4 inlet = 8,000 ppm, wet feed water vapour = 3.2 %.

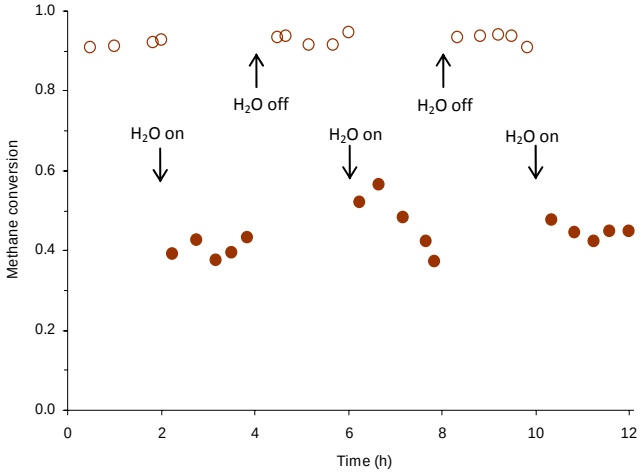

Fig. 5.2. Time-on-stream evolutions under dry and wet feed over 1.2 wt% Pd/Al_2O_3 catalyst at temperature of 320 ºC. GHSV = 100,000 h^{-1}, CH_4 inlet = 8,000 ppm, wet feed water vapour = 3.2 %. ○ = dry feed, ● = wet feed.

Repeating the jump experiments up to 12 h does not disclose significant loss in activity over a relatively short time period. This behaviour suggests a competition

for sites between water and methane [11, 18] occurring in this period. Over this relatively short time period we suggest that, species described as responsible for catalyst deactivation such as $Pd(OH)_2$ are absent, which is supported by our XPS findings (see below).

Our findings are consistent with the results published by others, especially the pulse experiments as reported previously over palladium catalysts [10, 11, 19, 20] under different reaction conditions. Over 4 % Pd/Al_2O_3 catalyst, Burch *et al.* [10] observed reversible deactivation (an instantaneous drop from 40 % to nearly 10 % conversion at 325 ºC) in catalytic activity. Likewise when 2.7 % of H_2O was added to a 1 % methane in air feed stream, other researchers concluded that, the formation of $Pd(OH)_2$ may not be important since palladium hydroxide under these conditions decomposes at the much lower temperature of approximately 250 ºC [21]. Roth and co-workers [11] also observed catalyst deactivation when exposed to a humid feed stream, with a slow initial deactivation stage followed by a dramatic drop in catalyst activity. The same authors suggested that, deactivation as a result of feed water vapour is reversible, while water produced in the reaction was suggested to cause irreversible catalyst deactivation. This was concluded from time-on-stream experiments for 6 h and 22 h runs respectively at 350 ºC over 1.9 wt% Pd/Al_2O_3 (1 % of H_2O was added to 1 % CH_4, 4 % O_2, balance N_2) [11]. It was suggested that, a progressive transformation of the active phase into less active phase occurred when water is present as a product [11]. In contrast to what can be presented in Fig. 2, within 2 h the activity is fairly

constant. This is most likely a result of the exposure time of the active Pd sites with wet feed being insufficient to transform PdO into $Pd(OH)_2$, therefore we do not observe any irreversible deactivation. It also might be because of the high space velocity we used in our experiment, the transformation rate of active sites into less active sites is slowed compared to what has been reported by Roth and co-workers [11].

5.3.2. Stability evaluation of Pd/Al_2O_3 catalyst

In order to understand the reasons for catalyst deactivation over long periods on stream, a 1.0 wt% Pd/Al_2O_3 catalyst was operated continuously for 1,150 hours. Prior to stability test, the activity of this catalyst has been tested and showed similar activities compared with 1.2 wt% Pd/Al_2O_3 catalyst (see Fig. S1 of supplementary information). The feed composition was 7,000 ppm CH_4, 10,000 ppm CO_2, 30,000 ppm H_2O balance air where GHSV was in the range of 75,000 h^{-1} – 110,000 h^{-1}. During the course of these experiments, the furnace temperature was periodically increased, in order to ensure that a conversion level of methane (in excess of 90 %) was achieved, mimicking the performance requirements for a large scale catalytic VAM mitigation system.

Fig. 5.3 shows the methane conversion as a function of reaction temperature for the system over this experimental period. The initial temperature of the system to achieve 90 % conversion was 350 °C, with this temperature increasing to 500 °C

at a time of 1,150 h. A significant rate of deactivation was observed during the first 80 h of reaction. In order to obtain high conversions, the bed temperature was increased from 320 °C to 420 °C during this period, ensuring the targeted 90 % conversion level of methane was re-established. The conversion level within the first 200 h of operation exhibits significant variation in activity. This is thought to be due to the initial deactivation phase of the catalyst, which appears to be comparatively fast. This result is detailed further in the ordinate which shows the catalyst bed temperature required to achieve 90 % methane combustion conversion. Please note that reoccurring of sharp drop in methane conversion is a result of a longer interval in bed temperature adjustment. The minor fluctuation in methane conversion level observed at nearly-fixed temperature of the furnace is mainly due the change in water vapour concentration which caused by changing in ambient temperature.

Following an initial deactivation period of the catalyst, methane conversion was maintained at 90 %, however it can be seen that after approximately 950 h, the conversion decreases to approximately 70 %. At this stage of the time-on-stream experiment, the GHSV was slowly reduced from 100,000 h^{-1} to 75,000 h^{-1} whilst maintaining the system temperature.

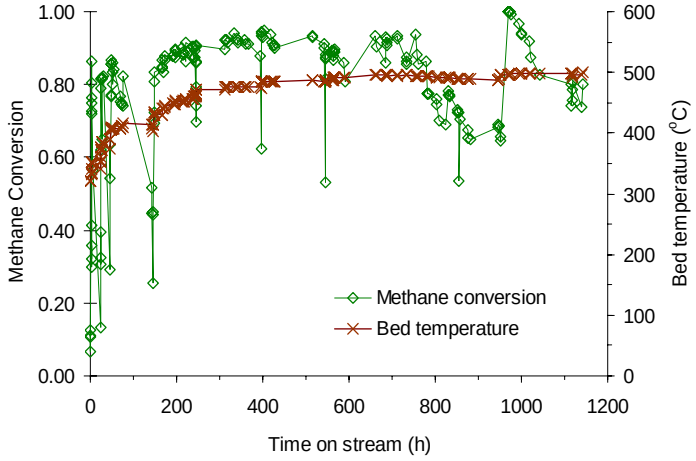

Fig. 5.3. Time-on-stream fractional methane conversion and corresponding reactor bed temperature over 1.0 wt% Pd/Al_2O_3 catalyst. Feed = 7,000 ppm CH_4, 10,000 ppm CO_2, 30,000 – 40,000 ppm H_2O balance air. GHSV = 75,000–110,000 h^{-1}. ◊= methane conversion, × = bed temperature.

This was done in an attempt to maintain the targeted 90 % methane conversion without having to further increase the catalyst temperature. This test, however, did not have a significant effect on methane conversion. The GHSV was then increased to 110,000 h^{-1} and the catalyst bed temperature increased to return the system to 90 % methane conversion. The catalyst bed temperature tends to plateau in the final stages of the run, suggesting that for long term use a constant temperature can be used to obtain stable conversion.

In order to investigate the long term effect of water produced from reaction, a VAM experiment under dry feed conditions was carried out for 1,600 h where the reactant was 7,000 ppm methane balance air at space velocity of 100,000 h^{-1}. The variation of the T_{90} temperatures is compared to VAM in a wet feed stream in Fig. 5.4. Similar to the conversion of a wet VAM feed stream, the temperature required to achieve in excess of 90 % conversion of CH_4 (T_{90}) increased over the

duration of the experiment. Under wet feed conditions, the experiment was run continuously for a total of 1,150 h with a catalyst bed temperature of 500 °C required to achieve 90 % methane conversion, while the dry VAM gas feed experiment was run for a total of 1,610 h with a final catalyst bed temperature of 450 °C required for T_{90}. To estimate the conversion of methane and in order to assess the influence of the different conditions for the long term, the data for both the dry and wet run were extrapolated. Empirically, a logarithmic function was found to yield the best fit for the experimental data. The estimation results in a final bed temperature of 555 °C for the wet feed and 500 °C for the dry feed over a period of duration of 8,760 h (1 year).

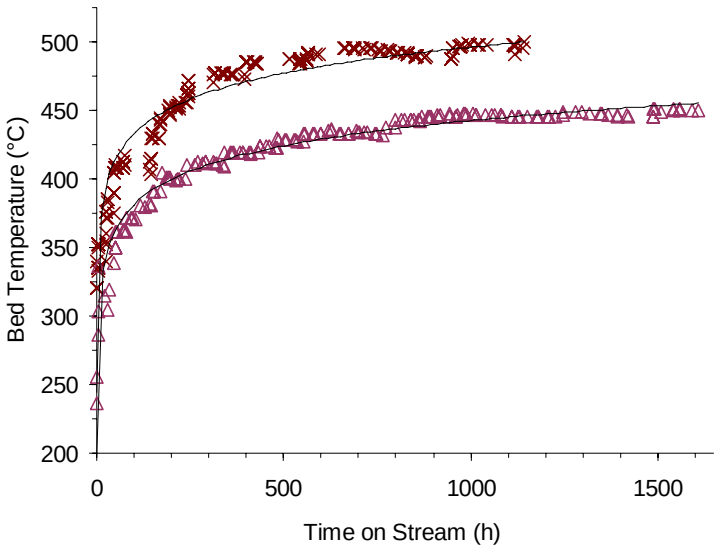

Fig. 5.4. Catalyst bed temperature required for 90 % CH_4 conversion for wet (30 000 – 40 000 ppm H_2O) and dry time on stream runs over 1.0 Pd/Al_2O_3 catalyst. Feed: 7000 ppm CH_4 balance air, GHSV = 100 000 h^{-1}. × = wet feed run; Δ = dry feed run.

The effect of coal mine ventilation air dust on the conversion of methane was assessed and a wet VAM stream was operated continuously for over 7 weeks, where 60.8 mg VAM dust was packed in front of the 200 mg of catalyst. This quantity of VAM dust corresponds to the amount of dust deposited on the catalyst over a year of continuous operation. Time-on-stream variability, and reaction bed temperature over a 1.0 wt% Pd/Al_2O_3 catalyst, is shown in Fig. 5.5. The feed was 7,000 ppm CH_4, 10,000 ppm CO_2, 32,000 ppm H_2O and balance air at space velocity of 100,000 h^{-1}. Significantly higher fluctuations in the conversion levels and temperatures of the bed were observed in these experiments compared to the long term experiments in the absence of dust. One of the reasons for this fluctuation is likely to be a result of the combustion of coal particles present in the VAM dust and channelling with resulting changes in the pressure drop across the catalyst and dust beds (ca. 0.1 bar). After ca. 700 h on stream, it was noticed that there was a significant decrease in methane conversion.

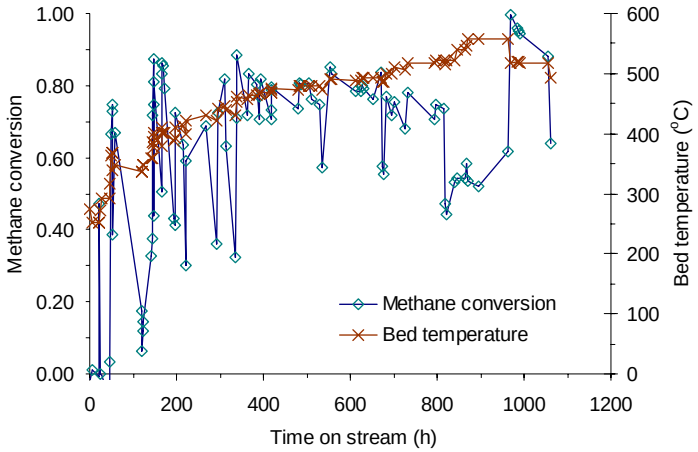

Fig. 5.5. Time-on-stream evolutions and reactor bed temperature over 1.0 wt% Pd/Al_2O_3 catalyst in the presence of VAM dust. Feed = 7,000 ppm CH_4, 10,000 ppm CO_2, 32,000 ppm H_2O balanced air. GHSV = 100,000 h^{-1}. ◇ = methane conversion, × = bed temperature.

The bed temperature was continually increased to 550 ºC over a period of 150 h (time on stream 950 h) in order to restore the conversion level to 90 %. As the conversion did not increase, it was suspected that the catalyst bed had shifted slightly, into a lower temperature zone of the furnace. The bed was then opened and it was confirmed that the catalyst bed had moved. After that, the catalyst was repacked and the experiment continued. Subsequent to repacking, the catalyst exhibited similar conversion levels observed before the bed movement. No difference in methane conversion and temperature were observed within the experimental error. This is an experimental artefact due to high volumes of VAM dust, which would not be present in a real VAM mitigation system.

5.3.3. Characterization of catalysts

The nitrogen adsorption isotherm experiment results in estimates of the Langmuir surface areas of 98.4 $m^2 \cdot g^{-1}$, 92.8 $m^2 \cdot g^{-1}$ and 193.4 $m^2 \cdot g^{-1}$ for γ-δ-Al_2O_3, 1.2 wt% Pd/γ-δ-Al_2O_3, and 1.0 wt% Pd/γ-Al_2O_3 (commercial catalyst), respectively. Note that the alumina phase used for catalysts prepared in these experiments is somewhat different to what has been used for commercial catalysts, confirmed by our XRD results. The surface area of the commercial catalyst is somewhat higher, although the activity of the catalysts is similar. Thus, as expected, the support surface area appears to have very little influence on catalytic activity. ICP-OES confirms the loading of 1.0 and 1.2 wt% of Pd on their supports respectively.

The XRD pattern of Pd/Al_2O_3 catalysts reveal minute reflections attributed to Pd or PdO phases (overlapping with support peaks, thus they were identified by slightly increased intensities and widths of support reflections), consistent with a low net metal loading and suggests small noble metal particles. The overlap with the support reflections and the small size makes particle size estimation from XRD difficult. As reported in our previous works, the particle size of the palladium was estimated from the results of pulse H_2-chemisorption at 109.1 ºC showing that the average catalyst particle diameter is 12.2 nm, corresponding to a 9.2 % level of metal dispersion [22]. This particle size estimation agrees with what has been observed with TEM analysis, where particle sizes were measured to vary between 6 and 13 nm [22].

The influence of water vapour adsorption on the active site and the support was investigated using TPD analysis. The intensity of water desorbed from the support material (γ-δ-Al_2O_3) and 1.2 wt% Pd/Al_2O_3 catalysts are plotted in Figure 5.6(a) for fresh active catalyst and 5.6(b) for the used catalyst (7 hours at 320 °C). Prior to water adsorption, fresh catalysts were pre-heated for 1 h at 500 ºC with a ramp of 5 ºC·min^{-1} and H_2O adsorption was at 110 °C, while on Pd/Al_2O_3 (used catalyst) the water was adsorbed during combustion of methane with a wet feed at 320 °C for 7 h.

In all cases, high and low temperature desorption peaks can be observed. The low temperature peak is observed at ca 240 °C and the high temperature peak was

observed between 350 °C and 700 °C. The low temperature desorption is attributed to weakly bound water, whereas the high temperature peak is attributed to adsorption on coordinatively unsaturated sites [23, 24].

Over a fresh alumina surface (Figure 5.6a), a second desorption peak is observed at ca 600 °C. On fresh Pd-containing catalysts, the second temperature desorption peak of water was observed at higher temperatures than on the support, indicating that water is more strongly bound on the Pd-containing surface. The higher temperature peak (600 °C) observed for the support material shifts to 700 °C, which suggests either a change in the interaction strength of the sites or structural and chemical changes of the sites by Pd. We suggest that Pd is deposited on sites that can interact strongly with water and transforms into sites that bind even more strongly with water. A small quantity of water is retained on the catalyst at temperatures as high as 700 ºC, similar to what was observed by Mowery and co-workers [12]. This further underscores the formation of catalyst sites interacting strongly with water.

Over the used catalyst (Figure 5.6b), the maximum water desorption rate was observed at ca 350 °C. A quantified amount of water remains on the catalyst at these temperatures (as indicated by the relative area under the peak), suggesting significant number of sites are interacting with water/form hydroxides. The desorption peak around 350 °C most likely is due to water desorption from hydroxides, consistent with the decomposition temperature of $Pd(OH)_2$ [21]. The

high temperature peak at ca. 700 °C was not observed, suggesting the absence of sites that are able to strongly adsorb water. Highly coordinatively unsaturated sites could be crucial as site for oxygen activation and would result in deactivation of the catalyst, similar to what has been suggested in [8]. These coordinatively unsaturated sites often are described as edge or corner or surface sites on metal and metal oxides [25]. Our estimation of the amount of water adsorbed during experiment is 0.9×10^{-3} mol·g^{-1} and 1.1×10^{-3} mol·g^{-1} for the support and the Pd/Al_2O_3 catalyst, respectively. The ratio of water desorbed from catalyst versus amount of Pd is 10, which means majority of water is adsorbed on the support. However, the presence of palladium on alumina increases the quantity of $H_2O_{(v)}$ adsorbed and also results in significant water desorption peak shift toward higher temperatures. This suggests significant interaction of Pd with water.

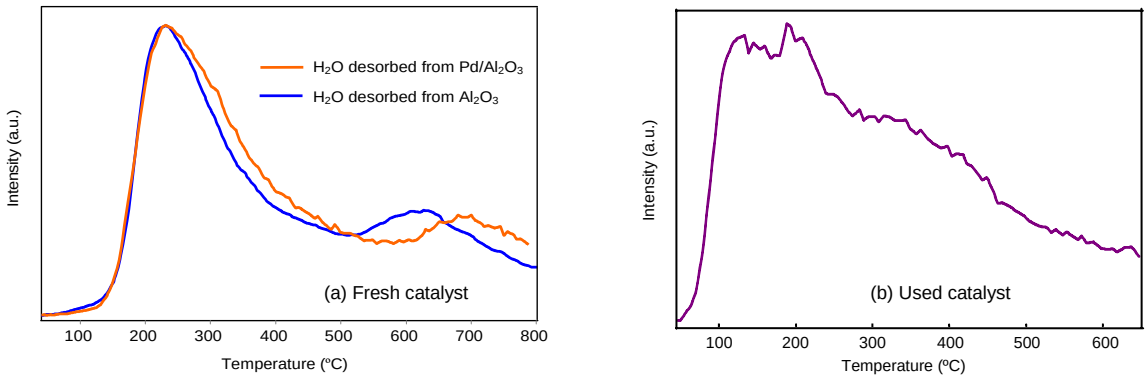

Fig. 5.6. TPD curves of water desorption from (a) fresh catalyst (1.2 wt% Pd/Al_2O_3) and catalyst support (γ-δ Al_2O_3) from and (b) used catalyst time on stream 7 h, Feed; 6000 ppm CH_4, ca. 30 000 ppm H_2O, reaction temperature 320 °C.

XPS spectra of activated (calcined-reduced) and used 1.2 wt% Pd/Al_2O_3 catalyst are displayed in Fig. 5.7. The binding energies (BE) and Pd/Al ratios are provided in Table 5.1 for all samples. XPS spectra of the activated and reduced 1.2 wt% Pd/Al_2O_3 catalyst (Fig. 5.7a), reveal two distinct Pd peaks representing the Pd $3d_{5/2}$ core level transitions. The palladium species at 335.0 eV and 336.3 eV can be attributed to Pd^0 and Pd^{2+} respectively. These species are formed during catalyst activation under air and hydrogen. The presence of metallic Pd and PdO has been assigned, by comparison with shifts reported in the literature [3, 26, 27].

The XPS spectra of the 1.2 wt% Pd/Al_2O_3 catalyst used for 2 h under dry and wet feed at 335 ºC are plotted in Fig. 5.7b. Two species with a binding energy (BE) of 335.0 eV and 336.4 eV were observed. The binding energies are similar to the BE obtained from the calcined-reduced sample (Fig. 5.7a) which suggests little change in the chemical nature of Pd^0 and Pd^{2+}. This observation supports our experimental data presented in Fig. 5.2 where the loss of activity 2 h under wet stream is completely reversible and no structural or chemical changes in the catalyst were detected.

Following reaction with lean air-methane mixtures at a temperature of 290 ºC for 10 h, the 1.2 wt% Pd/Al_2O_3 catalyst was deactivated and the XPS spectra of this sample is shown in Fig. 5.7c. The shape and width of the peak (FWHM = 2.3 eV at Pd $3d_{5/2}$ line) suggests the presence of multiple palladium species. Similar to the spectra of the fresh sample, asymmetry toward higher binding energies

indicates that multiple peaks should be fitted. Assuming Gaussian-Lorentzian curves (70 % Gaussian), the peak fitting results in two different photoelectron energies at BE of 336.0 eV and 337.1 eV ($3d_{5/2}$ core level). Adding additional peaks results in little improvements in the Chi^2 fit and is thus statistically not significant. The lower energy peak at BE of 336.0 eV is identified as bulk Pd^{2+} as reported in the literature [3, 27]. The presence of PdO corresponds to Pd species identified in Fig. 5.7a, which indicates transformation of Pd metal into the oxidized form under reaction conditions. The signal at a higher BE of 337.1 eV can be interpreted as palladium hydroxide (*vide infra*), which appears to be related to the deactivation observed during time on stream.

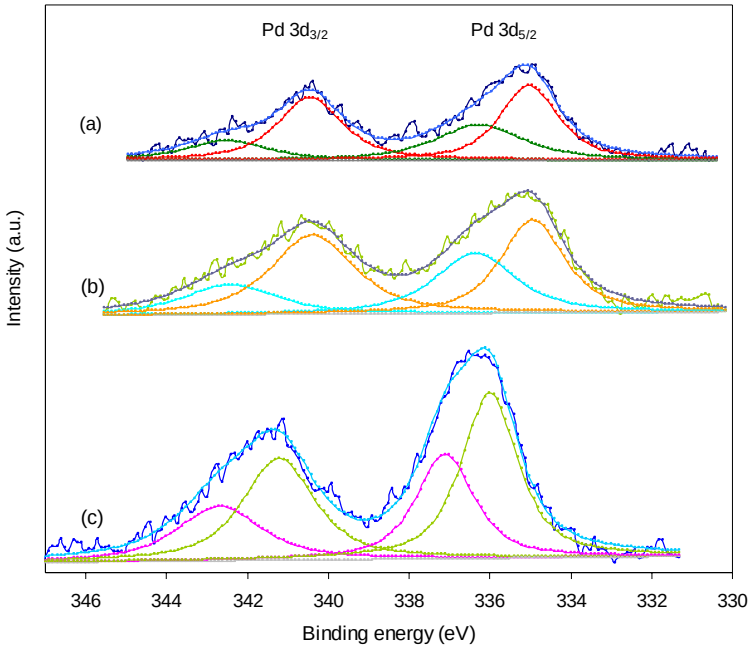

Fig. 5.7. XPS spectra of Pd 3d core level of 1.2 wt% Pd/Al_2O_3, (a) calcined-reduced sample; (b) used sample of 2 h TOS under humid condition; (c) used sample of 10 h TOS under humid condition.

Table 5.1. XPS peak positions and Pd/Al ratio

Fig.	Sample	Pd $3d_{5/2}$ peak position (eV)		Pd/Al ratio
		Pd^0	Pd^{2+}	
7a.	1.2 Pd/Al_2O_3, calcined-reduced	335.0	336.3	0.0046
7b.	1.2 Pd/Al_2O_3, 2 h usage	335.0	336.4	0.0040
7c.	1.2 Pd/Al_2O_3, 10 h usage	-	336.0 337.1	0.0077
8a.	1.0 Pd/Al_2O_3, fresh	334.7	336.1	0.0045
8b.	1.0 Pd/Al_2O_3, calcined-reduced	335.2	336.4	0.0045
8c.	1.0 Pd/Al_2O_3, 1,150 h usage	-	336.3	0.0040
9a.	1.0 Pd/Al_2O_3, used in the presence of dust	-	335.9	0.0048
9b.	Dust contaminated with Pd/Al_2O_3, used	-	336.2	0.0018

A limited body of research describing hydroxyl compounds was identified, and correlations between progressive alterations in chemical bonding and shifts in XPS binding energies with the nature of hydrogen bonding have been proposed [28]. A change in the binding energy of $Pd(OH)_2$ was reported by Barr [29] when a hydroxide layer is present on the palladium surface. Experimentally, Barr found that the Pd^0 peak at a BE of 335.4 eV was shifted to 336.9 eV and 338.6 eV upon formation of PdO and $Pd(OH)_4$, respectively [28, 29]. These shifts in binding energies are similar to what has been observed for Pd $3d_{5/2}$ in our samples (see Fig. 5.7). The presence of O-H groups on palladium metal can result in a shift of the peak of 1.1 eV toward a higher binding energy. The formation of palladium hydroxide is further substantiated by the re-generation of the active sites when a deactivated catalyst was heated in He (15 $ml \cdot min^{-1}$) at 500 ºC for 1 h. H_2 was detected in the exit stream, which most likely originates from OH groups on the catalyst surface. The TPD spectra plotted in Figure 5.6 also support the argument

of palladium hydroxide being present in the deactivated sample and are responsible for deactivation.

The spectra of a fresh, activated and used samples of 1.0 wt% Pd/Al_2O_3 catalyst in the Pd 3d core level region are shown in Fig. 5.8. For the fresh (as received, Fig. 5.8a) and activated (calcined-reduced, Fig. 5.8b) samples, the peak deconvolution results in two species detected at Pd $3d_{5/2}$ core level. These species are having similar binding energies as reported in Fig. 5.7a and 5.7b.

Figure 5.8c shows the spectra of used 1.0 wt% Pd/Al_2O_3 catalyst after 1,150 h operation using a surrogate VAM gas (refer to catalyst activity data plotted in Figure 5.3). XPS analysis of the catalyst discloses a single peak of Pd $3d_{5/2}$ core level at 336.3 eV. The presence of a single Pd^{2+} species is proposed as the full width at half maximum of Pd $3d_{5/2}$ is only 1.8 eV, which is indicative of a single species. Fitting more peaks under Pd 3d spectra, does not significantly decrease Chi^2.

XPS spectra in figure 5.8c suggest no palladium hydroxide is present on the catalyst. The increased bed temperature leads to decomposition of hydroxyl species, resulting in a single peak which is interpreted as PdO species dispersed on the support. An increase in Pd crystallite size is suggested to be an important contributor for deactivation as formation of $Pd(OH)_2$ was not found most likely due to the higher temperature.

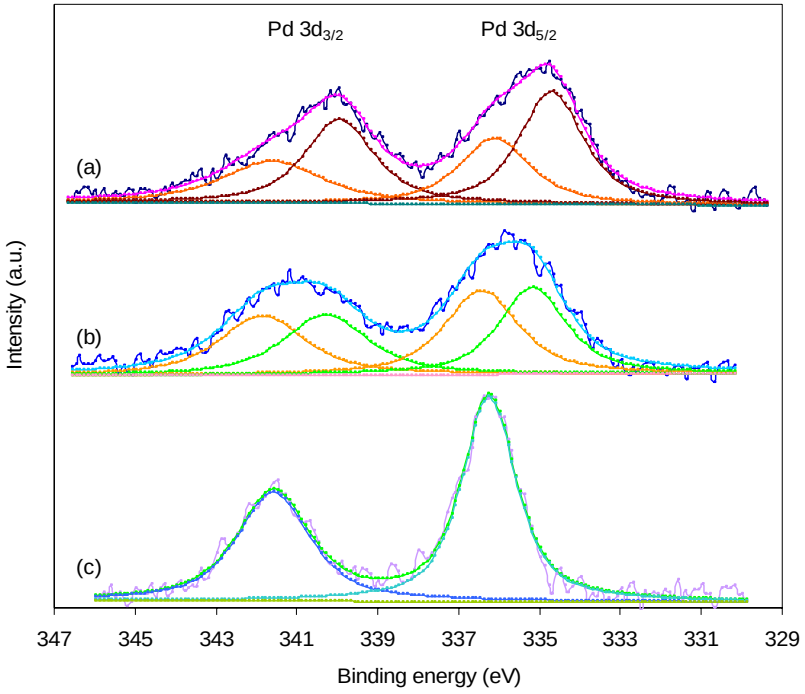

Fig. 5.8. XPS spectra of Pd 3d core level of 1.0 wt% Pd/Al_2O_3, (a) fresh sample; (b) calcined-reduced sample; (c) used sample of 1150 h stability test.

The accumulation of H_2O on the catalyst increases the surface mobility and results in particle agglomeration as well as potentially hinders the oxygen transfer from the bulk in a Mars van Krevelen type reaction mechanism [8]. As suggested by Lee and Trimm, thermal deactivation is caused by either sintering of the catalyst or support material [30]. This sintering involves surface/volume diffusion and other transformations. At reaction temperatures close to 0.3 × melting point (Hüttig temperature), the transformation becomes significant [31]. In our study, after ca. 300 h, the bed temperatures were adjusted toward 500 ºC close to the Hüttig temperature for Pd at 466 °C, and thus, a significant level of sintering would be expected. Please note that the binding energy of the Pd^{2+} of catalyst used in humid conditions for 1,150 h slightly

decreases compared to the fresh samples, similar to the catalyst aged in the presence of VAM dust. This is consistent with sintering (see below).

The used 1.0 wt% Pd/Al_2O_3 catalyst from VAM-dust time on stream experiment was analyzed by XPS in order to determine the surface composition of catalyst and dust after 1,100 h operation. Fig. 5.9 shows the palladium 3d photoelectron spectra of used catalyst (a) and used dust mixed with catalyst (b). The binding energies compiled along with Pd/Al atomic ratio are provided in Table 5.1. Deconvolution of the peak at Pd $3d_{5/2}$ core level suggests a single peak at a binding energy of 335.9 eV for the used catalyst. This peak is identified as Pd^{2+}, which is similar species detected from samples in Fig. 5.7 and Fig. 5.8, and is in agreement with the previous discussion suggesting palladium oxide is the primary species present on the surface after long term time on stream experiment. Note the decreased binding energy of the used sample (Fig. 5.9a) compared to the activated sample (Fig. 5.8b). The decreased binding energy can originate from chemical shift but also final state effects due to relaxation of the core hole. For larger particles, this relaxation effect is less important compared to smaller particles. Thus, the shift can be evidence for larger particles in the used samples, i.e., sintering. Despite a lower intensity, an identical peak is detected also from the XPS spectra of used dust at similar binding energies. As suggested by the overall surface composition of the used catalyst in Table 5.2, impurities such as Na, Cl and F were also present. It is important to note that the deactivation was little affected by the presence of the VAM dust and these species play a minor role in deactivation.

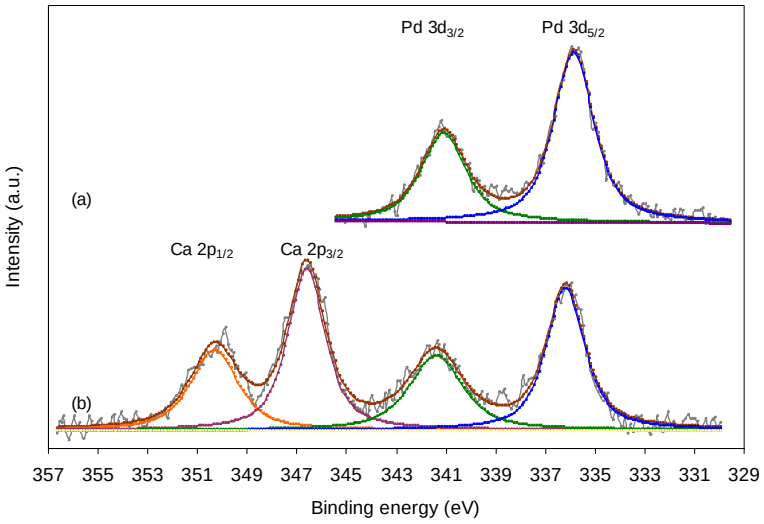

Fig. 5.9. XPS spectra of Pd 3d core level of used 1.0 wt% Pd/Al_2O_3 catalyst in the presence of dust, (a) used catalyst; (b) used dust mixed with catalyst.

Table 5.2. Surface composition of used catalyst and a mixture of VAM dust and used catalyst.

	Sample	Composition (at.%)												
		Pd	O	Al	C	Na	N	Cl	F	Si	Mg	Ca	S	Fe
(a)	Used Pd/Al_2O_3 (in the presence of dust)	0.18	57.9	37.2	3.85	0.15	0.22	0.24	0.29	-	-	-	-	-
(b)	Used Dust+ Pd/Al_2O_3 contamination	0.09	43.3	49.1	4.48	0.45	0.33	-	0.22	0.99	0.31	0.44	0.33	-
(c)	VAM dust (fresh)	-	39.4	3.2	34.0	0.8	1.4	3.5	-	6.0	5.1	6.2	-	0.4

From the used catalyst, XPS evidence disclosed that ca. 0.24 % of chlorine deposited on used catalyst while chlorine was not detected in the fresh catalyst and used dust (see Table 5.2). Others have suggested that chlorine ions behaves as a powerful inhibitor during methane oxidation over supported Pd catalyst [11, 32, 33] and removing the chlorine from the surface takes a minimum 10 h reaction even at temperatures as high as 600 ºC [11]. Since our reaction temperature is below 550 ºC, it appears that chlorine remains on the surface of the catalyst and inhibits catalytic activity. As can be seen in Figure 5.5 over 1,100 h reaction, an increase in bed temperature can increase methane conversion. However, it is important to note that in maintaining an average methane conversion > 75 % over 1,100 h our reaction temperature does not exceed 600 ºC.

5.3.4. Characterization of the VAM dust

The XRD trace of VAM dust (Fig. S2 of SI) following long term catalytic reaction discloses the presence of calcium carbonate, quartz and iron oxide as distinct phases. Consistent with the phase analysis by XRD, elemental analysis reveals the presence of Ca, Fe and Si (see Table 5.2). In addition aluminium, magnesium and titanium were also detected in the samples. These elements may be present as amorphous silicates. Surface analysis by XPS resulted in similar composition as determined by ICP-OES.

XPS analysis of the used catalyst and dust reveals the presence of chlorine on the catalyst. Chlorine can have a significant effect on the activity of the noble metal catalysts and has been detected in the catalyst after 1,200 h of reaction. As indicated in Table 5.2, XPS of the separated VAM-dust revealed that chloride was likely removed

from VAM gas and deposited on the catalyst surface. Note that complete separation of dust and catalyst was not possible. The presence of Cl in the XPS (Table 5.2) and its absence in ICP-OES suggests surface enrichment of chlorine on the catalyst that was operating in the presence of VAM dust. As already noted, the VAM dust influenced the overall activity (T_{90} at 1,100 h was 550 °C compared to experiment without dust T_{90} = 500 °C) but the deactivation was not dramatic. Thus, chlorine does have some but not a significant impact on the deactivation under our conditions.

5.4. Conclusions

The stability of a palladium supported on alumina has been evaluated during short and long term experiments in the presence of water and VAM dust. Within 2 h during, alternating experiments in dry and wet VAM feed suggests ca. 50 % reversible drop in activity, most likely due to competition between water and methane to adsorb on the active sites. For short term VAM oxidation, palladium hydroxide was not detected. Prolonged exposure to water leads to formation of palladium hydroxide and progressively deactivates Pd/Al_2O_3 catalyst. A long term stability test with humid synthetic ventilation air methane reveals that 90 % conversion can be achieved for a period of 1,150 h at temperatures ≤ 500 °C. The water vapour present in the feed stream is the primary factor responsible for catalyst deactivation. Introducing VAM dust into reactor lead to some reduced activity most likely due to an inhibition effect of chloride ions on the surface of catalyst. Nevertheless, in the presence of ventilation air dust an average methane conversion higher than 75 % can be achieved over 1,100 h at a reaction temperature below 600 ºC.

References

1. Solomon, S., D. Qin, M. Manning, R.B. Alley, T. Berntsen, N.L. Bindoff, Z. Chen, A. Chidthaisong, J.M. Gregory, G.C. Hegerl, M. Heimann, B. Hewitson, B.J. Hoskins, F. Joos, J. Jouzel, V. Kattsov, U. Lohmann, T. Matsuno, M. Molina, N. Nicholls, J. Overpeck, G. Raga, V. Ramaswamy, J. Ren, M. Rusticucci, R. Somerville, T.F. Stocker, P. Whetton, R.A. Wood, and D. Wratt, *Technical summary*, in *Climate change 2007: the physical science basis. contribution of working group I to the fourth assessment report of the intergovernmental panel on climate change*, S. Solomon, et al., Editors. 2007: Cambridge, United Kingdom and New York, NY, USA p. 996.

2. Schultz, H.L., P. Carothers, R. Watts, and R. McGuckin, *Assessment of the worldwide market potential for oxidising coal mine ventilation air methane*. 2003, United States Environmental Protection Agency, Air and Radiation (US-EPA).

3. Stasinska, B., A. Machocki, K. Antoniak, M. Rotko, J.L. Figueiredo, and F. Gonçalves, *Importance of palladium dispersion in Pd/Al_2O_3 catalysts for complete oxidation of humid low-methane-air mixtures.* Catalysis Today, 2008. 137(2-4): p. 329-334.

4. Su, S., H. Chen, P. Teakle, and S. Xue, *Characteristics of coal mine ventilation air flows.* Journal of Environmental Management, 2008. 86: p. 44 - 62.

5. Su, S., A. Beath, H. Guo, and C. Mallett, *An assessment of mine methane mitigation and utilization technologies.* Progress in Energy and Combustion Science, 2005. 31: p. 123-170.

6. Karakurt, I., G. Aydin, and K. Aydiner, *Mine ventilation air methane as a sustainable energy source.* Renewable and Sustainable Energy Reviews, 2011. 15(2): p. 1042-1049.

7. Gelin, P. and M. Primet, *Complete oxidation of methane at low temperature over noble metal based catalysts: a review.* Applied Catalysis B: Environmental, 2002. 39: p. 1-37.

8. Schwartz, W.R., D. Ciuparu, and L.D. Pfefferle, *Combustion of methane over palladium-based catalysts: catalytic deactivation and role of the support.* The Journal of Physical Chemistry C, 2012. 116(15): p. 8587-8593.

9. Ribeiro, F.H., M. Chow, and R.A. Dallabetta, *Kinetics of the complete oxidation of methane over supported palladium catalysts.* Journal of Catalysis, 1994. 146(2): p. 537-544.

10. Burch, R., F.J. Urbano, and P.K. Loader, *Methane combustion over palladium catalysts: The effect of carbon dioxide and water on activity.* Applied Catalysis A: General, 1995. 123(1): p. 173-184.

11. Roth, D., P. Gélin, M. Primet, and E. Tena, *Catalytic behaviour of Cl-free and Cl-containing Pd/Al_2O_3 catalysts in the total oxidation of methane at low temperature.* Applied Catalysis A: General, 2000. 203(1): p. 37-45.

12. Mowery, D.L., M.S. Graboski, T.R. Ohno, and R.L. McCormick, *Deactivation of $PdO-Al_2O_3$ oxidation catalyst in lean-burn natural gas engine exhaust: aged catalyst characterization and studies of poisoning by H_2O and SO_2.* Applied Catalysis B: Environmental, 1999. 21(3): p. 157-169.

13. Ciuparu, D., N. Katsikis, and L. Pfefferle, *Temperature and time dependence of the water inhibition effect on supported palladium catalyst for methane combustion.* Applied Catalysis A: General, 2001. 216(1-2): p. 209-215.

14. Schwartz, W.R. and L.D. Pfefferle, *Combustion of methane over palladium-based catalysts: support interactions.* The Journal of Physical Chemistry C, 2012. 116(15): p. 8571-8578.

15. Carlo, G.D., G. Melaet, N. Kruse, and L.F. Liotta, *Combined sulfating and non-sulfating support to prevent water and sulfur poisoning of Pd catalysts for methane combustion.* Chemical Communication, 2010. 46: p. 6317-6319.

16. Yamamoto, H. and H. Uchida, *Oxidation of methane over Pt and Pd supported on alumina in lean-burn natural-gas engine exhaust.* Catalysis Today, 1998. 45(1–4): p. 147-151.

17. Liu, Y., S. Wang, T. Sun, D. Gao, C. Zhang, and S. Wang, *Enhanced hydrothermal stability of high performance lean fuel combustion alumina-supported palladium catalyst modified by nickel.* Applied Catalysis B: Environmental, 2012. 119–120(0): p. 321-328.

18. Burch, R., *Low NO_x options in catalytic combustion and emission control.* Catalysis Today, 1997. 35(1–2): p. 27-36.

19. Kikuchi, R., S. Maeda, K. Sasaki, S. Wennerström, and K. Eguchi, *Low-temperature methane oxidation over oxide-supported Pd catalysts: inhibitory effect of water vapor.* Applied Catalysis A: General, 2002. 232(1-2): p. 23-28.

20. Gelin, P., L. Urfels, M. Primet, and E. Tena, *Complete oxidation of methane at low temperature over Pt and Pd catalysts for abatement of lean-burn natural gas fuelled vehicles emissions: influence of water and sulphur containing compounds.* Catalysis Today, 2003. 82: p. 45-57.

21. Card, R.J., J.L. Schmitt, and J.M. Simpson, *Palladium-carbon hydrogenolysis catalysts: The effect of preparation variables on catalytic activity.* Journal of Catalysis, 1983. 79(1): p. 13-20.

22. Setiawan, A., E.M. Kennedy, B.Z. Dlugogorski, A.A. Adesina, O. Tkachenko, and M. Stockenhuber, *Evidence of the formation of surface palladium carbide during the catalytic combustion of lean methane/air mixtures.* Energy Technology (Weinheim, Ger.), 2014.

23. Liu, X., *DRIFTS study of surface of γ-alumina and its dehydroxylation.* The Journal of Physical Chemistry C, 2008. 112(13): p. 5066-5073.

24. Backman, L.B., A. Rautiainen, M. Lindblad, and A.O.I. Krause, *The interaction of cobalt species with alumina on Co/Al_2O_3 catalysts prepared by atomic layer deposition.* Applied Catalysis A: General, 2009. 360(2): p. 183-191.

25. Busca, G., *The surface acidity and basicity of solid oxides and zeolites*, in *Metal oxides: Chemistry and applications*, J.L.G. Fierro, Editor. 2006, CRC Press, Taylor & Francis Group: Boca Raton. p. 247.

26. Yasuda, K., T. Masui, T. Miyamoto, and N. Imanaka, *Catalytic combustion of methane over Pt and PdO-supported CeO-ZrO-Bi_2O_3/γ-Al_2O_3 catalysts.* Journal of Materials Science, 2011. 46(11): p. 4046-4052.

27. Naumkin, A.V., A. Kraut-Vass, S.W. Gaarenstroom, and C.J. Powell, *NIST standard reference database 20, version 4.1*. 2012.

28. Kerber, S.J., J.J. Bruckner, K. Wozniak, S. Seal, S. Hardcastle, and T.L. Barr. *The nature of hydrogen in x-ray photoelectron spectroscopy: General patterns from hydroxides to hydrogen bonding*. 1996. Mineapolis, Minnesota (USA): AVS.

29. Barr, T.L., *An ESCA study of the termination of the passivation of elemental metals.* The Journal of Physical Chemistry, 1978. 82(16): p. 1801-1810.

30. Lee, J.H. and D.L. Trimm, *Catalytic combustion of methane.* Fuel Processing Technology, 1995. 42: p. 339-359.

31. Trimm, D.L., *Thermal stability of catalyst supports*, in *Studies in surface science and catalysis*, H.B. Calvin and B.B. John, Editors. 1991, Elsevier. p. 29-51.

32. O. Simone, D., T. Kennelly, N. L. Brungard, and R. J. Farrauto, *Reversible poisoning of palladium catalysts for methane oxidation.* Applied Catalysis, 1991. 70(1): p. 87-100.

33. Gao, D., S. Wang, C. Zhang, Z. Yuan, and S. Wang, *Methane combustion over Pd/Al_2O_3 catalyst: effects of chlorine ions and water on catalytic activity.* Chinese Journal of Catalysis, 2008. 29(12): p. 1221-1225.

CHAPTER 6

The stability of Co_3O_4, Fe_2O_3, Au/Co_3O_4 and Au/Fe_2O_3 catalysts in the catalytic combustion of lean methane mixtures in the presence of water

---

Published in:

Catalysis Today, 2014,

http://dx.doi.org/10.1016/j.cattod.2014.11.031

Appendix D supplied the supporting information of this chapter.

6.1. Introduction

The anthropogenic emission of methane is emerging as an important environmental issue due to the volumes of the gas being emitted and the significant impact this has on the environment. Approximately 70 % of methane emissions can be attributed to ventilation air methane (VAM) emitted from coal mines [1, 2]. The large volumetric flow rate and the low methane concentration (≤ 1 %) of VAM stream presents a major challenge in developing technologies to mitigation or utilize this emission. A number of processes have been developed to mitigate these emissions. One potential solution for reducing methane emission is catalytic combustion, where methane is oxidised to carbon dioxide on a catalytically-active solid surface. This flameless combustion is ideal for highly diluted air/methane streams, as the production of NO_x is essentially absent and the reaction temperature is relatively low.

The catalytic combustion of methane has been extensively investigated over noble metals, transition metal oxides and mixed metal oxides. Pd-based catalysts are considered as one of the most active [3], however susceptibility to poisoning by water is a major practical problem when the catalyst is employed in a VAM stream as the humidity level of the stream is at or near saturation. As reported in our previous work, the water vapour present in the feed is the primary factor leading to catalyst deactivation observed during catalytic combustion of simulated VAM stream over 1,100 h [4]. Therefore, the application in the VAM combustion necessitates the development of durable catalysts, characterized by improved resistance to water vapour-poisoning.

Gold was initially believed to be inactive as a catalyst because of its inability to chemisorb most gases under typical reaction conditions [5]. However, in a seminal study pioneered by Haruta et al., it was shown that carbon monoxide could be oxidized over gold catalysts [6] at temperatures as low as 77 K. This success was followed by the development of a gold catalyst for the total methane oxidation [7], in which nano-sized gold catalysts were supported on various metal oxides [8, 9] with the aim of improving the activity and stability of catalysts. The activity of supported gold catalysts during total oxidation of methane was reported recently [10, 11], and although supported gold catalysts are not as active as palladium-based catalysts, an understanding on the nature of nano-sized gold can further our understanding of the deactivation process and in turn how to enhance the catalyst activity and stability. Limited measurements exist regarding the characteristics and catalytic activity of supported gold catalyst specifically for combustion of lean methane-air mixtures. Methane combustion in the presence of water over gold-based catalysts has not yet been investigated in detail.

Transition metal oxides have been considered as catalysts for total oxidation of methane due to their higher stability and lower cost when compared to noble metals [12]. Earlier work reported the use of single-metal oxides (such as Cr_2O_3, NiO, Mn_2O_3, Co_3O_4, and CuO) and these studies evaluated the activities and deactivation phenomena during lean methane combustion [13]. Among those tested, Co_3O_4 was the most active catalyst but was less stable compared to Mn_2O_3. Preparing different morphologies of cobalt oxide was demonstrated recently as a strategy for improving the catalytic activity [14]. Enhanced activity and stability was reported for Co_3O_4 nanotubes prepared using a morphology-directed technique [15]. The higher activity observed from these nanotubes catalysts was reported to be due to the prominence and exposure of the (112) crystal

plane and high reactivity of the surface oxygen. However, the issue of catalyst stability in the presence of water vapour in the feed has not been addressed yet.

This paper reports the effect of water vapour present in catalytic combustion of lean methane mixture over pure oxide (Co_3O_4 and Fe_2O_3) and supported gold (Au/Fe_2O_3, Au/Co_3O_4) catalysts. The catalyst characteristics and catalytic activities under dry and wet feed are investigated at gas hourly space velocities (GHSVs) up to 100,000 h^{-1}, mimicking the requisite conditions of a catalytic reactor used in large scale treatment of ventilation air methane stream. An understanding of the inhibitory effect of water vapour is explored by performing the temperature-programmed desorption of water from fresh and used samples supported by other characterization techniques such as N_2 adsorption desorption, XRD, TEM, SEM and XPS analyses.

6.2. Experimental

6.2.1. Catalyst preparation

Cobalt oxide was prepared using a precipitation method. $Co(NO_3)_2.6H_2O$ (Sigma-Aldrich) was dissolved in water (0.1 M), the solution was stirred at 80 ºC and cobalt species precipitated by adjusting to a pH of 9 using Na_2CO_3 solution (0.25 M). The resulting precipitate was filtered, washed with hot and cold water and dried in an oven at 110 °C for 20 h. Prior to catalyst activity measurement, the sample was pre-treated ex-situ in air at 400 °C for 4 h.

In order to investigate the effect of surface area on the catalytic activity and stability of iron oxide, a high surface area Fe_2O_3 catalyst was prepared by adding 0.33 mL of an aqueous solution of 0.36 M $Al(H_2PO_4)_3$ (Alfa Aesar) into 15.1 mL of 2.33 M $Fe(NO_3)_3$ (Sigma-Aldrich) [16]. The mixture was then placed in a rotary evaporator at 60 ºC for 2 h before being heated in a furnace to 380 ºC at a ramp of 4 ºC min^{-1} for 1 h. The resulting paste was then dried in an oven at 110 °C for approximately 20 h and calcined in static air at 400 °C for 4 h to activate the catalyst as well as remove any residual phosphorus and nitrate originating from sample precursors. Finally the sample was purged with helium for 30 min prior to reaction.

Supported gold catalysts were prepared using a co-precipitation method [10]. For Au/Fe_2O_3 catalyst, a solution of 35.1 g of $Fe(NO_3)_3 \cdot 9H_2O$ (Sigma-Aldrich) was dissolved to form a solution of approximately 0.1 M. This solution was mixed with 0.3 g of $HAuCl_4 \cdot 3H_2O$ (Acros-Organic) dissolved in HCl (0.58 M). The solution was adjusted to a pH of 9 while being stirred at 80 °C using Na_2CO_3 solution (0.1 M). The resulting precipitate was filtered under vacuum and washed with hot and then cold water several times. The precipitate was collected and dried in an oven at 110 °C for approximately 16 h and pressed and sieved to 250-400 μm. The sample was then pre-treated ex-situ in air at 400 °C for 4 h, activating the catalyst as well as ensuring the removal of any residual precursors.

A similar method was used for preparing 2.2 wt. % Au/Co_3O_4 catalyst where 23.97 g of $Co(NO_3)_2.6H_2O$ (Sigma-Aldrich) dissolved in water (0.1 M) was mixed with 307.2 mg of $HAuCl_4.9H_2O$ (Acros-Organic) dissolved in HCl at 0.58 $mol.L^{-1}$. The solutions were stirred at 80 ºC and Na_2CO_3 solution (0.25 M) was added drop wise until a pH of 8.2

was reached [10]. The resulting paste was then filtered, washed, dried and calcined under the same procedure as described above.

6.2.2. Catalytic activity measurement

Catalytic activity measurements were performed in a tubular stainless steel micro reactor. The inlet methane concentration was set at 0.6 %, balanced with air at GHSVs between 27,000 and 200,000 h^{-1}. The inlet and outlet mixtures were analyzed using a gas chromatograph equipped with a thermal conductivity detector (TCD) and concentric packed column (Alltech CTR-I). For humid feed experiments, the reactant mixture was passed through a saturator operated at 25 °C ± 3 ºC with a humidity probe installed at the outlet. The actual reaction temperatures were measured by placing a K-type thermocouple into the reactor close to the catalyst bed.

6.2.3. Catalyst characterization

The surface areas of catalysts were measured by nitrogen adsorption at 77 K using Gemini 11 2370 surface area analyser according to the Brunauer-Emmet-Teller (BET) method. Powder X-ray diffraction (XRD) patterns of catalysts were examined using Cu Kα radiation performed by a Philips X'Pert diffractometer in the range of 2θ angles from 2° to 90° with 0.008° 2θ step resolution. Temperature-programmed desorption (TPD) analyses were performed using a purpose built TPD apparatus equipped with Pfeiffer Prisma quadrupole mass analyser. Zeiss Sigma VP FESEM served to capture the Scanning Electron Microscopy (SEM) images of the sample using a secondary electron (SE) detector and back-scattered electron (BE) detector. Bruker light element

SSD Energy-dispersive X-ray spectroscopy (EDS) detector allowed the elemental analysis while capturing the SEM images. A JEOL 2100 Transmission Electron Microscope (TEM) was used for TEM imaging of supported gold catalysts. The gold loadings were quantified using Varian 715-ES inductively coupled plasma optical emission spectrometer (ICP-OES).

For surface analysis, ex situ X-ray photoelectron spectroscopy (XPS) was carried out using mono-chromated Al K alpha (energy 1486.68 eV) radiation and the emitted photoelectrons were analyzed using an ESCALAB250Xi manufactured by Thermo Scientific, UK. The energy scale was shifted relative to the adventitious carbon at 284.6 eV and the spectrometer was calibrated against binding energies of Au $4f_{7/2}$ = 83.96 eV, Ag $3d_{5/2}$ = 368.21 eV and Cu $2p_{3/2}$ = 932.62 eV.

6.3. Results and discussions

6.3.1. The activity and stability of Co_3O_4 and Fe_2O_3 catalysts

The catalytic activity tests of single oxide catalysts were performed by feeding the reactor tube with 6,000 ppm methane (balance air) at gas hourly space velocity (GHSV) of 100,000 h^{-1}. The light-off curves were recorded at temperatures from 250 to 650 °C. A blank experiment was carried our prior to catalytic activity test and confirmed that no methane conversion was observed up to a temperature of 650 °C [17]. Fig. 6.1 shows the temperature dependency of methane conversion over Co_3O_4 and Fe_2O_3 catalysts. The temperature of 90 % conversion varies significantly, with the Co_3O_4 exhibiting the lowest light-off temperature. The temperature at 90 % methane conversion (T_{90}) for

Co_3O_4 is 440 °C, while T_{90} of Fe_2O_3 is about 510 °C. These light-off curves clearly suggest that the nano-sized cobalt oxide is more active compared to Fe_2O_3 catalysts.

The stability of each catalyst was observed during time-on-stream (TOS) experiments under dry and humid feed conditions at reaction temperature of 455 ˚C and gas hourly space velocity of 100,000 h^{-1}. Initially, the methane combustion was carried out using a dry feed and after 1 h the reaction mixture was passed through a saturator and remained so continuously for 1 or 2 days. Fig. 6.2 shows the time-on-stream evolution of methane oxidation over Co_3O_4 and Fe_2O_3 catalysts. Adding water vapour into the feed produced no measurable drop in activity over the Co_3O_4 catalyst within 24 h TOS. Prolonging the operation up to 55 h under humid feed condition, the methane conversion level remained relatively constant, ranging from 95 % to 98 %. When compared to the Fe_2O_3 catalyst, a significant deactivation was observed where the methane conversion dropped from ca. 70 % to 20 % within 24 h under humid feed, suggesting that iron oxide activity is very sensitive to water compared to cobalt oxide.

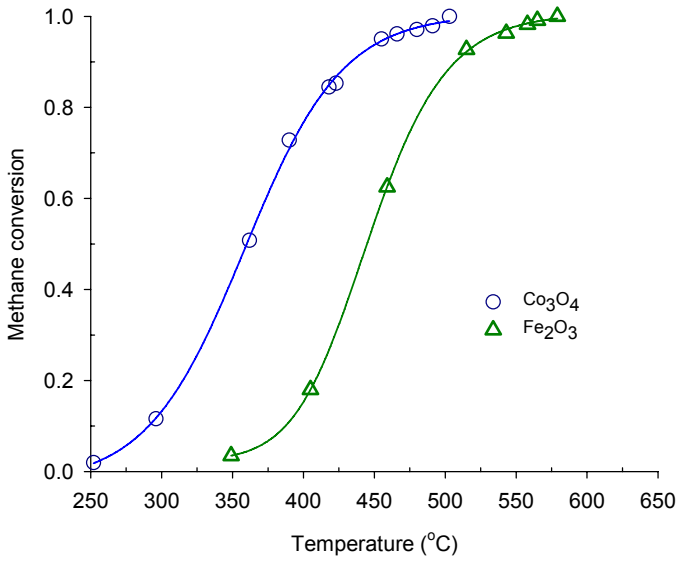

Fig. 6.1. Methane conversion as a function of temperature over (○) Co_3O_4 and (Δ) Fe_2O_3 catalysts. Reaction condition: 6,000 ppm CH_4 balance air at GHSV = 100,000 h^{-1}.

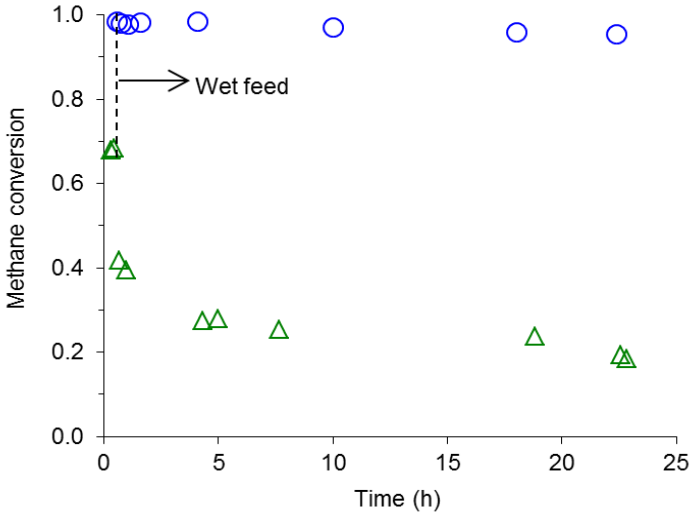

Fig. 6.2. Time on stream behavior under dry and wet feed over Co_3O_4 (○) and Fe_2O_3 (Δ) catalysts. Feed: 6,000 ppm CH_4, 3 vol.% H_2O (for wet feed) balance air. GHSV = 100,000 h^{-1}, bed temperature = 455 °C.

6.3.2. The characteristic of Co_3O_4 and Fe_2O_3 catalysts

Nitrogen adsorption-desorption isotherms of Co_3O_4 and Fe_2O_3 catalysts are provided in Fig. S1 of supplementary information (SI), suggesting type IV isotherms from hysteresis loop observed within a relative pressure (p/p_0) range of 0.4-0.9 [18]. The surface area of the samples, calculated using the BET equation, results in 31.1 m^2 g^{-1} and 86.6 m^2 g^{-1} for cobalt oxide and iron oxide, respectively.

XRD patterns of cobalt oxide and iron oxide catalysts are shown in Fig. 6.3. The peak of XRD reflections are sharp and intense, suggesting well-crystallized phases of Co_3O_4 and Fe_2O_3 (hematite). The topography of iron oxide and cobalt oxide was investigated using Scanning Electron Microscopy (SEM). In the supplementary information (SI), the SEM images of Co_3O_4 and Fe_2O_3 are provided in Fig. S2 and Fig. S3 respectively, showing the surface morphologies of both samples. From these images we can see that

the size distribution of cobalt oxide particles is narrower than iron oxide. Cobalt oxide has a nearly spherical shape and larger pore size compared to iron oxide.

The higher activity of Co_3O_4 catalyst compared to Fe_2O_3 catalyst was investigated using temperature-programmed desorption (TPD) of oxygen. Initially, both samples were heated in situ under vacuum up to 550 °C to remove any pre-adsorbed compounds. Oxygen (99.5 %) was adsorbed at 400 °C followed by cooling to room temperature (RT). The TPD experiment was carried out with a temperature ramp of 5 ºC.min^{-1} heating from RT to 550 °C. Fig. 6.4 shows the TPD profile of O_2 (m/z = 32) desorption over Co_3O_4 and Fe_2O_3 catalysts.

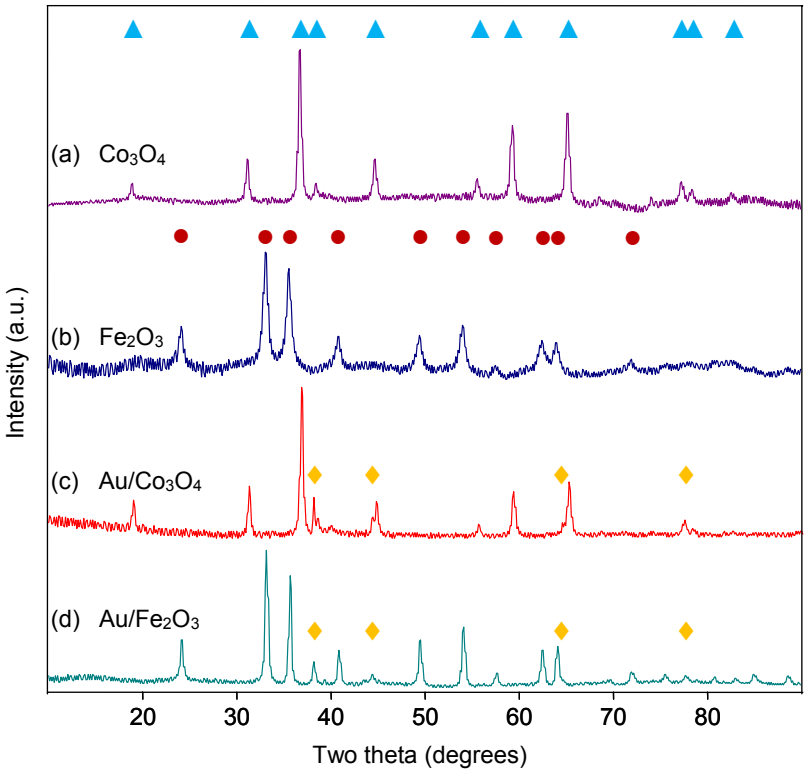

Fig. 6.3. X-ray diffraction patterns of (a) Co_3O_4; (b) Fe_2O_3; (c) Au/Co_3O_4 and (d) Au/Fe_2O_3 catalysts. Crystalline phase: ▲ = Co_3O_4, ● = Fe_2O_3, ♦ = Au.

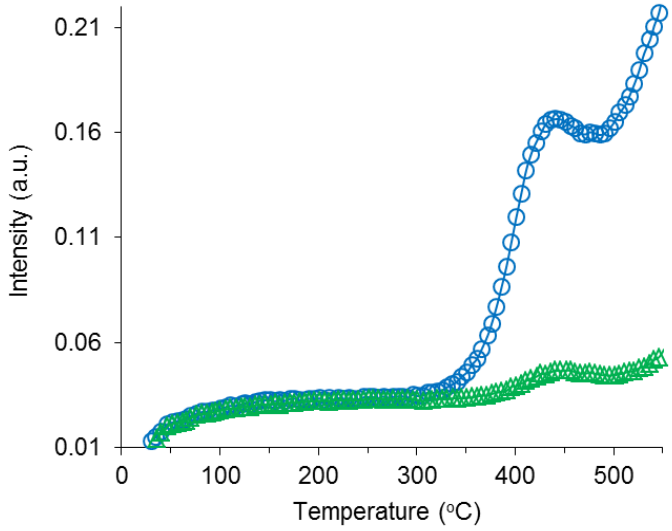

Fig. 6.4. TPD profile of O_2 desorption of Co_3O_4 (○) and Fe_2O_3 (Δ) catalysts at heating rate of 5 ºC.min^{-1}. O_2 was adsorbed at 400 ºC.

TPD spectra of Co_3O_4 suggests at temperature of 350 °C a significant concentration of oxygen is present on the surface, resulting in a maximum in the desorption rate of oxygen at 440 °C. Meanwhile, over the surface of Fe_2O_3 the oxygen desorption starts at higher temperature (400 °C) and with a lower intensity. This is consistent with data from light-off curves plotted in Fig. 6.1 where between 300-400 °C observeable conversions were detected over both catalysts. The peaks at temperature in range of 350 °C to 500 °C indicate that the oxygen adsorption capacity of Co_3O_4 catalyst is higher compared to Fe_2O_3 catalyst. The higher oxygen surface coverage of Co_3O_4 is suggested to be responsible for activity difference of the catalysts. As reported in the literature, it is inferred that, the re-oxidation of the reduced cobalt oxide sites is rate limiting [19, 20].

The inhibiting effect of water was investigated using temperature-programmed-desorption analysis. Fig. 6.5 shows H_2O (m/z = 18) TPD spectra of (a) Co_3O_4 and (b) Fe_2O_3 catalysts where the water was adsorbed at 150 ºC and TPD spectra recorded

during desorption from RT to 650 ºC with a heating rate of 5 ºC min^{-1}. Prior to water adsorption, each sample was activated in-situ at 400 ºC for 1 h with a ramp of 5 ºC min^{-1}. Peak deconvolution of TPD spectra suggests four desorption states of water from both catalysts. The peak positions after curve fitting for all TPD samples are provided in Table S1 of SI. Three peaks were detected below 400 °C. These peaks are related to desorption from weakly bond H_2O from the oxide surfaces. Above 400 °C, a stronger bond of H_2O was detected from both samples. However, the intensity of water desorbed from Fe_2O_3 is higher than that of Co_3O_4 which suggests more water is bound to iron oxide than to Co_3O_4. Furthermore, the water desorption peak at ca 500 °C was found over Fe_2O_3 indicative of strongly bound water (hydroxyl) species. In light of this finding, the difference in catalytic activity can be explained by competition of the reactants with water or irreversible destruction of active sites. Rapid deactivation was observed over Fe_2O_3 catalyst (see Fig. 6.2) where the activity dropped from ca. 70 % to 25 % within 5 h methane oxidation using humid feed.

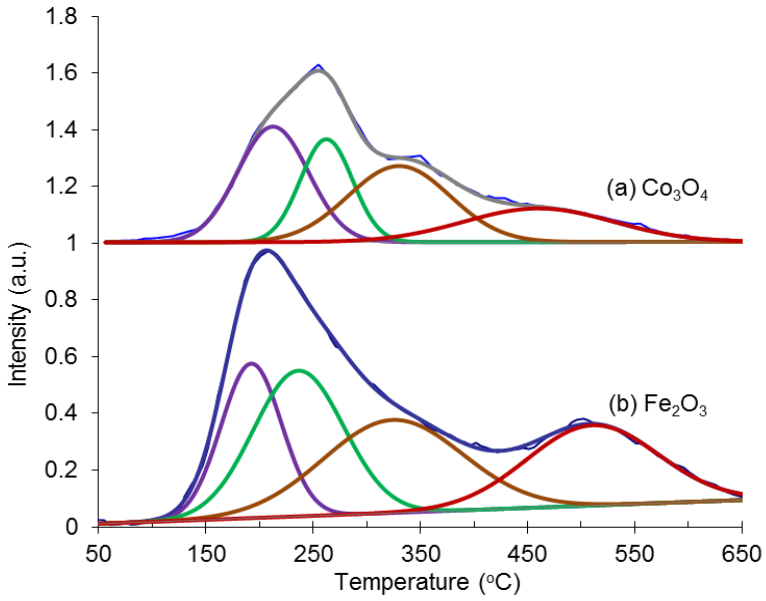

Fig. 6.5. TPD profile of H_2O desorption of (a) Co_3O_4 and (b) Fe_2O_3 catalysts at heating rate of 5 ºC.min^{-1}, H_2O adsorption at 150 ºC. TPD spectra of Co_3O_4 were offset by 1 a.u. for clarity.

The surface composition and oxidation state of fresh and used samples were analyzed using XPS of Co_3O_4 and Fe_2O_3 catalysts. For this analysis, the fresh samples are the sample which has been activated (as mentioned in experimental section) and kept in a sealed container. The used samples are catalyst which have been used in time-on-stream (TOS) experiments, as plotted in Fig. 2. After the TOS run was terminated, the catalyst was transferred into the XPS sample chamber for analysis.

The experimental and fitted Co 2p spectra of fresh and used cobat oxide catalysts are presented in Fig. S4 of SI. As expected, the spectra of both samples are essentially identical, highlighting no change in oxidation state or surface composition following the time-on-stream experiments. This argument was cross-checked with fitted peak of O 1s spectra from both samples as shown in Fig. S5 of SI. At Co $2p_{3/2}$ the peak fitting suggests two cobalt species were detected at binding energies of 779.2 eV and 780.3 eV. Over the fresh sample, the peak at binding energy of 779.2 eV is identified as Co^{3+} and the peak at 780.3 eV is Co^{2+} [18, 21]. It is noteworthy that no significant shift in binding energy was observed from the used sample. This XPS result is in line with the excellent stability of Co_3O_4 as observed during time-on-stream experiment (see Fig. 6.2).

Exploring an explanation for the rapid deactivation phenomena observed from iron oxide catalyst was investigated by collecting XPS of fresh and used Fe_2O_3 samples. The spectra at Fe 2p core level for both samples are shown in Fig. S6 of SI. Comparison of these two spectra does not indicate any significant changes in oxidation state of Fe. Deconvolution of the peak under Fe $2p_{3/2}$ spectra results in two peaks at binding

energies of 710 ± 0.2 eV and 711.3 ± 0.1 eV. As suggested in the literature, these peaks are attributed to Fe^{3+} species [22, 23] which is typically the oxidation state of Fe_2O_3 (haematite). This argument is consistant with the XRD patterns of both samples, the result suggesting the dominance of haematite phase in these samples.

The fitted peak and the experimental spectra of O 1s core-level of fresh and used Fe_2O_3 are plotted in Fig. 6.6. The spectra of fresh sample (Fig. 6.6a) suggests two peaks at binding energies of 529.9 eV and 531.4 eV while deconvolution of the used Fe_2O_3 spectra (Fig. 6.6b) results in three peaks at binding energies of 529.9 eV, 531.7 eV and 533.4 eV. The presence of a peak at binding energy of 533.4 eV over the used sample is most-likely related to the formation of hydroxyl species on the surface of Fe_2O_3, which is consistent with data reported in the literature [24, 25].

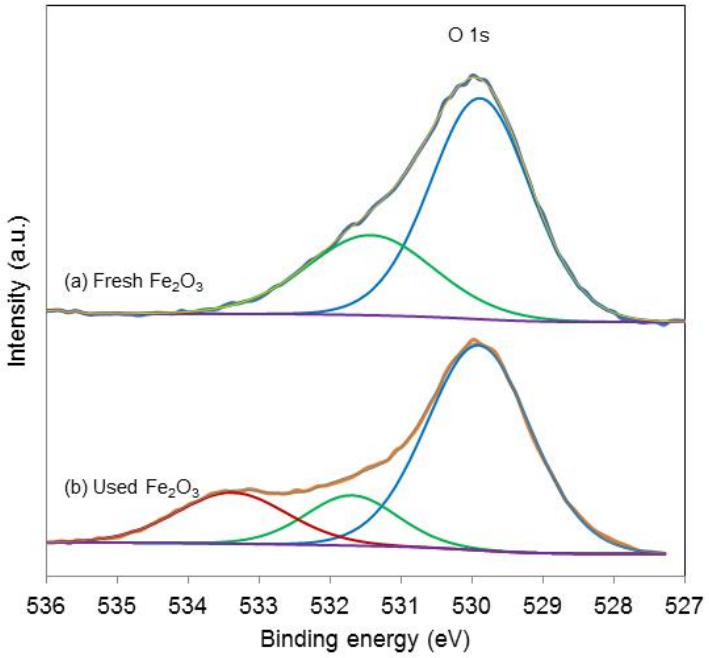

Fig. 6.6. XPS spectra of O 1s core level of (a) fresh Fe_2O_3 and (b) used Fe_2O_3.

6.3.3. Dependency of activity and stability of Au supported on Co_3O_4 and Fe_2O_3

The catalytic activity and stability of cobalt oxide and iron oxide were further evaluated following the loading of Au particles on these supports using a co-precipitation method, as outlined in the experimental section. Fig. 6.7 shows the temperature dependency of methane conversion over Au/Co_3O_4 and Au/Fe_2O_3 catalysts compared with the data plotted for single oxide catalysts in Fig. 6.1.

The temperature of 10 % conversion varies significantly, with the Co_3O_4 exhibiting the lowest light-off temperature. This figure suggests that the nano-sized cobalt oxide is the most active catalyst, followed by Au/Co_3O_4, Fe_2O_3 and Au/Fe_2O_3 catalysts. The temperatures at 10 % methane conversion (T_{10}) for Co_3O_4 and Au/Co_3O_4 are similar (suggesting similar intrinsic rates). The T_{90} of Co_3O_4 is about 50 °C lower than the temperature of 90 % methane conversion over Au/Co_3O_4. Comparison of Fe_2O_3 and Au/Fe_2O_3 light-off curves also suggests that the support material is more active than the supported gold catalyst. At 500 °C methane oxidation over Fe_2O_3 catalyst achieves 90 % conversion level while Au/Fe_2O_3 catalyst can only convert 60 % of CH_4 into CO_2. Surprisingly, the presence of gold on cobalt oxide or iron oxide does not enhance the activity of the catalyst, if it has any influence that effect appears to be detrimental in terms of catalytic activity. This behaviour suggests potential poisoning of transition metal sites by gold, the details of which are currently under investigation.

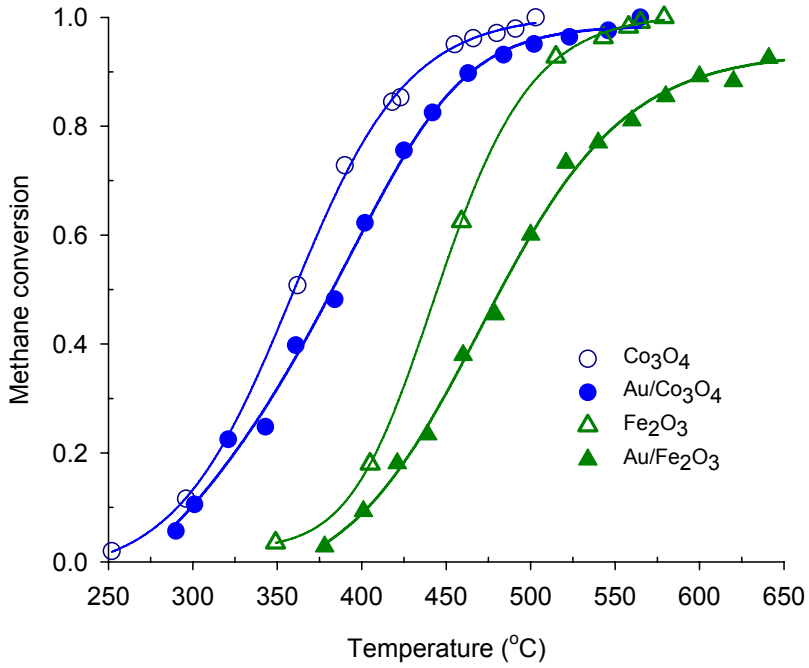

Fig. 6.7. Methane conversion as a function of temperature over (○) Co_3O_4; (●) Au/Co_3O_4; (Δ) Fe_2O_3 and (▲) Au/Fe_2O_3 catalysts. Reaction condition: 6,000 ppm CH_4 balance air at GHSV = 100,000 h^{-1}.

The activity of the catalysts at different space velocities was investigated over Au/Co_3O_4 and Au/Fe_2O_3 catalysts. In Fig. S7 and Fig. S8 of the supplementary information (SI), we plot the light-off curves for methane oxidation over Au/Co_3O_4 and Au/Fe_2O_3 catalysts. A drop in T_{90} of 30 °C in activity was observed from Au/Co_3O_4 catalyst when varying the GHSV from 27,000 h^{-1} to 100,000 h^{-1}, whilst over Au/Fe_2O_3 catalyst the temperature at 90 % conversion (T_{90}) was shifted up about 100 ˚C upon increasing the space velocity from 35,000 h^{-1} to 100,000 h^{-1}. This result is consistent with the data reported by Choudhary et al where the activity of Au/Fe_2O_3 catalyst was significantly affected by changing GHSVs [11].

The stability of gold supported on cobalt oxide and gold supported on iron oxide catalysts were evaluated under similar condition as mentioned above. Initially, the experiment was started by feeding the reactor with dry feed for 45 min, and then

switched to wet feed (dry and wet conditions). Fig. 6.8 shows the time-on-stream evolution of methane combustion over these catalysts for 24 h. For comparison, TOS data of Fe_2O_3 (dry wet conditions) and Au/Fe_2O_3 tested under dry feed conditions are plotted also in this figure. The activity of Au/Co_3O_4 catalyst is fairly constant before and after water vapour was introduced into the feed, similar to what was observed from Co_3O_4 catalyst (see Fig. 6.2). In contrast, over Au/Fe_2O_3 catalyst, the presence of water in the feed leads to significant deactivation. However, the deactivation rate of Au/Fe_2O_3 catalyst is lower compared to deactivation rate of Fe_2O_3 catalyst. This observation is likely due to a higher reaction temperature for TOS experiment of Au/Fe_2O_3 catalyst. As suggested by TPD spectra (see below), at 530 °C less water remains on the surface. In addition, the dry feed TOS experiment of Au/Fe_2O_3 catalyst at 530 °C indicates that removing water from the feed decreases the deactivation rate. This is consistent with our findings from TPD and XPS analyses from which we conclude that the hydroxyl species are strongly bonded on the surface.

The surface area of the samples calculated from N_2-physisorption data using BET equation are provided in Table 6.1. Compared with co-precipitated gold on iron oxide catalyst, the pure iron oxide exhibits higher surface area due to modified preparation method. Meanwhile, pure cobalt oxide and supported gold on cobalt oxide catalyst have similar specific surface areas. The ICP-OES results confirm the presence of 1.7 wt% and 2.2 wt% of gold on iron oxide and cobalt oxide, respectively.

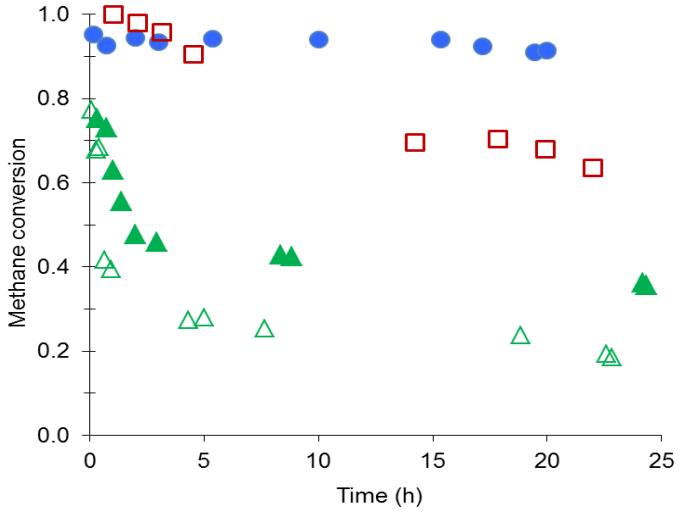

Fig. 6.8. Time on stream methane oxidation (●) under dry and wet conditions over Au/Co_3O_4 catalyst at 455 ºC; (□) under dry conditions over Au/Fe_2O_3 catalyst at 530 ºC; (▲) under dry and wet conditions over Au/Fe_2O_3 catalyst at 530 ºC; (△) under dry and wet conditions over Fe_2O_3 catalyst at 455 ºC. Reactant: 6,000 ppm CH_4 balanced air, water vapour = 3 vol%, GHSV = 100,000 h^{-1}.

Table 6.1. Surface area and Au particle size

Sample	BET Surface area ($m^2.g^{-1}$)	Average Au particle size measured by TEM (nm)
1.7 wt. % Au/Fe_2O_3	55.5	15
2.2 wt. % Au/Co_3O_4	32.9	18
Co_3O_4	31.1	-
Fe_2O_3	86.6	-

XRD patterns of gold supported on cobalt oxide and iron oxide catalysts are shown in Fig. 6.3c-d. The XRD reflections are sharp and intense suggesting well-crystallized phases of Au, Fe_2O_3 and Co_3O_4. The line broadening of the highest intensity of the gold reflection peak suggests that the crystallite size of both samples is similar. This is supported by particle size measurement using TEM analysis where the average gold particle size of Au/Co_3O_4 and Au/Fe_2O_3 are 18 nm and 15 nm, respectively. It was also observed that the line broadening at half the maximum intensity (FWHM) of Co_3O_4 reflection at 36.8° 2θ decreased slightly following gold deposition. Our calculation

suggests that the cobalt oxide particle size increased about 3 nm upon loading gold on the oxide. This is supported by the surface area calculation results in Table 6.1 where no significant increase was observed after gold deposition on Co_3O_4. Please note that the differences in FWHM of Fe_2O_3 reflections observed in our samples are due to different precursor used.

The distribution of gold nano particles on Fe_2O_3 (Fig. S9 of SI) and Co_3O_4 (Fig. S10 of SI) was successfully recorded by using backscattered electron (BE) detector. From these images, well dispersed bright-colour-dots are evident, which are identified as gold particles and later confirmed by EDS analysis. High resolution micrographs of gold catalysts captured by TEM are presented in Fig. 6.9. The gold particle deposited on Fe_2O_3 is shown in Fig. 6.9a and the gold supported on Co_3O_4 is in Fig. 6.9b. In general, the Au particle size observed is in the range of 8-30 nm. TEM image and particle distribution are provided in Fig. S11 of SI and suggests an average particle size of 18 nm, significantly higher than the particle size suggested for optimal activity of supported Au catalysts [26].

The influence of gold particle size in methane oxidation was reported by Blick et al [27], who found that gold particles with diameter of 5-10 nm supported on MgO were active for converting methane into CO and CO_2. The same effect was observed also over Au/Al_2O_3 catalysts prepared by impregnation and deposition-precipitation methods where the smallest particle sizes (3-5 nm) were found to be the most active [28]. An enhanced catalytic activity of the nano-sized gold (8-9 nm) was demonstrated recently upon loading 10 wt% of Au on Co_3O_4 [21]. However, in our samples, the gold loading was below 3 wt% and the average gold particle size is 18 nm for Au/Co_3O_4 catalysts

(based on TEM analysis). It was expected that loading the gold to the metal oxide catalyst surface would produce an increase in catalytic activity, however the gold particle in the samples tested does not enhance methane conversion (see Fig. 6.7).

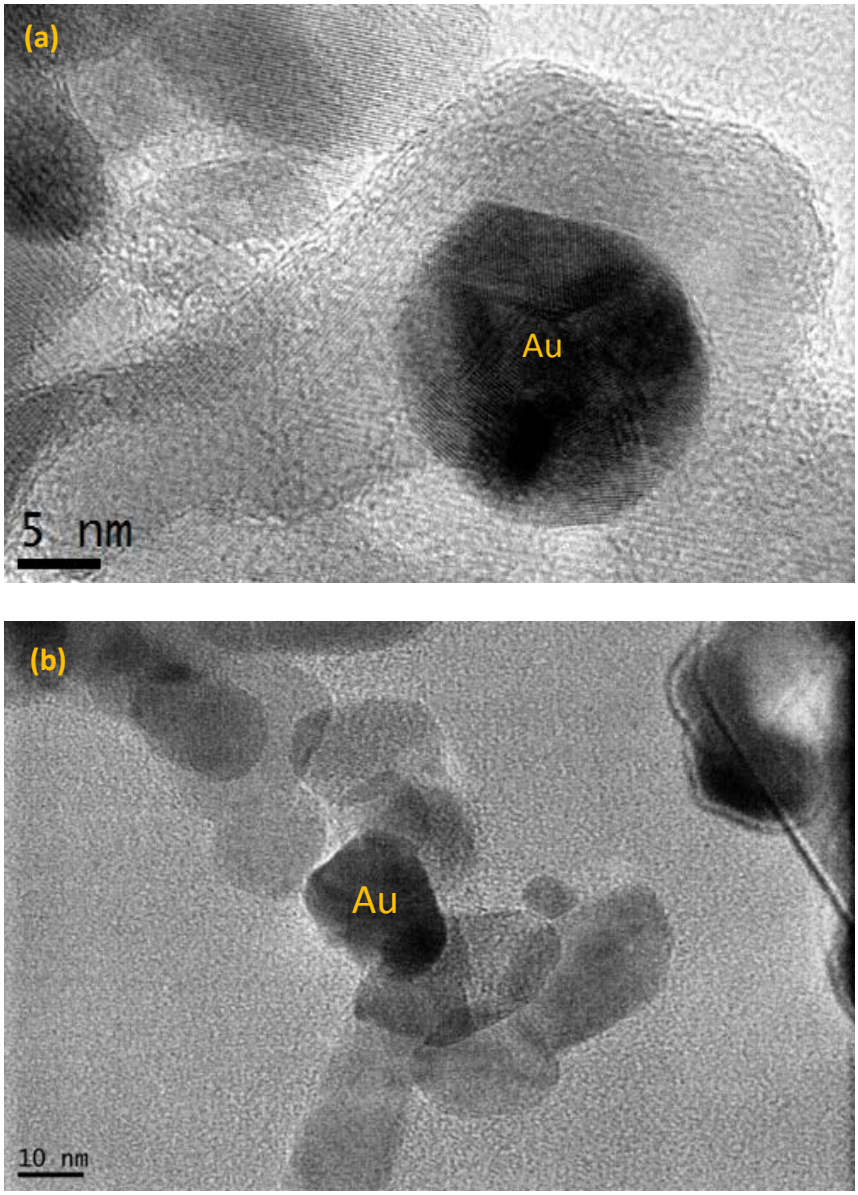

Fig. 6.9. HR-TEM images of (a) Au/Fe_2O_3 and (b) Au/Co_3O_4 catalysts.

The inhibiting effect of water was investigated for Au supported on Co_3O_4 and Fe_2O_3 catalysts. Fig. 6.10 shows H_2O-TPD spectra of Au/Co_3O_4 in comparison with spectra of Co_3O_4 catalysts where the water was adsorbed under similar condition as described above. Peak fitting of TPD spectra suggests four desorption states of water from Au/Co_3O_4 catalysts at temperatures of 195 °C, 243 °C, 309 °C and 498 °C. These peak positions have shifted slightly in comparison to the position of the peaks found for desorption from Co_3O_4 which is related to the loading Au on Co_3O_4.

TPD spectra of water desorbed from Fe_2O_3 catalyst were compared with the spectra obtained from Au/Fe_2O_3 catalysts, in order to explore the interaction between the hydroxyl groups on the catalyst, the gold and support. Both spectra are shown in Fig. 6.11. Gaussian peak fitting of Au/Fe_2O_3 TPD spectra suggests four adsorption states of water resulting in desorption peaks at temperatures of 192 °C, 224 °C, 294 °C and 469 °C. These peaks are similar to those found for water desorption from Fe_2O_3. It is interesting to see that upon loading gold on the iron oxide, no new adsorption sites (desorption peaks) were detected. Evidence for interaction between water and gold was essentially absent from these spectra. This suggests that most of water was adsorbed on Fe_2O_3. This is consistent with our XPS result below, where hydroxyl species were detected on the sample that was used for time-on-stream experiments under humid condition.

The water and catalyst interaction during catalytic combustion of methane was investigated using TPD analysis of used gold catalysts (TOS experiments as plotted in Fig. 6.8). After the TOS experiment was terminated, the catalyst was purged with helium while cooling in the furnace to room temperature. The sample was immediately

transferred into a TPD tube. Desorption of H_2O was then started from 30 ºC until 650 ºC at heating rate of 5 ºC min^{-1}. Fig. 6.12 shows the TPD spectra of water which was adsorbed on the surface of Au/Fe_2O_3 and Au/Co_3O_4 catalysts during TOS experiments.

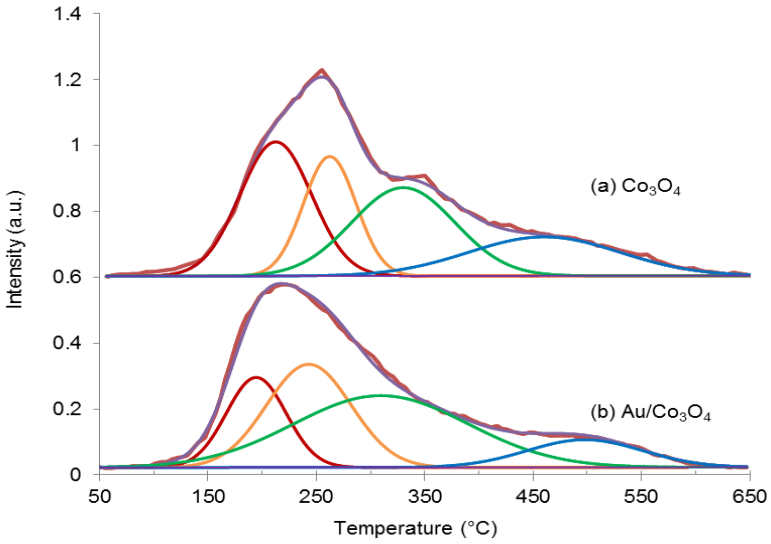

Fig. 6.10. TPD profile of H_2O desorption of (a) Co_3O_4 and (b)Au/Co_3O_4 catalysts at heating rate of 5 ºC.min^{-1}, H_2O adsorption at 150 ºC. Plot (a) was offset by 0.6 a.u. to improve clarity.

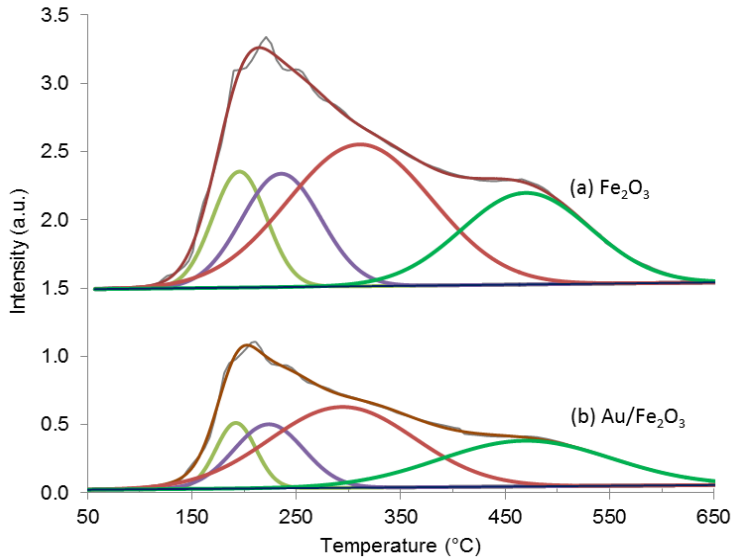

Fig. 6.11. TPD profile of H_2O desorption of (a) Fe_2O_3 and (b) Au/Fe_2O_3 catalysts at heating rate of 5 ºC·min^{-1}, H_2O adsorption at 150 ºC. Plot (a) was offset by 1.5 a.u. for clarity.

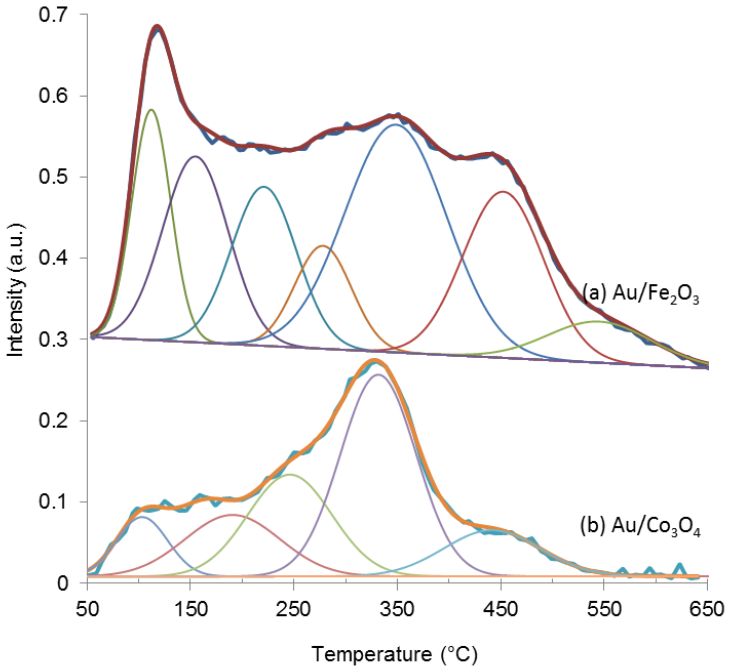

Fig. 6.12. TPD profile of H_2O desorption over (a) used Au/Fe_2O_3 and (b) used Au/Co_3O_4 catalysts. H_2O was adsorbed during TOS experiment as plotted in Fig. 6.8. Plot (a) was offset by a straight line for better visualization.

As shown in Fig. 6.12, TPD spectra of Au/Fe_2O_3 catalyst can be fitted based on seven distinct sites for H_2O adsorption. The main water desorption sites were observed at 120 ºC, 350 ºC and 450 ºC. The peak at 120 ºC is the most intense peak, which can be interpreted as the weakest bond of hydroxyl compounds adsorbed on Au/Fe_2O_3 catalyst, whereas the peaks at higher temperatures are mostly related to hydroxyl compounds adsorbed during time-on-stream experiment under wet feed as described in Fig. 6.8. As expected, TPD analysis of used Au/Co_3O_4 catalyst results in a lower net H_2O coverage and in turn less prominent desorption peaks compared to that of Au/Fe_2O_3 catalyst. Curve fitting suggests that there are five peaks at temperatures of 103 ºC, 161 ºC, 246 ºC, 332 ºC and 441 ºC, respectively. The most intense peak is at 332 ºC while the smallest peak is at 441 ºC. It is suggested that at 441 ºC, very little H_2O is adsorbed on the surface of Au/Co_3O_4 catalyst when compared to Au supported on Fe_2O_3. As a result,

we speculate that the presence of water during time-on-stream experiment over Au/Co_3O_4 (see Fig. 6.8) has, similar to the Co_3O_4 support, little effect on methane combustion.

The oxidation state and surface composition of 1.7 wt% Au/Fe_2O_3 and 2.2 wt% Au/Co_3O_4 catalysts were analysed with XPS. Both samples were calcined ex-situ in air at 400 °C for 4 h before loading to the XPS sample holder. The spectra of Au 4f core level region are plotted in Figure 6.13 and the surface composition is provided in Table 6.2. Deconvolution of the peak under the curve at Au $4f_{7/2}$ core-level was performed using Gaussian-Lorentzian (30:70) peak shapes. There is a single element detected at binding energies (BE's) of 84.1 eV and 84.4 eV for Au/Fe_2O_3 and Au/Co_3O_4, respectively (FWHM = 0.84-0.89 eV). From each sample, the single peak is identified as Au^0 which is consistent with the binding energies reported in the literature [21, 29].

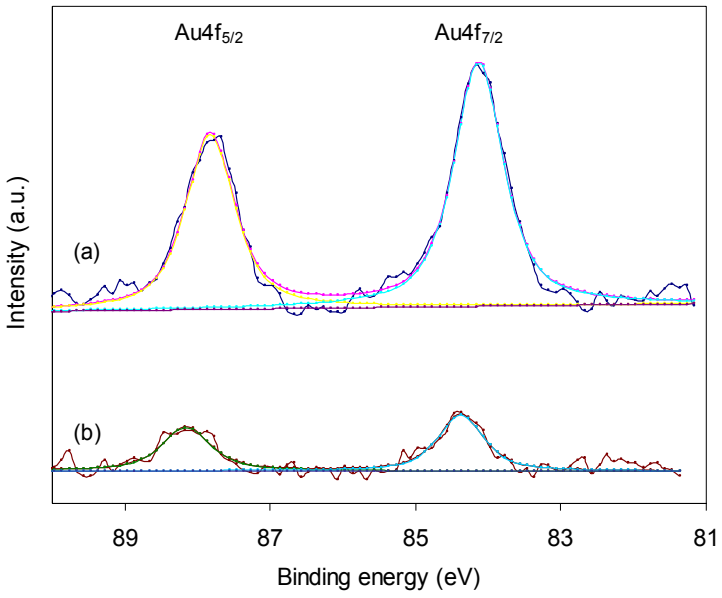

Fig. 6.13. XPS spectra of Au 4f core level of (a) Au/Fe_2O_3 and (b) Au/Co_3O_4catalysts.

Table 6.2. XPS peak position and surface composition

Sample	Au 4f peak position (eV)		Surface composition (%)				
	$Au4f_{7/2}$	$Au4f_{5/2}$	Au	O	Fe	Co	C
a. 1.7 Au/Fe_2O_3	84.1	87.8	0.14	61.6	32.6	-	4.21
b. 2.2 Au/Co_3O_4	84.4	88.2	0.05	58.9	-	35.6	2.94

It is interesting to note that the Au peak on Au/Co_3O_4 is small, (see Table 6.2), indicating only a low surface concentration of Au. This result is consistent with our finding from TPD analysis. Comparison of Co_3O_4 and Au/Co_3O_4 TPD spectra (Fig. 6.10) suggests that the H_2O desorption temperatures and in turn adsorption energies of both samples are similar.

6.4. Conclusions

The activity and hydrothermal stability of Co_3O_4, Fe_2O_3, Au/Co_3O_4 and Au/Fe_2O_3 catalysts were evaluated for catalytic combustion of lean air-methane mixtures. Excellent stability was observed over nano-particle Co_3O_4 and Au/Co_3O_4 during time-on-stream experiments. No changes in oxidation/chemical states were observed from Co_3O_4 catalyst, before and after TOS experiments. The presence of strongly bonded adsorption of hydroxyl species on the surface of all catalysts studied, as observed by TPD and XPS analyses, highlights the role of water as being responsible for the rapid deactivation over Fe_2O_3 and Au/Fe_2O_3 catalysts. Nevertheless, co-precipitating gold with cobalt oxide or iron oxide does not enhance the activity of the catalyst.

References

1. Solomon, S., D. Qin, M. Manning, Z. Chen, M. Marquis, K.B. Averyt, M. Tignor, and H.L. Miller, *Climate change 2007: The physical science basis*, in

Contribution of working group I to the fourth assessment report of the intergovernmental panel on climate change. 2007, Cambridge University Press: Cambridge, United Kingdom and New York, NY, USA

2. Stolaroff, J.K., S. Bhattacharyya, C.A. Smith, W.L. Bourcier, P.J. Cameron-Smith, and R.D. Aines, *Review of methane mitigation technologies with application to rapid release of methane from the arctic.* Environmental Science & Technology, 2012. 46(12): p. 6455-6469.

3. Gelin, P. and M. Primet, *Complete oxidation of methane at low temperature over noble metal based catalysts: a review.* Applied Catalysis B: Environmental, 2002. 39: p. 1-37.

4. Setiawan, A., J. Friggieri, E.M. Kennedy, B.Z. Dlugogorski, and M. Stockenhuber, *Catalytic combustion of ventilation air methane (VAM) – long term catalyst stability in the presence of water vapour and mine dust.* Catalysis Science & Technology, 2014.

5. Bond, G.C., *Gold: a relatively new catalyst.* Catalysis Today, 2002. 72: p. 5-9.

6. Haruta, M., T. Kobayashi, H. Sano, and N. Yamada, *Novel gold catalysts for the oxidation of carbon monoxide at a temperature far below 0 ^oC.* Chemistry Letters, 1987: p. 405-408.

7. Waters, R.D., J.J. Weimer, and J.E. Smith, *An investigation of the activity of coprecipitated gold catalysts for methane oxidation.* Catalysis Letters, 1995. 30: p. 181-188.

8. Grisel, R.J.H. and B.E. Nieuwenhuys, *A comparative study of the oxidation of CO and CH_4 over $Au/MOx/Al_2O_3$ catalysts.* Catalysis Today, 2001. 64(1–2): p. 69-81.

9. Miao, S. and Y. Deng, *Au-Pt/Co_3O_4 catalyst for methane combustion.* Applied Catalysis B: Environmental, 2001. 31: p. L1-L2.

10. Solsona, B.E., T. Garcia, C. Jones, S.H. Taylor, A.F. Carley, and G.J. Hutchings, *Supported gold catalysts for the total oxidation of alkanes and carbon monoxide.* Applied Catalysis A: General, 2006. 312: p. 67-76.

11. Choudhary, V.R., V.P. Patil, P. Jana, and B.S. Uphade, *Nano-gold supported on Fe_2O_3: A highly active catalyst for low temperature oxidative destruction of methane green house gas from exhaust/waste gases.* Applied Catalysis A: General, 2008. 350: p. 186-190.

12. Choudhary, T.V., S. Banerjee, and V.R. Choudhary, *Catalysts for combustion of methane and lower alkanes.* Applied Catalysis A: General, 2002. 234(1-2): p. 1-23.

13. Paredes, J.R., E. Diaz, F.V. Diez, and S. Ordonez, *Combustion of methane in lean mixtures over bulk transition-metal oxides: evaluation of the activity and self-deactivation.* Energy Fuels, 2009. 23(1): p. 86-93.

14. Hu, L., Q. Peng, and Y. Li, *Selective synthesis of Co_3O_4 nanocrystal with different shape and crystal plane effect on catalytic property for methane combustion.* Journal of the American Chemical Society, 2008. 130(48): p. 16136-16137.

15. Fei, Z., S. He, L. Li, W. Ji, and C.-T. Au, *Morphology-directed synthesis of Co_3O_4 nanotubes based on modified Kirkendall effect and its application in CH_4 combustion.* Chemical Communication, 2012. 48(6): p. 853-855.

16. Liu, Y., H. Tuysuz, C.-J. Jia, M. Schwickardi, R. Rinaldi, A.-H. Lu, W. Schmidt, and F. Schuth, *From glycerol to allyl alcohol: iron oxide catalyzed dehydration and consecutive hydrogen transfer.* Chemical Communication, 2010. 46(8): p. 1238-1240.

17. Setiawan, A., E.M. Kennedy, B.Z. Dlugogorski, A.A. Adesina, O. Tkachenko, and M. Stockenhuber, *Evidence of the formation of surface palladium carbide during the catalytic combustion of lean methane/air mixtures.* Energy Technology (Weinheim, Ger.), 2014. 2.

18. Liu, Y., H. Dai, J. Deng, S. Xie, H. Yang, W. Tan, W. Han, Y. Jiang, and G. Guo, *Mesoporous Co_3O_4-supported gold nanocatalysts: highly active for the oxidation of carbon monoxide, benzene, toluene, and o-xylene.* Journal of Catalysis, 2014. 309(0): p. 408-418.

19. Bahlawane, N., *Kinetics of methane combustion over CVD-made cobalt oxide catalysts.* Applied Catalysis B: Environmental, 2006. 67(3–4): p. 168-176.

20. Liotta, L.F., H. Wu, G. Pantaleo, and A.M. Venezia, *Co_3O_4 nanocrystals and Co_3O_4-MOx binary oxides for CO, CH_4 and VOC oxidation at low temperatures: a review.* Catalysis Science & Technology, 2013. 3(12): p. 3085-3102.

21. Liotta, L.F., G. DiCarlo, A. Longo, G. Pantaleo, and A.M. Venezia, *Support effect on the catalytic performance of Au/Co_3O_4-CeO_2 catalysts for CO and CH_4 oxidation.* Catalysis Today, 2008. 139: p. 174-179.

22. Zhang, Y., T. Ma, and J. Zhao, *Study on the conversion of glycerol to nitriles over a $Fe_{19.2}K_{0.2}/\gamma$-Al_2O_3 catalyst.* Journal of Catalysis, 2014. 313(0): p. 92-103.

23. Grosvenor, A.P., B.A. Kobe, M.C. Biesinger, and N.S. McIntyre, *Investigation of multiplet splitting of Fe 2p XPS spectra and bonding in iron compounds.* Surface and Interface Analysis, 2004. 36(12): p. 1564-1574.

24. Senanayake, S.D., D. Stacchiola, P. Liu, C.B. Mullins, J. Hrbek, and J.A. Rodriguez, *Interaction of CO with OH on Au(111): HCOO, CO_3, and HOCO as key intermediates in the water-gas shift reaction.* Journal of Physical Chemistry C, 2009. 113(45): p. 19536-19544.

25. Naumkin, A.V., A. Kraut-Vass, S.W. Gaarenstroom, and C.J. Powell, *NIST Standard Reference Database 20, Version 4.1*. 2012.

26. Haruta, M., *Size and support dependency in the catalysis of gold.* Catalysis Today, 1997. 36(1): p. 153-166.

27. Blick, K., T.D. Mitrelias, J.S.J. Hargreaves, G.J. Hutchings, R.W. Joyner, C.J. Kiely, and F.E. Wagner, *Methane oxidation using Au/MgO catalysts.* Catalysis Letters, 1998. 50: p. 211-218.

28. Grisel, R.J.H., P.J. Kooyman, and B.E. Nieuwenhuys, *Influence of the preparation of Au/Al_2O_3 on CH_4 oxidation activity.* Journal of Catalysis, 2000. 191(2): p. 430-437.

29. Solsona, B., M. Pérez-Cabero, I. Vázquez, A. Dejoz, T. García, J. Álvarez-Rodríguez, J. El-Haskouri, D. Beltrán, and P. Amorós, *Total oxidation of VOCs on Au nanoparticles anchored on Co doped mesoporous UVM-7 silica.* Chemical Engineering Journal, 2012. 187(0): p. 391-400.

CHAPTER 7

Understanding the hydrothermal stability of palladium supported on TS-1 catalyst in catalytic combustion of lean methane in air mixtures

Submitted to:

Journal of Catalysis

Appendix E supplied the supporting information of this chapter.

7.1. Introduction

Catalytic combustion of methane is a potential solution to mitigate methane emissions as it can operate outside the flammability range and production of NO_x is essentially absent due to its relatively low reaction temperatures. Supported Pd catalysts are considered to be excellent catalysts for this reaction [1]. Poisoning by water and other contaminants can have long-term deleterious effects, and significantly reduce the potential for their use in catalytic combustion of fugitive methane emission from coal mines ventilation air [2].

Earlier studies reported that water significantly inhibits the activity of Pd on Al_2O_3 [3, 4] and Pd on zeolites [5, 6] at lower temperatures, which is due to competition between water and methane for adsorption on catalyst active sites [3, 4, 7]. Furthermore, an irreversible deactivation can be induced by the presence of water where the active site (palladium oxide) transforms into a less active site (palladium hydroxide) [3, 4, 7]. Ciuparu et al suggested that the hydroxyl groups produced by the methane combustion reaction are bound strongly on the surface [8] and accumulate on the support [9]. Therefore, when external water is introduced the surface becomes saturated and the rate of desorption is decreased [8].

In addition to its well defined, crystalline microporous nature and redox activity, the TS-1 zeotype is known as a more hydrophobic material compared to other zeolites [10]. Due to their microporous and well defined pore structure, zeolites often are used to support redox functionalities because of their ability to stabilise small clusters. The

titanium silicalite-1 (TS-1) materials initially prepared by Taramasso et al. were effectively used as a catalyst for the selective oxidation of alkenes and alcohol substrates using hydrogen peroxide [11-13]. Using photoassisted deposition (PAD) method, nanosize Pd particles were successfully deposited on TS-1 and tested for direct synthesis of H_2O_2 from H_2 and O_2 [14]. Very recently, the preparation of Au-Pd nano-particles supported on hierarchical TS-1 catalysts was evaluated for selective oxidation of benzyl alcohol using in situ generated hydrogen peroxide [15]. It was found that the use of TS-1 as catalyst support improved metal dispersion [15]. It is generally agreed that the dispersion of the noble metal is one of the key factors for improving the activity of palladium catalysts for methane oxidation [1]. These properties are thought to improve the long term stability of a combustion catalyst and thus we investigated TS-1 as a support material for palladium catalysts under long-term reaction conditions. To our knowledge, for catalytic combustion of lean methane mixtures, palladium supported on TS-1 has not been previously reported.

Attempts to improve the tolerance against water poisoning were undertaken by supporting palladium on composite materials such as $LaMnO_3$-ZrO_2 [16] and TiO_2-SiO_2 [17]. As reported in the literature [17], mixing titanium and silica oxides avoids or delays the reaction between Pd and H_2O. A hydrothermal stability test was reported recently by Liu et al. [4] by using Ni-modified alumina as support at a reaction temperature of 600 ºC. Our recent work on a long term stability test (1,150 h) over Pd/Al_2O_3 catalyst disclosed that the level of 90 % methane conversion is achievable at temperatures ≤ 500 ºC in the presence of water in the feed [2].

For the current work, we prepared a new palladium catalyst using titanium silicalite (TS-1) zeolite as support for methane combustion to gain a better understanding of the underlying principles that govern catalyst stability. The resistance of this catalyst was evaluated during catalytic combustion of lean methane in air over an extended period of time. The long term stability test was performed under conditions where the level of methane conversion was maintained at or above 90 % at a gas hourly space velocity of 100,000 h^{-1}. The physical and chemical properties of Pd/TS-1 catalyst were investigated in order to understand the advantages of this catalyst in comparison with conventional palladium on alumina catalysts.

7.2. Experimental

7.2.1. Catalyst preparation

Catalyst containing 1.4 wt% Pd/TS-1 was prepared by wet impregnation of a commercial titanium silicalite (TS-1) support (ENI-Polimeri Europa SpA) with an aliquot of Pd (II) nitrate solution (10 wt% in 10 wt% nitric acid, Sigma-Aldrich) mixed using a mortar and pestle. Water was added drop-wise while mixing, until a paste was formed. The resulting paste was dried in an oven at 110 °C for approximately 20 h. The dried catalyst was then ground, pressed and sieved to 250-400 μm. A tubular fixed-bed reactor was employed for the calcination of the dried solid catalyst in air at 500 ºC for 2 h followed by purging in helium while slowly cooling the catalyst to desired reaction temperature. For comparison, a commercially available 1.0 wt% Pd/Al_2O_3 (Sigma-Aldrich) was used and activated under conditions as reported in our previous work [2].

7.2.2. Catalyst characterization

The surface areas of the catalysts were measured by nitrogen adsorption at 77 K using a Gemini 11 2370 surface area analyzer. A volumetric glass apparatus was employed to assess the active particle size and metal dispersion by performing hydrogen chemisorption at 35 ºC, in the pressure range between 30 and 90 mbar (vacuum measurement by Pfeiffer CMR 362-TPG 261, data logging by LabVIEW version 7.1.1). A H/Pd = 1/1 stoichiometry was assumed for H_2 chemisorption on metallic palladium [18]. Mean particle diameter was estimated based on dispersion values using the following formula [19]:

$dp = \frac{6 \times C_a \times M \times 10^9}{\rho \times D \times N_a}$, where Ca is concentration of surface metal atom (equal to 1.27×10^{19} atoms m^{-2}) [19], M is Pd atomic mass, ρ is Pd volumetric mass (equal to 12.02×10^6 g m^{-3}) [19], D is metal dispersion and Na is Avogadro number. Temperature-programmed desorption (TPD) analysis was undertaken using a purpose built TPD apparatus with a Pfeiffer Prisma quadrupole mass analyser for detection. Zeiss Sigma VP FESEM served to capture the Scanning Electron Microscopy (SEM) images of the sample using a secondary electron (SE) detector and backscattered electron (BE) detector. A JEOL 2200 FS transmission electronic microscope (TEM) with EDS and a scanning transmission electron microscope (STEM) system was used for imaging nano-sized Pd particles and support as well as measuring the particle size distribution. Palladium loading was quantified using a Varian 715-ES inductively coupled plasma optical emission spectrometer (ICP-OES). Powder X-Ray diffraction patterns of catalysts were examined using Cu Kα radiation with a Philips X'Pert diffractometer.

Diffractograms were collected in the 2θ angle range from 2° to 90° with 0.008° 2θ step resolution.

For surface analysis, X-ray photoelectron spectroscopy (XPS) was conducted using monochromated Al K alpha (energy 1486.68 eV) radiation and the emitted photoelectrons were analyzed using an ESCALAB250Xi manufactured by Thermo Scientific, UK. To minimize the possibility of sample contamination, spent samples were immediately transferred into sealed containers after stopping the reaction by cooling in helium. The sample was mounted on the stub using indium tape. The energy scale of the XPS spectra was referenced to the adventitious carbon adsorption at 284.6 eV. The spectrometer was calibrated against binding energies of Au $4f_{7/2}$ = 83.96 eV, Ag $3d_{5/2}$ = 368.21 eV and Cu $2p_{3/2}$ = 932.62 eV.

7.2.3. Catalytic activity assessment

The activity of the catalyst was measured in a tubular stainless steel micro reactor. The inlet methane concentration was fixed at 7,000 ppm balanced with air (for the wet feed 3.2 vol% H_2O was added) at a gas hourly space velocity (GHSV) of 100,000 h^{-1}. The inlet and outlet gas mixtures were analyzed using an online gas chromatograph equipped with a thermal conductivity detector (TCD) and concentric-packed single column (Alltech CTR-I). For wet feed experiments, the reactant mixture was passed through a saturator and a humidity probe was installed at the outlet. The reaction temperature was measured with a K-type thermocouple placed into the catalyst bed.

For catalytic stability studies, a second, separate reactor set-up was used and operated continuously under varying reaction conditions (temperature was increased in order to achieve a 90 % level of conversion for methane). Throughout the study, the feed concentration of methane and carbon dioxide were kept constant at 7,000 ppm and 10,000 ppm, respectively. The saturator system was operated at ambient temperature (25 ºC ± 3 ºC) resulting in a relative humidity of ca. 85 % (corresponding to a $H_2O_{(v)}$ pressure of between 30 000 – 40 000 ppm). This humidity is well within the range of a typical coal mine as reported in the literature [20]. The targeted 90 % methane conversion was maintained by increasing the catalyst bed temperature as the catalyst deactivated during time on stream up to 1,900 h.

Kinetic measurements were carried out over the fresh and long-term used catalysts using a wet feed containing 7,000 ppm CH_4, 3.2 % H_2O balanced with air. Carbon dioxide was not added to the feed since the reaction rate is independent of the partial pressure of CO_2 [21]. The turn-over frequency (TOF), defined as the moles of methane converted per second and per mole of active site was calculated under conditions where the methane conversion level was below 15 %. The number of active sites on the catalyst was estimated based on palladium dispersion measurements. Pd dispersion was also calculated based on the average Pd particle size measured by TEM analysis (for fresh and used catalysts) using the formula mentioned above.

7.3. Results and discussion

7.3.1. Catalyst activity and stability under wet feed conditions

In addition to catalytic activity measurements in the micro-reactor, the surface reactions involved in methane combustion over the Pd/TS-1 were studied using temperature programmed desorption (TPD) analysis. The sample was heated under vacuum at 500 °C for 1 h to remove any pre-adsorbed compounds. At 110 °C, methane (99.99 %) was adsorbed. Subsequently, the products were desorbed and the gas phase was analysed. During the desorption experiments, a significant quantity of CO_2 was produced, suggesting methane is being oxidised by lattice oxygen of the catalyst. This result suggests that the surface oxygen participates in the methane oxidation reaction, following a Mars-van Krevelen mechanism under these conditions [22, 23]. Fig. 7.1 shows TPD profiles of CO_2 (m/z = 44) desorbed from Pd/TS-1 catalyst. TPD spectra indicate that a significant rate of desorption of CO_2 was detected at temperatures ranging from 270 °C to 400 °C with a maximum desorption rate at 395 °C. It is expected that in the plug-flow reactor study, methane oxidation can utilize lattice oxygen from the catalyst over this temperature range.

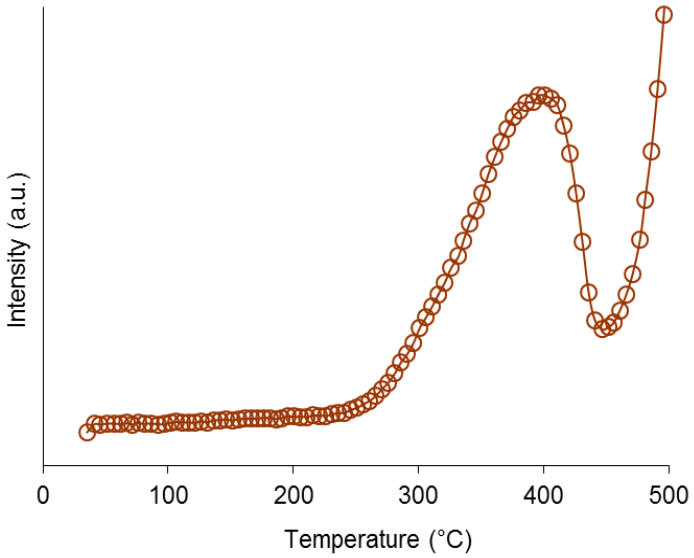

Fig. 7.1. TPD spectra of CO_2 (m/z = 44) desorbed from Pd/TS-1 catalysts. CO_2 was produced under vacuum on the surface of catalysts subsequent to CH_4 *in-situ* adsorption at 110 °C in presence of water. Heating ramp = 5 °C·min^{-1}.

The catalytic performance of Pd/TS-1 catalyst was measured for total oxidation of methane in the presence of water vapour in the feed. For initial activation, the catalyst was calcined in air at 500 °C for 2 h then cooled to 200 °C in a flow of helium. A feed of 7,000 ppm methane and 3.2 vol.% H_2O in air was passed through the catalyst bed with a GHSV of 100,000 h^{-1}. The experiment was then started by gradually increasing the furnace temperature.

Methane conversion as a function of reaction temperature (light off curve) over Pd/TS-1 catalyst is plotted in Fig. 7.2. As a comparison, the activity of Pd/Al_2O_3 catalyst was tested under similar conditions and also plotted in Fig. 7.2. Comparison of the light off curves suggests that palladium supported on TS-1 has similar activity to Pd/Al_2O_3 catalyst. Methane was converted to CO_2 within a similar temperature range as suggested by TPD experiment in Fig. 7.1. The temperature of 90 % conversion of methane (T_{90}) over Pd/TS-1 is only 20 °C (approximately) lower than the T_{90} of the Pd/Al_2O_3 catalyst. Note that a TS-1 sample (without Pd loading) was also tested under similar condition as described previously and conversion of methane was not detected at temperatures as high as 510 °C confirming that TS-1 zeolite itself is not an active catalyst for methane oxidation under our reaction conditions. The deposited palladium particles on TS-1 are responsible for converting methane to carbon dioxide.

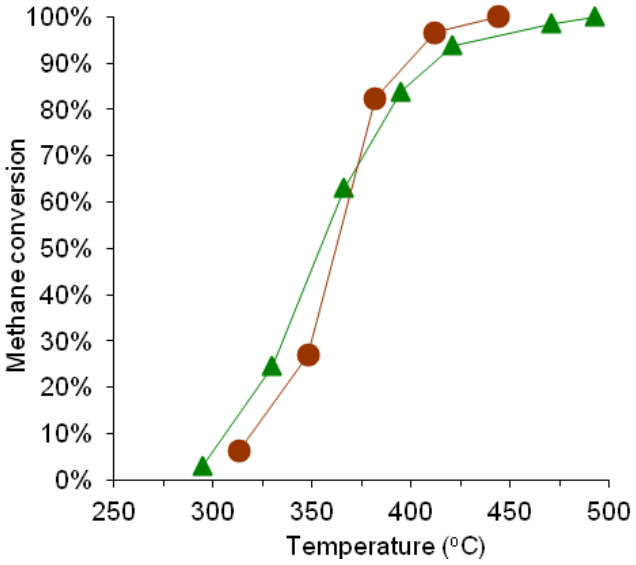

Fig. 7.2. Methane conversion as a function of reaction temperature of methane oxidation over (▲) Pd/Al_2O_3 and (●) Pd/TS-1 catalysts. GHSV = 100,000 h^{-1}, feed: 7,000 ppm CH_4, 3.2 vol.% H_2O balance air.

Evaluation of the catalyst stability of the Pd/TS-1 was performed using a separate reactor configuration which was operated continuously under varying reaction temperatures in order to maintain a 90 % level of methane conversion. The feed composition for these long term stability tests was adjusted mimicking the ventilation air composition typically emitted from a coal mine (7,000 ppm CH_4; 10,000 ppm CO_2; 30,000 to 40,000 ppm H_2O balance air). Fig. 7.3 shows the catalyst bed reactor temperature required for maintaining a 90 % conversion of methane of Pd/TS-1 catalyst over 1,900 h.

At beginning of the run, the initial temperature to achieve 90 % conversion (T_{90}) was 430 °C and after 1,900 h time on stream, the bed temperature was slowly increased up to 451 °C. Methane conversion level was maintained at 90 % conversion after 160 h reaction without any drop in activity (constant T_{90}) over the experimental run. It has been confirmed previously that the water vapour present in the feed would be the

primary factor for catalyst deactivation in addition to the water produced from reaction [2]. A very stable activity was observed from this catalyst. As plotted in Fig. 7.3, the bed temperature to achieve 90 % conversion curve appears to plateau starting from 160 h until 1,900 h time-on-stream which indicates that the deactivation process occurred at a very slow rate. This experiment suggests that using TS-1 as a support material can successfully reduce the rate of deactivation of Pd-based catalyst and achieved an almost constant activity after 160 h on stream.

The catalyst bed reactor temperature required for maintaining a 90 % conversion of methane using Pd/TS-1 catalyst is compared with data that we reported earlier [2] and plotted in Fig. 7.3. Surprisingly, the bed temperature of Pd/TS-1 catalyst after 1,100 h under a humid feed is approximately 55 °C lower when compared to the temperature of Pd/Al_2O_3 catalyst. This suggests the rate of deactivation of TS-1 supported Pd catalyst is very slow compared to the rate observed over Pd/Al_2O_3 catalyst. The difference in the stability of the catalytic activity between Pd/Al_2O_3 and Pd/TS-1 catalysts is due to the difference in the nature of support material, reducing the formation of hydroxyl groups on the surface (please see below). The higher rate of deactivation of Pd/Al_2O_3 was suggested to be due to the hydroxyl accumulation on the oxide support inhibits oxygen mobility on the supports [9]. This accumulation prevents the migration of oxygen from support to active site and participation in combustion reaction. Moreover, hydroxyl accumulation can block the active site and promote the formation of Pd-OH bond [2, 9].

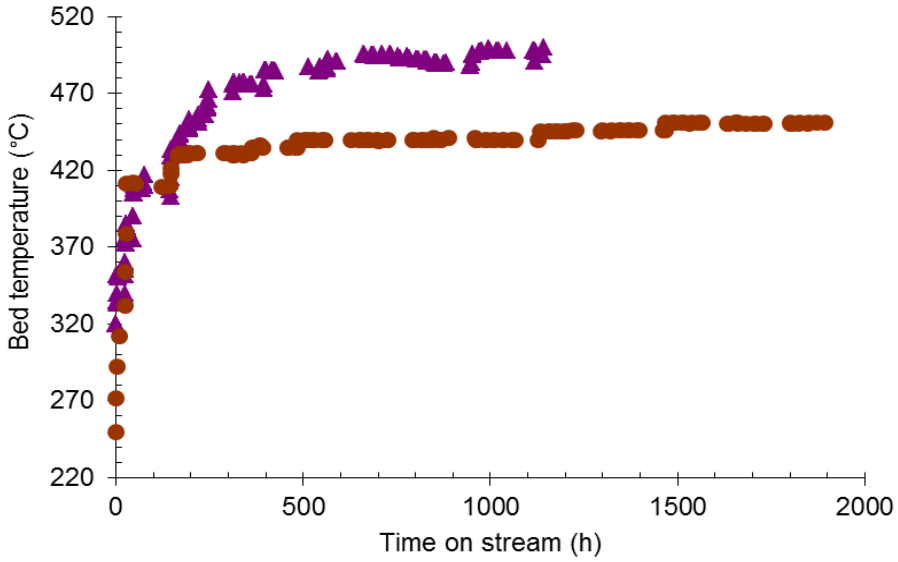

Fig. 7.3. Catalyst bed temperature required for 90 % CH_4 conversion over Pd/TS-1 and Pd/Al_2O_3 catalysts. Feed: 7,000 ppm CH_4; 10,000 ppm CO_2; 30,000 – 40,000 ppm H_2O balance air, GHSV = 100,000 h^{-1}. ▲ = TOS experiment over Pd/Al_2O_3; ● = TOS experiment over Pd/TS-1.

The temperature dependency of the rate of reaction in lean methane combustion at low conversion over Pd/TS-1 and Pd/Al_2O_3 catalysts was investigated under the procedures as mentioned in experimental section. Fig. 7.4 provides the Arrhenius plots of fresh catalysts under dry and wet feed conditions. The apparent activation energies for methane combustion under dry feed condition were 117 and 95 kJ mol^{-1} for fresh Pd/TS-1 and Pd/Al_2O_3 catalysts, respectively. This data are comparable with the activation energies reported in the literature [24, 25]. Our calculation on turn-over frequency (TOF) at 260 °C resulted in 0.009 s^{-1} for Pd supported on TS-1 and 0.015 s^{-1} for Pd supported on alumina.

In the presence of water in the feed, observable activities over fresh Pd/TS-1 and Pd/Al_2O_3 catalysts were shifted to higher reaction temperature (at 312 °C) resulting in TOF's of 0.007 s^{-1} and 0.015 s^{-1}, respectively. Estimation of the apparent activation

energy resulted in 247 kJ mol^{-1} for Pd/TS-1 compared to 159 kJ mol^{-1} for Pd/Al_2O_3 catalyst. The activation energy of the conversion over the fresh Pd/Al_2O_3 catalyst is consistent with the data reported by van Giezen et al [21]. As suggested in the literature, the influence of water on the rate of reaction of methane combustion over palladium catalysts is temperature dependent and negative first order [7, 21]. The inhibiting effect of water decreases with increasing the temperature and becomes insignificant at temperatures above 450 °C [3, 8].

The comparison indicates that with a dry feed, the activation barrier over the Pd/TS-1 and Pd/Al_2O_3 catalysts is significantly smaller than under conditions when the combustion gas was saturated with water vapour. A possible explanation for this behaviour can be related to the availability of labile oxygen for the combustion. As indicated above, at least some of the catalytic combustion is occurring via a Mars van Krevelen type mechanism. Clear evidence can be found in Fig. 7.1, where the reaction with methane and the absence of any oxidant results in the formation of CO_2, suggesting the reaction of methane occurs with stored surface oxygen. Evidence for the existence of mobile, stored oxygen can also be observed in Fig. 7.5, please see below for a detailed description. It is important to note that, below 300 °C very little oxygen was desorbed from both Pd/Al_2O_3 and Pd/TS-1. Thus, it can be inferred that below 300 °C either a different reaction mechanism is operating that does not depend on the availability of the mobile oxygen species from the solid or the low "effective" oxygen surface coverage (oxygen available for the reaction) results in a lower activation energy [26] (also see below). During oxidation experiments in the presence of water vapour, the reaction temperature was higher (> 45 °C) than without the addition of water and thus more mobile surface oxygen species are available for reaction on the catalyst. The

"effective" surface coverage of oxygen is expected to be higher than at lower temperatures. Thus, the activation energy of methane oxidation over the fresh catalysts would be higher than at lower temperatures, consistent with what is observed experimentally. In contrast, competitive adsorption between O_2 and H_2O is expected to have an effect, which would result in lower oxygen surface coverage over the Pd/Al_2O_3 catalyst, in turn resulting in a lower apparent activation energy contradicting the observation (Fig 7.4). However, increasing the reaction temperature will result in a reduced relative coverage of water/O_2 (heat of adsorption of water on supported Pd catalysts is lower than that of oxygen [27, 28]) only partially offsetting the effect of the increased availability of oxygen.

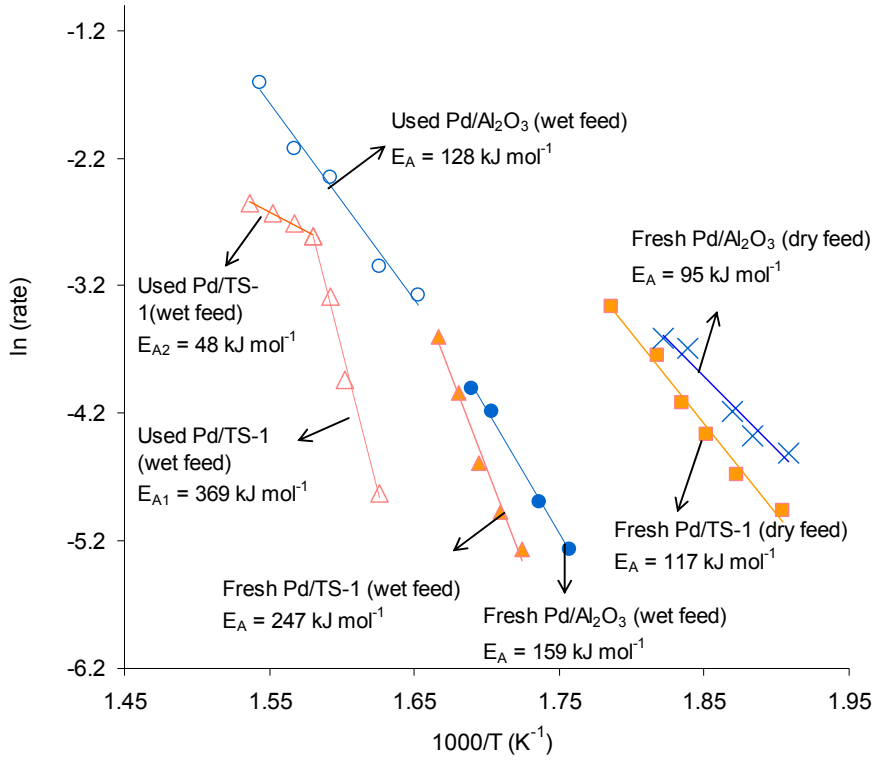

Fig. 7.4. The Arrhenius plots of Pd/TS-1 and Pd/Al_2O_3 catalysts before (fresh) and after long-term stability tests (used). The reactions were run under wet feed conditions consisting of 7,000 ppm CH_4, 3.2 vol% H_2O in air at GHSV = 100,000 h^{-1}. ■ = fresh Pd/TS-1 (dry feed); × = fresh Pd/Al_2O_3 (dry feed); ▲= fresh Pd/TS-1 (wet feed); ● = fresh Pd/Al_2O_3 (wet feed); △ = used Pd/TS-1 (wet feed) and o = used Pd/Al_2O_3 (wet feed)

The Arrhenius plots of Pd/TS-1 and Pd/Al_2O_3 measured following long-term time on stream experiments are also plotted in Fig. 7.4. Our estimation of the rate of reaction over the used Pd/TS-1 and Pd/Al_2O_3 catalysts at 365 °C results in the TOF of 0.066 s^{-1} and 0.120 s^{-1}, respectively. It is observed that over the used Pd/TS-1 catalyst the slope of the line (and in turn the activation energy) changes at *ca* 360 °C while over the used Pd/Al_2O_3 catalyst no mechanistic change in the apparent activation energy was observed. At reaction temperatures below 360 °C, the Arrhenius plot of Pd/TS-1 suggests the activation energy is 369 kJ mol^{-1}. Above this reaction temperature, the activation energy decreases to 48 kJ mol^{-1}. In principle, this behaviour can be due to i) diffusion effects, ii) change in the mechanism and iii) due to coverage dependency of the apparent activation enthalpy [26]. External diffusion can be excluded, because the variation of the flow rate keeping space velocity constant did not result in a variation of the conversion. Steady state conversion at a GHSV of 100,000 h^{-1} only varied within the experimental error, from 6.4 % to 6.9 % when flowrate was changed from 80 ml min^{-1} to 120 ml min^{-1}. Internal diffusion for the TS-1 catalyst would be possible, but the Thiele modulus was significantly smaller than 1 (0.11) clearly suggesting (together with the lack of external diffusion) the absence of Knudsen diffusion [29]. Furthermore, the change in apparent activation energy is significantly less than 50 %, also suggesting the absence of internal diffusion [30].

The changes in activation energy in methane combustion over supported noble metal catalysts have been reported in the literature [29-31]. It was found that at lower temperatures, higher activation energies were observed which was suggested to be related to the heat of adsorption of oxygen on precious metal. The apparent higher activation energy at lower temperatures may be expressed as the sum of activation

energies for oxidation of palladium and for methane oxidation by the resulting palladium oxide [30]. As shown in Fig. 7.5, oxygen TPD from Pd on TS-1 (after co-adsorption with water at 300 °C) discloses a desorption peak of O_2 at *ca*. 480 °C whereas this peak was not observed over Pd on alumina subject to the same conditions. This suggests that at a reaction temperature of 365 °C, most of the labile oxygen will have desorbed reducing the surface coverage of oxygen. This in turn (as suggested in [26]) results in a decreasing apparent activation energy, as was observed in Fig. 7.4. The Arrhenius plot of the used Pd/TS-1 catalyst also suggests that the water molecules on the surface of Pd/TS-1 catalyst start to desorb at temperature of 360 °C resulting in an increase in rate of reaction. No accumulation of hydroxyl is expected at this temperature which is supported by TPD spectra as plotted in Fig. 7.6 and Fig. 7.7 below. On the other hand, TPD spectra of water desorbed from Pd/Al_2O_3 catalyst at temperatures < 500 °C shows a very high intensity of water adsorbed on the surface of catalyst which persistently inhibits the reaction.

7.3.3. Characterization of catalysts

The surface properties of Pd/TS-1 in comparison with Pd/Al_2O_3 catalysts were investigated utilizing TPD of oxygen. Prior to analysis, the sample was pre-treated under vacuum at 500 °C for 1 h at a heating ramp of 5 °C min^{-1}. Oxygen was co-adsorbed with H_2O at 300 °C and desorbed at 550 °C. Fig. 7.5 shows the oxygen TPD spectra (*m/z* = 32) of Pd/TS-1 and Pd/Al_2O_3 catalysts. In the presence of water, Fig. 7.5 shows that maximum rate of O_2 desorption over Pd/TS-1 was observed at 480 °C whereas in contrast over Pd/Al_2O_3 no peak was observed at this temperature range. These observations can be interpreted that the oxygen adsorption capacity is higher on

the Pd/TS-1 catalyst. Similar phenomena were reported in the literature where a highly-dispersed palladium catalyst resulted in a higher oxygen mobility [32]. As observed from TEM and chemisorption results below that, the Pd dispersion is larger on Pd/TS-1 compared to Pd/Al_2O_3 catalyst. The support has also been suggested to influence on the ability of palladium to adsorb oxygen and there was a strong correlation between the oxygen adsorption capacity of precious metal and its catalytic activity [30, 33].

The effect of water vapour on palladium supported on TS-1 catalyst was investigated using TPD analysis. Water was naturally selected as the adsorbate with the purpose of investigating the interactions between water, active sites and the support material. The intensity of water (m/z = 18) desorbed from the support material (pure TS-1) and Pd/TS-1 catalyst are provided in Fig. S1 of supplementary information (SI).

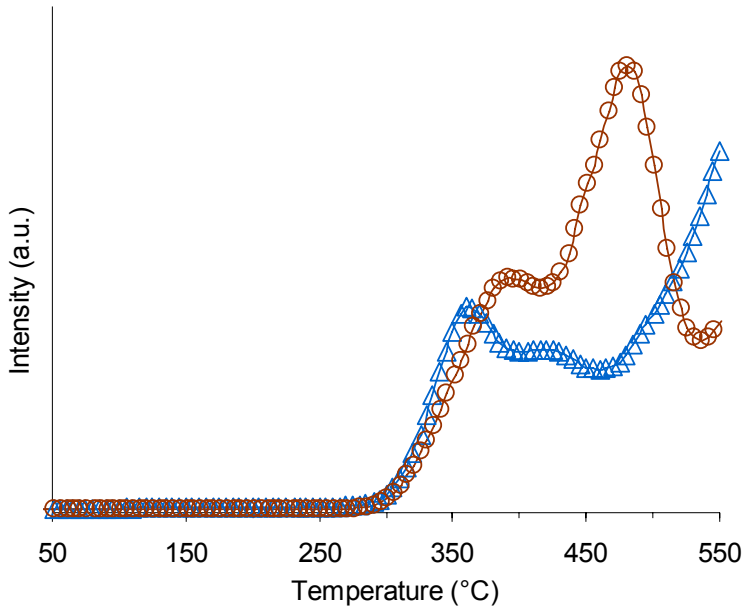

Fig. 7.5. TPD spectra of oxygen (*m/z* = 32) desorbed from Pd/Al_2O_3 and Pd/TS-1 catalysts. Oxygen was co-adsorbed with H_2O at 300 °C. Heating ramp = 5 °C·min^{-1}. Δ = Pd/Al_2O_3; ○ = Pd/TS-1.

Prior to adsorption, both samples were pre-heated for 1 h at 500 °C with a heating rate of 5 °C min^{-1} to remove any pre-adsorbed compounds. Water was adsorbed at 110 °C to avoid any weakly bound adsorbate retained on the sample. Fig. S5 of SI suggests that the TPD spectra of Pd/TS-1 are identical to what was observed in water desorption from the unmodified TS-1 support material. There are high and low temperature desorption peaks observed in both samples spectra. A low intensity peak detected at 240 °C indicates that there is a small number of water molecules adsorbed on the catalyst surface. The higher temperature peaks appearing at 510 °C and 660 °C are attributed to desorption of surface hydroxyl groups resulting in partial destruction of the lattice suggested in the literature [34-36].

Fig. 7.6 shows the comparison of TPD spectra of water desorbed from Pd/Al_2O_3 and Pd/TS-1 catalysts. The TPD spectra of Pd/Al_2O_3 suggest the presence of multiple desorption peaks at temperature below 500 °C and a higher desorption state at 610 °C. The area of the low temperature water desorption peak from Pd/Al_2O_3 is much bigger compared to the higher temperature peak (ratio = 0.73/0.27). Our data suggests that Pd/Al_2O_3 catalyst adsorbs more water at lower temperature, while Pd/TS-1 catalyst shows significantly reduced adsorption capacity for water at lower temperatures, which are relevant for the catalytic methane combustion.

Further investigation of the H_2O-TPD phenomena were carried-out over Pd/TS-1 and Pd/Al_2O_3 catalysts by adsorbing water at 110 ˚C and heating to 350 ˚C for 1 h, then cooling to room temperature. TPD analysis started from room temperature increasing to a temperature of 850 ˚C. Prior to these experiments, both catalysts were heated under vacuum at 500 ˚C for 1 h. The spectra of H_2O desorbed from both catalysts are plotted

in Fig. 7.7. This plot discloses a significant desorption peak at 450 ˚C over Pd/Al_2O_3 catalyst highlighting a stronger adsorption state of water on the surface. The opposite behaviour is observed from Pd/TS-1 catalyst, where no significant peak was detected at temperature below 500 ˚C.

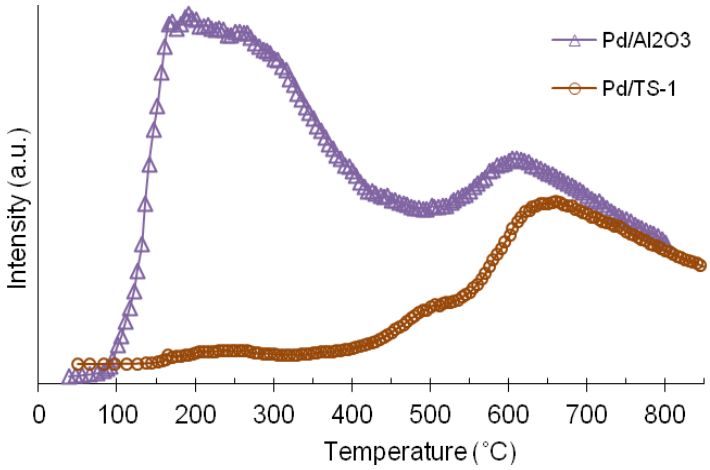

Fig. 7.6. TPD curves of water desorption from Pd/TS-1 and Pd/Al_2O_3 catalysts. H_2O was adsorbed at 110 °C. Heating ramp = 5 °C·min^{-1}. ○ = Pd/TS-1; Δ = Pd/Al_2O_3.

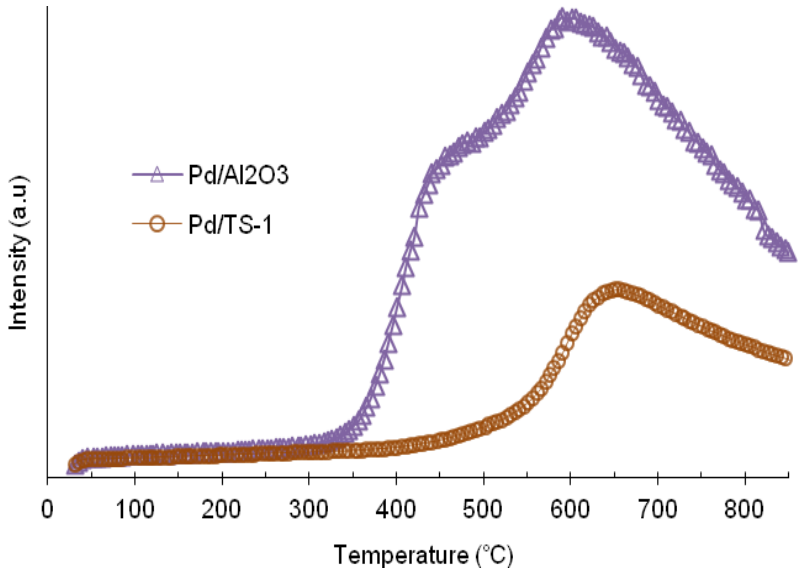

Fig. 7.7. TPD curves of water desorption from Pd/TS-1 and Pd/Al_2O_3 catalysts after heating at 350 °C for 1 h. H_2O adsorption at 110 °C. Heating ramp = 5 °C·min^{-1}. ○ = Pd/TS-1; Δ = Pd/Al_2O_3.

The complexity of water adsorption-desorption for MFI-zeolitic adsorbents has been reported in the literature, especially for TS-1, ZSM-5 and silicalite-1 (pure silica) [10]. It was found that among these zeolites, TS-1 is the most demonstrably hydrophobic material. It was reported that for hydrocarbons adsorption, TS-1 exhibited behaviour similar to that of ZSM-5 zeolite, however for water adsorption the intensity of TS-1 was as low as the rate of water desorbed from pure silica [10]. This argument is in line with what has been observed in TPD curves plotted in Fig. 7.6 and 7.7. TS-1 has very low concentration of adsorbed water and in turn helps to maintain the stability of Pd active sites during reaction. The hydrophobicity of TS-1 was suggested due to the absence of surface acidity (strong acid and hydrogen bonding), instead of an increased dispersion interaction [37]. More recent investigation also reported that the hydrophobic properties of TS-1 is due to the titanium atoms in the tetrahedral position of the MFI structure which create the hydrophobic environment [10].

The adsorption and desorption of nitrogen was performed on pure TS-1 support, Pd/TS-1 and Pd/Al_2O_3 catalysts in order to measure the surface area and the pore sizes. The adsorption-desorption isotherm of Pd/TS-1 and Pd/Al_2O_3 catalysts are plotted in Fig. S2 of the SI. The textural properties of all samples tested are provided in Table 7.1.

In general, the isotherm adsorption plots of our samples fall into type-IV as classified by IUPAC which is typically the behaviour of mesoporous materials [38]. Interestingly, the desorption curves of Pd/TS-1 catalyst (Fig. S2a of SI) is shifted slightly to a higher volume over the pressure range while Pd/Al_2O_3 catalyst desorption plot (Fig. S2b of SI) is shifted only at a relative pressure higher than 0.7. As reported in the literature, these shifts indicate enhanced adsorption over the range of relative pressures, which suggests

the coexistence of micro and mesopores within these catalysts [39]. As shown in Table 7.1, the average pore diameter calculated using Barrett-Joyner-Halenda (BJH) method results in 5.4 nm and 16.8 nm for Pd/TS-1 and Pd/Al_2O_3 catalysts, respectively. Not surprisingly the surface area of Pd/TS-1 catalyst is much higher compared to Pd supported on alumina catalyst. The surface area estimated by Langmuir method discloses a decrease from 641.9 $m^2 g^{-1}$ to 492.8 $m^2 g^{-1}$ in the presence the Pd nano-particles on TS-1 which confirms the deposition of Pd on TS-1 support. This is further substantiated by ICP-OES, SEM, TEM and XPS results below.

Nitrogen physisorption analysis over the used Pd/TS-1 catalyst suggests that the surface area decreased only *ca.* 3 % after 1,900 h time-on-stream experiment. In contrast, a significant loss in surface area was observed over the used Pd/Al_2O_3 catalyst where the surface area decreased from 212.9 $m^2 g^{-1}$ to 146.5 $m^2 g^{-1}$ (*ca.* 31 % drop) after 1,100 h TOS experiment.

Table 7.1. N_2-physisorption calculation results

Parameter	Sample				
	TS-1	Pd/TS-1	Used Pd/TS-1	Pd/Al_2O_3	Used Pd/Al_2O_3
Langmuir Surface Area ($m^2 g^{-1}$)	641.9	492.8	476	212.9	146.5
BJH Average Pore Diameter (Å)	30.7	54.1	23.6	167.6	158.7
BJH Adsorption Pore Volume ($cm^3 g^{-1}$)	0.07	0.11	0.06	0.66	0.4

The crystallinity of palladium supported on TS-1 was investigated using powder X-ray diffraction (XRD) analysis. Fig. S3 of SI shows XRD patterns for Pd/TS-1 catalyst in comparison to XRD pattern of pure TS-1 support material. Diffraction reflections of both samples confirm the presence of MFI-type zeolite structure and high crystallinity of these samples [10, 15]. A very small, broad reflection at 34.8 ˚2θ observed from

XRD pattern of calcined Pd/TS-1 catalyst suggesting the existence of palladium oxide (0 1 2) on TS-1 support. This is consistent with a low net metal loading (from ICP-OES result) and suggests a well-dispersed nature of palladium particles on TS-1 zeolite (from H_2-chemisorption result). However, the low intensity (high FWHM) of PdO reflections does not enable an estimation of the palladium particle size. The PdO is x-ray amorphous. An estimation of the active particle size calculated from the results of H_2-chemisorption at 35 ºC shows that average particle diameter is 7.6 nm resulting in 14.8 % dispersion. A comparable result was obtained from hydrogen chemisorption of Pd/Al_2O_3 catalyst which is suggesting a palladium dispersion of 14.2 % with an average particle size of 7.9 nm.

Exploring the possibility of a morphological transformation during catalyst preparation and methane oxidation was carried out using scanning electron microscopy (SEM). Fig. 7.8 shows SEM images of TS-1 zeolite and Pd/TS-1 catalysts at the same magnifications. The topography of fresh TS-1 zeolite was captured by a secondary electron (SE) detector and shown in Fig. S4 of SI. Using a backscattered electron **(**BE) detector, the images of TS-1 support material and Pd/TS-1 catalyst were captured as shown in Fig. 7.8a and 7.8b. Comparing both images, SEM micrograph of fresh Pd/TS-1 catalyst reveals very small, brighter particles distributed over the whole area of TS-1 surface which are interpreted as signal from palladium particles. In this image, the palladium particle is recognized as the brighter particle due to its higher atomic weight (see the arrows). This has been confirmed by Energy Dispersive Spectroscopy (EDS) which was performed during analysis.

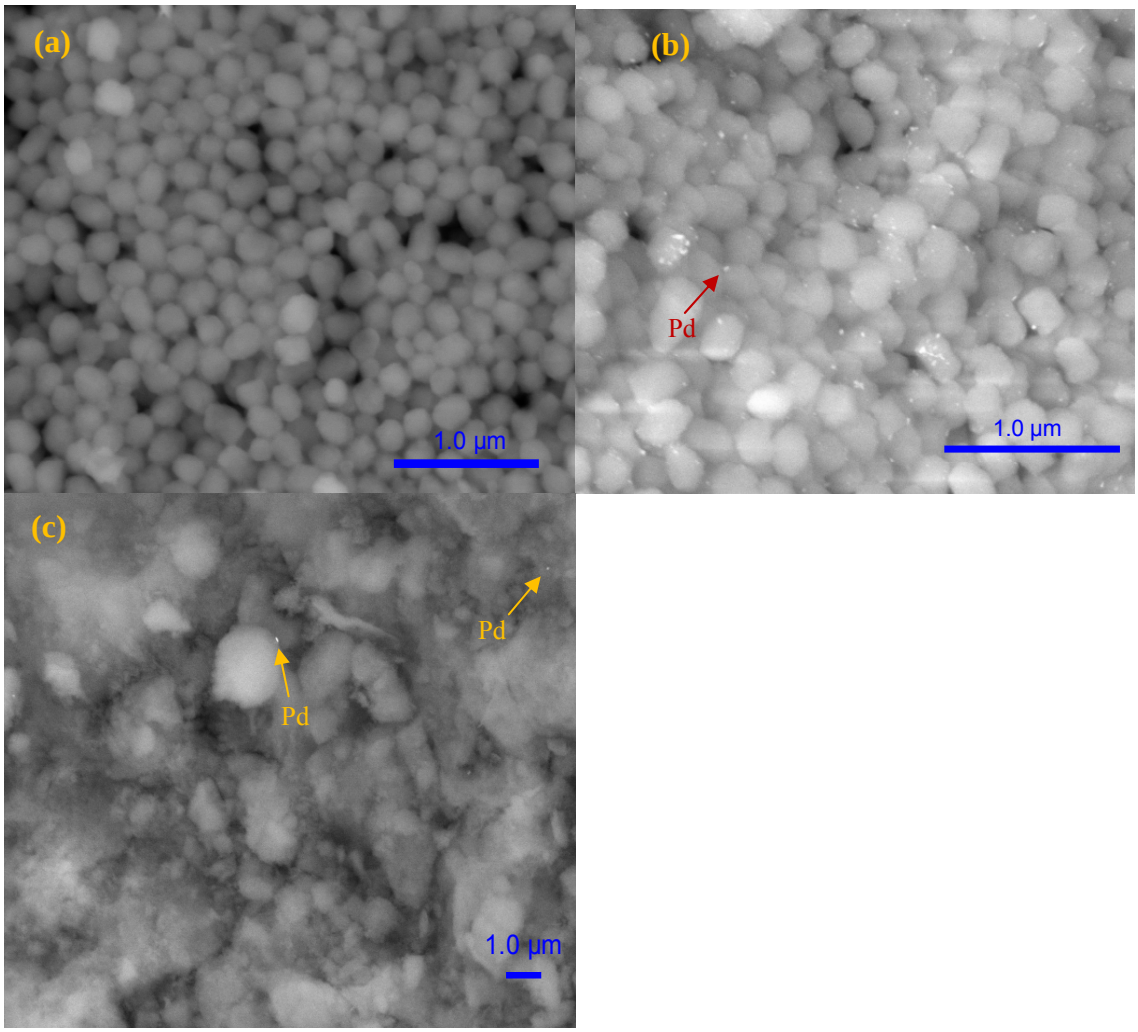

Fig. 7.8. SEM images of (a) TS-1 zeolite; (b) Pd/TS-1; and (c) Pd/Al_2O_3 catalyst.

A less bright particle distribution is observed from Pd/Al_2O_3 SEM image (see Fig 7.8c). These images suggest that the nature of TS-1 support helps in establishing a better palladium particle distribution. This is in a good agreement to what has been reported in the literature that the morphology and microstructure of nano-sized Pd particle is affected by the nature of its support [4].

The SEM images of fresh and used Pd/TS-1 catalysts are compared in Fig. S5 of SI. It can be seen that no significant measurable change in morphology was observed under SEM. This is consistent with N_2-physisorption results where only 3 % of surface area

decreased during 1,900 h TOS experiment. This minor change is most-likely related to the transformation of palladium particle. This argument is further substantiated by our finding from TEM analysis below. It is suggested that the formation and removal of hydroxide compounds from the surface of catalyst can potentially accelerate the sintering process [40], either sintering of the catalyst or support material [41]. The surface diffusion of the single phase solid is significantly increased at temperatures near to the Hüttig temperature (0.2 - 0.3 × melting point) [40]. Assuming the melting point of palladium is 1,552 ºC, the Hüttig temperature is then in the range of 310 ºC to 466 ºC. In Fig. 3 we can see that after 150 h, the bed temperatures were increased from 410 ºC to 430 ºC which is inside the Hüttig temperature range, and thus, a surface diffusion of palladium nano-particle would be expected.

Palladium particle size and distribution of Pd/TS-1 catalyst was observed under transmission electron microscope (TEM) before and after long-term stability test. Fig. 7.9a shows the representative TEM micrograph of fresh catalyst, including particle size distribution plot and the representative image of the used catalyst is provided in Fig. 7.9b. According to our statistical analysis, the size of palladium particle distributed on the surface of the fresh catalyst ranged from 1 nm to 11 nm with the average size of 4 nm. An increase in particle size was observed over the used catalyst, where the average particle size of palladium was 8 nm. This increase is most likely related to the deactivation observed over 1,900 h time-on-stream experiment. A similar phenomena was reported over Pd/Al_2O_3 catalyst, where the particle size of palladium increased after long-term stability test under wet feed conditions [2]. In Fig. 7.9c and 7.9d, the representative TEM images and particle distribution of fresh and used Pd/Al_2O_3

catalysts are shown. The average Pd particle size of Pd/Al_2O_3 catalyst increased from 2.6 nm to 8.2 nm after high humidity, long time-on-stream catalyst evaluation.

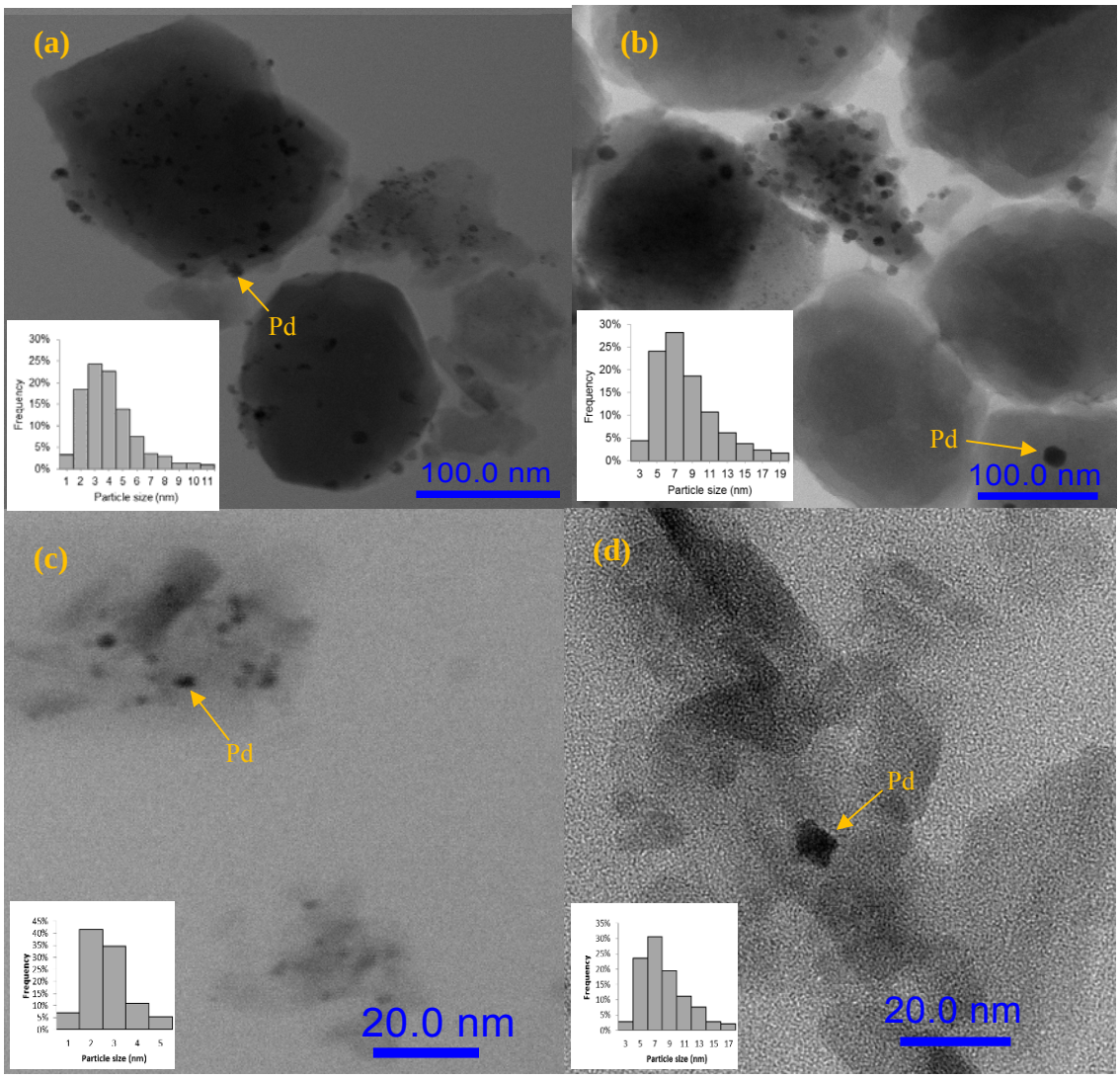

Fig. 7.9. TEM images of fresh and used catalysts: (a) fresh Pd/TS-1; (b) used Pd/TS-1; (c) fresh Pd/Al_2O_3 and (d) used Pd/Al_2O_3.

XPS spectra of fresh and used Pd/TS-1 catalyst are displayed in Fig. 7.10. The binding energies (BE) and surface composition are provided in Table 7.2. Prior to analysis, the fresh sample was calcined in air at 500 °C for 2 h, while the used sample was directly taken from the long term (1,900 h) stability tests as plotted in Fig. 7.3. The spectra of the fresh catalyst sample (Fig. 7.10a) reveals a single distinct peak representing the Pd $3d_{5/2}$ core level transitions, similar to what can be observed from the used sample (Fig. 7.10b). No metallic Pd was detected from the surface of the used sample. The presence of PdO_2 at binding energies of 337.2 - 337.4 eV has been assigned by comparing with shifts reported in the literature [42-44] with the oxide most likely formed during calcination of Pd/TS-1 catalyst.

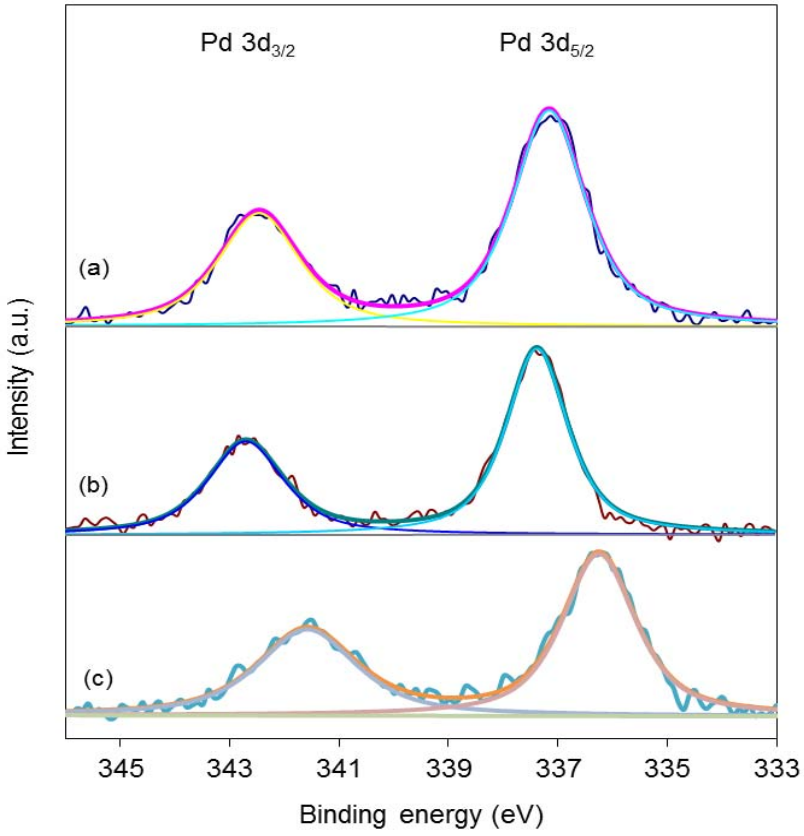

Fig. 7.10. XPS spectra of Pd 3d core level of (a) fresh Pd/TS-1, (b) used Pd/TS-1 and (c) used Pd/Al_2O_3 catalysts.

Table 7.2. Surface composition and binding energies at Pd 3d core level

Sample		Pd $3d_{5/2}$ peak position (eV)	Surface composition (%)					
			Pd	O	Ti	Si	Al	C
(a)	Pd/TS-1, fresh	337.2	0.5	64.1	0.3	33.1	-	2.12
(b)	Pd/TS-1, used	337.4	0.3	63.6	0.2	32.7	-	3.12
(c)	Pd/Al_2O_3, used	336.3	0.2	59.2	-	-	37.1	

The unique formation of Pd^{4+} on zeolite supported Pd catalyst has been confirmed by Bi and Lu who studied Pd/NaZSM-5 calcined at 600 ˚C where a binding energy was observed at 337.7 eV [45]. On the other hand, they also observed that upon calcination of Pd/Al_2O_3, the binding energy of Pd $3d_{5/2}$ was 336.6 eV (which can be identified as Pd^{2+}), relatively similar to what was found from our Pd/Al_2O_3 catalysts (Fig. 7.10c). This suggests the formation of Pd^{4+} on Pd/Al_2O_3 catalysts is unlikely. Meanwhile, palladium supported on zeolite can stabilize the presence of PdO_2 through the special space structure of zeolite [45].

The binding energy of a peak at Pd $3d_{5/2}$ core level of the 1,900 h time-on-stream used catalyst (Fig 7.10b) is shifted 0.2 eV towards a higher BE compared to the fresh catalyst. However, the shape of deconvoluted peak at Pd $3d_{5/2}$ core level of the used catalyst is virtually identical to the fresh catalyst peak pattern. As shown in Table 7.2, the ratios of Pd to Ti or Pd to Si are similar for used and fresh catalyst. In addition, comparison of a plot of Ti 2p core-level of fresh and used Pd/TS-1 spectra (see Fig. S6 and Table S1 of SI) indicates no shift in binding energy. These suggest no significant changes in chemical/oxidation state of Pd/TS-1 catalyst following the long term operation under surrogate VAM gas, and that the Pd phase in Pd/TS-1 catalyst is stable and less sensitive to water poisoning as no other species was able to be detected from

this spectra. In contrast, Pd on alumina shows significant variation of the Pd signature [2] which can be attributed to the formation of palladium hydroxide. The argument is inline with TPD plots (Fig. 7.6 and Fig. 7.7) as well as the comparison bed furnace temperatures plotted in Fig. 7.3.

4. Conclusion

The catalytic activity and stability of palladium supported on TS-1 catalyst was investigated in catalytic combustion of lean methane in air mixture and compared with Pd/Al_2O_3 catalyst. A notable increase in hydrothermal stability was observed over 1,900 h time-on-stream experiments, where a constant steady state activity to obtain 90 % conversion was achieved below 500 °C. The Arrhenius plot of Pd-TS-1 catalyst obtained after long-term stability test indicates two linear regions with different apparent activation energies and consequently a change in the oxygen surface coverage dependent on the reaction temperature is proposed. Catalyst characterization suggests that water adsorption and in turn the hydrophobicity of the catalyst support plays important role in enhancing the stability of the catalyst. The data obtained disclose that the activity of Pd/TS-1 catalyst was hindered at lower temperature by water present in the feed, however at temperatures higher than 350 °C water is not present on the surface resulting in a lower activation energy compared to Pd/Al_2O_3. The hydrophobic properties of titanium silicalite support helps in preventing the accumulation of hydroxyl on the support and also increase the amount of available oxygen.

References

1. Gelin, P. and M. Primet, *Complete oxidation of methane at low temperature over noble metal based catalysts: a review.* Applied Catalysis B: Environmental, 2002. 39: p. 1-37.

2. Setiawan, A., J. Friggieri, E.M. Kennedy, B.Z. Dlugogorski, and M. Stockenhuber, *Catalytic combustion of ventilation air methane (VAM) – long term catalyst stability in the presence of water vapour and mine dust.* Catalysis Science & Technology, 2014. 4(6): p. 1793-1802.

3. Burch, R., F.J. Urbano, and P.K. Loader, *Methane combustion over palladium catalysts: the effect of carbon dioxide and water on activity.* Applied Catalysis A: General, 1995. 123(1): p. 173-184.

4. Liu, Y., S. Wang, T. Sun, D. Gao, C. Zhang, and S. Wang, *Enhanced hydrothermal stability of high performance lean fuel combustion alumina-supported palladium catalyst modified by nickel.* Applied Catalysis B: Environmental, 2012. 119–120(0): p. 321-328.

5. Gao, D., S. Wang, C. Zhang, Z. Yuan, and S. Wang, *Methane combustion over Pd/Al_2O_3 catalyst: effects of chlorine ions and water on catalytic activity.* Chinese Journal of Catalysis, 2008. 29(12): p. 1221-1225.

6. Shi, C., L. Yang, and J. Cai, *Cerium promoted Pd/HZSM-5 catalyst for methane combustion.* FUEL, 2007. 86(1–2): p. 106-112.

7. Ribeiro, F.H., M. Chow, and R.A. Dallabetta, *Kinetics of the complete oxidation of methane over supported palladium catalysts.* Journal of Catalysis, 1994. 146(2): p. 537-544.

8. Ciuparu, D., N. Katsikis, and L. Pfefferle, *Temperature and time dependence of the water inhibition effect on supported palladium catalyst for methane combustion.* Applied Catalysis A: General, 2001. 216(1-2): p. 209-215.

9. Schwartz, W.R., D. Ciuparu, and L.D. Pfefferle, *Combustion of methane over palladium-based catalysts: catalytic deactivation and role of the support.* The Journal of Physical Chemistry C, 2012. 116(15): p. 8587-8593.

10. Serrano, D.P., G. Calleja, J.A. Botas, and F.J. Gutierrez, *Characterization of adsorptive and hydrophobic properties of silicalite-1, ZSM-5, TS-1 and beta zeolites by TPD techniques.* Separation and Purification Technology, 2007. 54(1): p. 1-9.

11. Taramasso, M., G. Perego, and B. Notari, U. Patent, Editor. 1983: United States.

12. Qiu, F., X. Wang, X. Zhang, H. Liu, S. Liu, and K.L. Yeung, *Preparation and properties of TS-1 zeolite and film using Sil-1 nanoparticles as seeds.* Chemical Engineering Journal, 2009. 147(2–3): p. 316-322.

13. Notari, B., *Titanium silicalites.* Catalysis Today, 1993. 18(2): p. 163-172.

14. Mori, K., Y. Miura, S. Shironita, and H. Yamashita, *New route for the preparation of Pd and PdAu nanoparticles using photoexcited Ti-containing zeolite as an efficient support material and investigation of their catalytic properties.* Langmuir, 2009. 25(18): p. 11180-11187.

15. Moreno, I., N.F. Dummer, J.K. Edwards, M. Alhumaimess, M. Sankar, R. Sanz, P. Pizarro, D.P. Serrano, and G.J. Hutchings, *Selective oxidation of benzyl alcohol using in situ generated H_2O_2 over hierarchical Au-Pd titanium silicalite catalysts.* Catalysis Science & Technology, 2013. 3(9): p. 2425-2434.

16. Specchia, S., P. Palmisano, E. Finocchio, M.A.L. Vargas, and G. Busca, *Catalytic activity and long-term stability of palladium oxide catalysts for natural gas combustion: Pd supported on $LaMnO_3$-ZrO_2.* Applied Catalysis B: Environmental, 2009. 92(3–4): p. 285-293.

17. Carlo, G.D., G. Melaet, N. Kruse, and L.F. Liotta, *Combined sulfating and non-sulfating support to prevent water and sulfur poisoning of Pd catalysts for methane combustion.* Chemical Communication, 2010. 46: p. 6317-6319.

18. Castellazzi, P., G. Groppi, and P. Forzatti, *Effect of Pt/Pd ratio on catalytic activity and redox behavior of bimetallic Pt-Pd/Al_2O_3 catalysts for CH_4 combustion.* Applied Catalysis B: Environmental, 2010. 95: p. 303-311.

19. Anderson, J.R. and K.C. Pratt, *Introduction to characterization and testing of catalysts*. 1985, Sydney ; Orlando: Academic Press. ix, 457 p.

20. Su, S., H. Chen, P. Teakle, and S. Xue, *Characteristics of coal mine ventilation air flows.* Journal of Environmental Management, 2008. 86: p. 44 - 62.

21. van Giezen, J.C., F.R. van den Berg, J.L. Kleinen, A.J. van Dillen, and J.W. Geus, *The effect of water on the activity of supported palladium catalysts in the catalytic combustion of methane.* Catalysis Today, 1999. 47(1-4): p. 287-293.

22. Fujimoto, K.-i., F.H. Ribeiro, M. Avalos-Borja, and E. Iglesia, *Structure and reactivity of PdOx/ZrO_2 catalysts for methane oxidation at low temperatures.* Journal of Catalysis, 1998. 179(2): p. 431-442.

23. Mars, P. and D.W. van Krevelen, *Oxidations carried out by means of vanadium oxide catalysts.* Chemical Engineering Science, 1954. 3, Supplement 1(0): p. 41-59.

24. Li, Y. and J.N. Armor, *Catalytic combustion of methane over palladium exchanged zeolites.* Applied Catalysis B: Environmental, 1994. 3(4): p. 275-282.

25. Helfferich, F.G., *Kinetics of multistep reactions*. 2nd ed. Chemical Kinetics, ed. N.J.B. Green. Vol. 40. 2004, UK: Elsevier.

26. Lynggaard, H., A. Andreasen, C. Stegelmann, and P. Stoltze, *Analysis of simple kinetic models in heterogeneous catalysis.* Progress in Surface Science, 2004. 77(3–4): p. 71-137.

27. Li, G., P. Xiao, and P. Webley, *Binary adsorption equilibrium of carbon dioxide and water vapor on activated alumina.* Langmuir, 2009. 25(18): p. 10666-10675.

28. Zakumbaeva, G.D. and S.V. Artamonov, *Calorimetric study of the interaction of oxygen with Pd-black and Pd/Al_2O_3.* Reaction Kinetics and Catalysis Letters, 1979. 10(2): p. 183-186.

29. Trimm, D.L. and C.-W. Lam, *The combustion of methane on platinum-alumina fibre catalysts-I.* Chemical Engineering Science, 1980. 35: p. 1405-1413.

30. Cullis, C.F. and B.M. Willatt, *Oxidation of methane over supported precious metal catalysts.* Journal of Catalysis, 1983. 83: p. 267-285.

31. Baldwin, T.R. and R. Burch, *Catalytic combustion of methane over supported palladium catalysts. II. Support and possible morphological effects.* Applied Catalysis, 1990. 66: p. 359-381.

32. Stasinska, B., A. Machocki, K. Antoniak, M. Rotko, J.L. Figueiredo, and F. Gonçalves, *Importance of palladium dispersion in Pd/Al_2O_3 catalysts for complete oxidation of humid low-methane-air mixtures.* Catalysis Today, 2008. 137(2-4): p. 329-334.

33. Ivanov, D.V., L.G. Pinaeva, L.A. Isupova, E.M. Sadovskaya, I.P. Prosvirin, E.Y. Gerasimov, and I.S. Yakovleva, *Effect of surface decoration with $LaSrFeO_4$ on oxygen mobility and catalytic activity of $La_{0.4}Sr_{0.6}FeO_3-\delta$ in high-temperature N_2O decomposition, methane combustion and ammonia oxidation.* Applied Catalysis A: General, 2013. 457(0): p. 42-51.

34. Peri, J.B., *A model for the surface of gamma-alumina.* Journal of Physical Chemistry, 1966. 69(1): p. 220-230.

35. Zamora, M. and A. Cordoba, *A study of surface hydroxyl groups on gamma-alumina.* Journal of Physical Chemistry, 1978. 82(5): p. 584-588.

36. Egashira, M., M. Nakashima, S. Kawasumi, and T. Seiyama, *Temperature programmed desorption study of water adsorbed on metal oxides. 2. Tin oxide surfaces.* Journal of Physical Chemistry, 1981. 85(26): p. 4125-4130.

37. Drago, R.S., S.C. Dias, J.M. McGilvray, and A.L.M.L. Mateus, *Acidity and Hydrophobicity of TS-1.* The Journal of Physical Chemistry B, 1998. 102(9): p. 1508-1514.

38. Sing, K.S.W., *Reporting physisorption data for gas/solid systems.* Pure and applied Chemistry, 1982. 54(11): p. 2201-2218.

39. Serrano, D.P., R. Sanz, P. Pizarro, I. Moreno, and S. Medina, *Hierarchical TS-1 zeolite as an efficient catalyst for oxidative desulphurization of hydrocarbon fractions.* Applied Catalysis B: Environmental, 2014. 146(0): p. 35-42.

40. Trimm, D.L., *Thermal stability of catalyst supports*, in *Studies in surface science and catalysis*, H.B. Calvin and B.B. John, Editors. 1991, Elsevier. p. 29-51.

41. Lee, J.H. and D.L. Trimm, *Catalytic combustion of methane.* Fuel Processing Technology, 1995. 42: p. 339-359.

42. Gao, D., C. Zhang, S. Wang, Z. Yuan, and S. Wang, *Catalytic activity of Pd/Al_2O_3 toward the combustion of methane.* Catalysis Communications, 2008. 9(15): p. 2583-2587.

43. Venezia, A.M., G.D. Carlo, G. Pantaleo, L.F. Liotta, G. Melaet, and N. Kruse, *Oxidation of CH_4 over Pd supported on TiO_2-doped SiO_2: effect of Ti(IV) loading and influence of SO_2.* Applied Catalysis B: Environmental, 2009. 88(3–4): p. 430-437.

44. Chenakin, S.P., G. Melaet, R. Szukiewicz, and N. Kruse, *XPS study of the surface chemical state of a $Pd/(SiO_2 + TiO_2)$ catalyst after methane oxidation and SO_2 treatment.* Journal of Catalysis, 2014. 312(0): p. 1-11.

45. Bi, Y. and G. Lu, *Catalytic CO oxidation over palladium supported NaZSM-5 catalysts.* Applied Catalysis B: Environmental, 2003. 41(3): p. 279-286.

CHAPTER 8

Accelerated hydrothermal ageing of Pd/Al_2O_3 for catalytic combustion of ventilation air methane

---

Appendix F supplied the supporting information of this chapter.

8.1. Introduction

Methane is a gas with significant greenhouse warming potential whose atmospheric sources and sinks are well documented [1]. Nearly 10 % of total anthropogenic methane emissions originate from coal mining activities [2], and almost two-thirds of these emissions originate from mine ventilation air. Reducing the greenhouse impact of this particular source presents significant challenges to mine operators, the most notable being that ventilation air methane (VAM) is a low concentration, high volume stream that prevents the use of conventional combustion and energy recovery technologies. Low temperature catalytic combustion offers an alternative treatment method, which, when compared to high temperature combustion, offers the advantage to eliminate the generation of additional emissions to the air, such as nitrogen oxides. However, its viability depends on maintaining the activity of the catalyst bed during its exposure to high volumes of ventilation air that contains several components which have the potential to affect performance, such as water vapour and particulate matter.

It is widely accepted that supported palladium catalysts are one of the most effective in the low temperature oxidation of methane [3]. The oxidation proceeds through a Pd-PdO redox cycle in which oxygen present in the support is also thought to play a role [4]. Our recent evaluation of Pd/Al_2O_3 catalysts over long-term time-on-stream (TOS) experiments suggests that the deactivation process is a complex phenomenon, although, as highlighted in other studies, the presence of water in the feed stream is perhaps the most significant factor contributing to catalyst deactivation [5].

Despite considerable effort, the mechanism of catalyst deactivation is not fully understood [6]. Deactivation can occur through chemical, mechanical and thermal processes [7]. Thermal deactivation processes include the loss of active-site surface area as a result of particle aggregation and collapse of the support pore structure through re-crystallization. Chemical transformation can also result in the loss of active metal sites [7]. Pd/Al_2O_3 catalyst activity can be affected by both thermal and chemical transformations [4].

These deactivation processes can be accelerated under high-temperature hydrothermal ageing. A study of hydrothermal ageing on methane combustion over Ce-promoted PdO/ZrO_2 catalysts highlighted the impact that ageing temperature plays on catalyst deactivation [8]. Hydro-thermal treatments for two weeks on various supported Pd catalysts at 900 °C under simulated domestic boiler exhaust gas were performed to understand the ageing mechanism in natural gas combustion [9]. Deactivation studies were reported recently for natural-gas vehicle catalysts [10] and diesel oxidation catalysts [11] where significant changes in morphology and chemical poisoning were observed. A very recent article reported that support phase transformation and particle sintering were found after thermal (at 900 °C in air) and stoichiometric (at 900°C, air-fuel equivalent ratio = 1) ageing over $Pd/YFeO_3$ three-way-catalyst [12]. However, the effects caused by thermal ageing and chemical poisoning are still inconclusive, and, in particular, the ageing process under simulated VAM gas has not been considered.

In this contribution, we report the properties of Pd/Al_2O_3 catalyst after long-term stability tests in the presence of water and coal mine dust in lean-methane combustion. Catalyst deactivation has also been explored using four accelerated ageing procedures.

Catalysts were aged under a wet feed at 780 °C and 830 °C for 18 h (the wet feed containing CH_4, H_2O and air), under a wet-oxygen in helium mixture at 780 °C for 18 h, and in an autoclave at 175 °C for 3 days. The properties of the aged catalysts were compared with the properties of used catalysts tested in long-term stability experiments. Our overarching aim is to gain a better understanding of the deactivation phenomena and to explore effective strategies for accelerating the ageing process in order to reduce the time that is typically required for catalyst stability tests.

8.2. Experimental

8.2.1. Catalyst treatment

The material used in the study (1.0 wt% Pd/Al_2O_3) was supplied by Sigma-Aldrich. Following our previously reported procedure [5], prior to use, the material was activated by calcining in air at 500 ºC for 2 h then reduced by purging in H_2 for 2 h at 300 ºC. We subsequently denote this sample as "calcined-reduced" while the "fresh" catalyst is referred to "as received catalyst".

We begin by characterising samples used in ventilation air methane (VAM) treatments reported earlier [5]. Three samples were selected from the long-term studies, which will be referred to as "dry-VAM", "wet-VAM" and "wet-dust-VAM". The dry-VAM sample was tested for 1600 h time on stream (TOS) in a feed consisting of 0.7 % CH_4 balanced with air. The wet-VAM sample was subjected to a feed of 0.7 % CH_4, 1 % CO_2, 3 % – 4 % H_2O balanced with air for 1,150 h TOS. A similar feed was used for the wet-dust-VAM sample, with the addition of VAM dust being packed in front of the catalyst bed.

The experimental procedures of these long-term experiments were detailed in our previous report [5].

In an effort to identify an accelerated ageing protocol that emulates the deactivation processes occurring in the long-term experiments, four aging treatments were examined. The possibility of increasing bed temperatures caused by coal-dust channelling/combustion observed in our previous work also motivates our assessment of the catalyst performance at higher temperatures. Treatment I involved aging at a bed temperature of 780 ºC for 18 h under a feed of 0.7 % CH_4, 3 vol% H_2O balance air. Treatment II used the same feed as I, but was aged at 830 ºC for 18 h. Treatment III involved aging at 780 ºC for 18 h under a mixture of 60 vol% O_2, 3 vol% H_2O and the balance being helium. Aging under a wet oxygen bath gas was chosen to promote the formation of palladium oxide, which was observed to be the only Pd species present after the long-term studies [5]. Treatment IV employed hydrothermal aging in an autoclave set at 175 ºC for three days to promote the deactivation of the catalyst by water. After the ageing treatments, the catalytic activity of each sample was tested for methane oxidation under humid conditions (feed consisted of 0.7 % CH_4, 3.2 % H_2O, balance air) at a gas hourly space velocity (GHSV) of 100,000 h^{-1}.

8.2.2. Catalyst characterization

The surface area, pore size and pore volume of the catalyst samples were measured by nitrogen adsorption-desorption at 77 K using a Micromeritics TriStar 3000 physisorption analyzer. Palladium loading was quantified using a Varian 715-ES inductively coupled plasma optical emission spectrometer (ICP-OES). Zeiss Sigma VP

FESEM served to capture the Scanning Electron Microscopy (SEM) images of the sample using a secondary electron (SE) detector and backscattered electron (BE) detector. Bruker light element SSD Energy-dispersive X-ray spectroscopy (EDS) detector allowed the elemental analysis while capturing the SEM images. A JEOL 2200 FS transmission electronic microscope (TEM) featured with EDS and scanning transmission electron microscope (STEM) system was used for imaging nano-sized Pd particles and support as well as measuring the particle size distribution. TEM particle analysis was carried out using Gatan DigitalMicrograph software. Powder X-Ray diffraction patterns of fresh and used catalysts were collected using Cu Kα radiation with a Philips X'Pert diffractometer. Diffractrograms were recorded in the 2θ angle range from 2° to 90° with 0.008° 2θ step resolution.

For surface analysis, ex-situ X-ray photoelectron spectroscopy (XPS) was carried out using mono-chromated Al K alpha (energy 1486.68 eV) radiation and the emitted photoelectrons were analyzed using an ESCALAB250Xi manufactured by Thermo Scientific, UK. To avoid sample contamination, the used samples were immediately transferred into sealed container after terminating the reaction by cooling in helium. The exposure time of samples in air was minimized to reduce the likelihood of experimental artefacts especially those related to adsorption of water vapour from ambient air. The sample was mounted on the sample holder using indium foil. The energy scale was shifted relative to the adventitious carbon at 284.6 eV. The shift was cross checked with the position of O 1s from Al_2O_3 which is found at 531eV. Fitting of component contributions to the peaks was performed using a mixed Gaussian-Lorentzian (30:70) line-shape.

8.2.3. Catalytic activity measurement

The activity of the catalyst was measured in a tubular stainless steel micro reactor. For accelerated ageing experiments, the feed was 7,000 ppm CH_4, 30,000 ppm H_2O balanced with air at a GHSV of 100,000 h^{-1}. The inlet and outlet mixtures were analyzed using a gas chromatograph equipped with a thermal conductivity detector (TCD) and concentric packed column (Alltech CTR-I). Water was added as a reactant by passing the feed through a saturator and a humidity probe (Pico HumidProbe AT329/21) was installed at the outlet. The actual reaction temperature was observed by placing a thermocouple close to the catalyst bed. For the long-tern catalytic stability tests, a separate set-up was prepared and running continuously under wet condition as reported in our earlier work [5].

8.3. Results and discussion

8.3.1. The nature of fresh and used Pd/Al_2O_3 catalysts

In the long-term time-on-stream (TOS) studies catalyst deactivation was monitored as an increase in bed temperature required in order to maintain methane conversion at 90 %. Fig. 8.1 plots the variation of temperatures at 90 % conversion (T_{90}) versus time-on-stream for the three VAM sample conditions. In all cases, a significant level of catalyst deactivation occurs in the first 50 h TOS. This is followed by a much more gradual decay in bed activity, and after a few hundred hours the bed activity stabilises at a relatively constant value. At the end of the experiments the catalyst beds reached 450 °C (1,600 h) in the case of dry-VAM, and 500 °C for wet-VAM (1,110 h).

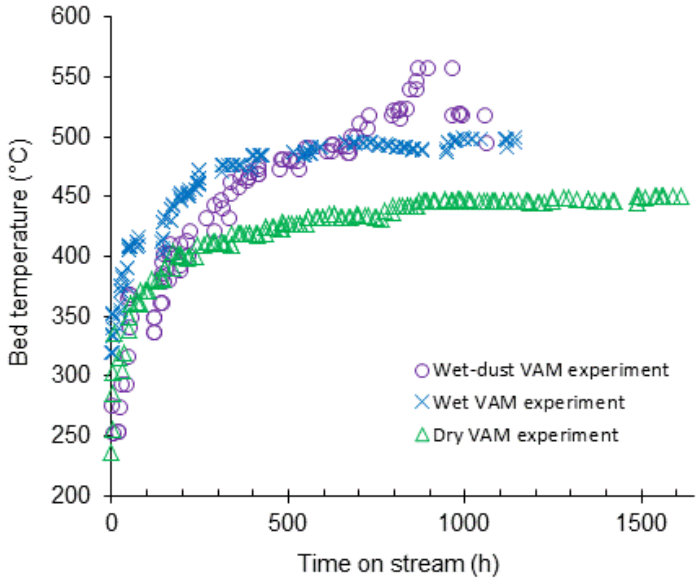

Fig. 8.1. Catalyst bed temperature required for 90 % CH_4 conversion over 1.0 Pd/Al_2O_3 catalyst. Feed = 0.7 % CH_4, 1 % CO_2, 3–4 % H_2O (for wet feeds) balance air. GHSV = 100,000 h^{-1}. Δ = dry VAM experiment; × = wet VAM experiment and ○ = wet-dust VAM experiment.

The reduction in catalyst activity resulting from the presence of water in the feed is readily apparent in these data. The wet-dust VAM experiment displayed some instability in the bed temperature set point, which was attributed to coal particle combustion and channelling during the run [5]; after repacking the bed, the final bed temperature was similar to that of wet-VAM experiment. After long-term stability tests, the used catalysts were transferred carefully into sealed containers and subsequently characterized using XPS, N_2-physisorption, XRD, SEM and TEM analyses. The XPS analysis results are reported in [5].

The nitrogen adsorption-desorption isotherms of all tested samples are of type IV as classified by International Union of Pure and Applied Chemistry (IUPAC) [13], suggesting the materials are meso-porous, and that only minor changes in pore structure originate from the long-term stability tests. The surface area of the samples was

calculated using the Langmuir method, and the results are provided in Table 1. These data suggest that the pore structure of the supports changed at a very slow rate.

Table 8.1. N_2-physisorption analysis results of calcined-reduced and used catalysts

Description	Units	Calcined-reduced Pd/Al_2O_3	Used Pd/Al_2O_3, Dry VAM experiment	Used Pd/Al_2O_3, Wet-VAM experiment	Used Pd/Al_2O_3, Wet-dust-VAM experiment
Langmuir surface area:	$m^2.g^{-1}$	212.9	167.3	146.5	183.1
Micro-pore area:	$m^2.g^{-1}$	14.7	21.5	33.2	22.4
BJH adsorption cumulative pore volume	$cm^3.g^{-1}$	0.7	0.4	0.4	0.5
BJH adsorption average pore diameter	Å	167.6	145.5	158.7	143.7

XRD patterns of the samples are plotted in Fig. 8.2, and are dominated by reflections by γ- and θ-alumina phases. Reflections by Pd or PdO are expected to be very weak and overlapped by the alumina peaks, but can be distinguished as slightly increased intensities and widths of the support reflections [5]. These are very difficult to distinguish in the fresh or calcined-reduced sample, but peaks assigned to PdO can be seen in the used catalyst patterns (Fig. 2b-2d) [14, 15], suggesting agglomeration of Pd particle during the runs. In addition, peaks assigned to α-alumina can be seen in the dry-VAM and wet-VAM patterns.

At temperatures > 900 °C, γ-alumina is gradually transformed to δ-alumina, and to α-alumina via θ-alumina at temperatures > 1,100 °C [16]. These transformations result in a dramatic decrease in surface area. It is surprising that we observe such transformations of the support temperatures as low as 450 °C, admittedly over long periods of time, in the case of both dry- and wet-VAM samples. Whilst these two samples also display the most notable decrease in surface area (Table 8.1), the fact that the transition does not

occur in the sample with dust makes it difficult to attribute the loss in activity to this particular support phase transformation. This may reflect the fact that the reaction atmosphere plays a significant role in promoting structural changes and crystallisation of the support [17].

Fig. 8.3 shows the SEM images of calcined-reduced and used catalysts. No palladium particles are visible in the image of the calcined-reduced catalyst (Fig. 8.3a), most likely due to the low Pd loading and very small particle size. In contrast, after 1,600 h TOS under dry-VAM gas, the SEM image (Fig. 8.3b) reveals very small bright dots (see the arrow) spread over the surface of the support. Using EDS analysis, the bright dot on this image was identified as a palladium particle.

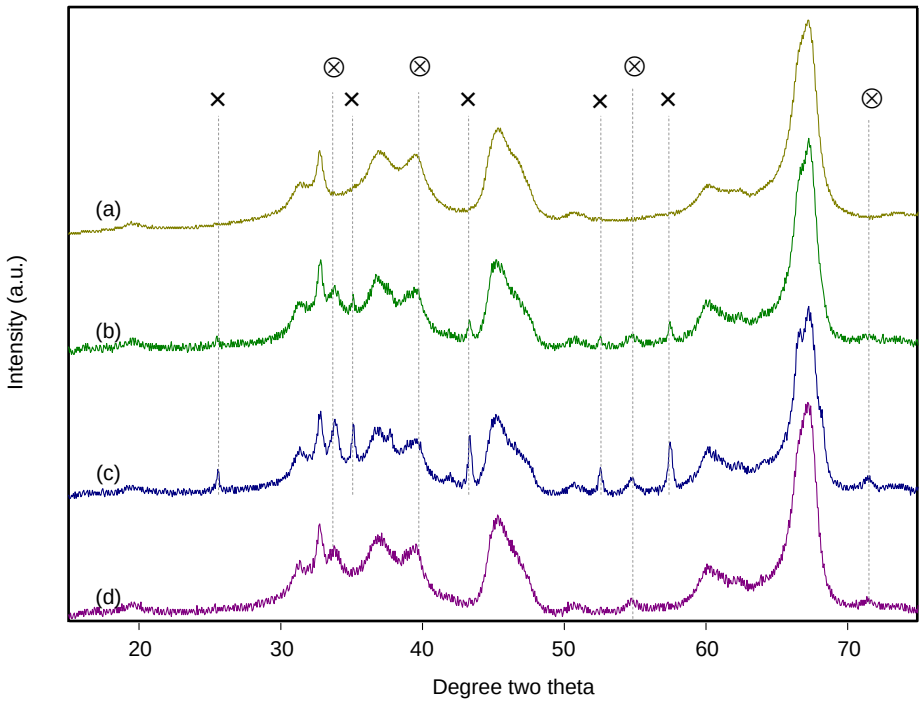

Fig. 8.2. XRD pattern of (a) calcined-reduced Pd/Al_2O_3, (b) used Pd/Al_2O_3 of dry-VAM experiment, (c) used Pd/Al_2O_3 wet-VAM experiment, (d) used Pd/Al_2O_3 of wet-dust VAM experiment. Phase: ⊗ = PdO and × = α-Al_2O_3.

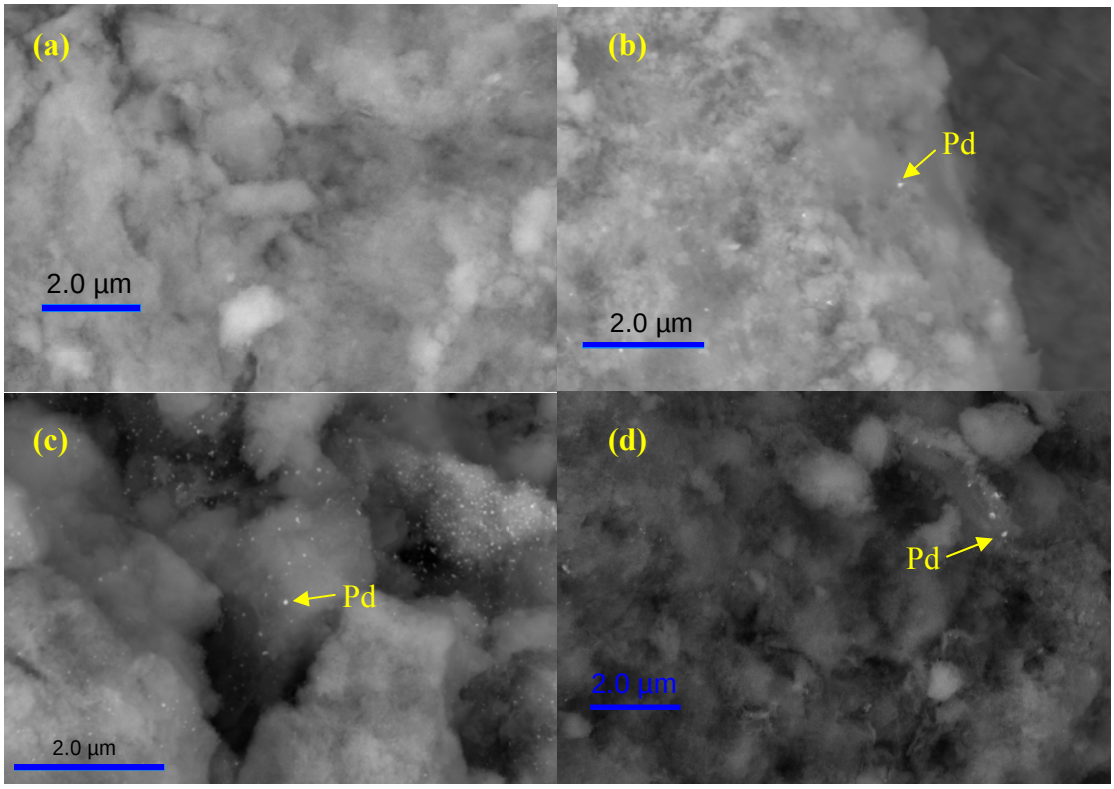

Fig. 8.3. SEM images of (a) calcined-reduced Pd/Al_2O_3; (b) used Pd/Al_2O_3 from dry-VAM experiment; (c) used Pd/Al_2O_3 from wet-VAM experiment; (d) used Pd/Al_2O_3 from wet-dust-VAM experiment.

Similar particles were observed also from used catalysts of wet-VAM and wet-dust-VAM experiments (Fig. 8.3c-3d), suggesting re-dispersion or particle agglomeration occurred during these long-term experiments. The SEM images therefore support the XRD data indicating that Pd agglomeration has occurred during the experiments, with the wet-VAM catalyst displaying the highest density of particles and strongest Pd-related diffraction peaks.

In order to understand the sintering and re-dispersion process of palladium particles during long-term experiments, the particle size and distribution was assessed using a transmission electron microscope (TEM), shown in Fig. S1 of Supplementary Information (SI). In the calcined-reduced catalyst the palladium particle size ranged

from 1 to 5 nm, with the average size of 2.6 nm, explaining why these were difficult to discern in XRD and SEM analyses. On the other hand, in the used samples the average particle size was of the order of 8 nm, indicating that diffusion and agglomeration of the particles occurred during use.

These data are consistent with a picture in which the inital decay in activity is the result of water adsorption on the support and/or active sites, which is know to occur at low temperatures. This probably accounts for the first stage of deactivation (see Fig. 8.1), and the presence of water vapour in the feed may simply serve to increase the extent to which this occurs. Thereafter deactivation continues through loss of active sites via particle agglomeration, and, more slowly, through loss of surface area through phase changes in the support. Both of these occur to a greater extent at higher bed temperatures, although the direct influence of water vapour itself cannot be ruled out. Palladium migration and particle growth occurs in all cases, and is the most prominent when water is present in the feed. Since the final bed temperature was also highest in this case, this could be a simple thermal effect rather than being directly caused by chemisorbed water. However, in the case of the wet feed, XPS suggests that all of the palladium is present as PdO [5], which presumably also has an impact on activity.

8.3.2. The activity of aged Pd/Al_2O_3 catalysts

Light-off curves of total oxidation of methane before and after each catalyst ageing treatment are shown in Fig. 8.4. In general, these plots suggest that high temperature hydrothermal treatment reduced catalyst activity to levels similar to those seen in the long term tests. The temperature at 90 % methane conversion (T_{90}) of the fresh catalyst

was 342 °C, whilst for treatment IV it was 412 °C, treatment I was 424 °C, treatment III was 445 °C, and treatment II was 530 °C. Increases in the T_{90} indicate catalyst deactivation, and these data suggest that the extent of this is influenced most by treament temperature, and less by the oxygen partial pressure. These results were used to establish the initial temperatures required for 90 % conversion in TOS testing of the hydrothermal stability of each of the aged catalyst samples.

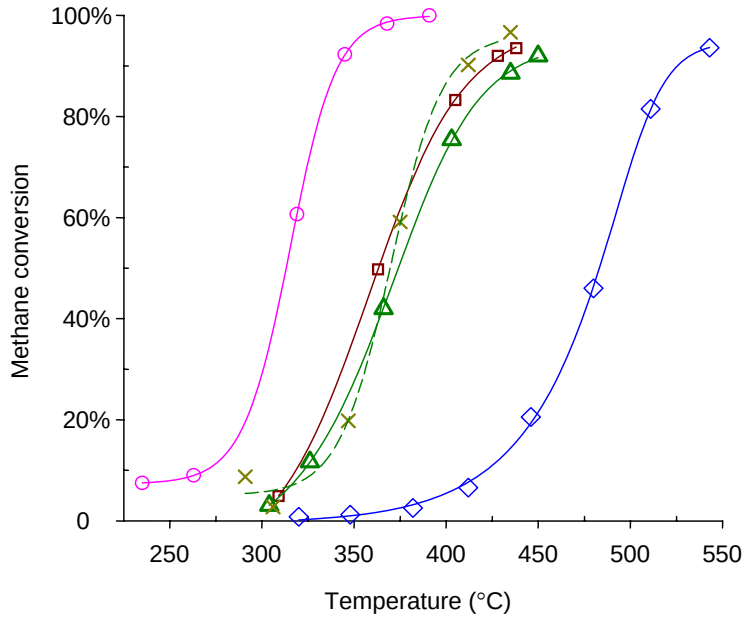

Fig. 8.4. Methane conversion as a function of temperature over fresh and aged Pd/Al_2O_3 catalysts. Feed: 0.7 % CH_4, 3.2 % H_2O balance air; GHSV = 100,000 h^{-1}. ○ = calcined-reduced catalyst; □ = Pd/Al_2O_3-I catalysts (aged 18 h in wet feed at 780 ˚C); ◇ = Pd/Al_2O_3-II catalysts (aged 18 h in wet feed at 830 ˚C); Δ = Pd/Al_2O_3-III catalysts (aged 18 h in wet O_2 at 780 ˚C); × = Pd/Al_2O_3-IV catalysts (aged 3 days in autoclave at 175 ˚C).

To observe the deactivation rate, time on stream experiments were performed over the aged catalysts starting at 90 % conversion without increasing the bed temperatures. Fig. 8.5 ilustrates the time on stream behaviours of aged catalysts under treatment I, III and IV. At their respective bed temperatures, the rate of deactivation of the catalyst aged in treatment IV is the lowest. Given the similarity in bed temperatures and light-off curves (Figure 8.4), this suggests that autoclave aged sample is more stable with respect to deactivation compared to the other two treatments.

The results for treatment III and IV were further examined by adjusting the bed temperature to maintain methane conversion at 90 %, as done in the earlier long-term studies. Fig. 8.6 indicates that the final bed temperature of treatment III needed to be raised to 500 °C to overcome the deactivation, which is a bed temperature similar to that seen after 1,100 h TOS under wet-VAM conditions (see Fig. 8.1).

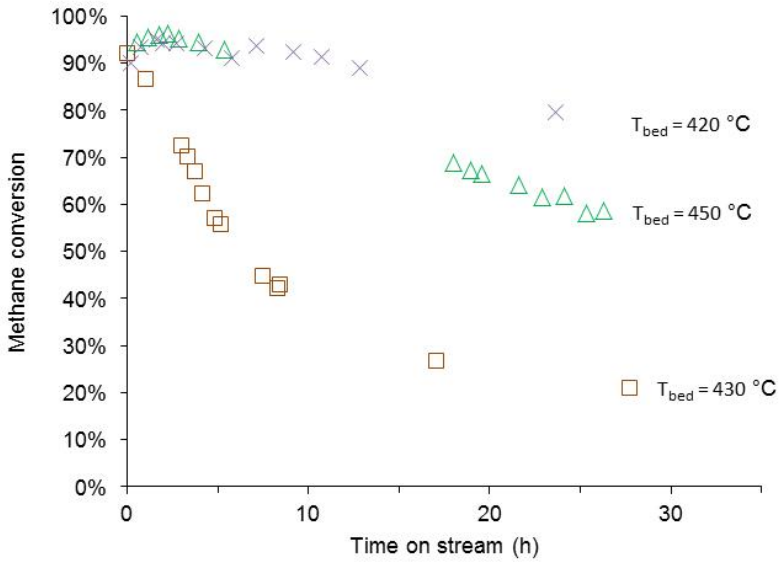

Fig. 8.5. Time on stream evolution of methane combustion over aged Pd/Al_2O_3 catalysts. Feed: 0.7 CH_4, 3.2 % H_2O balance air; GHSV = 100 000 h^{-1}. □ = Pd/Al_2O_3-I catalyst (aged 18 h under wet feed at 780 ˚C); Δ = Pd/Al_2O_3-III catalyst (aged 18 h in wet O_2 at 780 ˚C); × = Pd/Al_2O_3-IV catalysts (aged 3 days in autoclave at 175 ˚C).

On the other hand, treating the catalyst in autoclave leads to an increase in stability as the final bed temperature at 28 h TOS remained at 430 °C. However, the catalyst activity continued to decrease over the first 50 h in methane oxidation tests. The treatments tested, ageing in a wet oxygen in helium mixture at 780 °C for 18 h results in a catalyst behaviour that is the most similar to that of the long-term tests.

8.3.3. The nature of aged Pd/Al_2O_3 catalysts

Nitrogen adsorption-desorption isotherms of the aged catalysts show similarities in comparison to the isotherm of the fresh catalyst. Changes in pore structure and surface area of the aged catalysts are summarised in Table 8.2. As observed in the long term tests, these results indicate a relatively small change in surface area (of the order of 10 %) with aging in treatment I-III, even at the high bed temperatures used in treatment III.

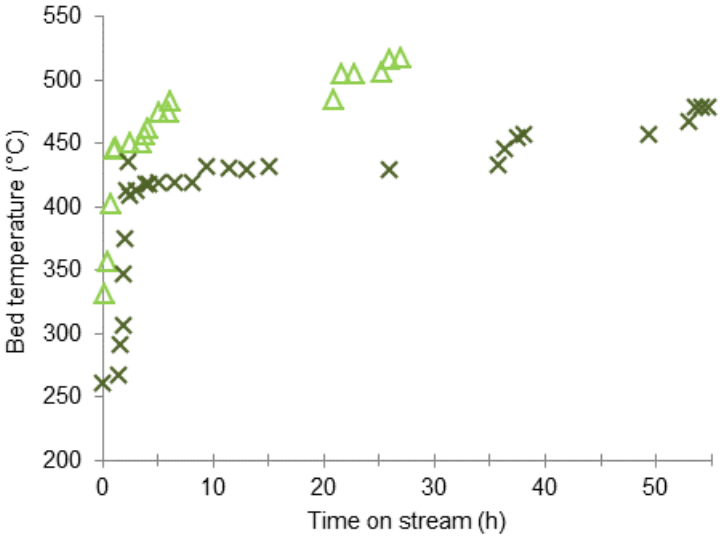

Fig. 8.6. Catalyst bed temperature required for 90 % CH_4 conversion over Δ = Pd/Al_2O_3-III catalyst (aged 18 h in wet O_2 at 780 ˚C) and × = Pd/Al_2O_3-IV catalysts (aged 3 days in autoclave at 175 ˚C). Feed = 0.7 % CH_4, 3.2 % H_2O balance air. GHSV = 100,000 h^{-1}.

A significant change was found in the catalysts aged in an autoclave where 55 % of the surface area is lost as a result of the treatment. However, the T_{90} of this catalyst is slightly lower compared to catalysts treatment I and III (see Fig. 8.4). In this case the significant change in support material pore structures does not result in any major change in active sites. This is supported by TEM results shown in Fig. S4d of SI, where no significant changes were seen in palladium particle size and distribution.

Table 8.2. N_2-physisorption analysis results of aged catalysts

Description	Units	Pd/Al_2O_3-I (aged 18 h in wet feed at 780 °C)	Pd/Al_2O_3-II (aged 18 h in wet feed at 830 °C)	Pd/Al_2O_3-III (aged 18 h In wet O_2 at 780 °C)	Pd/Al_2O_3-IV (aged 3 days in autoclave at 175 °C)
Langmuir surface area:	$m^2.g^{-1}$	193.4	184.5	180.1	96.0
Micro-pore area:	$m^2.g^{-1}$	2.0	3.8	15.4	13.8
BJH adsorption cumulative pore volume	$cm^3.g^{-1}$	0.4	0.5	0.5	0.2
BJH adsorption average pore diameter	Å	134.7	147.1	133.1	109.1

XRD patterns of the aged catalysts are shown in Fig. 8.7. From treatment I-III catalysts, no changes in the support phases were detected. Analysis of the reflections in the XRD patterns also suggests that no α-Al_2O_3 phase was detected in the samples despite the much higher temperatures used compared to the long-term tests, presumably because of the relatively short treatment times. PdO was only seen in treatment II, although there are some very weak features assigned to this phase in treatment III. The presence of this reflection suggests a growth in the palladium particle size through sintering. Interestingly, the XRD pattern of the treatment IV catalyst as shown in Fig. S2 suggests the formation of $AlHO_2$ (boehmite) after three days in autoclave at 175 °C. Sharp reflections with high intensity observed in this pattern indicate an increase in crystallinity of the alumina, which is supported by a significant decrease in surface area and the TEM image provided in Fig. S3.

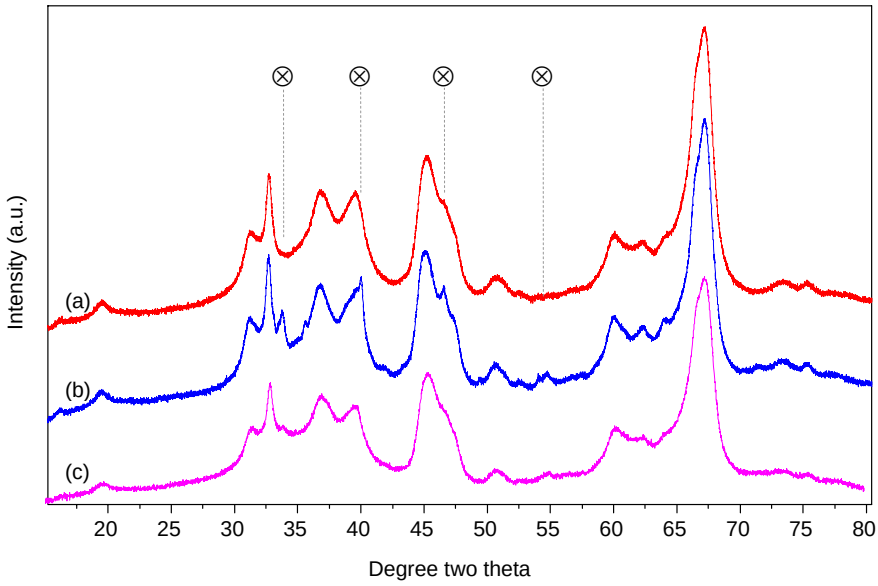

Fig. 8.7. XRD pattern of aged catalysts (a) Pd/Al_2O_3-I catalyst (aged 18 h in wet-feed at 780 ˚C); (b) Pd/Al_2O_3-II catalyst (aged 18 h in wet-feed at 830 ˚C); (c) Pd/Al_2O_3-III catalyst (aged 18 h in wet-O_2 at 780 ˚C). Phase: ⊗ = PdO.

Fig. 8.8 provides the SEM images of the aged catalysts. Over the surface of the treatment I catalyst, there are a few bright-dots as pointed by arrows in Fig. 8.8a which were identified as Pd particles by EDS. Upon increasing the ageing temperature to 830 °C (treatment-II), more Pd particles were detected, indicating significant redispersion and crystallite growth. As seen for the long term samples, this crystallite growth is consistent with the appearance of the reflections of a PdO phase seen in the XRD pattern of this sample. Some palladium particles are also seen on the surface of the treatment-III sample (Fig. 8.8c).

SEM is limited to detect relatively large particles present on the surface. Fig. S4 provides TEM images of the four aged catalysts including the distribution chart of Pd particle size. TEM particle analysis of the catalyst under treatment I and III (Fig. S4a

and S4b) indicates an average palladium particle size of 4 nm after ageing. An increase in particle size was observed in the treatment II sample (Fig. S4b), ranging from 3 to 8 nm. Note that the number of particles observed in the TEM image of the treatment II sample was significantly lower than that seen for the other two aged samples. This is consistent with the XPS data plotted in Fig. 9c where intensities of palladium species detected on the surface are very low compared to other samples, and suggests that Pd depletion occurred under the treatment II conditions. ICP analysis results of the aged samples substantiated the depletion where no decrease in Pd content was observable after the treatments. Depletion of Pd is consistent with the significant loss of catalyst activity for this sample that is seen in Figure 4. Both SEM and TEM analyses suggest that palladium migration and particle growth occurs in all cases, although final particle sizes are still smaller than observed in the long term samples.

Fig. 8.9 represents the XPS spectra of Pd 3d core level of calcined-reduced and aged catalysts. The binding energy (BE) of all fitted peaks and surface compositions are provided in Table 8.3. XPS analysis results of long-term used catalysts were reported previously [5]. Peak fitting under the spectra of calcined-reduced sample (Fig. 8.9a) reveals two components detected at Pd $3d_{5/2}$ core-level. These peaks can be identified as Pd^0 (at BE of 335.2 eV) and Pd^{2+} (at BE of 336.4 eV) by comparison with binding energies reported in the literature [18, 19].

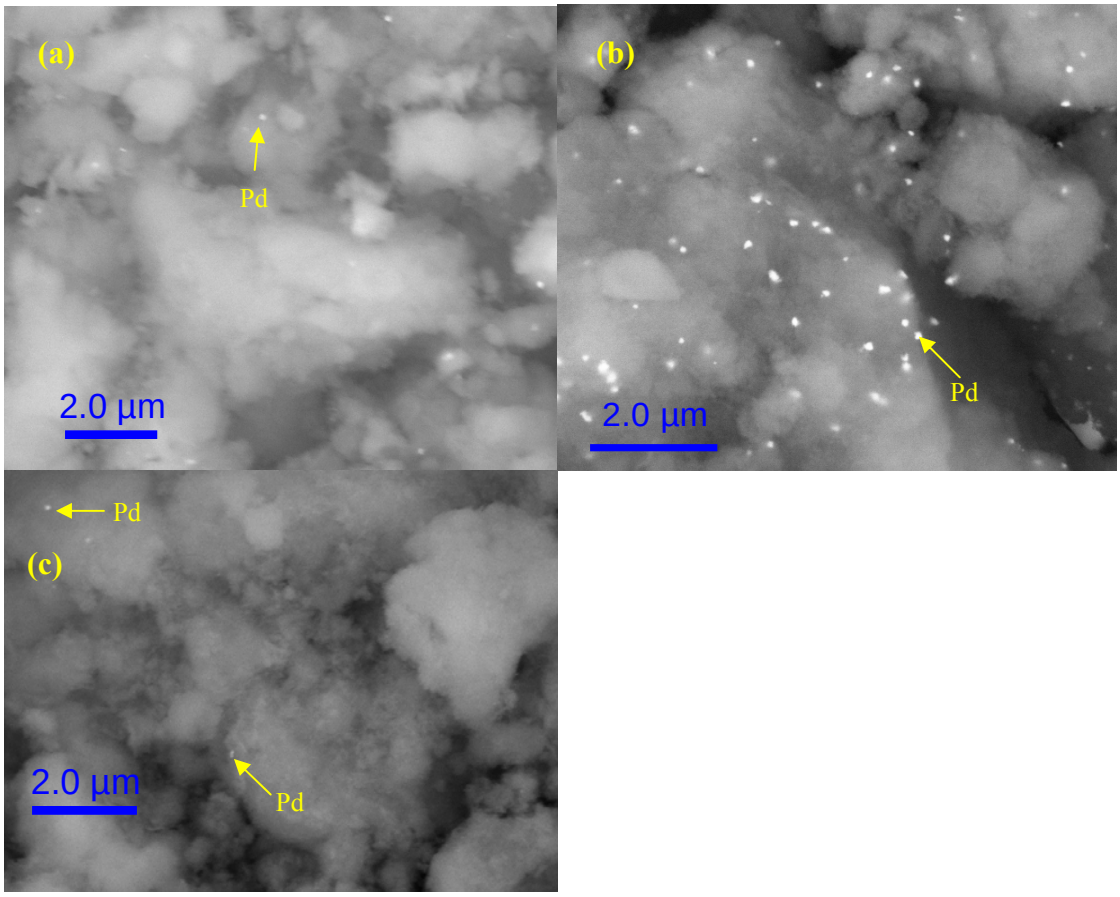

Fig. 8.8. SEM images of aged catalysts (a) Pd/Al_2O_3-I catalyst (aged 18 h in wet-feed at 780 ˚C); (b) Pd/Al_2O_3-II catalyst (aged 18 h in wet-feed at 830 ˚C); (c) Pd/Al_2O_3-III catalyst (aged 18 h in wet-O_2 at 780 ˚C).

For treatment I there are also two peaks at BE 334.8 eV and 336.5 eV which are similarly assigned to Pd^0 and Pd^{2+} respectively. The intensity of these spectra is lower than that of the fresh catalyst, suggesting a loss of Pd at the catalyst surface during the ageing process. This loss is more extensive in the case of treatment II (see Fig. 8.9c), and the TEM results suggest that at least some of this loss occurs throughout the sample rather than just at the surface. Treatment II sample also displays peaks assigned to Pd^0 and Pd^{2+}, although the PdO:Pd intensity ratio is the highest of all the samples. The palladium surface depletion is most likely due to diffusion of the Pd into the support to positions deeper than the photoelectron escape depth. This loss is greatest for ageing

treatment temperatures close to the decomposition temperature for PdO. This is supported by the XPS data of the long-term used catalysts where no palladium surface depletion was occurred during TOS experiment [5]. Our ICP analysis results over the aged catalyst also support this depletion argument where the total Pd content remains the same before and after the treatments.

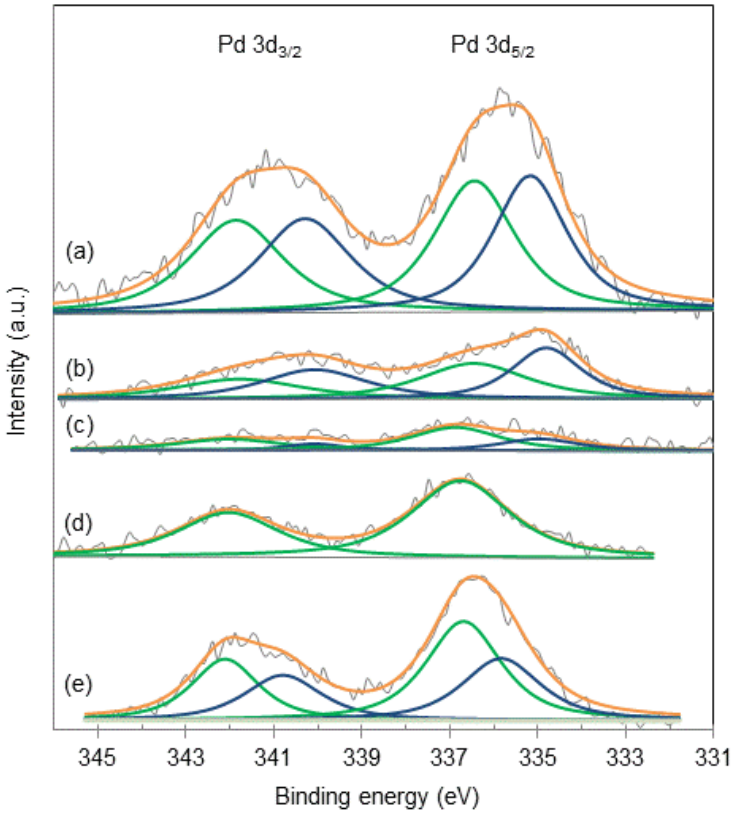

Fig. 8.9. XPS spectra of Pd 3d core level of 1.0 wt% Pd/Al_2O_3, (a) calcined-reduced sample; (b) Pd/Al_2O_3-I catalyst (aged 18 h in wet-feed at 780 ˚C); (c) Pd/Al_2O_3-II catalyst (aged 18 h in wet-feed at 830 ˚C); (d) Pd/Al_2O_3-III catalyst (aged 18 h in wet-O_2 at 780 ˚C); (e) Pd/Al_2O_3-IV catalysts (aged 3 days in autoclave at 175 ˚C).

Table 8.3. XPS peak position and surface composition

Sample	Pd $3d_{5/2}$ peak position (eV)		Surface composition (%)			
	Pd^0	Pd^{2+}	Pd	O	Al	C
a. Pd/Al_2O_3, calcined-reduced	335.2	336.4	0.2	59.6	37.7	1.6
b. Pd/Al_2O_3-I	334.8	336.5	0.1	59.6	38.5	1.8
c. Pd/Al_2O_3-II	335.0	336.9	0.03	59.9	37.9	2.1
d. Pd/Al_2O_3-III	-	336.8	0.1	55.1	31.3	10.8
e. Pd/Al_2O_3-IV	335.8	336.7	0.2	54.8	33.5	9.8

From treatment III catalyst, the XPS spectra after TOS experiment (plotted in Fig. 8.6) reveal that there is only one Pd species with BEs of 336.8 eV which can be assigned to Pd^{2+}. Fitting more peaks under the curve does not give any improvement in fit quality (χ^2). In addition, the Pd surface loss associated with the treatment was similar to treatment I. The oxidation state reached after treatment III is comparable to the oxidation state of catalyst after the long-term wet VAM test where only Pd^{2+} was observed in the sample at a concentration of 0.15 at% [5].

Fig. 8.9e shows the XPS spectra of treatment IV catalyst after a TOS experiment (plotted in Fig. 8.6). Similar to the other treatments catalysts, except for treatment III, at Pd 3d5/2 core level there are two peaks that can be fitted under the curve, Pd^0 at BE of 335.8 eV and Pd^{2+} at BE of 336.7 eV. As shown in Table 8.3, the surface composition of Pd species is similar to the calcined-reduced sample. This information is in-line with TEM analysis results where no significant re-dispersion of palladium particle was found after the treatment.

Activity loss as a result of the hydrothemal ageing appears as a consequence of Pd migration and sintering and possibly through loss of active species. Once used in a

VAM application, these aged catalysts suffer the same rapid decrease in activity thought to be caused by adsoprtion of water on the support and active sites. None of the ageing tests simulate the change in support phase observed in the long term experiment. These ageing treatments accelerate the deactivation caused by Pd particle sintering. This contibutes to activity loss that is likely to be irreversible, particularly if the particles are oxidised.

8.4. Conclusion

Insight into catalyst deactivation that occurred during long-term stability tests has been gained by characterizing the used catalysts under N_2-physisorption, XRD, SEM, TEM and XPS analyses. Deactivation is the result of palladium migration and particle growth and is the most prominent in the presence of water in the feed. The formation of α-Al_2O_3 during long-term stability tests explains the changes in pore structures occurred in conjunction with re-dispersion of Pd particles. On the other hand, with a target of mimicking the properties of long-term used catalysts, accelerated ageing of Pd/Al_2O_3 catalyst was performed under different procedures. XRD patterns of the aged catalysts revealed no α-alumina phase in the aged catalysts suggesting that the transformation of the alumina phase occurs at a very slow rate. Although it is clear that the aging treatments tested here do not necessarily mimic all of the behaviour observed in the catalyst beds tested on stream over the long-term, ageing under wet-oxygen in helium provides the catalyst bed that is perhaps the closest both in terms of performance and the characterization employed here. The oxidation state reached after treatment III is comparable to the oxidation state of catalyst after the long-term wet VAM test where only Pd^{2+} was observed in the sample at a concentration of 0.15 at%. Treating the

palladium catalysts at temperatures higher than 780 °C leads to palladium surface depletion which permanently reduces the performance of the catalyst.

References

1. Solomon, S., D. Qin, M. Manning, Z. Chen, M. Marquis, K.B. Averyt, M. Tignor, and H.L. Miller, *Fourth assessment report: climate change 2007. the physical science basis*, in *Contribution of working group I to the fourth assessment report of the intergovernmental panel on climate change, 2007*. 2007, Cambridge University Press: Cambridge, United Kingdom and New York, NY, USA
2. Schultz, H.L., P. Carothers, R. Watts, and R. McGuckin, *Assessment of the worldwide market potential for oxidising coal mine ventilation air methane*. 2003, United States Environmental Protection Agency, Air and Radiation (US-EPA)
3. Gelin, P. and M. Primet, *Complete oxidation of methane at low temperature over noble metal based catalysts: a review.* Applied Catalysis B: Environmental, 2002. 39: p. 1-37.
4. Peterson, E.J., A.T. DeLaRiva, S. Lin, R.S. Johnson, H. Guo, J.T. Miller, J. Hun Kwak, C.H.F. Peden, B. Kiefer, L.F. Allard, F.H. Ribeiro, and A.K. Datye, *Low-temperature carbon monoxide oxidation catalysed by regenerable atomically dispersed palladium on alumina.* Nature Communications, 2014. 5.
5. Setiawan, A., J. Friggieri, E.M. Kennedy, B.Z. Dlugogorski, and M. Stockenhuber, *Catalytic combustion of ventilation air methane (VAM) – long term catalyst stability in the presence of water vapour and mine dust.* Catalysis Science & Technology, 2014.
6. Schwartz, W.R., D. Ciuparu, and L.D. Pfefferle, *Combustion of methane over palladium-based catalysts: catalytic deactivation and role of the support.* The Journal of Physical Chemistry C, 2012. 116(15): p. 8587-8593.
7. Bartholomew, C.H., *Mechanisms of catalyst deactivation.* Applied Catalysis A: General, 2001. 212(1–2): p. 17-60.

8. Escandon, L.S., D. Nino, E. Diaz, S. Ordonez, and F.V. Diez, *Effect of hydrothermal ageing on the performance of Ce-promoted PdO/ZrO_2 for methane combustion.* Catalysis Communications, 2008. 9(13): p. 2291-2296.

9. Specchia, S., P. Palmisano, E. Finocchio, and G. Busca, *Ageing mechanisms on PdOx-based catalysts for natural gas combustion in premixed burners.* Chemical Engineering Science, 2009. 65(1): p. 186-192.

10. Honkanen, M., M. Kärkkäinen, V. Viitanen, H. Jiang, K. Kallinen, M. Huuhtanen, M. Vippola, J. Lahtinen, R. Keiski, and T. Lepistö, *Structural characteristics of natural-gas-vehicle-aged oxidation catalyst.* Topic in Catalysis, 2013. 56(9-10): p. 576-585.

11. Winkler, A., D. Ferri, and M. Aguirre, *The influence of chemical and thermal aging on the catalytic activity of a monolithic diesel oxidation catalyst.* Applied Catalysis B: Environmental, 2009. 93(1–2): p. 177-184.

12. Lu, Y., S. Keav, V. Marchionni, G.L. Chiarello, A. Pappacena, M. Di Michiel, M.A. Newton, A. Weidenkaff, and D. Ferri, *Ageing induced improvement of methane oxidation activity of $Pd/YFeO_3$.* Catalysis Science & Technology, 2014. 4(9): p. 2919-2931.

13. Sing, K.S.W., *Reporting physisorption data for gas/solid systems.* Pure and applied Chemistry, 1982. 54(11): p. 2201-2218.

14. Carlo, G.D., G. Melaet, N. Kruse, and L.F. Liotta, *Combined sulfating and non-sulfating support to prevent water and sulfur poisoning of Pd catalysts for methane combustion.* Chemical Communication, 2010. 46: p. 6317-6319.

15. Castellazzi, P., G. Groppi, P. Forzatti, A. Baylet, P. Marecot, and D. Duprez, *Role of Pd loading and dispersion on redox behaviour and CH_4 combustion activity of Al_2O_3 supported catalysts.* Catalysis Today, 2010. 155: p. 18-26.

16. Arai, H. and M. Machida, *Thermal stabilization of catalyst supports and their application to high-temperature catalytic combustion.* Applied Catalysis A: General, 1996. 138(2): p. 161-176.

17. Neyestanaki, A.K., F. Klingstedt, T. Salmi, and D.Y. Murzin, *Deactivation of postcombustion catalysts, a review.* Fuel, 2004. 83(4–5): p. 395-408.

18. Yasuda, K., T. Masui, T. Miyamoto, and N. Imanaka, *Catalytic combustion of methane over Pt and PdO-supported CeO-ZrO-BiO/γ-AlO catalysts.* Journal of Materials Science, 2011. 46(11): p. 4046-4052.

19. Teschner, D., E. Vass, M. Hävecker, S. Zafeiratos, P. Schnörch, H. Sauer, A. Knop-Gericke, R. Schlögl, M. Chamam, A. Wootsch, A.S. Canning, J.J. Gamman, S.D. Jackson, J. McGregor, and L.F. Gladden, *Alkyne hydrogenation over Pd catalysts: A new paradigm.* Journal of Catalysis, 2006. 242(1): p. 26-37.

CHAPTER 9

CONCLUSIONS AND RECOMMENDATIONS

9.1. Conclusions

Catalytic combustion of methane has been demonstrated to be a viable option for methane emission abatement where methane is totally oxidized to carbon dioxide at temperatures below 400 °C. This flameless combustion is applicable for highly diluted air-methane-water vapour streams and varied methane concentration. Production of NOx is essentially absent due to its relatively low reaction temperature. The humid conditions and the presence of coal dust in the VAM streams are the major issues in developing a catalytic combustion system.

Chapter 2 provides a summary of prior research related to the catalytic combustion of lean methane mixtures. It summarizes the characteristics of ventilation air methane streams and the various technological options available to mitigate and utilized these methane emissions. Supported Pd catalysts are generally agreed as the most active and durable materials for methane combustion and PdO are identified as the active catalytic phase. However, its sensitivity to and subsequent deactivation by water vapour presents a serious drawback to its use in catalytic combustion of ventilation air methane. Gold and cobalt oxide catalysts were considered as possible alternative catalytic materials for VAM application.

The effect of pre-treatment conditions on the activity of Pd/Al_2O_3 catalyst was examined and reported in Chapter 4. Pd/Al_2O_3 catalysts, calcined in air, exhibit a higher intrinsic activity at low temperatures compared to those activated in air and then reduced in hydrogen suggesting PdO is more active than Pd^0. Upon increasing the reaction temperature, the catalysts are reduced by methane and exhibit similar activity

to catalysts reduced with hydrogen. Interestingly, even under very lean conditions, PdO can activate methane at temperature as low as 180 °C and a carbonaceous solid phase is formed on palladium catalysts. XPS analysis suggests the carbonaceous solid phase formed at 180 °C is most likely in the form of a Pd-carbide species. Heating the carbonaceous solid phase to 320 °C in air oxidizes the carbide species to CO_2.

Chapter 5 evaluated the stability of Pd/Al_2O_3 catalysts during short and long term experiments in the presence of water and VAM dust. Experiment where the feed was oscillated between dry and wet feeds suggests that approximately 50 % of the catalytic activity (reversibly) decreased, most likely due to competition between water vapour and methane to adsorb on the active sites. Palladium hydroxide was not detected during these short term experiments. However, prolonged exposure to water resulted in the formation of palladium hydroxide and progressively deactivated the catalyst. Long term stability tests with humid, synthetic ventilation air methane reveals that methane conversion level can be maintained at 90 % for a period of 1,150 h at temperatures ≤ 500 °C. These long-term stability tests also highlight that water vapour present in the feed stream is the primary factor responsible for catalyst deactivation. Introducing VAM dust into the feed leads to a reduction in catalyst activity, likely due to an inhibitory effect of chloride ions on the surface of catalyst. Nevertheless, stability tests in the presence of water and VAM dust suggest that methane conversion level higher than 75 % can be achieved over 1,100 h at a reaction temperature below 600 ºC.

In Chapter 6, alternative catalysts i.e. Co_3O_4, Fe_2O_3, Au/Co_3O_4 and Au/Fe_2O_3 catalysts were prepared using several synthesis techniques. The activity and stability of these catalysts were evaluated for catalytic combustion of VAM mixtures under humid

conditions. Based on their activities, the order of intrinsic activity of the catalysts is: Co_3O_4 > Au/Co_3O_4 > Fe_2O_3 > Au/Fe_2O_3. The higher oxygen surface coverage of Co_3O_4 is suggested to be responsible for its higher activity compared to Fe_2O_3 catalysts. It is inferred that, the re-oxidation of the reduced cobalt oxide sites is rate limiting. Among those tested catalysts, nano-sized Co_3O_4 and Au/Co_3O_4 catalysts exhibit excellent stabilities during time-on-stream experiments. XPS analysis suggests that little or no change in oxidation/chemical states were observed from Co_3O_4 catalyst after time-on-stream experiments. TPD and XPS analyses reveal the presence of strongly bonded adsorption of hydroxyl species on the surface of catalysts highlighting the role of water as being responsible for the rapid deactivation over Fe_2O_3 and Au/Fe_2O_3 catalysts. Nevertheless, co-precipitating gold with cobalt oxide or iron oxide does not enhance the activity of the catalyst.

Chapter 7 assessed the activity and stability of a novel Pd supported on TS-1 catalyst in methane combustion and compared with Pd/Al_2O_3 catalyst. A notable increase in hydrothermal stability was observed over 1,900 h time-on-stream experiments, where a constant steady state activity at 90 % methane conversion level was achieved below 500 °C. The Arrhenius plot of Pd-TS-1 catalyst obtained after long-term stability test indicates two linear regions with different apparent activation energies and consequently a change in the oxygen surface coverage dependent on the reaction temperature is proposed. Catalyst characterization suggested that water adsorption and in turn the hydrophobicity of the catalyst support plays an important role in enhancing the stability of the catalyst. The data obtained disclose that the activity of Pd/TS-1 catalyst at lower temperature was hindered by water present in the feed. However, at temperatures higher than 350 °C water is not present on the surface resulting in lower activation energy in

comparison with Pd/Al_2O_3. The hydrophobic properties of titanium silicalite support helps in preventing the accumulation of hydroxyl on the support as well as increase the amount of available oxygen.

Chapter 8 investigated catalyst deactivation occurring during long-term stability tests. The characterization results showed that deactivation is due to palladium migration and particle growth and is the most prominent in the presence of water in the feed. The formation of α-Al_2O_3 during long-term stability tests explains the changes in pore structures which arise in conjunction with re-dispersion of Pd particles. On the other hand, accelerated ageing treatment of Pd/Al_2O_3 catalyst was performed under different procedures with a target of mimicking the properties of long-term used catalysts. XRD patterns revealed the absence of an α-alumina phase in the aged catalysts. This suggests that the transformation of the alumina phase takes place at a very slow rate. Although it is clear that the aging treatments described do not necessarily mimic all of the behaviour observed in the catalyst beds of the long-term tests, ageing under wet-oxygen in helium provides the catalyst bed that is perhaps the closest both in terms of performance and characteristics studied here. The oxidation state reached after treatment III is comparable to the oxidation state of catalyst after the long-term wet VAM test where only Pd^{2+} was observed in the sample at a concentration of 0.15 at%. Treating the palladium catalysts at temperatures higher than 780 °C leads to palladium surface depletion which permanently reduces the performance of the catalyst.

9.2. Recommendations

Catalytic combustion of lean methane in air has been extensively investigated highlighting the prospect of this method to be implemented in VAM mitigation and utilization. A number of previous studies were devoted to design of a suitable catalytic material which is capable of operation under humid conditions and in the presence of contaminants such as chlorine and sulphur containing compounds. However, implementation this technology for VAM abatement requires additional research work in order to understand the catalytic behaviour and develop a high performance and durable catalytic system. In this section, we suggest potential future work which focuses on the issues related to the combustion of coal mines ventilation air methane.

Although it is well recognised that water vapour strongly inhibits the activity of catalysts, a comprehensive understanding on the mechanism of catalyst deactivation has not been successfully established yet. Prior investigations suggest that the deactivation proceeds through the formation of hydroxyl groups on PdO which effectively deactivates the active site for methane oxidation [1, 2]. Other investigations showed that the activity of Pd/Al_2O_3 catalysts is partially restored upon removing water from the feed [3, 4]. In contrast, our data in Chapter 5 have shown that the drop in activity is reversible within 2 h time on stream experiment. Prolonged exposure to humid feed leads to the formation of palladium hydroxide and progressively deactivates the catalyst. This suggests that water inhibits methane oxidation on PdO through multiple mechanisms, depending on the reaction conditions and the structure of catalysts. Additional experiments on Pd catalysts using different support materials and different

reaction conditions would help in fully understands the mechanisms of catalyst deactivation.

The humid conditions of ventilation air streams urges future investigations to focus on low temperature reactions (in the range of 200-300 °C) where the hydroxyl is the most abundant surface species and the rate is limited by water desorption from the surface of the catalyst. In this case, the accumulation of hydroxyl groups on the catalyst support can prevent the migration of oxygen from the support to the Pd active site, as well as reducing the availability of oxygen involved in the oxidation of methane [5]. However, this requires more work such as kinetic and isotope experiments at different reaction conditions to clarify this argument. It is also possible that hydroxyls form on both the Pd site and the support in high concentration. Deactivation can potentially originate from the surface of either the support or palladium.

More effort in developing a comprehensive understanding of the sintering phenomena is incomplete due to the complexity of the elementary processes and lack of kinetic data for these processes. Very limited data is available for dispersion and particle-size distribution versus time which is necessary for validating sintering models [6]. In Chapter 7-8, the particle size of used Pd/TS-1 and Pd/Al_2O_3 catalysts after 1,100 h in operation were analysed using TEM suggesting an increase in the average Pd particle size. The particle size increases were also observed from Pd/Al_2O_3 catalysts after four rapid ageing treatments. Nevertheless, for process design/optimization and model development/validation, more statistically significant measurements of sintering rates are needed for supported metal catalysts under reaction conditions over several hundreds of hours and where possible in large scale processes. While spectroscopic

tools have been used effectively during the past two decades to advance our fundamental understanding of sintering and redispersion, additional insights into atomic and molecular processes occurred during sintering and redispersion are needed to develop more realistic models.

Another route to prepare efficient and durable catalysts for combustion of VAM gas should focus on improving the activity of cobalt oxide catalysts. Although the activity of this catalyst is currently is lower than palladium catalysts, its low-cost of production and higher stability would potentially result in more benefits for VAM application. Chapter 6 has disclosed the high stability of nano-sized Co_3O_4 catalyst tested under humid feed conditions. XPS data suggested that little or no change in oxidation state was observed over Co_3O_4 following time-on-stream experiments. A high oxygen adsorption capacity of the Co_3O_4 catalyst could be a key factor for the higher performance of this catalyst. It is generally observed that morphology or the crystal plane of Co_3O_4 nanocrystals can alter their catalytic performance [7]. Based on the current investigation results, the catalytic activity of Co_3O_4 is related to either the reactive [112]/[110]} planes or the surface oxygen species, bulk oxygen mobility, re-oxidation of cobalt species, and active oxygen vacancies of Co_3O_4 nanocrystals with controlled size [8]. To clarify this, more detail investigation should be performed under various reaction conditions and temperatures.

A combination of cobalt oxide with other oxides such as CeO_2, ZrO_2 *etc.* (Co_3O_4-MO_x binary oxides) are potential catalysts for VAM combustion. A number of studies have aimed at developing effective combinations as well as understanding the relationship between methane oxidation activity and redox properties. Although the number of

contributions on different Co_3O_4-MO_x binary oxides activities and their characteristics are growing, more research is still needed to explore optimum binary catalysts. Future research may be aimed for gaining a better understanding on the interactions between different kinds of binary oxide catalysts and their redox properties in relationship with the activity of catalysts. Future investigation can also be devoted in preparing three or more component in a catalytic system such as noble metal doped or noble metal alloys doped Co_3O_4-MO_x binary oxides. It is expected that combining different metal oxides and evaluating their activity under various reaction conditions will enable a more comprehensive understanding of the interaction between methane and active sites and therefore will improve catalytic activity and durability.

In order to meet the requirements of the VAM application, it seems to be essential that future investigations focus on catalyst modifications which enhance the durability of catalysts, especially developing greater resistance against water vapour and coal dust as well as enhancing the intrinsic activity of the catalyst. As reported in Chapter 7, the use of TS-1 as support material enhances the stability of Pd catalyst. Characterizations disclose that the hydrophobicity of TS-1 is higher compared to Al_2O_3 and leads to a lower desorption temperature of water vapour and reduces the accumulation of hydroxyl groups on the catalyst surface. As the hydroxyl groups are reduced, the stability of this catalyst increases significantly. This indicates that modification of the support material of palladium catalysts should be continued. As reported in the literature, the hydrophobicity of TS-1 can further be improved by applying fluorine or silylation modification procedures [9, 10]. The concept underpinning this approach is increasing the hydrophobicity of mesoporous silica by removing the unnecessary hydroxyl groups

or replacing them by other groups, which will assist the condensation of organic compounds in the pores.

The presence of coal dust in a catalytic system for VAM has been initially investigated and reported in Chapter 5. It was found that the VAM dust containing a mixture of fine coal, $CaCO_3$ and aluminosilicate particles has created a variation in catalytic activity originating from coal-dust ignition. Chloride ions were detected from the VAM dust and are suggested to be responsible for the drop in activity observed during time-on-stream experiments. Due to limited information available on the effect of VAM dust on catalysts, no clear explanation can be drawn. Indeed, coal dust investigation is still in very early stage and requires more investigations to understand the deactivation phenomena caused by VAM dust.

The application of a catalytic process for VAM abatement requires additional study on catalyst stability and durability in a larger reactor size under simulated VAM gas. Future studies should be devoted more in designing and testing a larger scale of catalytic reactor. The use of structure packing, such as a monolith in difference to a random packed bed reactor is more practical and provides additional benefits. Monoliths have been successfully used for the abatement of NO_x and CO emissions from automotive engines and in mass transfer operations such as distillation and absorptions. Designing the reactor of a scale which is industrially relevant is considerably easier when using monolith structure. The characteristic features of this generic structure are uniform flow distribution, low pressure drop, and improved mass transfer characteristics [11]. However, gas hourly space velocity of this type of structure is typically lower than those of packed beds. The key factor for improving their performance lies in the manner

how feed gas and catalyst are contacted. As the volumetric flow of VAM gas is high (~300 m^3 s^{-1}), it is important to fully understand catalyst dispersion/active site accessibility in the context of operating parameters such as reaction temperature, flow rate, feed composition and GHSV. The operating mode and flow distribution play important role on the performance of monolith reactors. To achieve a uniform flow distribution over the monolith cross section, the use of different type of flow distributor might prove adept and requires exploration [11]. The cell density and void fraction are also important parameter to be considered in designing a monolith for VAM.

.

The presence of coal dust and other particulates is a challenge in designing the catalytic system for VAM combustion. Particulates are heterogeneous in nature and can vary significantly. Additional studies on the characteristics of VAM dust are needed in order to provide comprehensive information for designing the structure of reactor. Understanding the physical and chemical properties of VAM dust will help in reducing blockage and deactivation of the monolithic catalyst, as well as minimising the rate of reactor corrosion.

References

1. Burch, R., F.J. Urbano, and P.K. Loader, *Methane combustion over palladium catalysts: the effect of carbon dioxide and water on activity.* Applied Catalysis A: General, 1995. 123(1): p. 173-184.

2. Ribeiro, F.H., M. Chow, and R.A. Dallabetta, *Kinetics of the complete oxidation of methane over supported palladium catalysts.* Journal of Catalysis, 1994. 146(2): p. 537-544.

3. Ciuparu, D., N. Katsikis, and L. Pfefferle, *Temperature and time dependence of the water inhibition effect on supported palladium catalyst for methane combustion.* Applied Catalysis A: General, 2001. 216(1-2): p. 209-215.

4. Ciuparu, D., M.R. Lyubovsky, E. Altman, L.D. Pfefferle, and A. Datye, *Catalytic Combustion of methane over palladium-based catalysts.* Catalysis Reviews, 2002. 44(4): p. 593-649.

5. Schwartz, W.R., D. Ciuparu, and L.D. Pfefferle, *Combustion of methane over palladium-based catalysts: catalytic deactivation and role of the support.* The Journal of Physical Chemistry C, 2012. 116(15): p. 8587-8593.

6. Bartholomew, C.H., *Mechanisms of catalyst deactivation.* Applied Catalysis A: General, 2001. 212(1–2): p. 17-60.

7. Xie, X. and W. Shen, *Morphology control of cobalt oxidenanocrystals for promoting their catalytic performance.* Nanoscale, 2009. 1(1): p. 50-60.

8. Liotta, L.F., H. Wu, G. Pantaleo, and A.M. Venezia, *Co_3O_4 nanocrystals and Co_3O_4-MOx binary oxides for CO, CH_4 and VOC oxidation at low temperatures: a review.* Catalysis Science & Technology, 2013. 3(12): p. 3085-3102.

9. Kuwahara, Y., K. Maki, Y. Matsumura, T. Kamegawa, K. Mori, and H. Yamashita, *Hydrophobic modification of a mesoporous silica surface using a fluorine-containing silylation agent and its application as an advantageous host material for the TiO_2 photocatalyst.* The Journal of Physical Chemistry C, 2009. 113(4): p. 1552-1559.

10. Kuwahara, Y., T. Kamegawa, K. Mori, and H. Yamashita, *Fabrication of hydrophobic zeolites using triethoxyfluorosilane and their application as supports for TiO_2 photocatalysts.* Chemical Communications, 2008(39): p. 4783-4785.

11. Roy, S., T. Bauer, M. Al-Dahhan, P. Lehner, and T. Turek, *Monoliths as multiphase reactors: a review.* AIChE Journal, 2004. 50(11): p. 2918-2938.

Appendix A

COSILAB calculation results

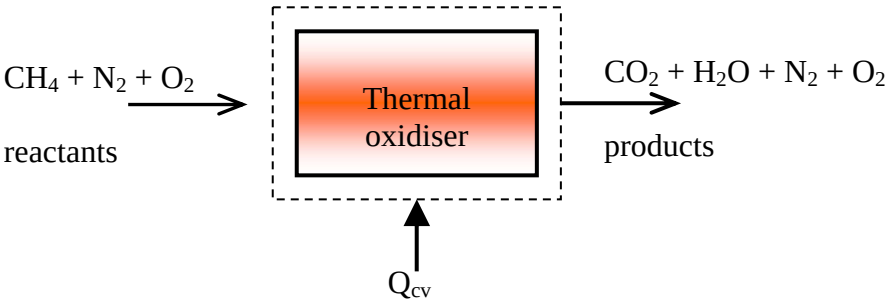

Assumptions:

Case : Equilibrium Calculation
(Calculation of chemical equilibria under a variety of conditions, and calculation of Chapman-Jouguet detonations)
Reaction temperature : 1273 K
Reactant pressure : 1 bar
Reactant composition : 0.2 % CH_4; 79.84 % N_2; 19.96 % O_2.
Equilibrium type : Enthalpy and Pressure Constant

Results:

```
================================================================

    COSILAB -- Equi Solver,  Version 3.1.2 from 05-Nov-2008

    Solver for Chemical-Equilibrium Problems

    Copyright (C) by SoftPredict 2003-2008

================================================================

Control data follow ...

BEGIN_COMMENT
Methane gas concentration is 0.2%
END_COMMENT

BEGIN_COS_VERSION
   2.3
END_COS_VERSION

reactant CH4 0.200000
reactant N2 79.840000
reactant O2 19.960000
TemperatureEstimate 1.400000E+003
Temperature 1.273000E+003
Pressure 1.000000E+000 bar
CONH
CONP
SIUnits
GivenMoleFractions
END
```

```
 Constant P and H

                          Reactants         Equilibrium
 ------------------------------------------------------
 P (atm)                 9.8692E-01          9.8692E-01
 T (K)                   1.2730E+03          1.3195E+03
 V (m3/kg)               3.6770E+00          3.8113E+00
 R (kg/m3)               2.7196E-01          2.6238E-01
 H (J/kg)                1.0719E+06          1.0719E+06
 U (J/kg)                7.0425E+05          6.9082E+05
 S (J/kg-K)              8.4683E+03          8.5161E+03
 W (kg/mol)              2.8785E-02          2.8785E-02


 Mole Fractions
 CH4                     2.0000E-03          0.0000E+00
 CO2                     0.0000E+00          2.0000E-03
 H2O                     0.0000E+00          4.0000E-03
 N2                      7.9840E-01          7.9840E-01
 O2                      1.9960E-01          1.9560E-01


 Mass Fractions
 CH4                     1.1147E-03          0.0000E+00
 CO2                     0.0000E+00          3.0578E-03
 H2O                     0.0000E+00          2.5034E-03
 N2                      7.7700E-01          7.7700E-01
 O2                      2.2189E-01          2.1744E-01

TASK COMPLETED: REGULAR STOP
```

Table S1 provides the COSILAB calculation results for methane concentration up to 0.7 with similar assumptions.

Table S1. COSILAB calculation result for various methane concentrations

Methane (%)	Nitrogen (%)	Oxygen (%)	Temperature (K)	H (kJ/kg)	S (kJ/kg.K)
0.2	79.84	19.96	1319.5	1.0719E+03	8.5161
0.3	79.76	19.94	1342.6	1.0708E+03	8.5455
0.4	79.68	19.92	1365.5	1.0697E+03	8.5741
0.5	79.6	19.9	1388.3	1.0685E+03	8.6023
0.6	79.52	19.88	1411.1	1.0674E+03	8.6299
0.7	79.44	19.86	1433.7	1.0662E+03	8.6571

Appendix B

Supporting Information for Chapter 4

Published in:

Energy Technology (Wiley-VCH Verlag GmbH&Co. KGaA, Weinheim) 2014, 2, 243 – 249, (DOI: 10.1002/ente.201300119)

Supporting information consists of five pages, seven figures and one table.

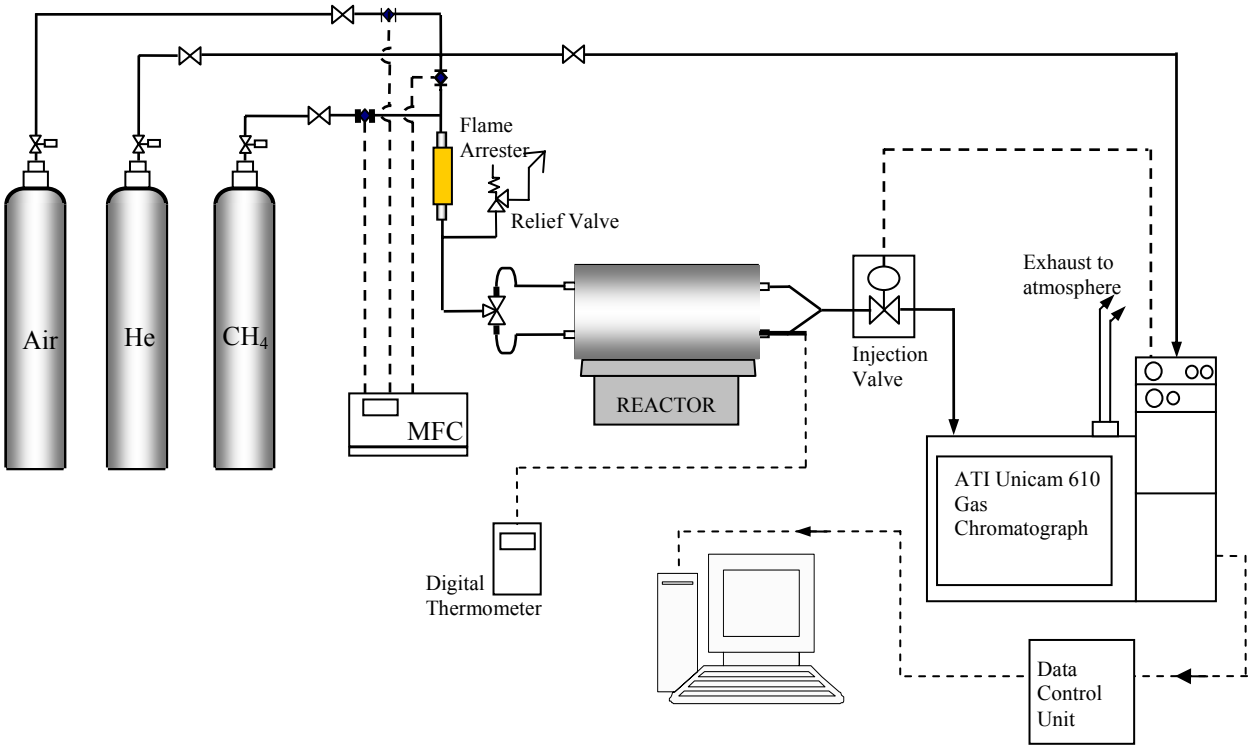

Fig. A.1. Experimental set-up for catalytic activity measurement.

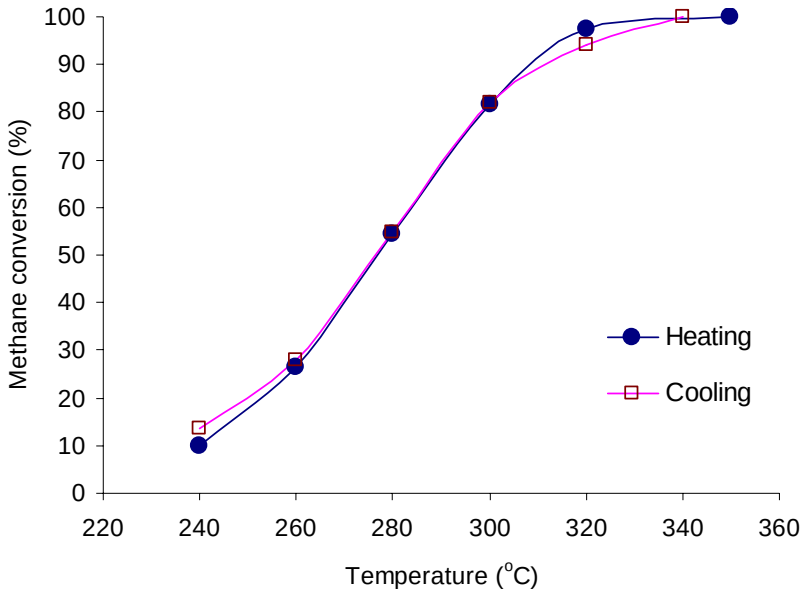

Fig. A.2. Methane conversion over 1.2 wt% Pd/Al_2O_3 catalysts as a function of temperature during heating and cooling. Feed: 6,000 ppm CH_4 balance air, GHSV = 33,000 h^{-1}.

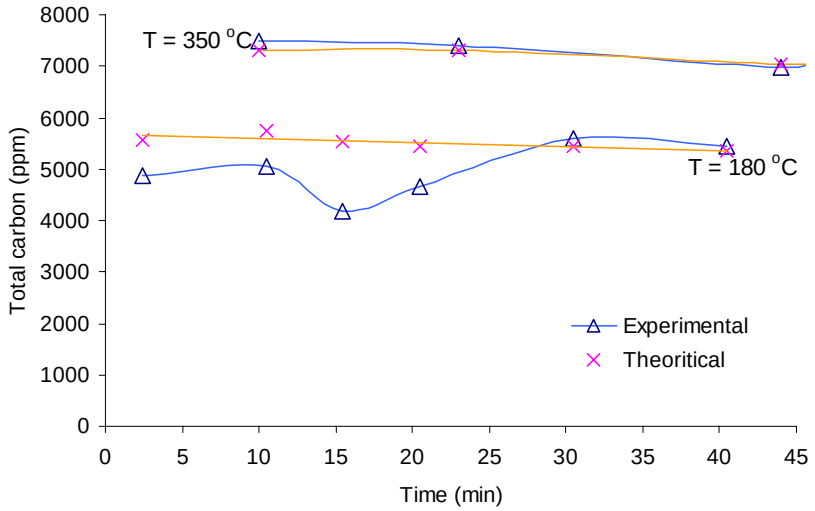

Fig. A.3. Total carbon detected and calculated during methane oxidation over 1.2 wt% Pd/Al_2O_3 catalysts calcined in air at T = 180 °C (feed = 5,000 ppm CH_4 in air) and T = 350 °C (feed = 7,000 ppm CH_4 in air) at space velocity of 33,000 h^{-1}. Δ = experimental; × = theoretical.

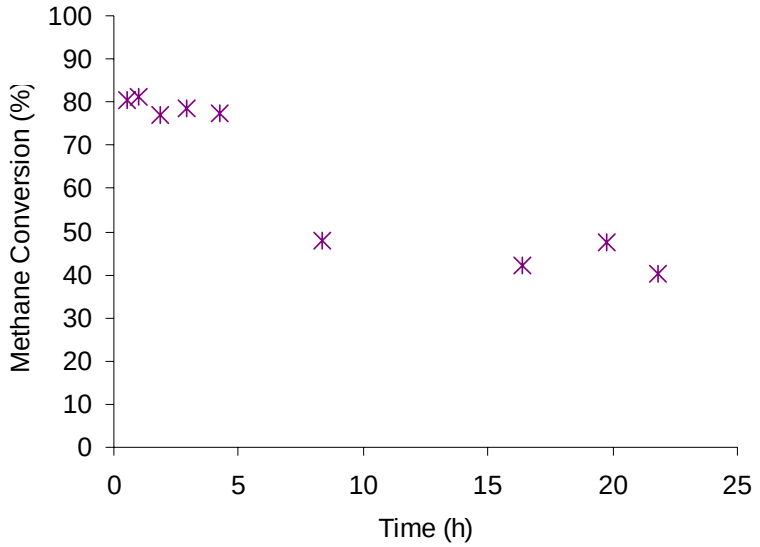

Fig. A.4. Evaluation of time-on-stream behaviour at 280 °C over 1.2 wt% Pd/Al_2O_3 catalysts calcined in air, feed = 6,000 ppm CH_4 in air at space velocity of 12,000 h^{-1}.

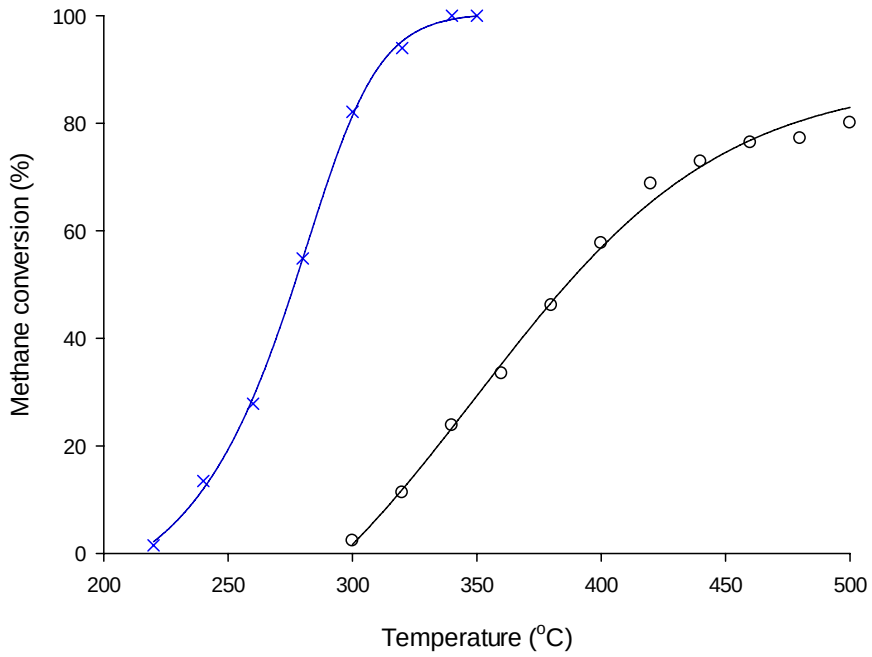

Fig. A.5. Methane conversion over Pd/Al_2O_3 catalysts as a function of temperature at different Pd loading. Feed: 6,000 ppm CH_4 balance air, GHSV = 33,000 h^{-1}. Calcined in air at 500 ºC for one h, purge with He for 30 min at 300 ºC and reduced in H_2 at 300 ºC for 2 h. × = 1.2 wt% Pd/Al_2O_3; ○ = 0.1 wt% Pd/Al_2O_3.

Table A.1. Metal dispersion and particle size

Sample	Metal dispersion (%)	Active particle diameter (nm)
1.2 wt% Pd/Al_2O_3 reduced in H_2	9	12.2
1.2 wt% Pd/Al_2O_3 calcined in air	68	1.6
0.1 wt% Pd/Al_2O_3 reduced in H_2	60	1.8

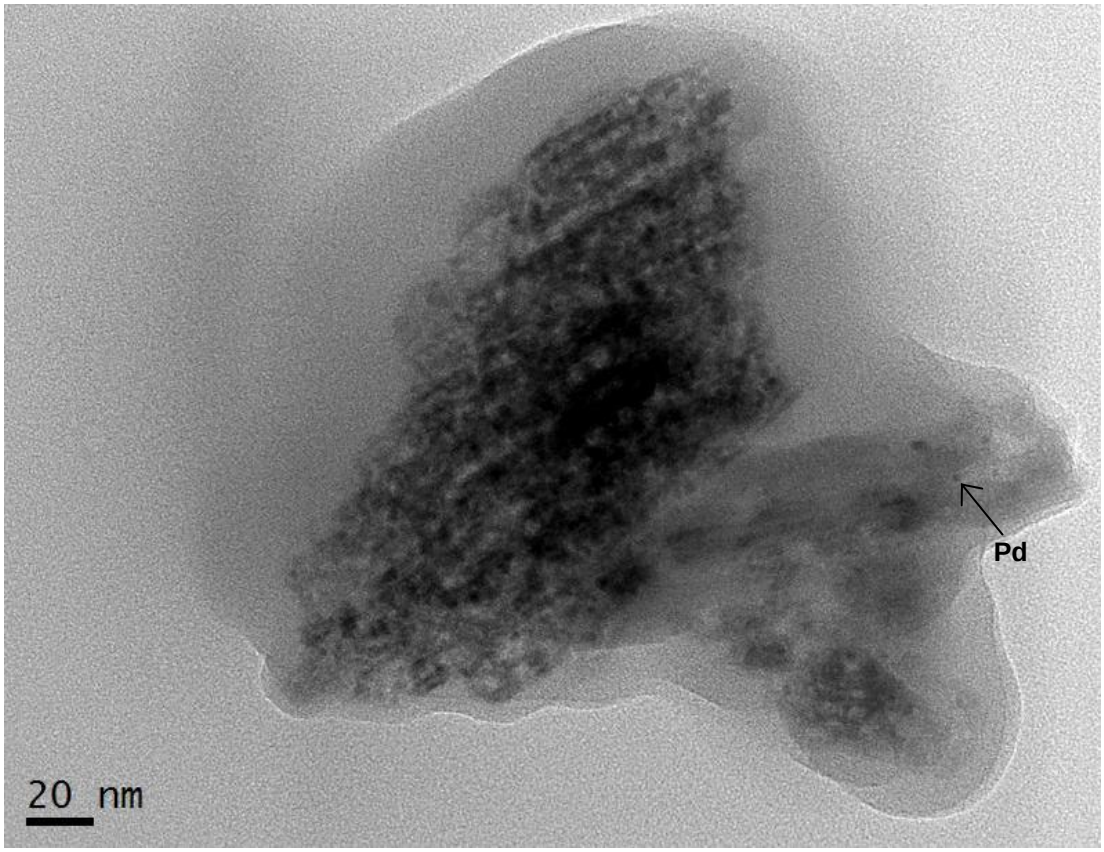

Fig. A.6. TEM images of calcined Pd/Al_2O_3 catalysts

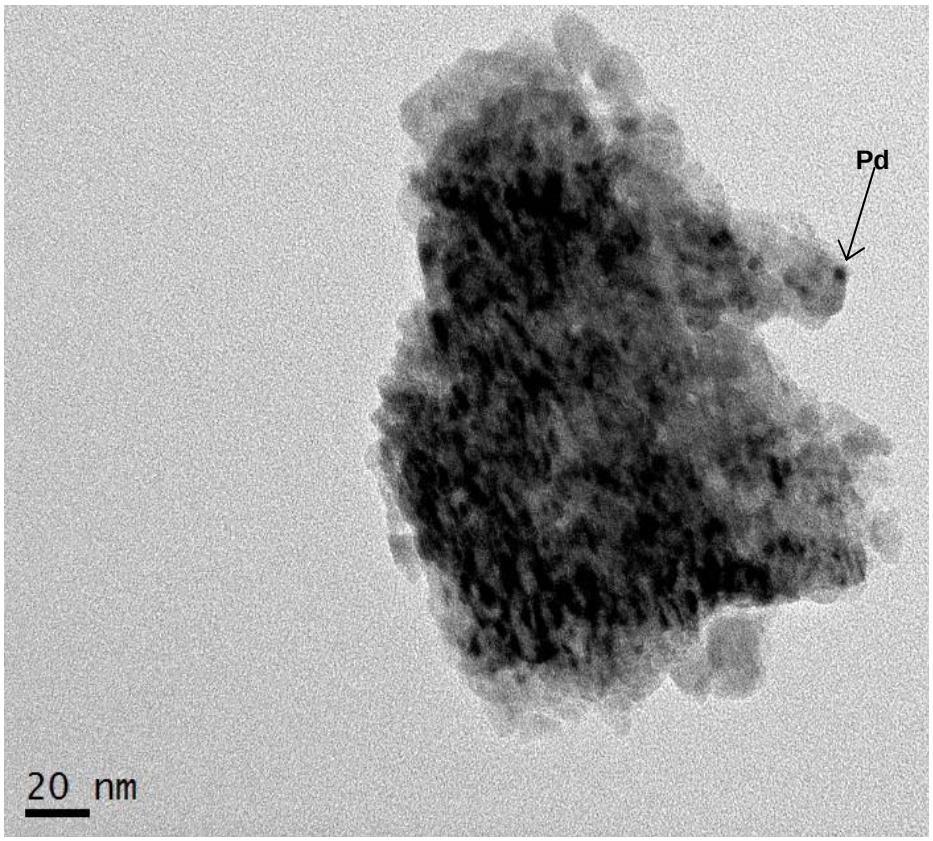

Fig. A.7. TEM images of calcined-reduced Pd/Al_2O_3 catalysts. The arrow indicates a Pd particle.

Appendix C

Supporting Information for Chapter 5

Published in:

Catalysis Science & Technology, 4(6):1793-1802 2014,

DOI: 10.1039/C4CY00120F

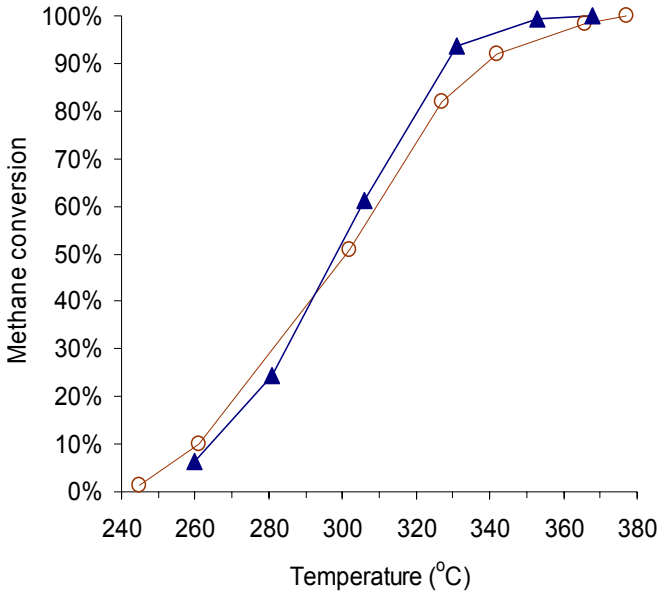

Fig. S1. Methane conversion as a function of reaction temperature of methane oxidation over 1.0 wt% Pd/Al_2O_3 and 1.2 wt% Pd/Al_2O_3 catalyst. Feed: 7,000 ppm CH_4 balance air at GHSV = 100,000 h^{-1}. ○ = 1.0 wt% Pd/Al_2O_3 catalyst; ▲ = 1.2 wt% Pd/Al_2O_3 catalyst.

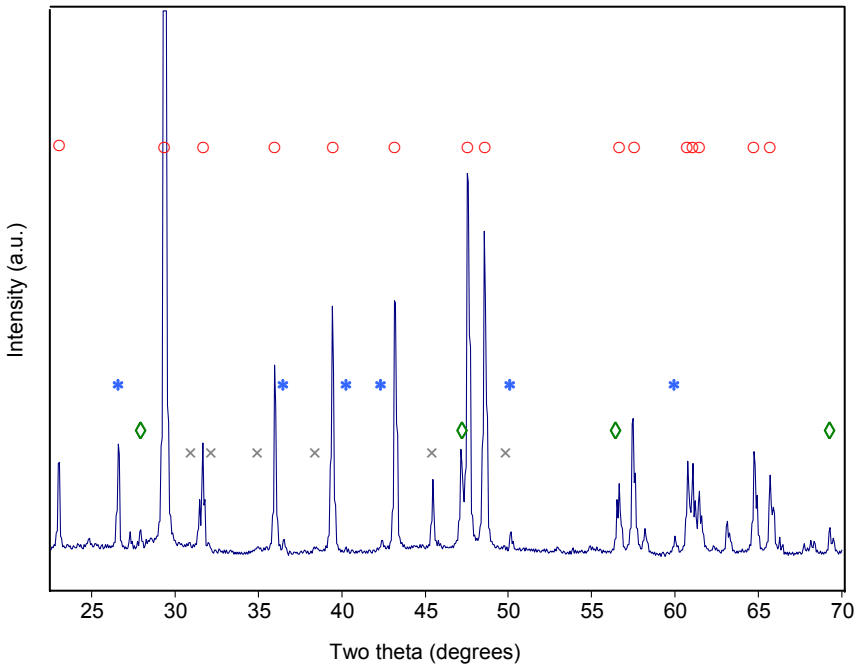

Fig. S2. X-ray diffraction patterns of VAM dust. Crystalline phase: ○ = $CaCO_3$, * = SiO_2, ◊ = Si, × = Fe_3O_4.

Appendix D

Supporting Information for Chapter 6

Published in:

Catalysis Today, 2014,

http://dx.doi.org/10.1016/j.cattod.2014.11.031

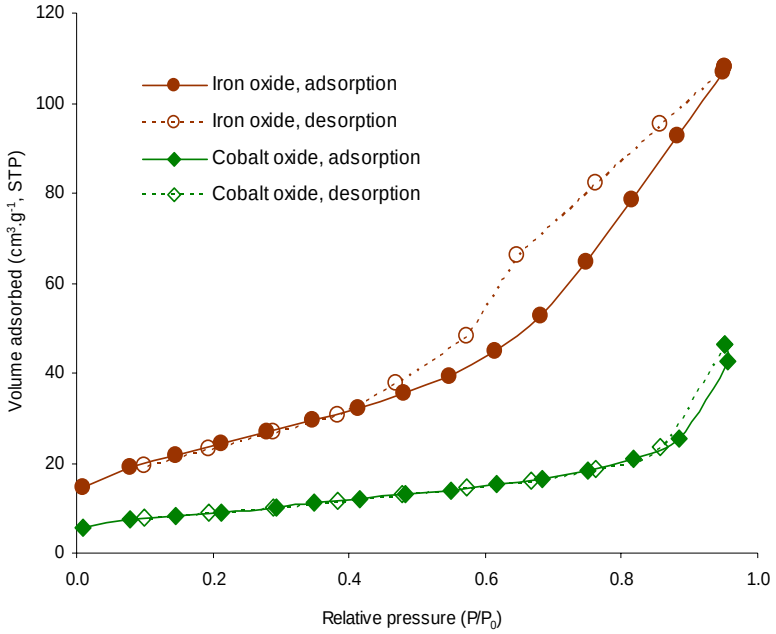

Fig. S1. Nitrogen adsorption-desorption isotherms of Co_3O_4 and Fe_2O_3 catalysts.

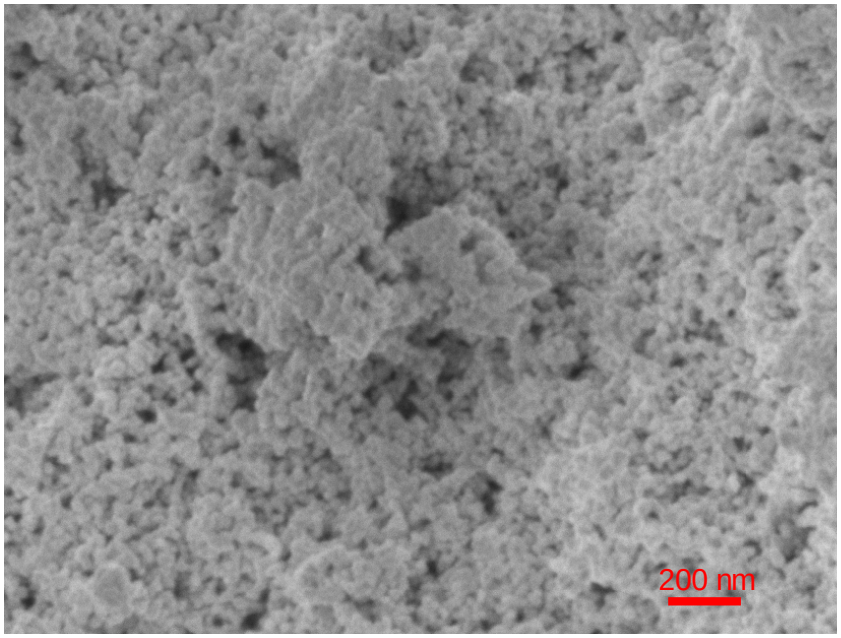

Fig. S2. SEM image of Co_3O_4

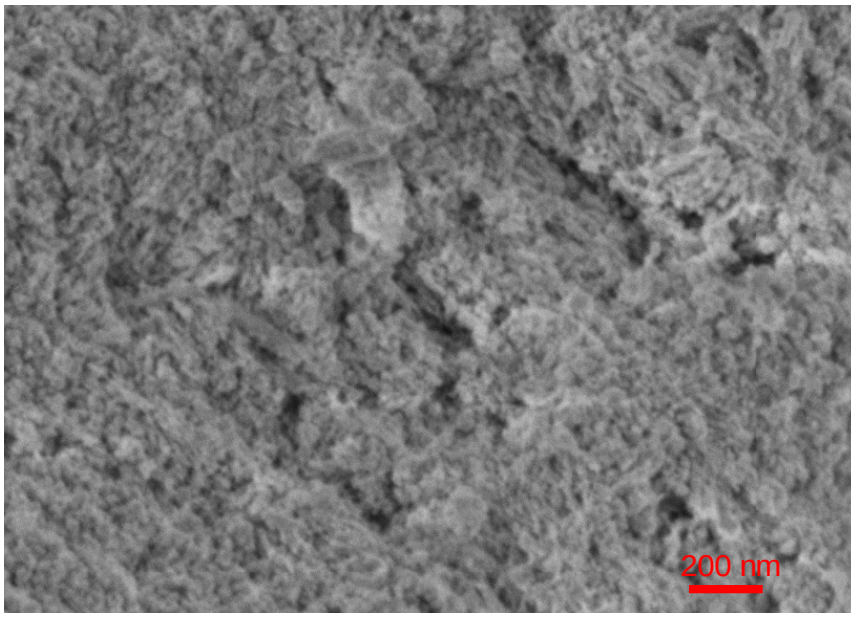

Fig. S3. SEM image of Fe_2O_3

Table S1. H_2O-TPD peak position

Sample	Peak position			
	Peak #1	Peak #2	Peak #3	Peak #4
Co_3O_4	212.5	262.3	330.1	460.1
Fe_2O_3	195.5	235.4	310.6	469.8
Au/Co_3O_4	194.5	243.0	309.4	497.6
Au/Fe_2O_3	192.2	223.7	294.0	469.0

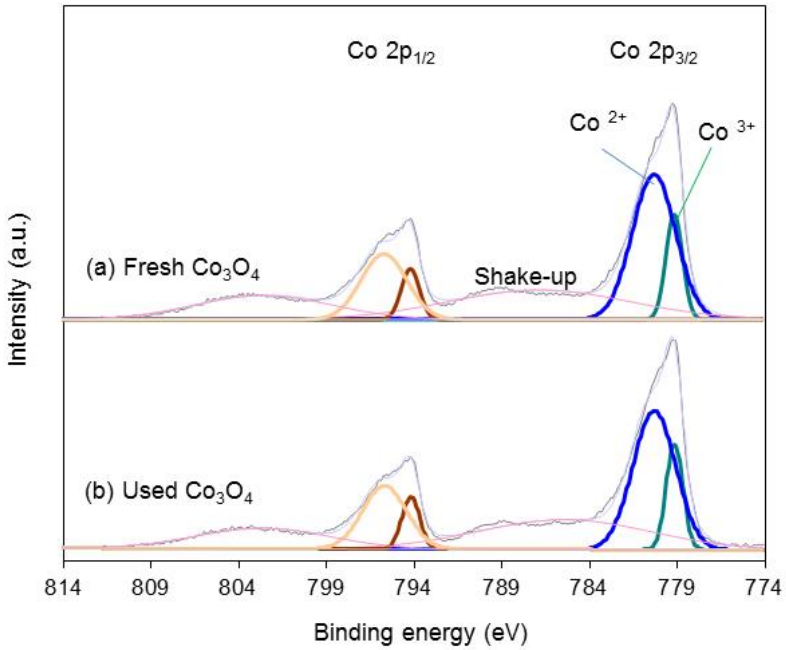

Fig. S4. XPS spectra of Co 2p core level of (a) fresh Co_3O_4 and used (b) fresh Co_3O_4

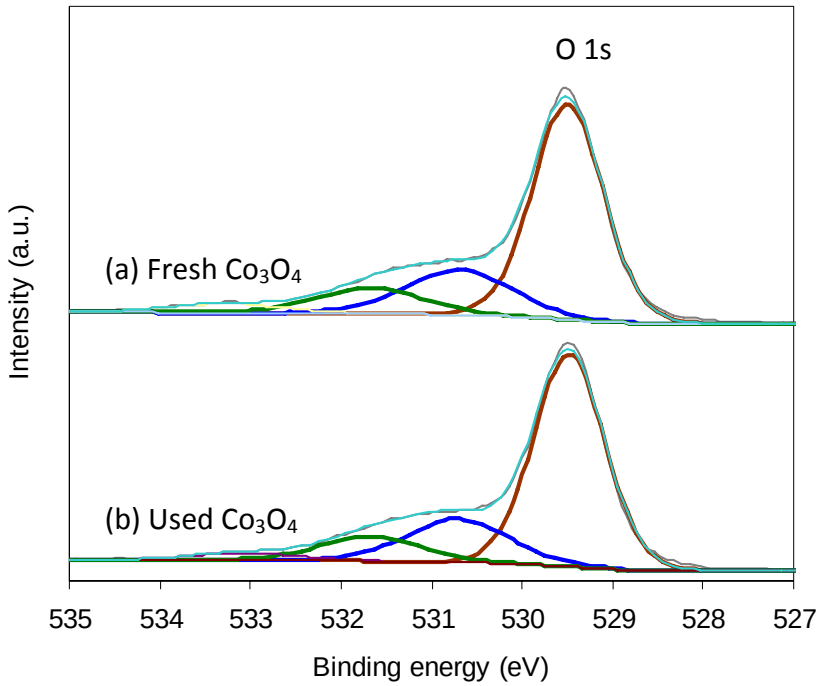

Fig. S5. XPS spectra of O 1s core level of (a) fresh Co_3O_4 and used (b) fresh Co_3O_4.

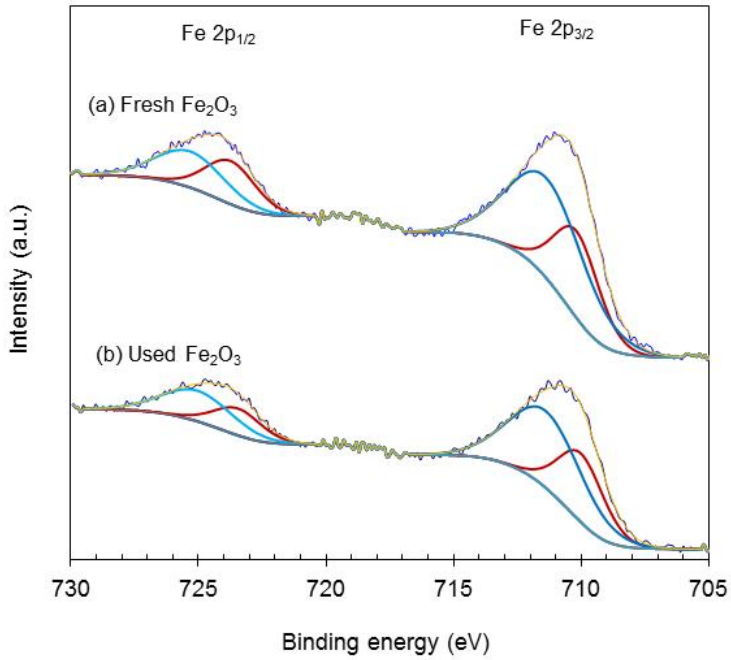

Fig. S6. XPS spectra of Fe 2p core level of (a) fresh Fe_2O_3 and used (b) fresh Fe_2O_3.

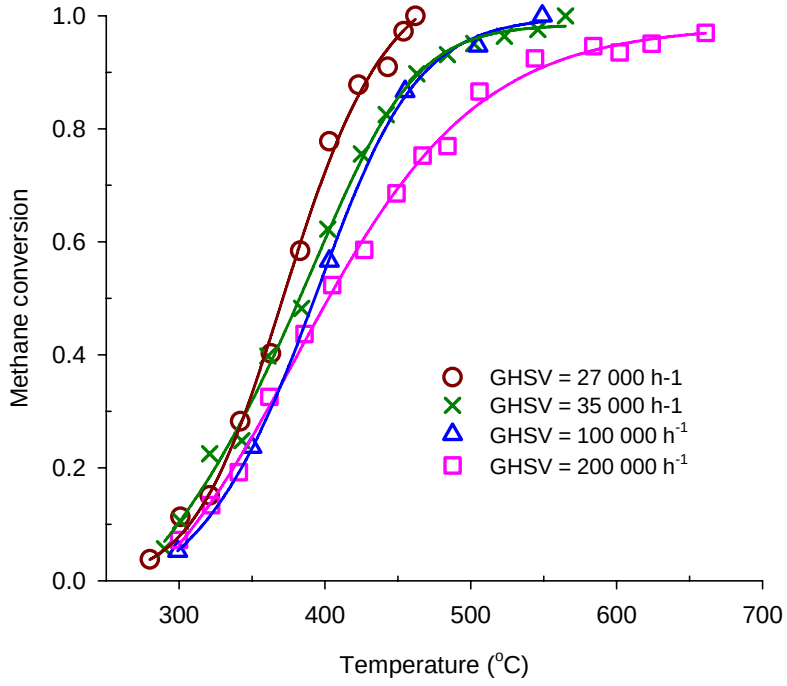

Fig. S7. Methane conversion as a function of temperature over Au/Co_3O_4 catalysts at different GHSV. Reaction condition: 6,000 ppm CH_4 balance air.

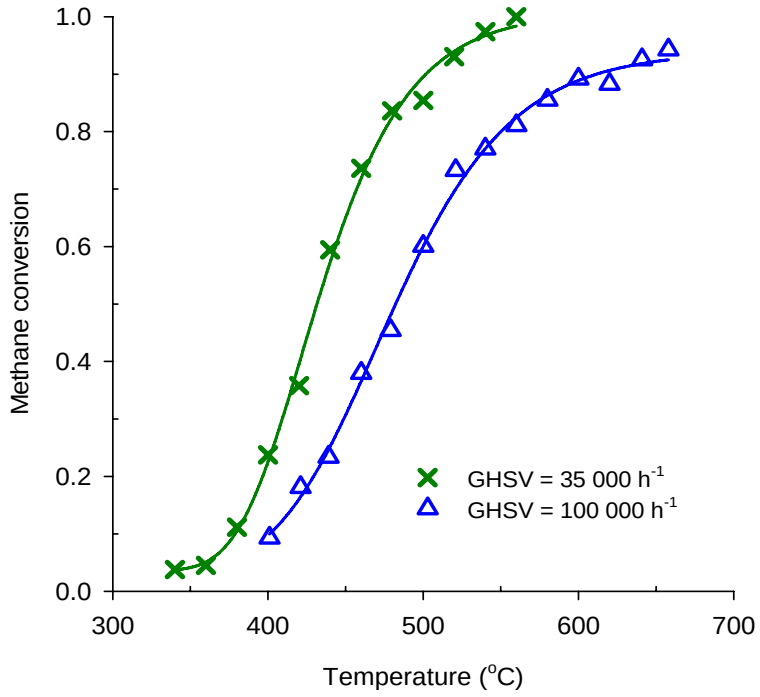

Fig. S8. Methane conversion as a function of temperature over Au/Fe_2O_3 catalysts at different GHSV. Reaction condition: 6,000 ppm CH_4 balanced with air.

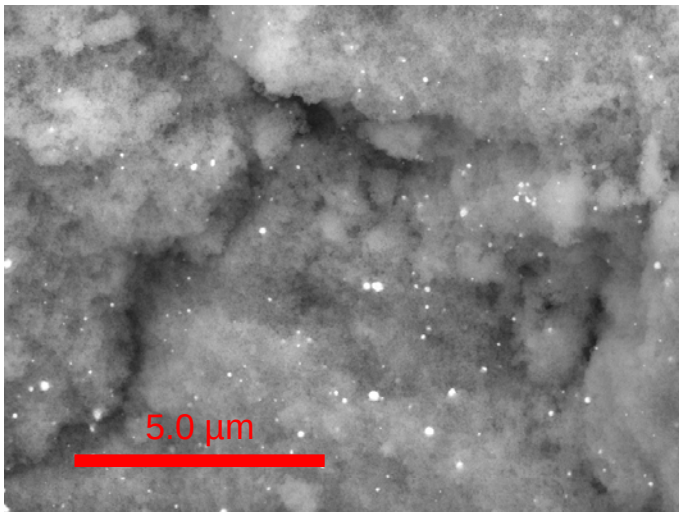

Fig. S9. SEM image of Au/Fe_2O_3

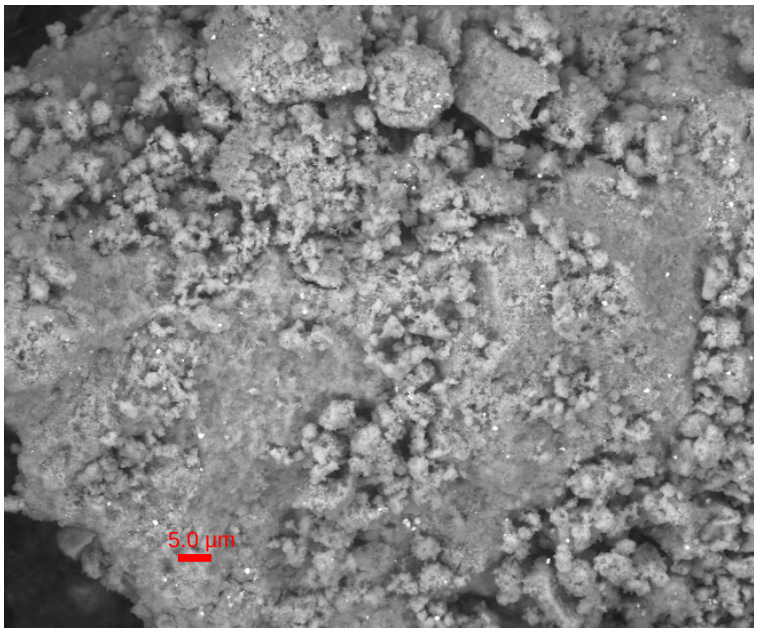

Fig. S10. SEM image of Au/Co_3O_4

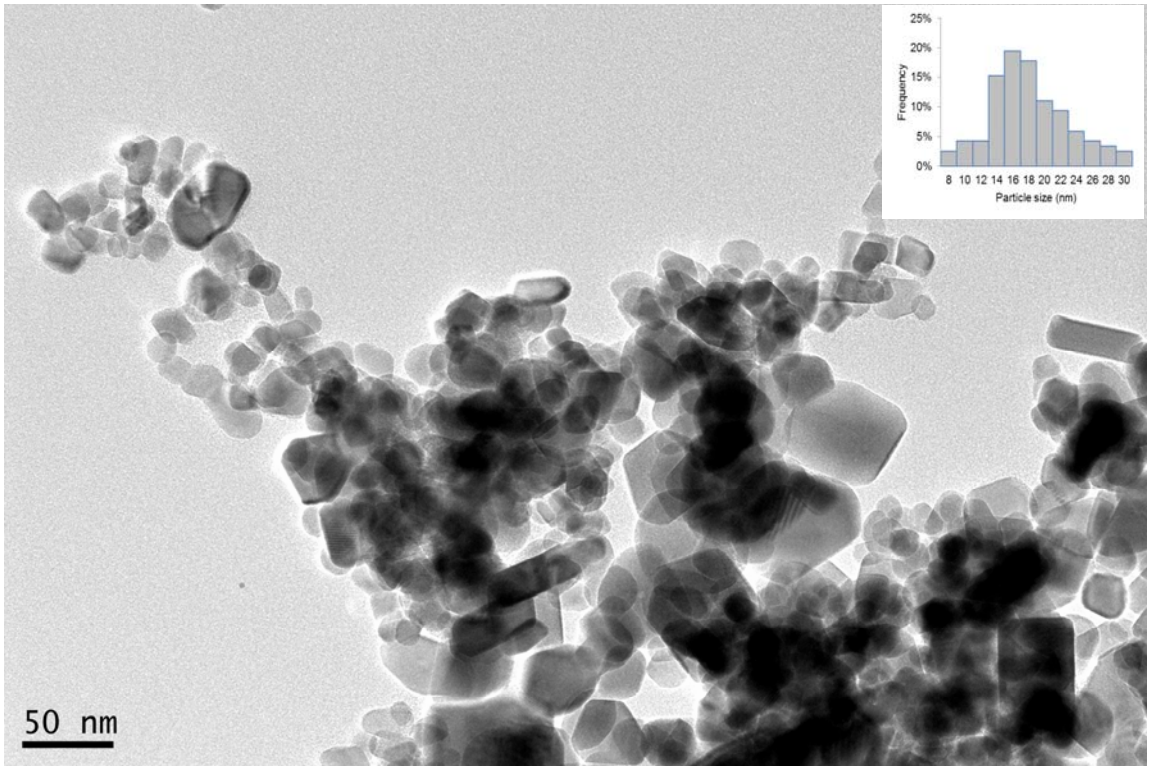

Fig. S11. TEM image and particle distribution of Au/Co_3O_4

Appendix E

Supporting Information for
Chapter 7

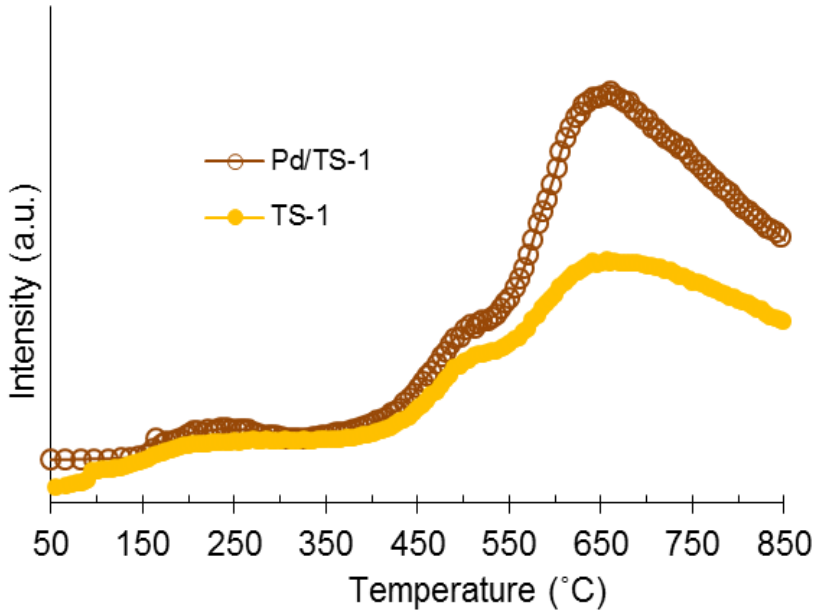

Fig. S1. TPD curves of water desorption from Pd/TS-1 catalyst and catalyst support (TS-1). H_2O was adsorbed at 110 °C. Heating ramp = 5 °C·min^{-1}. ○ = Pd/TS-1; ● = TS-1.

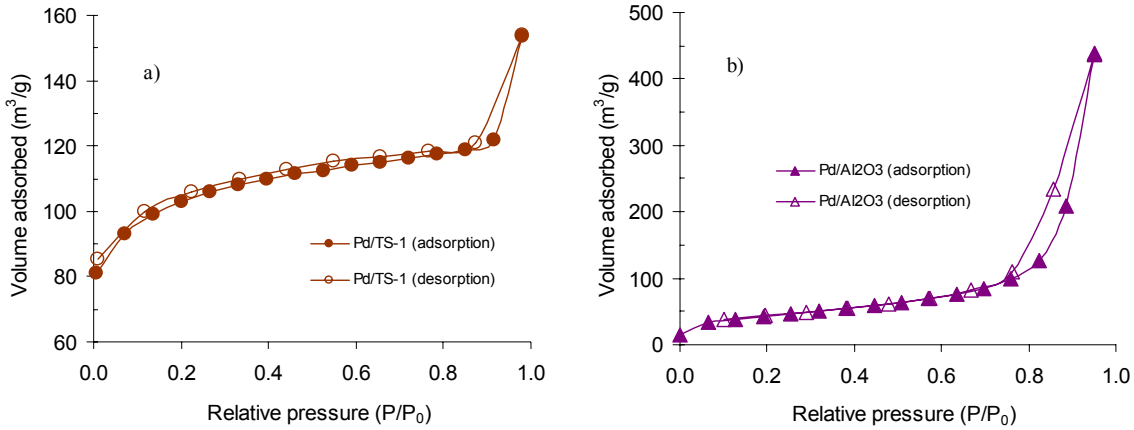

Fig. S2. Nitrogen-isotherm adsorption plot of Pd/TS-1 (a) and Pd/Al_2O_3 catalysts (b). ● = N_2-adsorption on Pd/TS-1; ○ = N_2-desorption from Pd/TS-1; ▲ = N_2-adsorption on Pd/Al_2O_3; Δ = N_2-desorption from Pd/Al_2O_3.

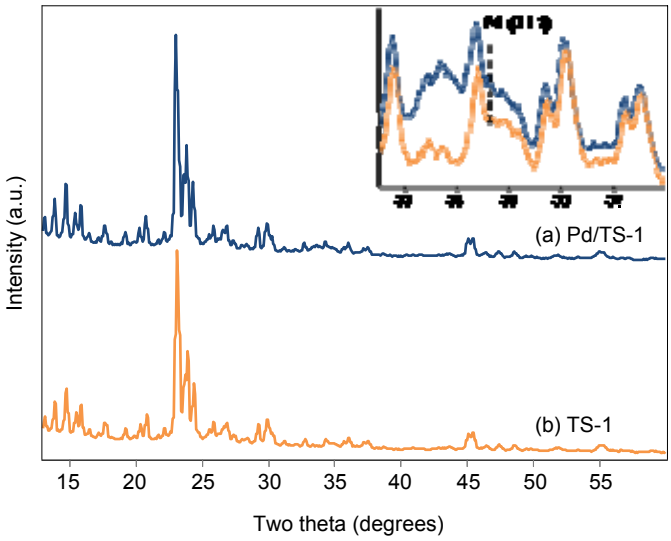

Fig. S3. X-ray diffraction patterns of (a) Pd/TS-1 catalyst and (b) TS-1 zeolite.

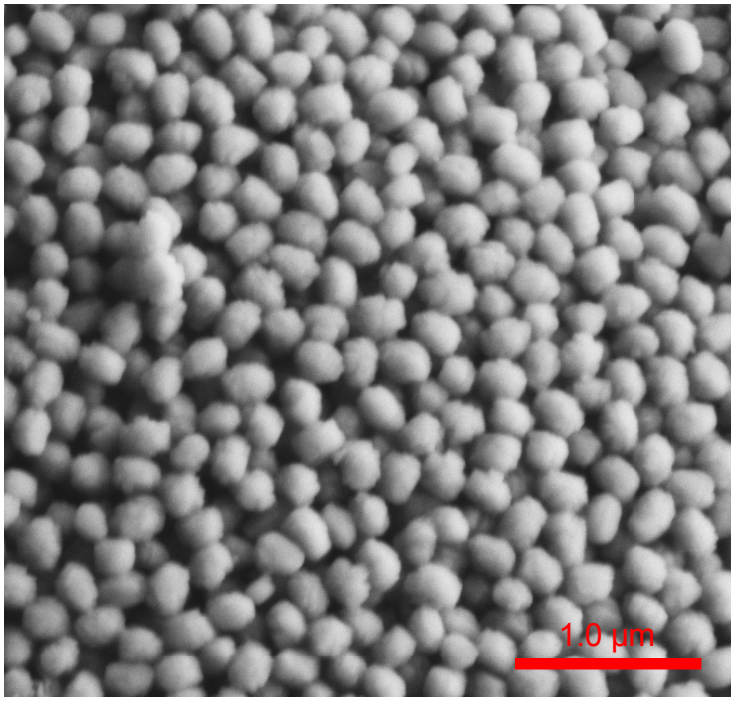

Fig. S4. SEM images of TS-1 zeolite captured by secondary electron detector.

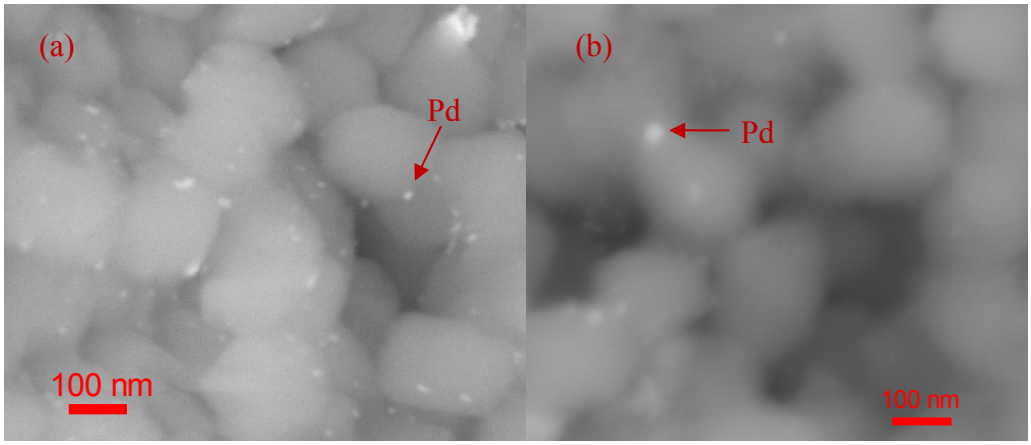

Fig. S5. SEM images of (a) fresh Pd/TS-1 and (b) used Pd/TS-1.

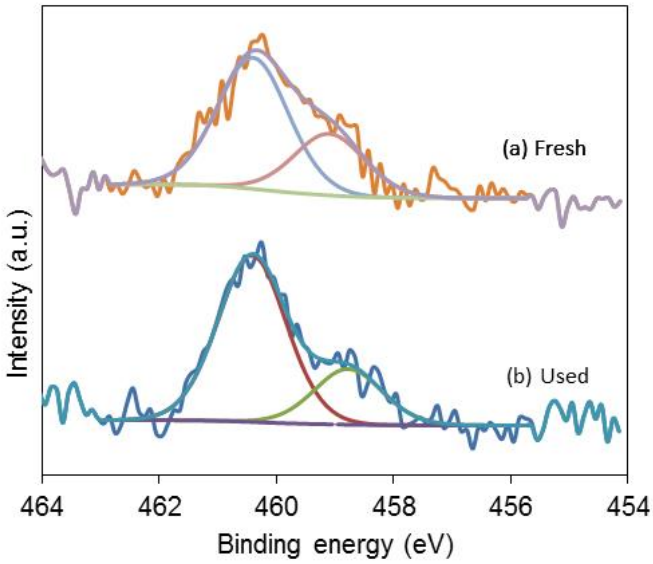

Fig. S6. XPS spectra of Ti 2p core level of Pd/TS-1 fresh (a) and used (b) catalysts

Table S1. Binding energies of Ti 2p core level

Sample		Ti 2p peak position (eV)	
		Peak 1	Peak 2
(a)	Pd/TS-1, fresh	460.4	459.1
(b)	Pd/TS-1, used	460.4	458.8

Appendix F

Supporting Information for
Chapter 8

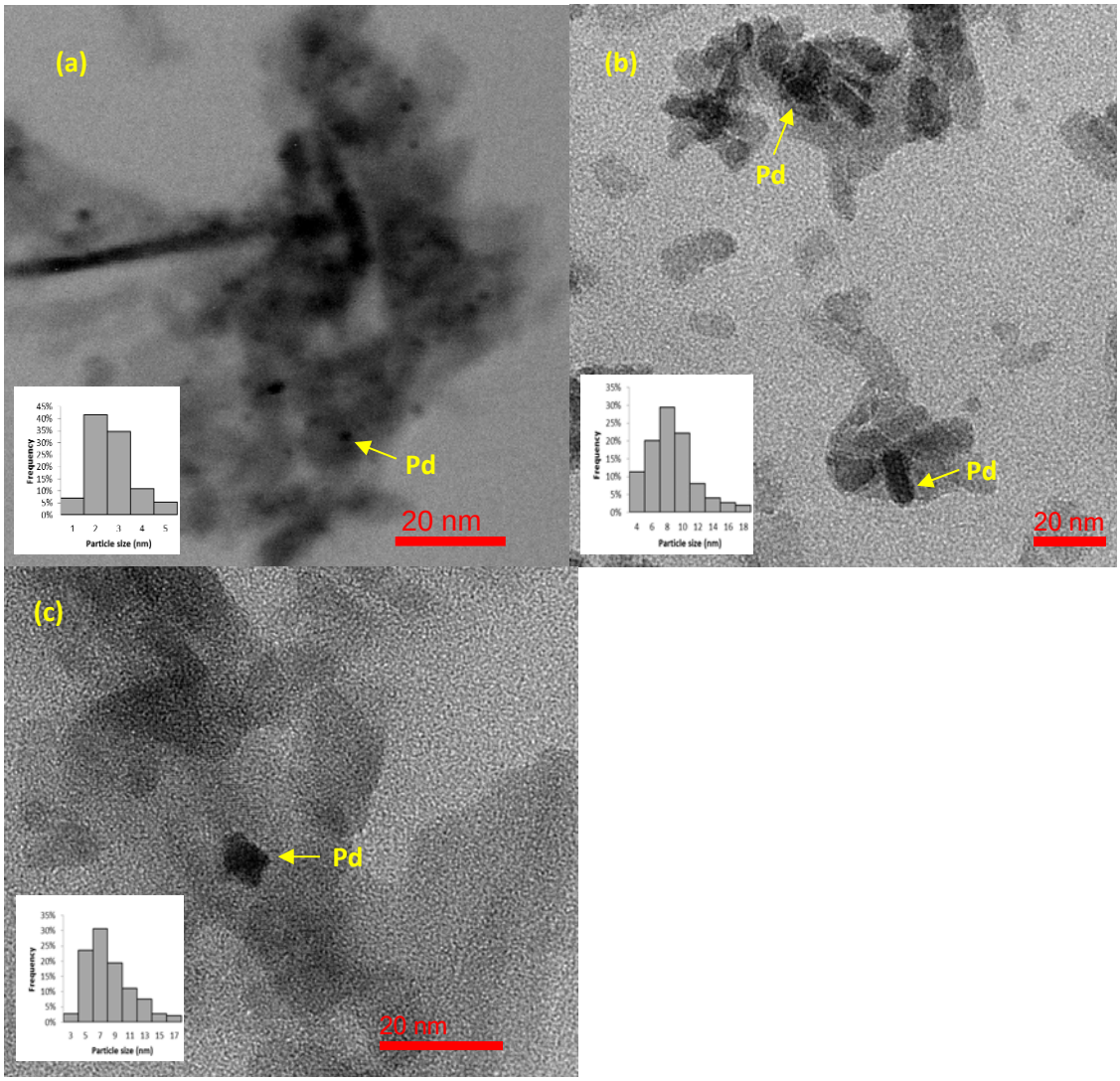

Fig. S1. TEM images of (a) fresh Pd/Al_2O_3; (b) used Pd/Al_2O_3 from dry-VAM experiment; (c) used Pd/Al_2O_3 from wet-VAM experiment;

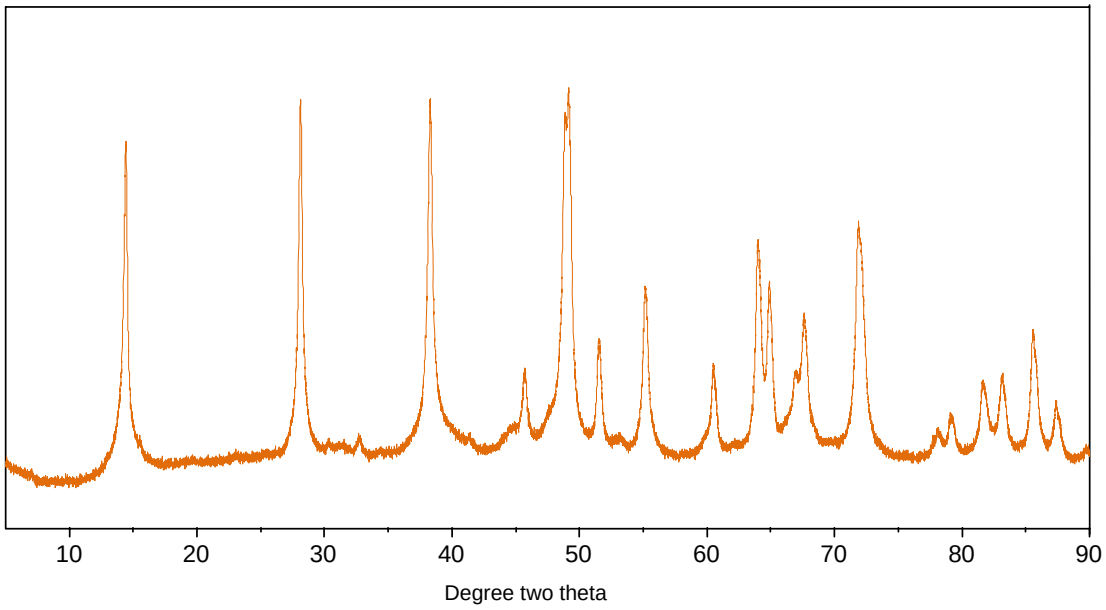

Fig. S2. XRD pattern of Pd/Al_2O_3-IV catalysts (aged 3 days in autoclave at 175 ˚C)

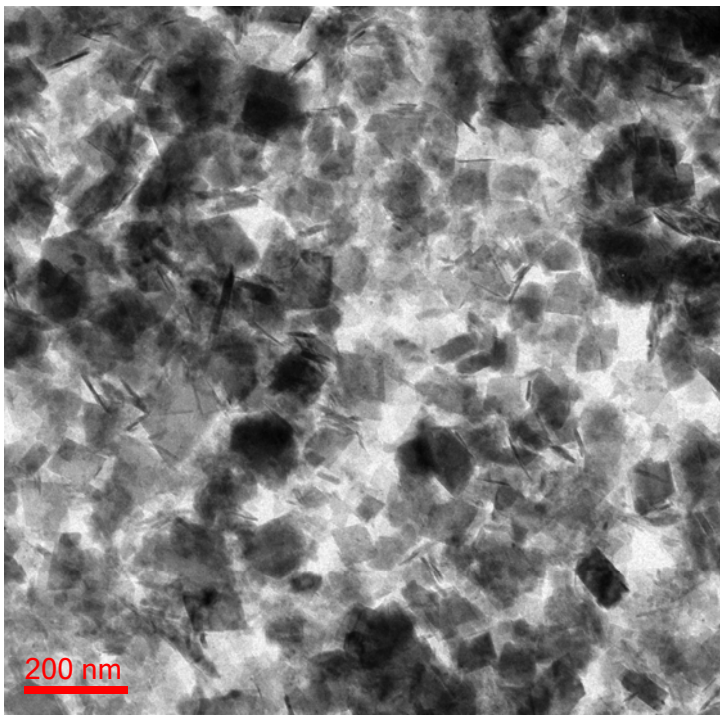

Fig. S3. TEM image of aged Pd/Al_2O_3-IV catalyst (aged in autoclave at 175 ˚C).

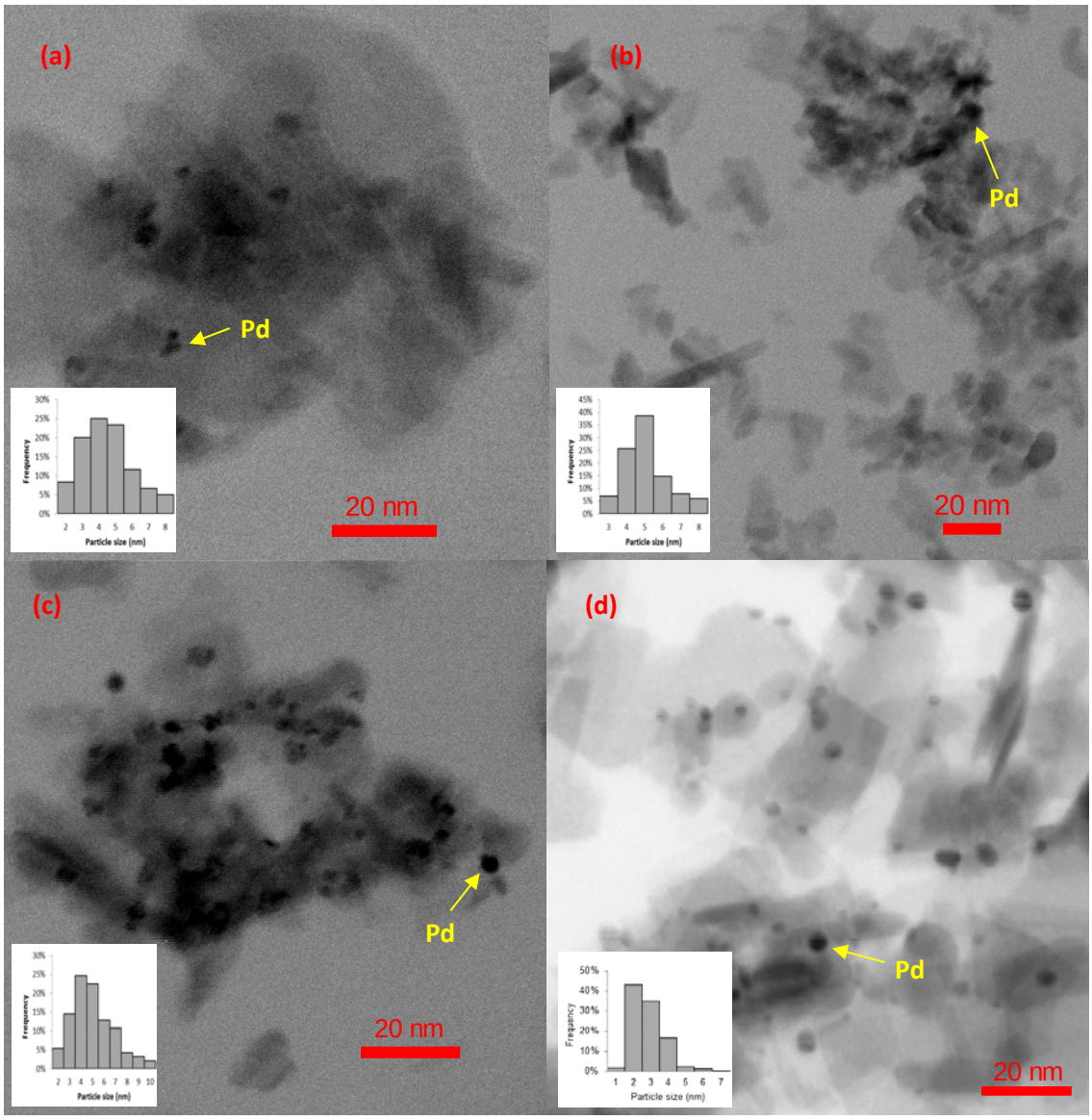

Fig. S4. TEM images of aged catalysts (a) Pd/Al_2O_3-I catalyst (aged 18 h in wet-feed at 780 ˚C); (b) Pd/Al_2O_3-II catalyst (aged 18 h in wet-feed at 830 ˚C); (c) Pd/Al_2O_3-III catalyst (aged 18 h in wet-O_2 at 780 ˚C); Pd/Al_2O_3-IV catalyst (aged in autoclave at 175 ˚C).